Langmuir-blodgett films of organic charge-transfer complexes

C. Pearson

LANGMUIR-BLODGETT FILMS OF ORGANIC CHARGE-TRANSFER COMPLEXES

by

C. Pearson BSc.

A Thesis submitted in partial fulfilment

of the requirements for the degree of PhD.

School of Engineering

University of Durham

December 1996

DECLARATION

I hereby declare that the work carried out in this thesis has not been previously submitted for any degree and is not currently being submitted in candidature for any other degree.

Signed .....

Candidate

The work in this thesis was carried out by the candidate

Signed.....

Director of Studies

Signed.....

Candidate

Dedication

This thesis is dedicated to my Dad.

Acknowledgements

There are a number of people that I would like to thank for the assistance they have given to me in the course of my work. Firstly, I would like to thank my supervisor, Professor Mike Petty for the time and effort that he has invested throughout my project. Also, the other members of the Molecular Electronics group, all of whom have helped to make working at Durham enjoyable.

I would like to thank Dr. A.S. Dhindsa and Dr. A.J. Moore in the Department of Chemistry for synthesising the organic compounds, Mr. B. Blackburn and the mechanical workshop and Mr. P Friend and the electronics workshop for helping to keep the LB troughs working. Thanks also to Mr. N.F. Thompson and Mr. D. Pattinson for maintaining the electron microscopes, Mr. J.E Gibson for teaching me how to do the photolithography and Ms. J.M. Dodds and Mrs. K. Seaton for helping me with the diagrams and photographs for this thesis.

I am grateful to the UK Engineering and Physical Sciences Research Council for their financial support.

Lastly, I would like to thank my mother, my brother and his family, and most especially my girlfriend, Julie, for all of their encouragement.

Abstract

This thesis is concerned with the preparation of floating films of electrically conductive organic charge-transfer complexes and their subsequent transfer to solid substrates by the Langmuir-Blodgett (LB) technique. Characterisation of the morphology (using ellipsometry, surface profiling, optical and scanning electron microscopy, energy dispersive spectroscopy and optical absorption spectroscopy) and electrical properties (at room temperature and low temperature) of the resulting multilayer structures is discussed. Three different systems were investigated: (i) mixed films containing the long chain tetrathiafulvalene (TTF) derivative octadecanoyl-TTF (ODTTF) and either octadecanoic acid (OA) or pentacosa-10,12-diynoic acid (PA); (ii) pure films of the charge-transfer complex *N*-octadecylpyridinium-bis-(4,5-dimercapto-1,3-dithiole-2-thione) palladium (C_{18}Py-Pd(dmit)$_2$); and (iii) pure films of the charge-transfer complex *N*-octadecylpyridinium-bis-(4,5-dimercapto-1,3-dithiole-2-thione) nickel (C_{18}Py-Ni(dmit)$_2$). Some interesting electrical properties were observed in these films. Also, C_{18}Py-Ni(dmit)$_2$ has been incorporated as the active layer in a thin film field effect transistor structure. Carrier mobility values of $1.9 \pm 0.5 \times 10^{-5}$ cm^2 V^{-1} s^{-1} and 0.3 ± 0.1 cm^2 V^{-1} s^{-1} were calculated from the device characteristics, before and after doping with iodine, respectively

In the case of films containing ODTTF, a maximum room temperature in-plane dc conductivity after iodine doping of $2\pm1\times10^{-2}$ S cm^{-1} was recorded. This conductivity was found to be strongly dependent on the molar ratio of the two components present in the film. The behaviour has been explained using two-site percolation models.

For C_{18}Py-Pd(dmit)$_2$ and C_{18}Py-Ni(dmit)$_2$, the properties of the floating layers and transferred films were found to be influenced by the exact experimental conditions. C_{18}Py-Pd(dmit)$_2$ films were conductive as deposited, with a stable maximum room temperature in-plane dc conductivity value of $1.5\pm1.0\times10^{-1}$ S cm^{-1}. C_{18}Py-Ni(dmit)$_2$ samples became conductive after exposure to iodine vapour, with a stable peak conductivity value of $1.3\pm0.8 \times10^{-1}$ S cm^{-1}.

CONTENTS

Chapter 1

Introduction

In the last 25 years, there has been considerable interest in the synthesis and characterisation of organic materials that form charge-transfer salts with novel electrical properties. Chapter 2 begins with a historical review of this development. These compounds can exhibit interesting electrical properties, with conductivities ranging from insulating through semiconducting to metallic and, in some cases, superconducting. The crystal structure and the origin of the electrical conductivity of organic materials is discussed in Chapter 2, including metallophthalocyanines, conductive polymers and fullerenes.

Three methods that are commonly used to prepare thin organic thin films: Langmuir-Blodgett film deposition; thermal evaporation and spinning, are described in Chapter 3. Emphasis is placed on the Langmuir-Blodgett technique since this method was employed to produce the thin films used in the course of this work. Previous research involving conductive LB films of organic charge-transfer materials is reviewed in the second half of Chapter 3, including details of anion radical salts, cation radical salts, donor-acceptor complexes and organometallic systems.

Chapter 4 begins with the theory of the thin film transistor (TFT), followed by an explanation of the role of the gate insulator. A review of previous work involving TFTs using organic materials as the active layer is also included.

The experimental techniques and equipment used in this work are described in Chapter 5: LB film deposition, including the preparation of spreading solutions, recording of pressure versus area isotherms, substrate cleaning and film transfer; the measurement of

film thickness using ellipsometry and surface profiling; optical and electron microscopy; energy dispersive spectrometry; optical absorption; the measurement of room temperature and low temperature electrical properties; and the fabrication and characterisation of thin film transistors.

Chapter 6 is the first results chapter, where the LB film forming properties and the characteristics of transferred multilayer films containing the amphiphilic tetrathiafulvalene (TTF) derivative octadecanoyl-TTF (ODTTF) are described.

The preparation and deposition of floating layers, and subsequent characterisation of transferred LB multilayer films of *N*-octadecylpyridinium-Pd(dmit)$_2$ (C_{18}Py-Pd(dmit)$_2$) and *N*-octadecylpyridinium-Ni(dmit)$_2$ (C_{18}Py-Ni(dmit)$_2$) are described in Chapters 7 and 8, respectively.

The electrical characteristics of a thin film field effect transistor using an LB film as the active region are presented in Chapter 9, and used to calculate the mobilities of the charge carriers in the organic layer, before and after doping with iodine.

Finally, Chapter 10 draws conclusions from all of the work in the thesis and makes suggestions for further work.

Chapter 2

Conductive Organic Compounds

2.1 Introduction

Organic molecular crystals consisting of π-electron donor (D) and acceptor (A) molecules have a low lying charge-transfer excitation. They crystallise in structures consisting of molecular stacks. The majority of these materials are neutral in the ground state, are either insulating or semiconducting and never exhibit metallic properties. The strongest π- donors (such as those shown in Fig. 2.1) and π-acceptors (illustrated in Fig. 2.2) form ionic crystals consisting of stacks of D^+ and/or A^- ion radicals. Metallophthalocyanines and certain polymeric hydrocarbons have unsaturated π-electron systems. Both become conductive after chemical doping. The most recently discovered class of organic conductor contains the salts of the acceptor molecule buckminsterfullerene. Organic solids in all of these groups can exhibit unusual electrical properties.

In this chapter, the historical development of conductive charge-transfer complexes is described. The crystal structure and the origin of the electrical conductivity of these materials is explained. Metallophthalocyanines, conductive polymers and fullerenes are also considered.

2.2 History of the development of conductive organic charge-transfer complexes

Most molecular organic crystals such as anthracene, benzene or naphthalene are electrically insulating with conductivities of the order 10^{-10} to 10^{-14} S cm^{-1}. The possibility that organic materials might exhibit electrical conductivity as high as that of metals was suggested in the early part of the 20^{th} century,[1] but the first experimental

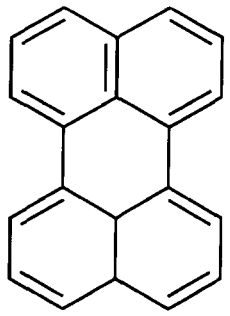

1 Perylene

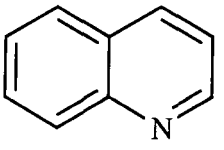

3 Quinoline

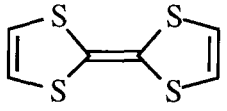

4 TTF

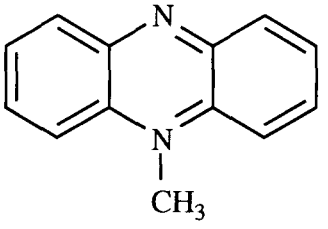

5 NMP

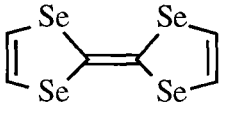

6 TSF

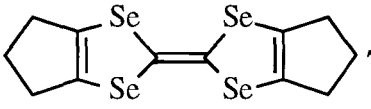

7 HMTSF

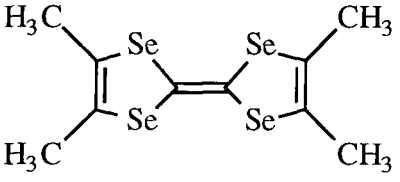

8 TMTSF

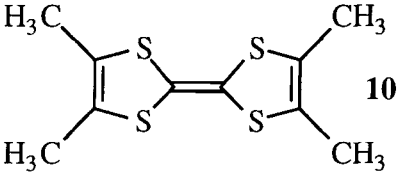

10 TMTTF

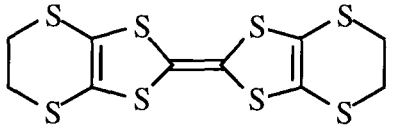

12 BEDT-TTF

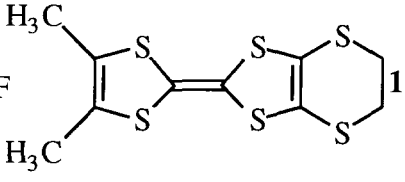

16 DMET

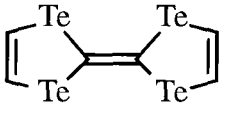

17 TTeF

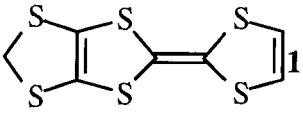

18 MDT-TTF

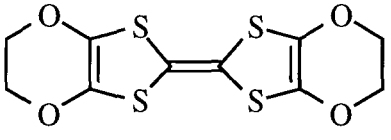

19 BEDO-TTF

Fig. 2.1 **Organic donor molecules.**

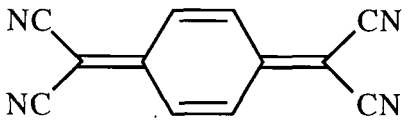

2 TCNQ

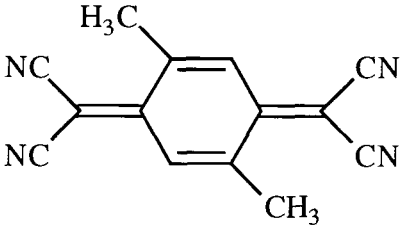

9 DMTCNQ

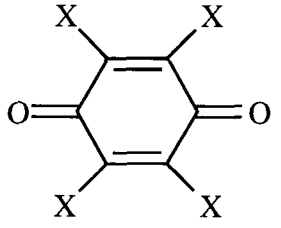

11 X_4BQ

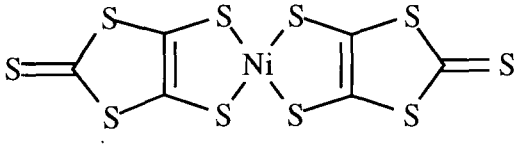

13 $Ni(dmit)_2$

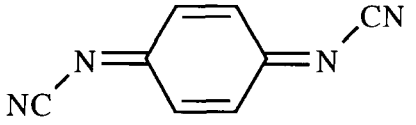

14 DCNQI

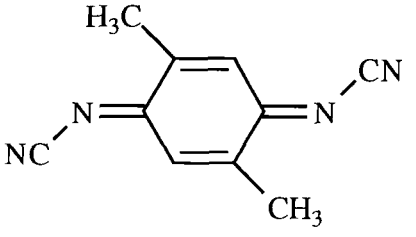

15 2,5-DM-DCNQI

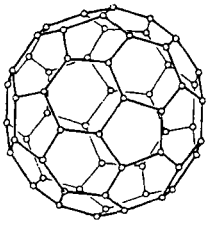

20 C_{60}

Fig. 2.2 **Organic acceptor molecules.**

evidence showing that molecular organic solids could exhibit interesting electrical properties was reported by Japanese workers in 1954.[2] They found that some complexes between polycyclic aromatic compounds (such as perylene(**1**)) and bromine had fairly high, thermally activated, electrical conductivity (~ $1x10^{-3}$ S cm^{-1} at room temperature) in the solid state. The conductivity of these compounds was found to decrease with time, however, and of the materials studied, the complex between perylene and bromine was the most stable.

In 1962, Melby and co-workers at the Dupont laboratories carried out fundamental work concerning the electrical properties of compounds containing a new powerful electron acceptor 7,7,8,8-tetracyano-*p*-quinodimethane (TCNQ)(**2**).[3] TCNQ is electron deficient and will accept an electron in order to become an anion radical. It is not electrically conductive on its own, however. Although the molecule will easily accept an electron from one of its neighbours, in pure TCNQ all of the molecules have the same electron affinity and there is no possibility of charge movement through the crystal. Consequently, pure TCNQ remains insulating. If TCNQ is combined in a crystal with an electron donating molecule, charge can be transferred from the donor to TCNQ. If the degree of charge-transfer is only partial, a conductive mixed-valence system will result in which charge can move between neighbouring TCNQ molecules, which form into face-to-face stacks. Many complexes of TCNQ with a variety of donors were found to be electrically conducting and quinolinium(**3**)-TCNQ was the most conductive organic material known at this time, with single crystal room temperature conductivity σ_{RT}=100 S cm^{-1}. In all cases, the conductivity of these compounds was found to decrease with decreasing temperature, i.e. the materials were semiconducting.

Attempts to manufacture a powerful reducing agent led to the synthesis, in 1970, of tetrathiafulvalene (TTF)(**4**)[4] and, in 1972, it was reported[5] that the chloride salt of this organic donor had high electrical conductivity (~ 0.3 S cm^{-1} at room temperature). The

following year, the salts TTF-TCNQ[6] and N-methylphenazinium (NMP)(**5**)/TCNQ[7] were prepared, where the ratio of donor to TCNQ was 1:1. In both cases, high conductivity was observed (σ_{RT} = 500 S cm^{-1} and 380 S cm^{-1}, respectively) as well as metallic behaviour, i.e. an increase in conductivity below room temperature. These materials were considered to be "organic metals". TTF-TCNQ had a maximum conductivity of 10^4 S cm^{-1} at around 60 K. If the temperature was reduced to below ~ 58 K, however, a phase transition from the metallic to a semiconducting state occurred.

The TTF/TCNQ system, consisting of segregated and uniform stacks of donor and acceptor molecules, provided a prototype for synthetic chemists, physicists and theoreticans in their attempts to design new, more highly conductive compounds. Information regarding the effect of minor changes in the structure of constituent molecules on the physical properties of the resulting solid was obtained. The synthesis of tetraselenofulvalene (TSF)(**6**) and the salt TSF/TCNQ, in 1974,[8] successfully reduced the temperature of the metal-insulator transition (T_{M-I}) to 40K, while the room temperature conductivity was increased to 800 S cm^{-1}. Substitution of the sulphur in the molecular structure with physically larger selenium atoms resulted in an increase in electronic interactions by enhancing the overlap of the molecular orbitals between the cations.

The first organic material to exhibit metallic character down to 45 mK, hexamethylene-TSF (HMTSF)(**7**)-TCNQ, was reported by Bloch *et al* in 1975.[9] This property was due to the increased dimensionality provided by close Se...N contacts between neighbouring stacks.

Suppression of the metal-insulator transition and stabilisation of the metallic state in tetramethyl-TSF (TMTSF)(**8**)-dimethyl-TCNQ (DMTCNQ)(**9**) by the application of hydrostatic pressure >10 kbar was demonstrated in 1979 by Andrieux *et al.*[10] Conductivities of 700 S cm^{-1} and ~ 10^5 S cm^{-1} were measured at 300 K and 4.2 K,

respectively.

In 1979, Torrance *et al* combined TTF and tetramethyltetrathiafulvalene (TMTTF)(**10**) with members of the tetrahalo-*p*-benzoquinone (X_4BQ where X=halogen)(**11**) family of molecules and successfully produced highly conducting compounds without the use of TCNQ, or a close derivative, as the acceptor.[11] For example, the pressed powder conductivity at 300 K of the 1:1 charge-transfer salt Cl_4BQ-TMTTF was found to be 20 S cm^{-1}.

Organic superconductivity was first reported in 1980 by Jérome *et al* [12] in the synthetic conductor $(TMTSF)_2PF_6$. A superconducting transition temperature T_c of 0.9 K under a pressure of 12 kbar was observed. Later, a superconducting state was found in $(TMTSF)_2ClO_4$.[13] A transition temperature of 1.3 K was observed, without the application of high pressure.

Bis-ethylenedithio-TTF$(BEDT\text{-}TTF)_2ClO_4$ $(1,1,2\text{-trichloroethane})_{0.5}$ was the first sulphur based system to exhibit metallic conductivity over a wide temperature range, from 298-1.4 K.[14] Two-dimensional transport properties were reported, where the conduction electrons predominantly moved through a framework of sulphur atoms in sheets of BEDT-TTF(**12**) atoms.

$(BEDT\text{-}TTF)_2ReO_4$ was the first sulphur-based superconducting organic material, observed by Parkin *et al* in 1983.[15] A transition temperature of 1.4 K under a pressure of 4 kbar was reported.

Further work on the BEDT-TTF molecule led to the discovery of ambient pressure superconductivity in the complex $(BEDT\text{-}TTF)_2I_3$ by Yagubskii *et al* in 1984.[16] A transition to the superconducting state was observed at a temperature of 1.4-1.5 K. This

transition temperature was increased to 8 K two years later by Schirber *et al*[17] by the application of anisotropic pressure. This resulted in a reduction in disorder and consequent rise in T_c.

In 1986, TTF-bis-[bis-(4,5-dimercapto-1,3-dithiole-2-thione) nickel II] ($TTF[Ni(dmit)_2]_2$) was reported as the first superconducting system based on the charge-transfer salt of a π-anion molecule[18], i.e. $Ni(dmit)_2$(**13**). At ambient pressure, a room temperature conductivity of 300 S cm^{-1} was reported, with metallic character retained down to 3 K and a conductivity of 1.5 x 10^5 S cm^{-1} at 4.2 K. Under pressure of 7 kbar, a superconducting transition was observed with T_c=1.62 K.

Work on the acceptor *N,N'*-dicyanoquinonediimine (DCNQI)(**14**) by Aumüller and co-workers[19] led to the synthesis of Cu(2,5-dimethyl-DCNQI)$_2$(**15**) in 1986. This complex exhibited extremely high conductivity in a radical anion salt, with room temperature conductivity of 800 S cm^{-1}, metallic behaviour down to 1.3 K and conductivity of 5 x 10^5 S cm^{-1} at 3.5 K.

The first superconducting compound based on an unsymmetrical donor molecule (all previous examples of organic superconductivity involved materials containing symmetrical donor and/or acceptor molecules) was reported by Japanese workers in 1987.[20] The complex dimethyl(ethylenedithio)-diselenadithiafulvalene(DMET)(**16**)$_2$-$Au(CN)_2$ exhibited a transition to the superconducting state at a temperature of 1.1 K under a pressure of 2.5 kbar.

Until 1987, all organic superconductors were based on π-donor molecules complexed with either a π-acceptor or a closed shell anion. The first example of superconductivity in a charge-transfer complex consisting of a π-anion and a closed shell cation was demonstrated by Kobayashi *et al* with the synthesis of $Me_4N[Ni(dmit)_2]_2$.[21] This

organic metal had a room temperature conductivity of 50 S cm^{-1} and a superconducting transition was observed at 5 K under a pressure of 7 kbar.

In 1988 the synthesis of tetratellurafulvalene (TTeF)(**17**) allowed investigation of the properties of the complex TTeF-TCNQ.[22] It was expected that the increased size of the tellurium atom over both sulphur and selenium would result in increased conductivity due to enhanced overlap of the π-electron system and raised dimensionality due to larger orbitals in the interstack directions. A room temperature conductivity of ~ 2000 S cm^{-1} was recorded, with metallic behaviour down to liquid nitrogen temperature.

Superconductivity in a sulphur based system with an unsymmetrical donor molecule was first reported by Papavassiliou et al in 1988.[23] The complex methylenedithio-tetrathiafulvalene(MDT-TTF)(**18**)-AuI_2 exhibited a superconducting transition at T_c = 3.5 K, under ambient pressure.

In 1988 a superconducting transition temperature at ambient pressure of 10.4 K was observed for the salt $(BEDT\text{-}TTF)_2Cu(SCN)_2$.[24]

The design of the bis(ethylenedioxy)tetrathiafulvalene (BEDO-TTF)(19) molecule by Wudl *et al* in 1990 led to the production of the first organic metal of an oxygen containing donor in the iodine salt[25] $(BEDO\text{-}TTF)_{2.4}\ I_3$ with room temperature conductivity of ~ 200 S cm^{-1} and subsequently, superconductivity in the complex $(BEDO\text{-}TTF)_2\ Cu_2(NCS)_3$[26] with a transition temperature T_c = 1.0 K at ambient pressure.

Currently, two salts of BEDT-TTF are the highest T_c organic superconductors. $(BEDT\text{-}TTF)_2\ Cu[N(CN)_2]Br$ has a transition temperature of 1.6 K at ambient pressure[27] and in $(BEDT\text{-}TTF)_2Cu[N(CN)_2]Cl$ T_c = 12.5 K under 0.3 k bar of hydrostatic pressure.[28]

2.3 Electrical conductivity and the band structure of solids

Electric current density, J, as a function of electric field, E, is given by Ohm's law

$$J = \sigma E \qquad 2.1$$

where the constant of proportionality, σ, is the electrical conductivity of a material. This conductivity is given by the product of charge density and mobility

$$\sigma = (ne)\mu \qquad 2.2$$

where e is the electronic charge and n and μ are the density and mobility of the charge carriers, respectively.

The most important feature for the formation of a highly conductive organic material is that the material should possess a partially occupied energy band. The band structure of an insulator, semiconductor, semimetal and metal are shown in Fig. 2.3. In an insulator, the energy gap E_g between the valence band and conduction band is large. At room temperature the electrons in the valence band have insufficient energy to move up to the conduction band and there is no mechanism for current flow. As the band gap decreases in size, it is possible for electrons to be thermally excited from the valence band to the conduction band. In this case the material is an intrinsic semiconductor and conductivity σ is given by

$$\sigma = \sigma_0 \exp\left(\frac{-E_g}{2kT}\right) \qquad 2.3$$

where k is Boltzmann's constant and T is the absolute temperature. Conductivity decreases with decreasing temperature and the plot of $\log_e(\sigma)$ versus reciprocal temperature has negative slope equal to $E_g/2k$ and intercept on the y-axis of σ_0, a

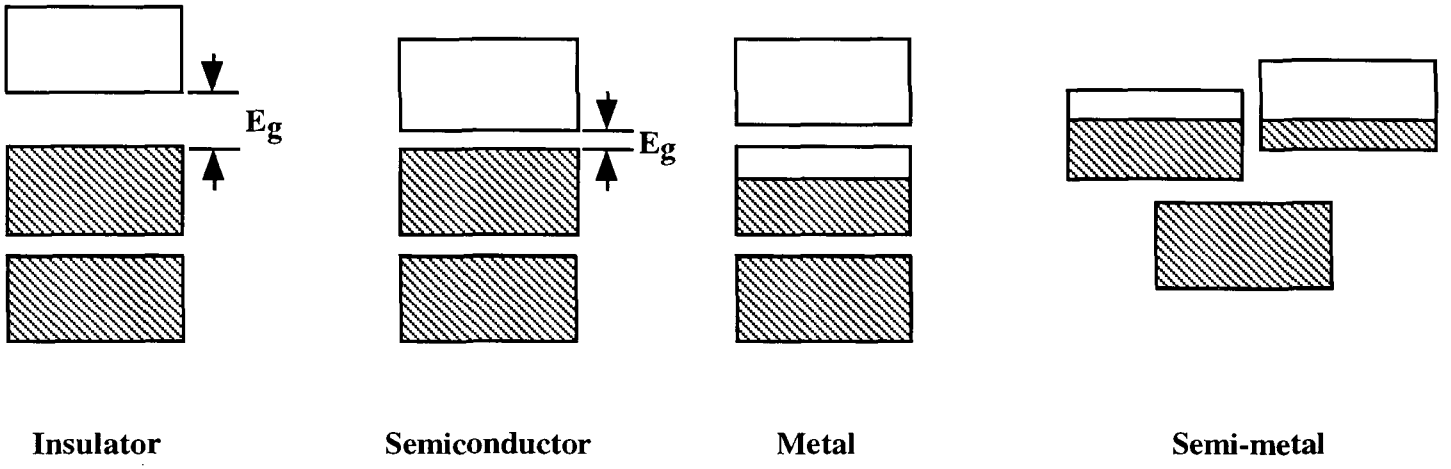

Fig. 2.3 The band structure of an insulator, semiconductor, metal and semi-metal.

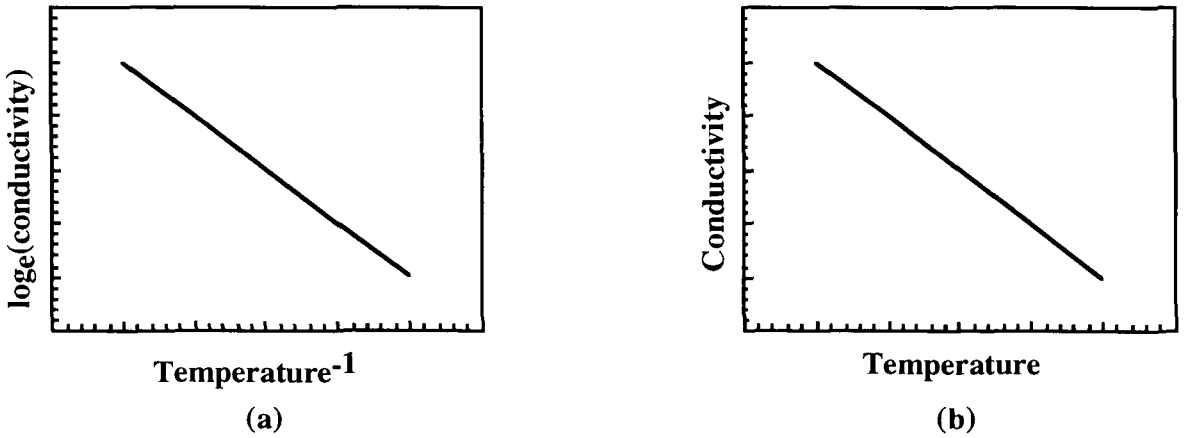

Fig. 2.4 Illustration of the temperature dependence of the conductivity of (a) a semiconductor and (b) a metal.

constant known as the pre-exponential factor. The temperature dependence of the conductivity of a semiconductor is depicted in Fig. 2.4(a). Metallic behaviour requires that a material should possess a partially filled band. In this case, many electrons can easily move to higher energy states within the same band and hence contribute to electrical conductivity. The temperature dependence of the conductivity of a metal is dominated by the scattering of conduction electrons by vibrations of the crystal lattice of the metal and hence, as the temperature decreases, there are fewer lattice vibrations and conductivity increases. The temperature dependence of the conductivity of a metal is illustrated in Fig. 2.4(b). In the case of a semi-metal, electrons are transferred from the highest occupied band of a donor to a low lying unoccupied band of an acceptor giving rise to two partially occupied bands.

2.4 Donor-acceptor complexes

Donor-acceptor (DA) charge-transfer (CT) complexes form from closed-shell molecules and have a neutral ground state. Crystalline DA complexes form molecular stacks in which the donor and acceptor molecules alternate along the stacking direction (...D A D A D A...) (Fig 2.5 (a) and (b)). This type of stacking is called mixed or intercalated. These materials are either insulators or semiconductors, with conductivities in the range 10^{-8}-10^{-14} S cm^{-1}, but never metals. Perylene-fluoranil, the crystal structure of which is shown in Fig 2.6, is an example of a donor-acceptor charge-transfer complex.[29] The alternation of donor and acceptor molecules along the c-axis can be seen. Electrical conductivity along this axis is 1.5 x 10^{-14} S cm^{-1}, about three times greater than that in the perpendicular directions.[30] The thermal activation energy for conduction is 0.73 eV in all directions.

2.5 Radical-ion salts

2.5.1 Crystal structure

Radical-ion salts are ionic in nature with a ground state consisting of positively and

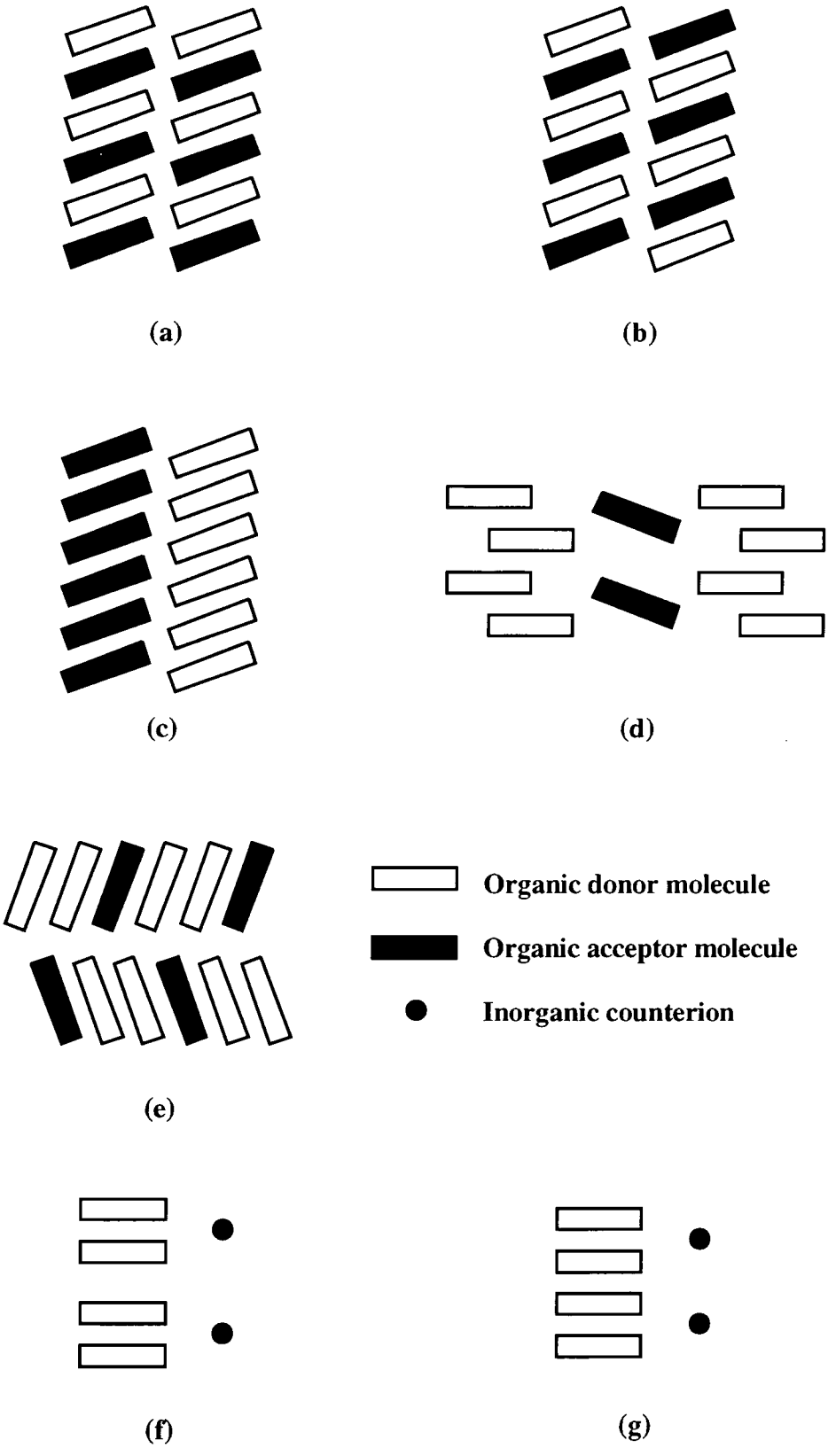

Fig. 2.5 Schematic diagram illustrating the different stacking patterns encountered in charge-transfer complexes and ion-radical salts.

(a) & (b) Mixed or intercalated stacking.
(c) & (d) Segregated stacking.
(e) Isolated dimers.
(f) & (g) Inorganic counterion.

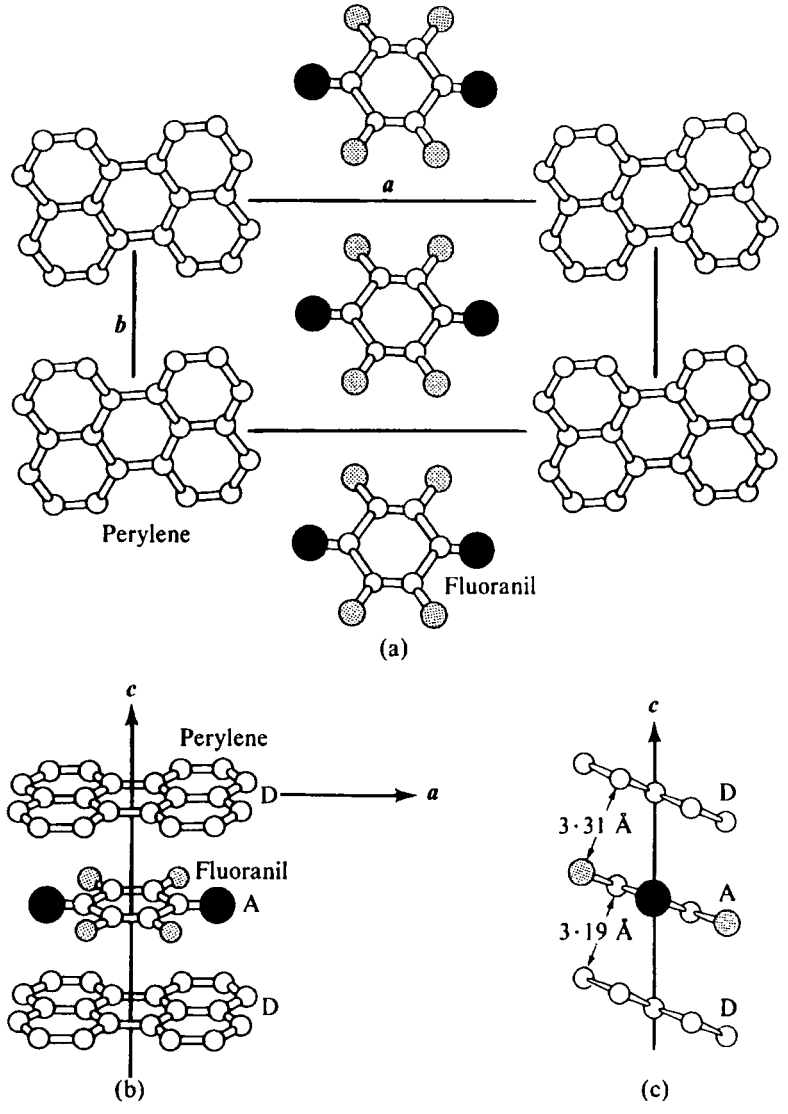

Fig. 2.6 **Crystal structure of the charge-transfer donor-acceptor complex perylene-fluoranil.**

(a) looking along c-axis (stacking direction).
(b) looking along b-axis, illustrating alternation of donors and acceptors.
(c) looking along a-axis with intermolecular spacing shown.

After Hanson.[29]

negatively charged donor and acceptor molecules. As with charge transfer complexes, the molecules in ion-radical salts pack into face-to-face stacks. There are several different ways in which these stacks form, as illustrated in Fig. 2.5, resulting in a variety of electrical properties. Ionic charge-transfer crystals often form mixed stacks in which donors (D) and acceptors (A) stack alternately face to face (...$D^+A^-D^+A^-$...)(Fig 2.5 (a) and (b)). The charge transfer excitation for a mixed stack crystal with an ionic ground state can be represented by

$$...D^+A^-D^+A^- \xrightarrow{h\upsilon_{CT}} D^+A\ DA^-... \qquad 2.4$$

where $h\upsilon_{CT}$ is the minimum energy needed to transfer charge between neighbouring sites. N,N,N',N'-tetramethyl-*p*-phenylenediamine (TMPD)-TCNQ crystallises in mixed stacks[31] with the molecular planes tilted with respect to the stacking axis (the c-axis) (Fig 2.7).

Free-radical crystals often exhibit segregated stacking (Fig 2.5 (c)) in which donors and acceptors form separate stacks

. . . .

. . . .

D^+ A^- D^+ A^-

D^+ A^- D^+ A^-

D^+ A^- D^+ A^-

. . . .

. . . .

In a donor stack with complete charge transfer, the lowest charge-transfer excitation is represented by

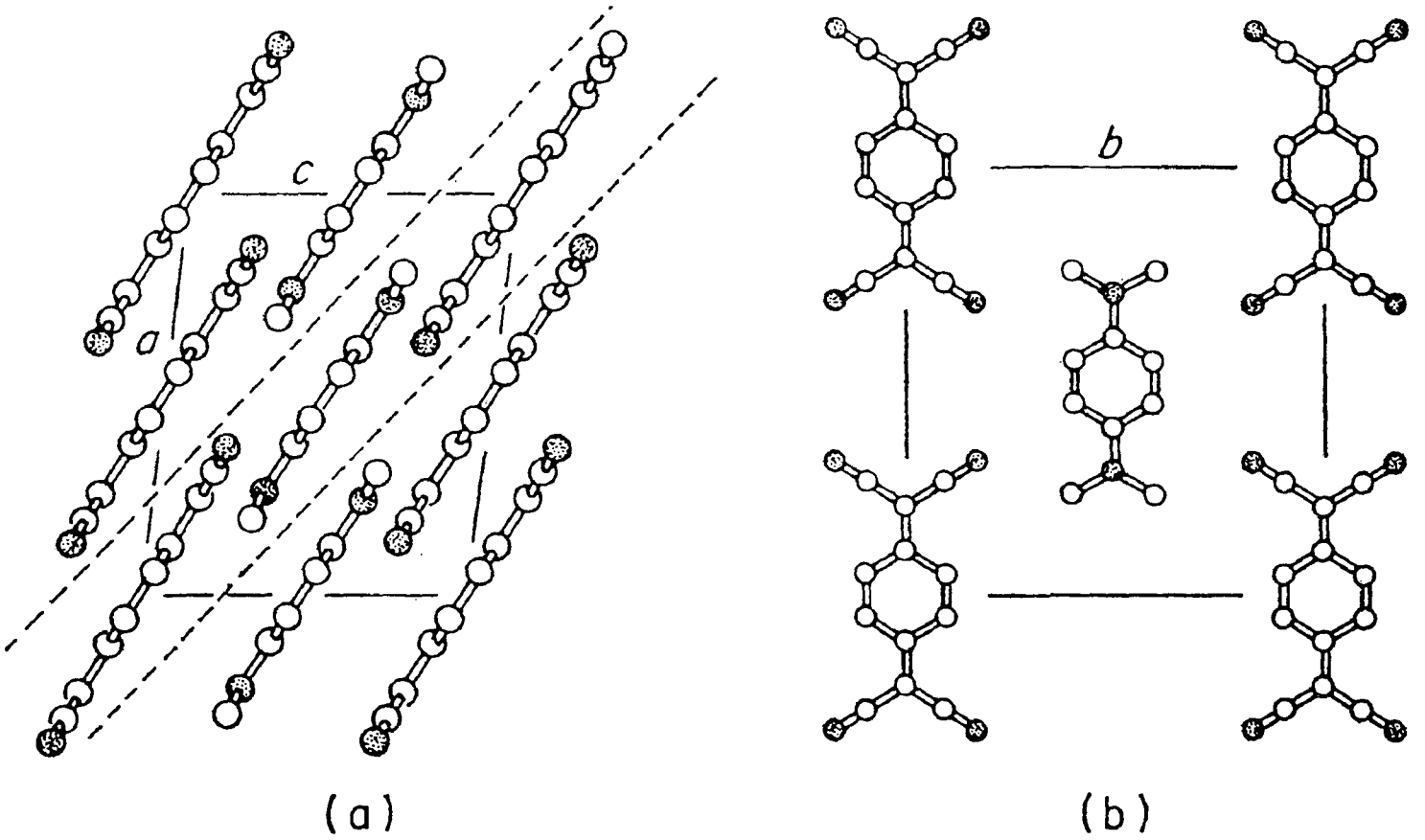

Fig. 2.7 **Crystal structure of TMPD-TCNQ**

(a) looking along b-axis.
(b) looking along c-axis showing the plane of molecules between the broken lines in (a).

After Hanson.[31]

$$\ldots D^{+}D^{+}D^{+}D^{+} \xrightarrow{h\upsilon_{CT}} D^{+}DD^{2+}D^{+}\ldots \qquad 2.5$$

and for an acceptor stack with complete charge transfer

$$\ldots A^{-}A^{-}A^{-}A^{-} \xrightarrow{h\upsilon_{CT}} A^{-}AA^{2-}A^{-}\ldots \qquad 2.6$$

Examples of ionic free-radical salts include the alkali metal-TCNQ compounds[3] and TTF-TCNQ.[6] The stacking of the molecules in TTF-TCNQ is illustrated in Fig 2.8.[32] The molecules in each column are tilted relative to the stacking axis (the b-axis) and neighbouring stacks arrange to form a herringbone pattern. In segregated stacks, a zigzag structure is possible along the columns (Fig 2.5 (d)). TMPD-$(TCNQ)_2$ exhibits this type of packing (Fig 2.9).[33] Here, the acceptor molecules are perpendicular to the stacking axis (the c-axis) while the donor molecules are inclined at an angle of about 70° to this axis. If the donor molecule is appreciably larger than the acceptor, a structure can result in which two acceptor molecules are sandwiched between each pair of donors in a mixed stack (Fig 2.5 (e)). Bis-8-quinolinolatocopper:$(picric\ azide)_2$ provides an illustration of this structure (Fig 2.10).[34] Each copper quinolinolate molecule is interleaved by two picric azide molecules. In salts containing inorganic counterions, dimerisation (Fig 2.5 (f)) or regularly spaced (Fig 2.5 (g)) packing may be observed. In TMPD-ClO_4, intermolecular cation distances are strongly alternated,[35] whereas in $(TMTSF)_2$-ClO_4, there is only slight dimerisation and a zigzag structure is seen, as shown in Fig. 2.11.[13]

2.5.2 Conductivity

Not all ion-radical salts exhibit high conductivity and it is possible to separate these materials into three classes on the basis of room temperature conductivity and the dependence of conductivity on temperature.[36]

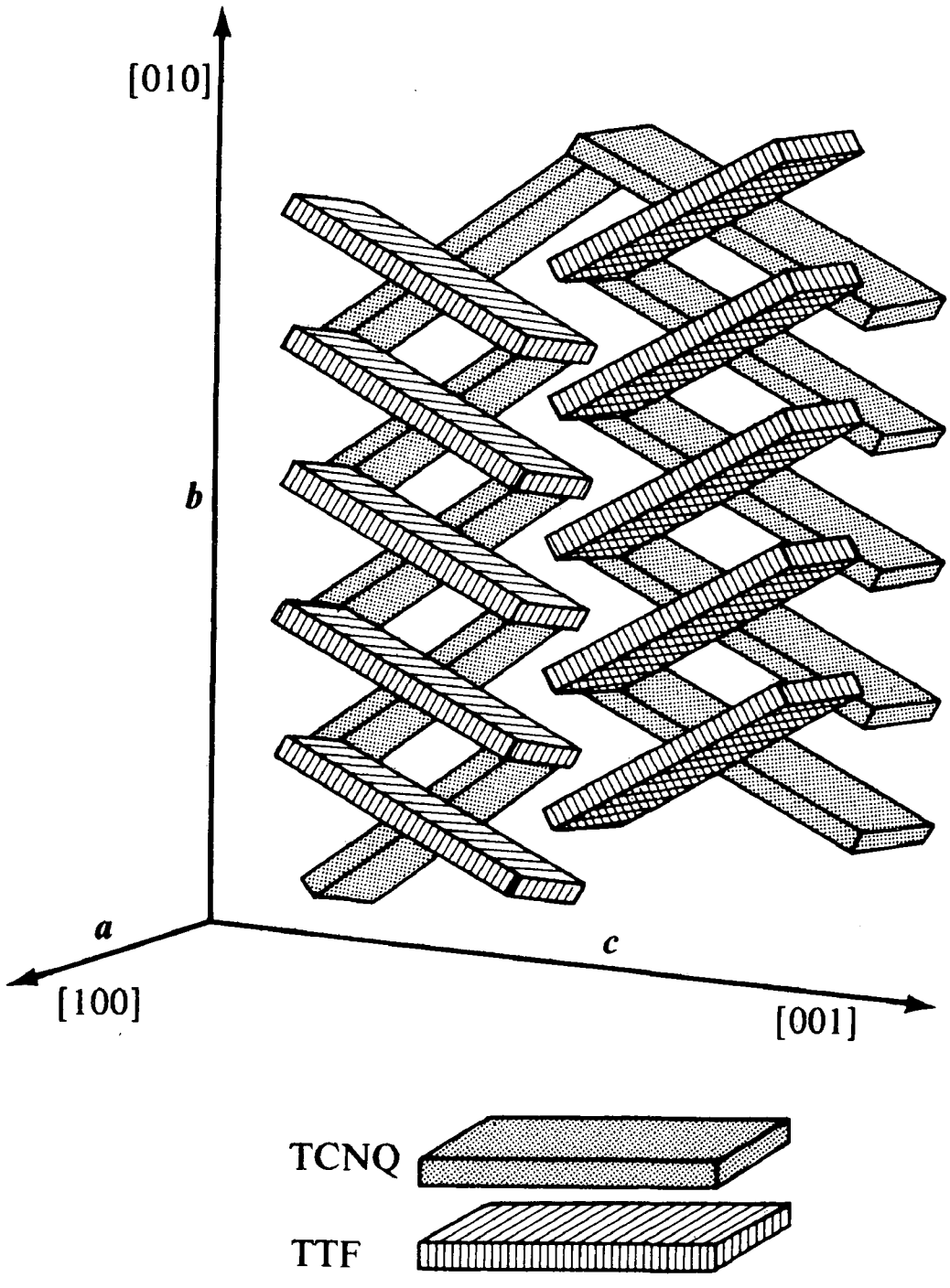

Fig. 2.8 **Schematic diagram illustrating the molecular packing found in single crystal TTF-TCNQ.**

After Comes.[32]

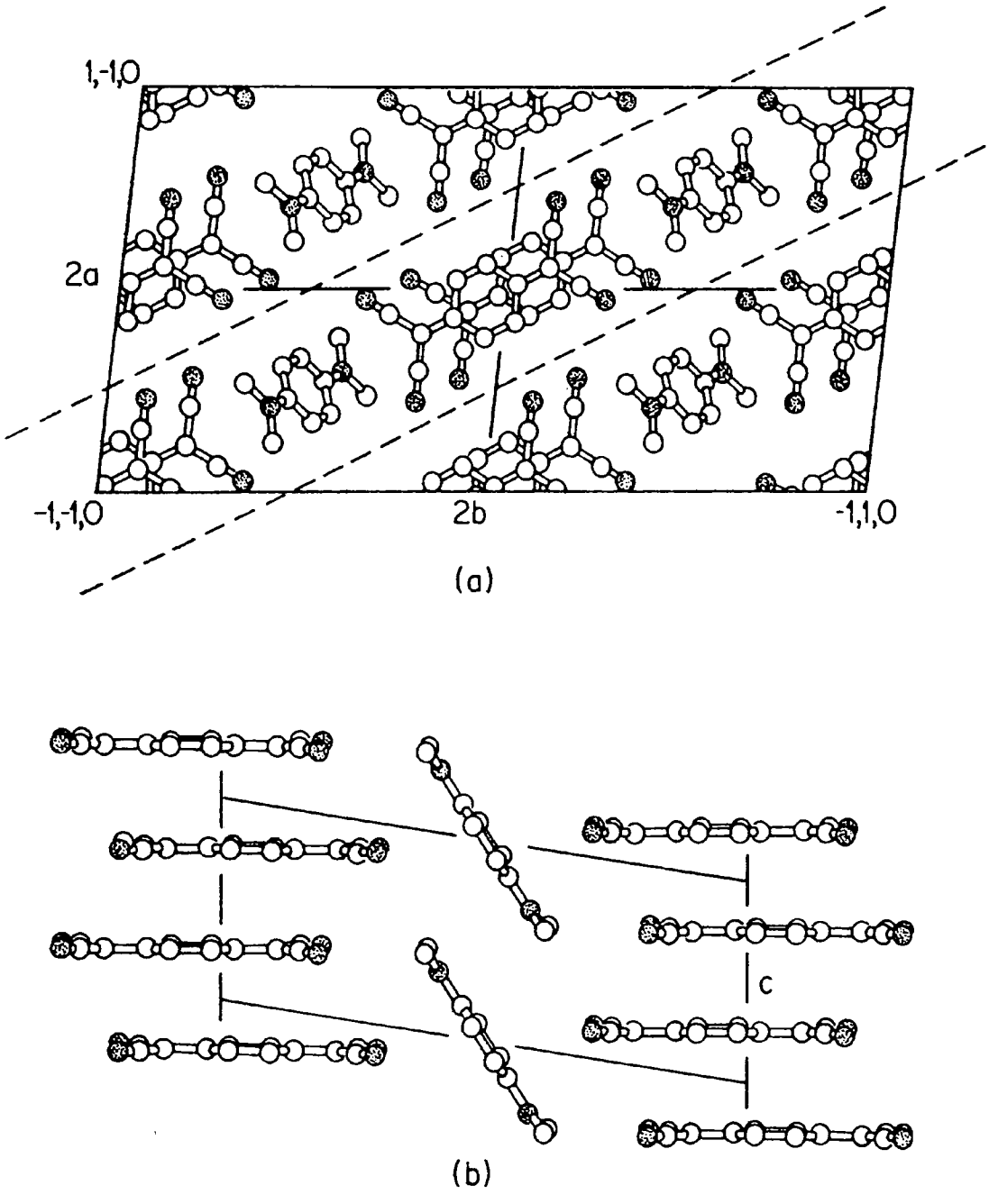

Fig. 2.9 **Molecular structure of TMPD-$(TCNQ)_2$**

(a) **looking along the c-axis.**

(b) **the molecules between the broken lines in (a) showing the zig-zag structure within the stacks.**

After Hanson.[33]

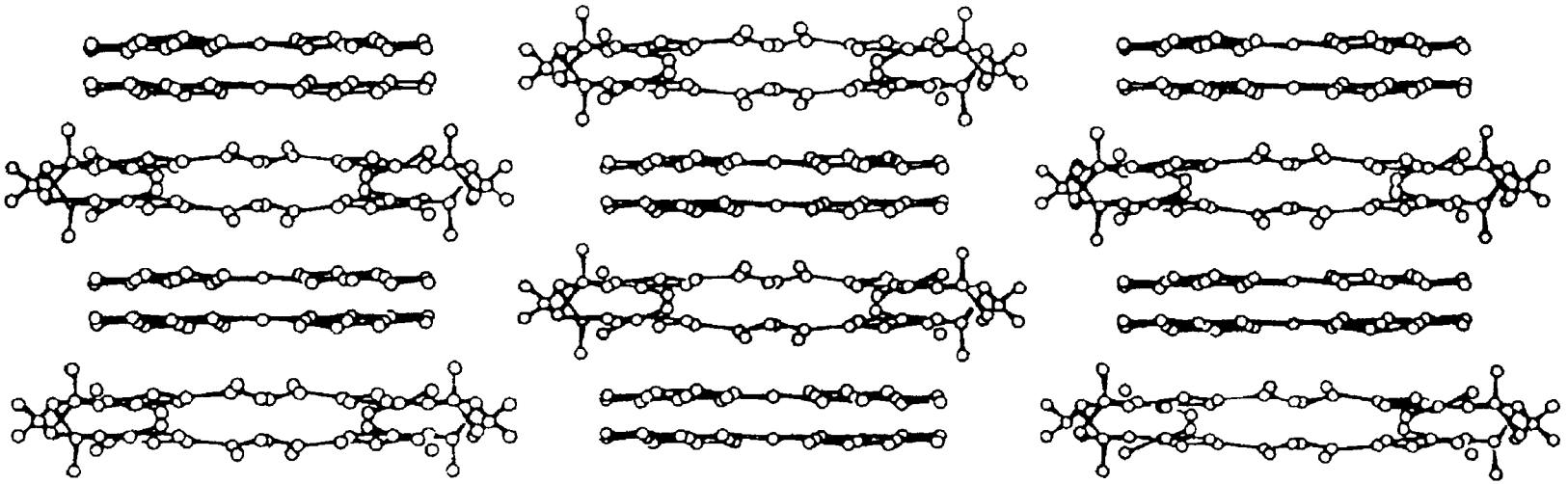

Fig. 2.10 **Crystal structure of bis-8-quinolinolatocopper:(picric azide)$_2$ showing pairs of acceptor molecules sandwiched between the donors.**

After Bailey and Prout.[34]

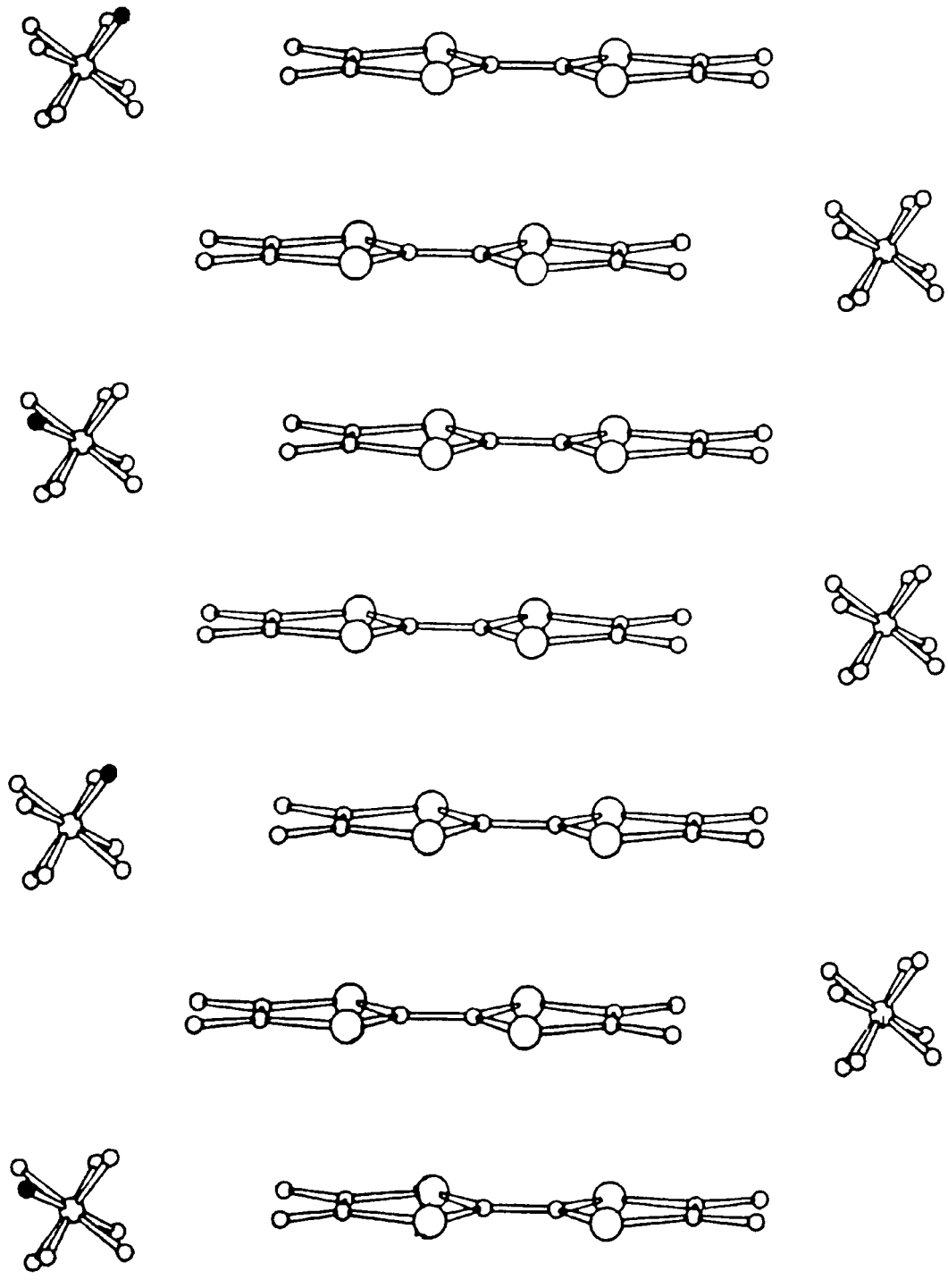

Fig. 2.11 Side view of the segregated columns in $(TMTSF)_2ClO_4$. Stacking occurs along the a-axis.

After Bechgaard *et al.*[13]

Class I - Room temperature conductivity σ_{RT} of the order of 10^{-6} to 1 S cm^{-1} and conductivity strongly thermally activated, with logσ versus T^{-1} linear, so that these materials may be considered to be semiconductors. Included in this class are the $(alkali^{+})_n(TCNQ^{-})_m$ compounds such as $Cs_2(TCNQ)_3$. Here, $\sigma_{RT} \sim 10^{-3}$ S cm^{-1} and the activation energy is 0.3-0.5 eV, depending on the temperature range studied.

Class II - A broad, weak maximum of conductivity σ_m at a temperature T_m is seen. The ratio $\sigma_m/\sigma_{RT} \leq 2$ and $\sigma_{RT} \sim 100$ S cm^{-1}. Examples of class II compounds are the ammonium derivatives of TCNQ such as NMP-TCNQ. Here, σ_{RT}=380 S cm^{-1}, $T_m \approx 160$ K and $\sigma_m/\sigma_{RT} \sim 1.2$.

Class III - These compounds exhibit a sharp maximum of conductivity σ_m at temperature T_m. The ratio $\sigma_m/\sigma_{RT} >> 2$ and σ_{RT} = 500-1000 S cm^{-1}. TTF-TCNQ is a typical class III material, with $\sigma_{RT} \approx 500$ S cm^{-1}, a conductivity peak at T_m=59 K and $\sigma_m/\sigma_{RT} = 20$.

Assuming the usual form of the relationship between conductivity, charge carrier density and carrier mobility

$$\sigma(T) = n(T)e\mu(T) \qquad 2.7$$

where e is the electronic charge, n(T) and μ(T) are the concentration and mobility of the charge carriers, which are both functions of temperature. The way in which the conductivity σ(T) varies with temperature is governed by the form of n and μ versus T. The following general expression can be used to describe the relationship between conductivity and temperature [37]

$$\sigma(T) = \sigma_0 T^{-\alpha} \exp(-\Delta/T) \qquad 2.8$$

where exp (-Δ/T) is the temperature dependence of the carrier concentration (here, Δ=ΔE/k with ΔE known as the thermal activation energy for conductivity) and $T^{-\alpha}$, where α is a constant, describes the variation of mobility with temperature. A schematic representation of the way in which σ, n and μ vary with temperature is shown in Fig. 2.12.[36] Equation 2.3 has a maximum at $T_m = \Delta/\alpha$. A class I compound has a $T_m >>$ 300 K, the carrier density is thermally activated and mobility is independent of temperature. Class II compounds follow equation 2.3 and T_m = 100-300 K. In the case of class III materials, carrier density is constant and mobility depends strongly on temperature. Here, T_m ~ 0 K. The conductivity versus temperature behaviour of a number of TCNQ salts is shown in Fig. 2.13 to illustrate the differences between these three classes. These differences can be partially attributed to the degree of charge transfer ρ from the donor to TCNQ. In the class I salts, charge transfer is complete, i.e. ρ=1, and all of the TCNQ molecules in a given stack are reduced. A minimum energy $h\upsilon_{CT}$ is required to transfer charge between neighbouring sites

$$TCNQ^{-}+TCNQ^{-} \xrightarrow{h\upsilon_{CT}} TCNQ^{0}+TCNQ^{2-} \qquad 2.9$$

This interband transition requires an activation energy and consequently the materials are insulators or semiconductors. A band arising from this transition is evident in the optical absorption spectrum of TCNQ salts. It is labelled B in Fig 2.14.[38] If ρ<1, however, there will be some neutral TCNQ molecules in a given column and the valence band is only partially filled allowing for the transport of charge along the stack. This leads to an absorption band (labelled A on Fig 2.14) as a result of the excitation of an excess charge to a neighbouring unoccupied site

$$TCNQ^{-}+TCNQ^{0} \xrightarrow{h\upsilon_{CT}} TCNQ^{0}+TCNQ^{-} \qquad 2.10$$

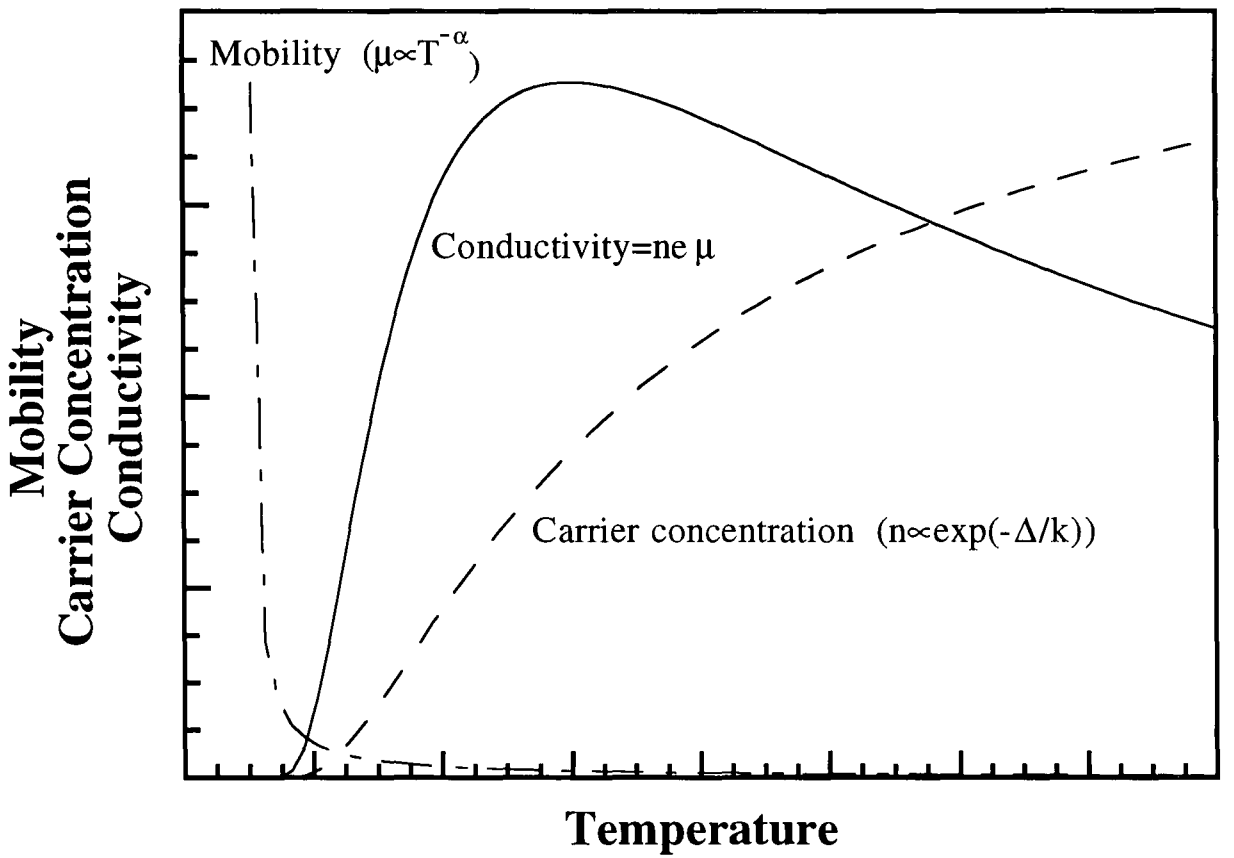

Fig. 2.12 **Temperature dependence of mobility, charge carrier concentration and conductivity.**

After Epstein *et al.*[36]

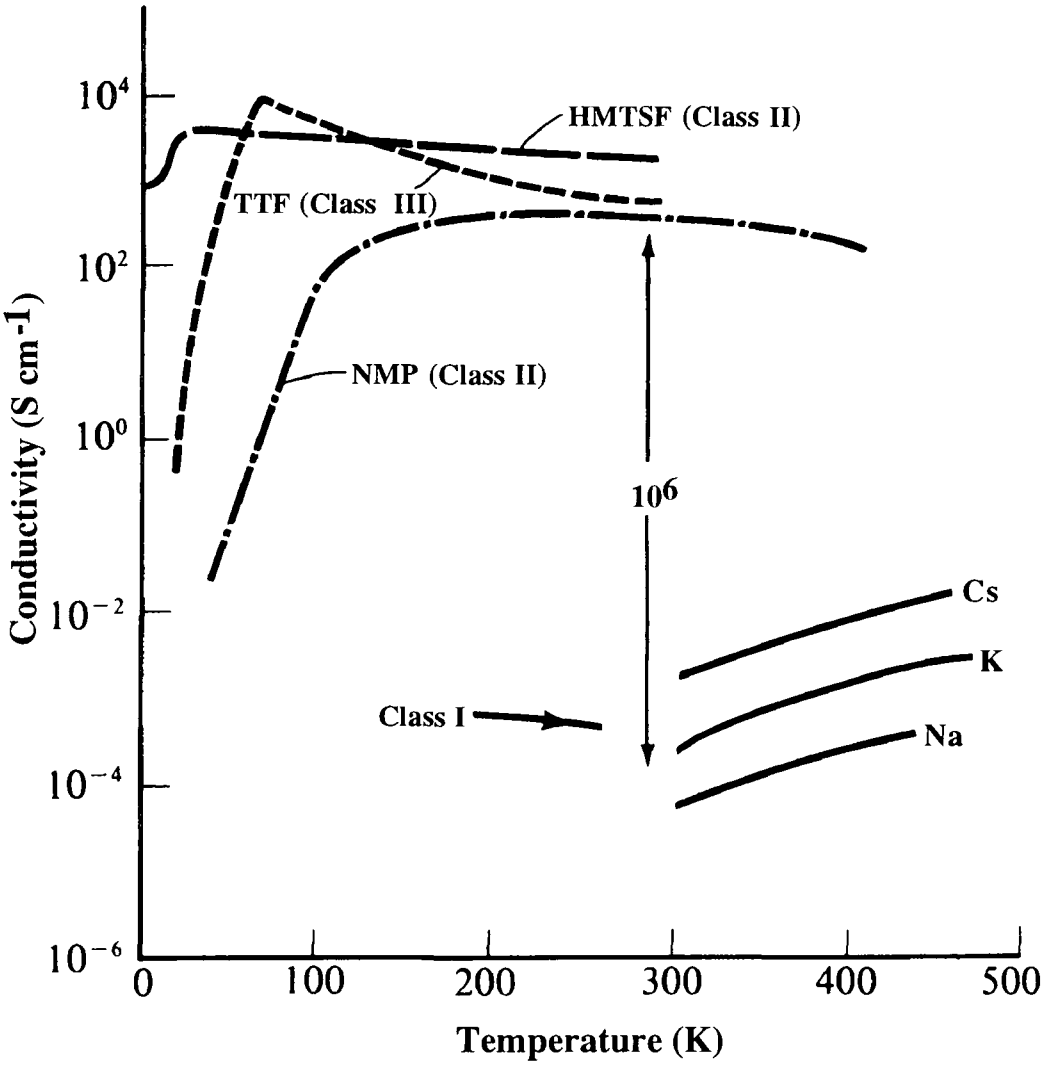

Fig. 2.13 **Single crystal dc conductivity along the stacking axis for a number of TCNQ salts illustrating the large differences in conductivity between classes I, II and III.**

After Torrance.[38]

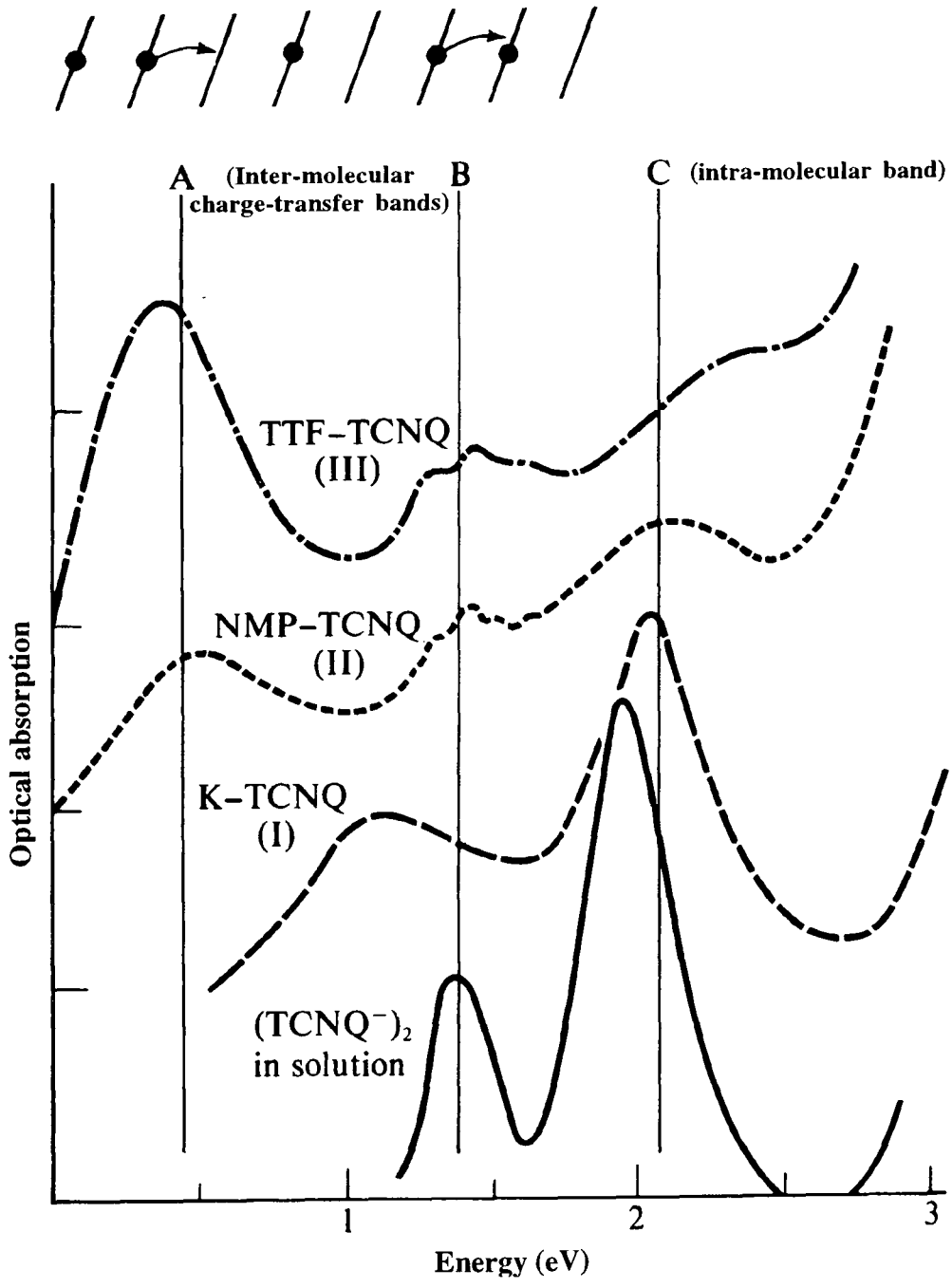

Fig. 2.14 Powder absorption spectra of several TCNQ salts from classes I, II and III. Above the bands A and B are schematic representations of the intrastack charge-transfer interactions that correspond to the observed peaks. The absorption spectrum of $(TCNQ^-)_2$ dimers in solution is also shown, which exhibits an intra-molecular band at 1.9 eV.

After Torrance.[38]

Band A is absent in simple TCNQ salts, such as K-TCNQ (Class I). These are Mott insulators, where charge is localised by the Coulomb repulsion between electrons on neighbouring sites.

2.6 Metal-dithiolate salts

Metal complexes of 1,2-dithiolene have recently emerged as π-anion molecules which form electrically conductive complexes with a variety of cations. The metal(dmit)$_2$ system is a planar molecule, the properties of which can be modified by varying the central metal ion. It crystallises in face-to-face stacks and the ten peripheral sulphur atoms can engage in intra-stack and inter-stack interactions, promoting three-dimensional electronic properties. Metals employed include Pd,Pt,Ag and Zn but compounds containing Ni have received the most attention. Salts are formed with open-shell organic cations such as TTF^+, closed shell organic cations like Me_4N^+ and inorganic cations e.g. Na^+. The salt TTF[Ni(dmit)$_2$]$_2$ behaves as an organic metal.[18] At room temperature, a conductivity of 300 S cm^{-1} is observed, increasing to ~ 10^5 S cm^{-1} at 4.2 K. In addition, under hydrostatic pressure of 7 kbar, a superconducting transition occurs at 1.62 K. In this compound, the molecules of TTF and Ni(dmit)$_2$ stack in distinct columns parallel to the b-axis. The arrangement of Ni(dmit)$_2$ molecules is illustrated in Fig 2.15(a). Alternating sheets of TTF and Ni(dmit)$_2$ are formed in the bc plane, as shown in Fig.2.15(b).

High conductivity has also been observed in salts of Ni(dmit)$_2$ with closed shell cations. The crystal structure of NMe_4[Ni(dmit)$_2$] is shown in Fig. 2.16.[21] Stacks of Ni(dmit)$_2$ molecules are separated by channels containing the cation, making this anion-stack conductor analogous to cation-stack conductor salts like TMTSF-ClO4 (cf. Fig. 2.11).

2.7 Metallophthalocyanines

A wide range of metallophthalocyanines (MPcs), dye molecules based on the molecular

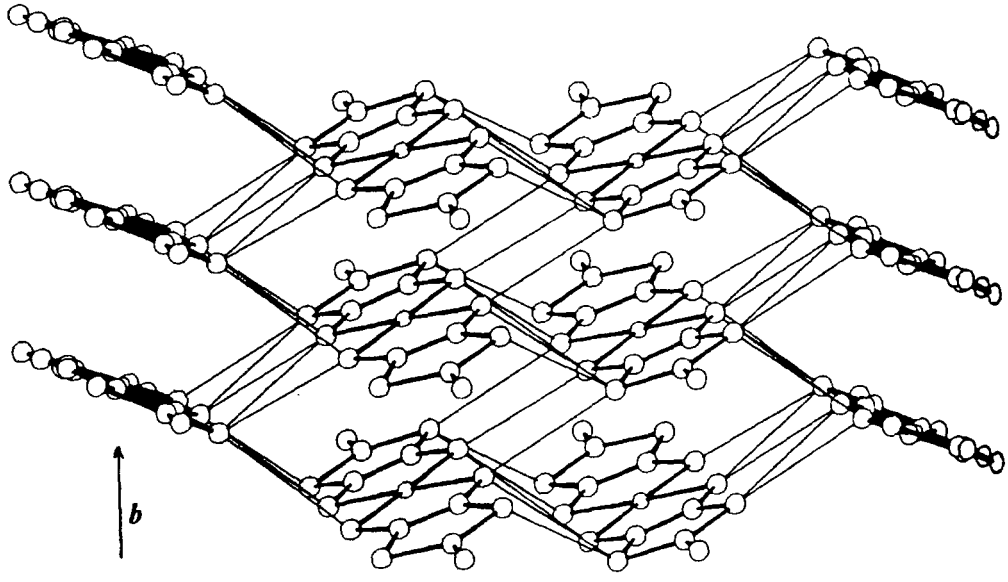

(a)

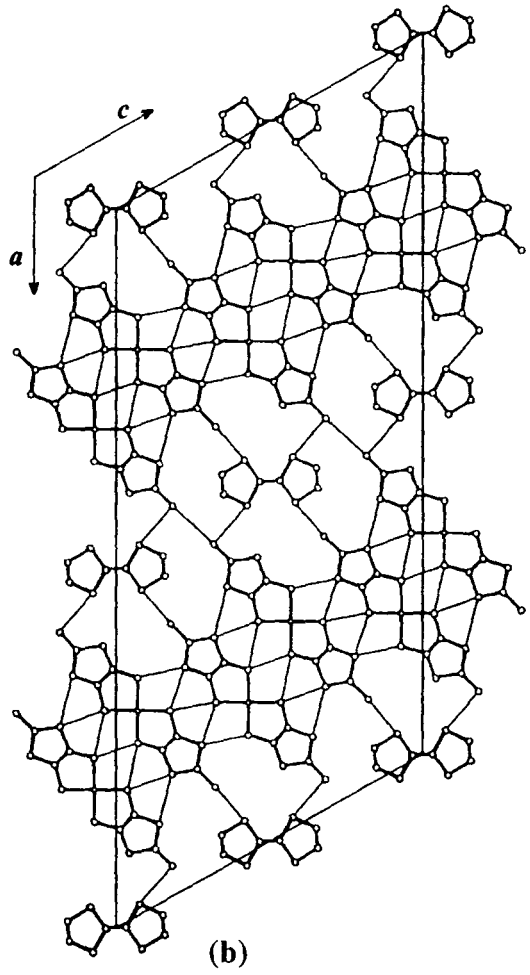

(b)

Fig. 2.15 **Structure of $TTF[Ni(dmit)_2]_2$**

(a) Stacks of $Ni(dmit)_2$ parallel to b-axis.
(b) Arrangement of TTF and $Ni(dmit)_2$ molecules in ac-plane.

After Brossard *et al.*[18]

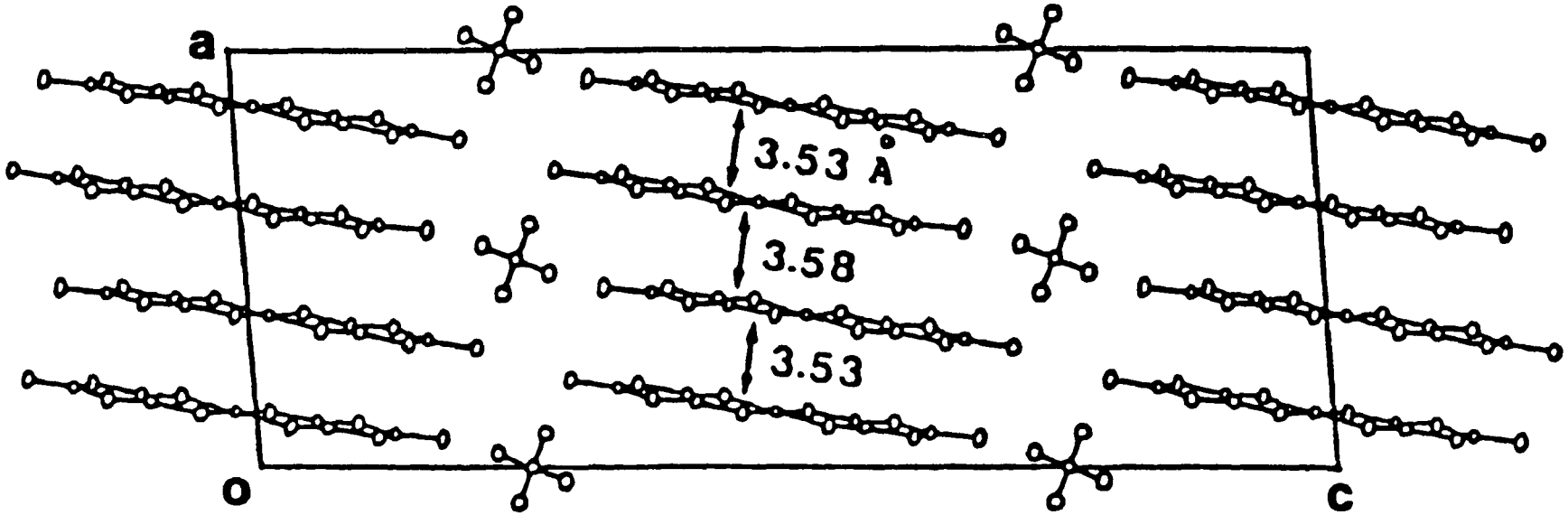

Fig. 2.16 Crystal structure of $NMe_4[Ni(dmit)_2]$ showing the molecular spacings.

After Kobayashi *et al.*[21]

structure shown in Fig 2.17, have been produced and studied. A number of special properties are exhibited by these compounds. They can be produced in exceptionally pure form since they are easily crystallised and sublimed. Remarkable chemical and thermal stability is observed and the materials are unaffected by strong acids and bases and are stable in air up to 400-500 °C. Their optical absorption spectra exhibit very intense bands at 400 nm and 700 nm due to their unsaturated π-electron system. Many elements can combine with the phthalocyanine ring and more than 70 different MPcs are known. Also, the nature of the central metal ion has a strong effect on the properties of the resulting compound. The properties of MPcs can be further varied by attaching substituents to the outside of the ring.

MPcs become conductive on oxidation, usually by a polyhalide such as I_3^- or an anion like PF_6^- or SbF_6^-. The charge carriers are associated with the conjugated π-electron system of the macrocycle. The phthalocyanine units pack in columns, with the anions in channels between the stacks. The crystal structure of $(NiPc)_2SbF_6$ is shown in Fig. 2.18.[39] This material has a room temperature conductivity of 200 S cm^{-1}, with metallic temperature dependence of conductivity observed between room temperature and 150 K. The central metal ion is not required to produce metallic properties. If the metal atom is replaced by two hydrogen atoms and the system oxidised by iodine, metallic conductivity is observed. The complex H_2PcI has room temperature conductivity of 700 S cm^{-1}, increasing to a maximum of 4000 S cm^{-1} at 15 K.

2.8 Conductive Polymers

In the past, polymers have been regarded as electrical insulators. Polyethylene, polystyrene and polytetrafluoroethylene are all excellent insulators with $\sigma < 10^{-16}$ S cm^{-1}. Polymers are mechanically strong, can easily be formed into any required shape and, recently, it has become possible to add chemical groups to the polymer backbone which will considerably increase the electrical conductivity. The addition of dopants to the

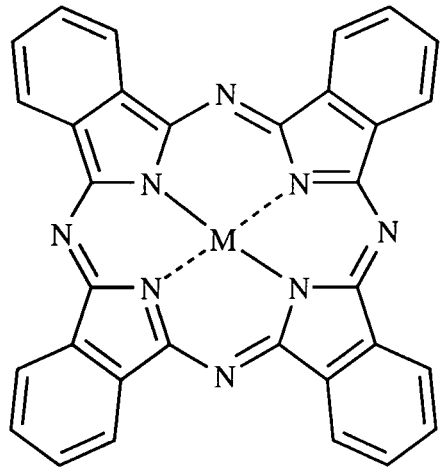

Fig. 2.17 Molecular formula of metallophthalocyanine.

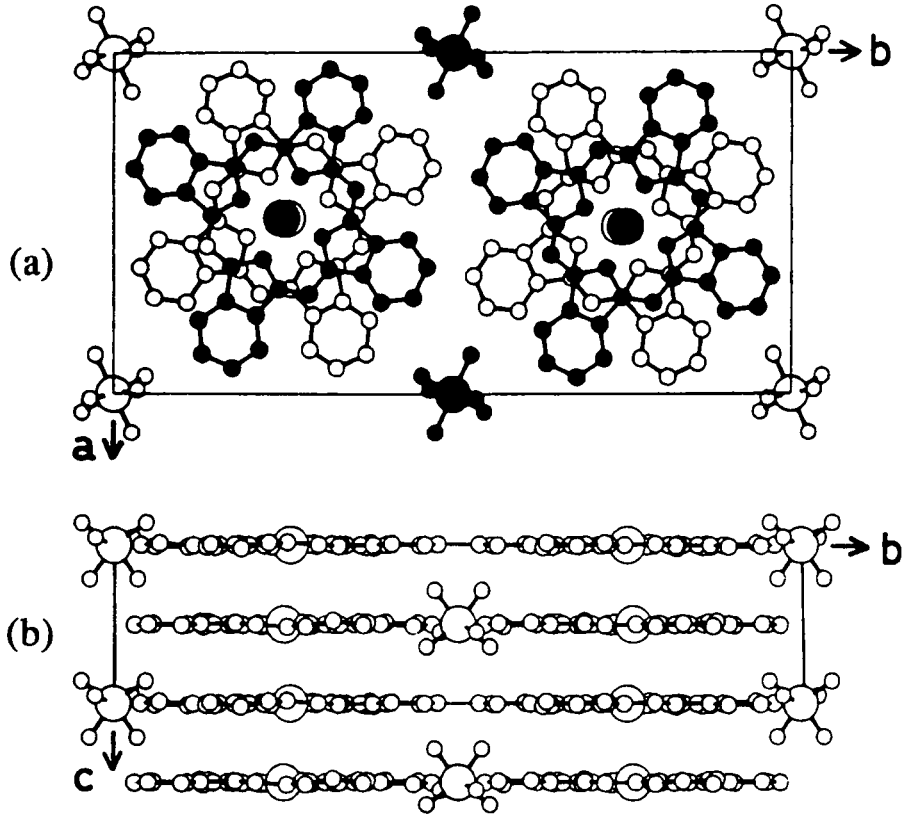

Fig. 2.18 Molecular structure of $(NiPc)_2SbF_6$

(a) looking along c-axis.
(b) looking along a-axis.

After Yakushi *et al.*[39]

polymer can increase the conductivity further. An example is trans-polyacetylene, the molecular structure of which is shown in Fig. 2.19. The electrical conductivity of this material can be varied over twelve orders of magnitude[40] from 10^{-9} S cm^{-1} to > 10^3 S cm^{-1}. It can be doped with donors such as AsF_5 and acceptors like I_2 and the n-type and p-type materials obtained will form p-n junctions. Stretching of the polymer produces an alignment of the polymer chains and results in considerable anisotropy of the electrical properties. For $[CH(AsF_5)_{0.1})]_x$, after stretching by a factor of three, the conductivity in the direction of stretching (σ_s) is > 2000 S cm^{-1} with an anisotropy of ~16. The conductivity of doped trans-polyacetylenes is comparable to that of TTF-TCNQ and metallic behaviour is also observed.

Polyaniline (PANi) is a polymer in which aromatic rings lie in the conjugation path along the backbone of the polymer. This material can exist in three oxidation states: reduced leucoemeraldine, oxidised emeraldine (Fig. 2.20) and doubly oxidised pergraniline. In all cases, the polymer is insulating but the emeraldine form has the property that upon doping with protons by exposure to a solution of pH < 3-4, the conductivity increases by up to 11 orders of magnitude and values up to 350 S cm^{-1} have been reported.[41] The emeraldine form of PANi has the added advantage that both the base and the protonated salt are soluble in N-methyl-2-pyrrolidone (NMP). This makes processing simple in that thin films can be cast or spun from a suitable solution. After removal of the solvent by baking in a vacuum oven, these films can subsequently be stretch aligned to produce films with electrical anisotropies of up to 25:1.[42]

2.9 Fullerenes

Salts of the electron acceptor molecule, buckminsterfullerene, formula C_{60} (**20**), are the most recently discovered class of organic conductors. The spherical nature of the C_{60} molecule leads to compounds having very different properties from those of systems containing flat donors and acceptors such as TTF and TCNQ. They exhibit three

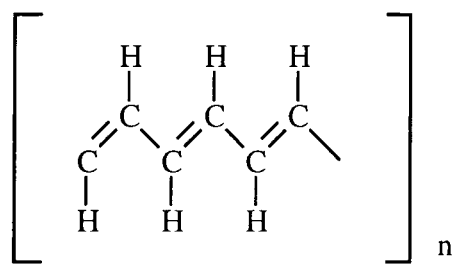

Fig 2.19 **Molecular formula of trans-polyacetylene.**

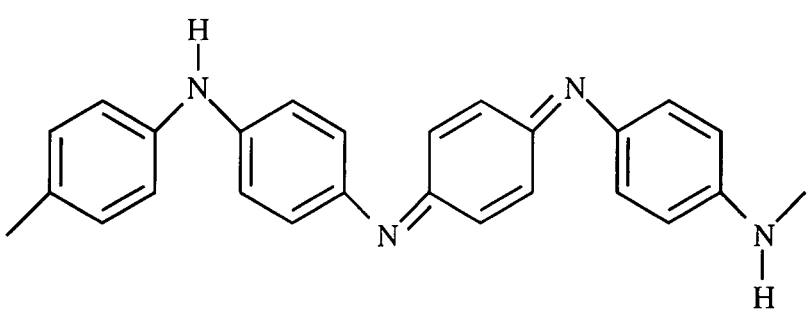

Fig 2.20 **Molecular formula of polyaniline (emeraldine base).**

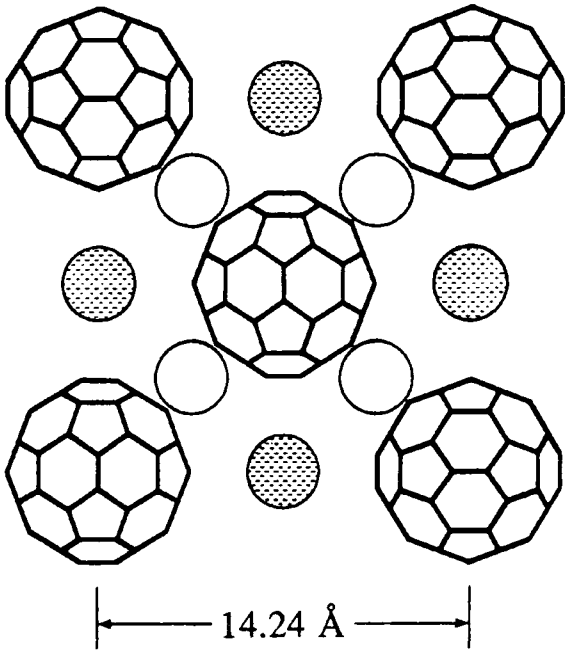

Fig 2.21 **Crystal structure of K_3C_{60}.**

After Stephens *et al.*[43]

dimensional electrical conductivity and the potassium and rubidium salts were found to be superconducting, with critical temperatures of 18K and 30K, respectively. These alkali metal fullerides crystallise in a cubic structure in which the cations fit into spaces between the C_{60}^{3-} anions. The crystal structure of K_3C_{60} is shown in Fig. 2.21.[43]

2.10 Summary

The historical review given in this chapter illustrates that in the field of organic materials, there exists a high potential for the chemical manipulation of electrical behaviour. Small variations in the molecular structure of a donor and/or acceptor can induce large changes in the behaviour of the charge transfer complex formed by them. Diverse properties have been reported, ranging from insulating and semiconducting to metallic and, in certain circumstances, superconducting behaviour.

References

1. H.N. McCoy, and W.C. Moore, J. Am. Chem. Soc., 33, (1911) 273-292.
2. H. Akamatu, H. Inokuchi and Y. Matsunaga, Nature, 173 (1954) 168-169.
3. L.R. Melby, R.J. Harder, W.R. Hertler, W. Mahler, R.E. Benson and W.E. Mochel, J. Am. Chem. Soc., 84 (1962) 3374-3387.
4. F. Wudl, G.M. Smith and E.J. Hufnagel, J. Chem. Soc., Chem. Commun., (1970) 1453-1454.
5. F. Wudl, G.M. Smith and E.J. Hufnagel, J. Am. Chem. Soc., 94 (1972) 670-672.
6. J. Ferraris, D.O. Cowan, V. Walatka and J.H. Perlstein, J. Am. Chem. Soc., 95 (1973) 948-949.
7. L.B. Coleman, J.A. Cohen, A.F. Garito and A.J. Heeger, Phys. Rev. B., 7 (1973) 2122-2128.
8. E.M. Engler and V.V. Patel, J. Am. Chem. Soc., 96 (1974) 7376-7378.
9. A.N. Bloch, D.O. Cowan, K. Bechgaard, R.E. Pyle, R.H. Banks and T.O.

Poehler., Phys. Rev. Lett., 34 (1975) 1561-1564.

10. A. Andrieux, C. Duroure, D. Jérome and K. Bechgaard, J. Physique Lett., 40 (1979) L381-L383.

11. J.B. Torrance, J.J. Mayerle, V.Y. Lee and K. Bechgaard, J. Am. Chem. Soc.,101 (1979) 4747-4748.

12. D. Jérome, A. Mazaud, M. Ribault and K. Bechgaard, J. Physique Lett., 41 (1980) L95-L98.

13. K. Bechgaard, K. Carneiro, F.B. Rasmussen and M.Olsen, J. Am. Chem. Soc., 103 (1981) 2440-2442.

14. G. Saito, T. Enoki, K. Toriumi and H. Inokuchi, Solid State Commun., 42 (1982) 557-560.

15. S.S.P. Parkin, E.M. Engler, R.R. Schumaker, R. Lagier, V.Y. Lee, J.C. Scott and R.L. Greene, Phys. Rev. Lett., 50 (1983) 270-273.

16. É.B. Yagubskii, I.F. Shchegolev, V.N. Laukhin, P.A. Kononovich, M.V. Karatsovnik, A.V. Zvarykina and L.I. Buravov, JETP Lett., 39 (1984) 12-16.

17. J.E. Schirber, L.J. Azevedo, J.F. Kwak, E.L. Venturini, P.C.W. Leung, M.A. Beno, H.H.Wang and J.M. Williams, Phys. Rev. B., 33 (1986) 1987-1989.

18. L. Brossard, M. Ribault, L. Valade and P. Cassoux, Physica B., 143 (1986) 378-380

19. A. Aumüller, P. Erk, G. Klebe, S. Hünig, J. U. von Schütz and H.-P. Werner, Angew. Chem. Int. Ed. Engl. 25 (1986) 740-741.

20. K. Kikuchi, K. Murata, Y. Honda, T. Namiki, T. Ishiguro, K. Kobayashi and I. Ikemoto. J. Phys. Soc. Jpn., 55 (1987) 3436-3439.

21. A. Kobayashi, H. Kim, Y. Sasaki, R. Kato, H. Kobayashi, S. Moriyama, Y. Nishio, K. Kajita and W. Sasaki, Chem Lett., (1987) 1819-1822.

22. M.D. Mays, R.D. McCullough, D.O. Cowan, T.O. Poehler, W.A. Bryden and T. J. Kistenmacher, Solid State Commun., 65 (1988) 1089-1092.

23. G.C. Papavassiliou, G.A. Mousdis, J.S. Zambounis, A. Terzis, A. Hountas,

B. Kilti, C.W. Mayer and J. Pfeiffer, Synth. Met., B27 (1988) 379-383.

24. H. Urayama, H. Yamochi, G. Saito, K. Nozawa, T. Sugano, M. Kinoshita, S. Sato, K. Oshima, A. Kawamoto and J. Tanaka, Chem. Lett., (1988) 55-58.

25. F. Wudl, H. Yamochi, T. Suzuki, H. Isotalo, C. Fite, H. Kasmai, K. Liou and G. Srdanov, J. Am. Chem. Soc., 112 (1990) 2461-2462.

26. M.A. Beno, H.H. Wang, A.M. Kini, K.D. Carlson, U. Geiser, W.K. Kwok, J.E. Thompson, J.M. Williams, J. Ren and M.-H. Whangbo, Inorg. Chem., 29 (1990) 1601-1602.

27. A.M. Kini, U. Geiser, H.H. Wang, K.D. Carlson, J.M. Williams, W.K. Kwok, K.G. Vandervoort, J.E. Thompson, D.L. Stupka, D Jung, M.-H. Whangbo, Inorg. Chem., 29 (1990) 2555-2557.

28. J.M. Williams, A.M. Kini, H.H. Wang, K.D. Carlson, U. Geiser, L.K. Montgomery, G.J. Pyrka, D.M. Watkins, J.M. Kommers, S.J. Boryschuk, A.V. Strieby Crouch, W.K. Kwok, J.E. Schirber, D.L. Overmyer, D. Jung, M.-H. Whangbo, Inorg. Chem., 29 (1990) 3274-3282.

29. A.W. Hanson, Acta. Crystallogr., 16 (1963) 1147-1151.

30. H. Kokoda, K. Hasegawa and w.G. Schneider, Can. J. Chem., 42 (1964) 1084-1087.

31. A.W. Hanson, Acta Crystallogr., 19 (1965) 610-613.

32. R. Comes, in *Chemistry and Physics of One-Dimensional Metals* (Ed. H.J. Keller), Plenum Press, New York (1977).

33. A.W. Hanson, Acta Crystallogr., B24 (1968) 768-778.

34. A.S Bailey and C.K Prout, J. Chem. Soc., (1965) 4867-4881.

35. J.L. DeBoer and A. Vos, Acta. Crystallogr., B28 (1972) 835-839.

36. J.S. Miller and A.J. Epstein, Ann. N.Y. Acad. Sci., 313 (1978).

37. A.J. Epstein and J.S. Miller, Solid State Commun., 27 (1978) 325-329.

38. J.B. Torrance, Accts. Chem. Res., 12 (1979) 79-86.

39. K Yakushi, M. Sakuda I. Hamada, H. Kuroda, A. Kawamoto, J. Tanaka, T.

Sugano and M. Kinoshita, Synth. Metals, 19 (1987) 769-774.

40. C.R. Fincher, M. Ozaki, A.J. Heeger and A.G. MacDiarmid, Phys. Rev. B, 19 (1979) 4140-4148.

41. A.P Monkman and P. Adams,Synth Met., 40 (1991) 87-96.

42. A.P. Monkman and P. Adams, Solid State Commun., 78 (1991) 29-31.

43. P.W. Stephens, L. Mihaly P.L. Lee, R.L. Whetten, S-M. Huang, R. Kaner, F. Deiderich and K. Holczer , Nature, 351 (1991) 632-634.

Chapter 3

Organic Thin Films

3.1 Introduction

In this chapter, three methods used for the formation of thin organic films on solid substrates, LB deposition, thermal evaporation and spinning, are discussed. Emphasis is placed on LB deposition since this is the technique used to prepare the films in this work. The background to conductive LB films is also considered, including details of anion radical salts, cation radical salts, donor-acceptor charge-transfer complexes and organometallic systems.

3.2 Thin film deposition techniques

3.2.1 Langmuir-Blodgett film deposition

LB films are prepared by first dissolving a suitable organic material in a solvent and spreading the resulting solution onto the surface of a liquid, usually high purity water, known as the subphase. Suitable materials are normally amphiphilic, having a 'water-loving', or hydrophilic, part and a 'water-hating', or hydrophobic, part. The solution spreads over the surface of the subphase and after evaporation of the spreading solvent the organic molecules remain as a monolayer floating on the subphase with the hydrophilic parts immersed in the water and the hydrophobic parts remaining outside. A schematic representation can be seen in Fig. 3.1(a). This monolayer is enclosed by a barrier system capable of varying the area available to it. If this area is now reduced, the film is compressed and, as a consequence, passes through various phases analogous to a two-dimensional 'gas', 'liquid' and 'solid'. These phases can be observed by measuring the surface pressure of the monolayer, which is equal to the reduction of the pure liquid surface tension due to the presence of the film. A plot of surface pressure versus area per molecule at constant temperature is known as an isotherm; its shape depends upon the

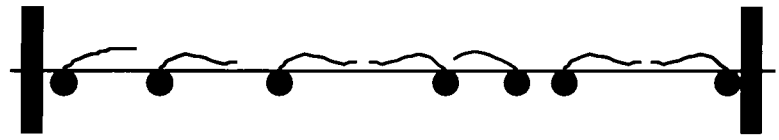

(a)

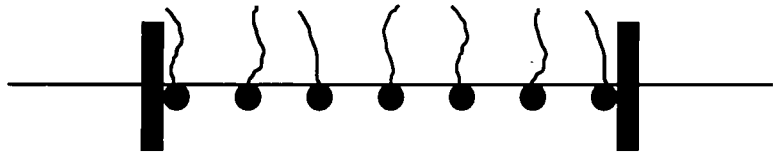

(b)

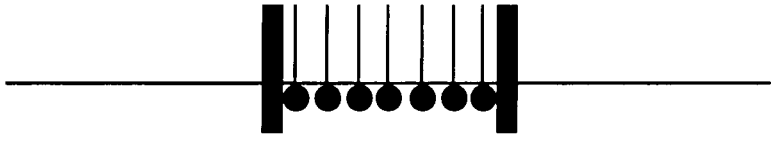

(c)

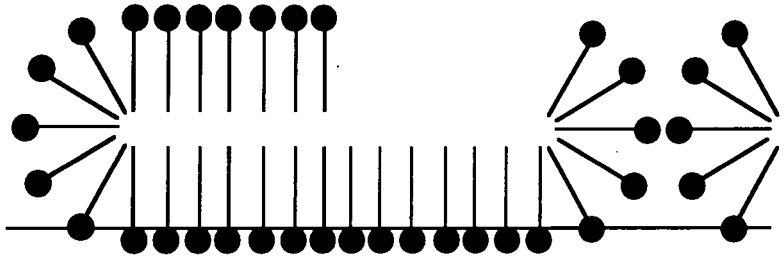

(d)

Fig. 3.1 **Schematic representation of a fatty acid monolayer on the surface of a water subphase.**

(a) Uncompressed
(b) Expanded
(c) Condensed
(d) Collapse

nature of the material spread. One of the simplest monolayer forming materials, the space-filling molecular formula of which is shown in Fig. 3.2, is octadecanoic acid (stearic acid). A typical surface pressure/area isotherm for this classic monolayer system on an acidified water subphase is shown in Fig. 3.3. Octadecanoic acid has a hydrophilic head group (COOH), which easily dissolves in water, and a long hydrophobic alkyl chain ($C_{17}H_{35}$). Observation of the isotherm reveals a number of different regions indicating the degree of order of the molecules on the surface of the subphase. The first region, labelled A, corresponds to the 'gaseous' phase where the distance between molecules is large (Fig. 3.1(a)). As the subphase area is reduced, the hydrophobic chains are lifted away from the surface of the water and as the monolayer becomes more ordered. The surface pressure rises (Fig. 3.3, regions B and C) and the molecules form close-packed solid-like phases. In region B, the hydrocarbon tails are tilted with respect to the subphase normal, whereas in region C, they are oriented perpendicular to the surface of the water (Fig. 3.1(c)). For fatty acids with shorter chain lengths, intermediate phases between the gaseous and solid regions may be observed. Here, the area per molecule is less than that expected for a gaseous monolayer, but still larger than the cross sectional area of the molecule. These are expanded, liquid-like phases, represented schematically in Fig. 3.1(b). If the monolayer in close-packed form continues to be compressed, collapse occurs and disordered multilayers form. This process is represented in Fig. 3.1(d) and corresponds to region D in Fig. 3.3.

When the film is in a close-packed solid form, monolayers may be transferred to a suitable substrate. In the most common deposition method, known as vertical dipping,[1] a substrate is coated by moving it up and down through the monolayer/air interface. As material is removed from the subphase surface an electrical signal derived from a surface pressure sensor is used to control the area available to the monolayer and maintain a constant surface pressure. The multilayer film obtained depends on the monolayer material used. In the most common mode of deposition, known as Y-type dipping, a

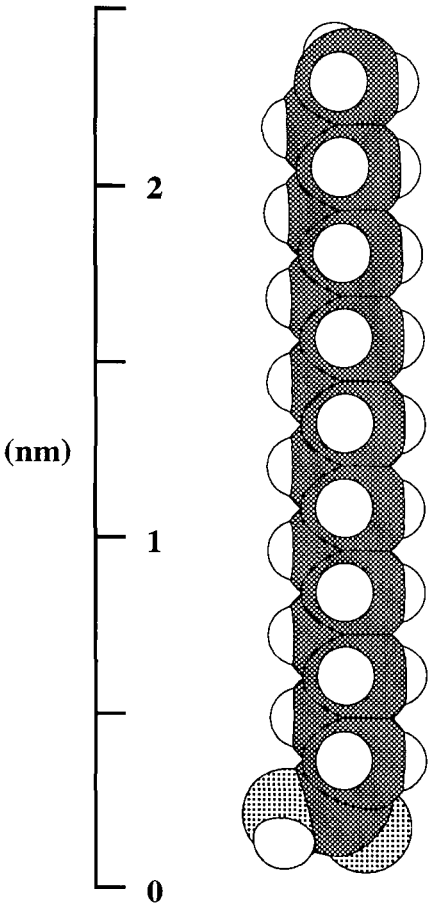

Fig. 3.2 Space filling molecular formula of octadecanoic acid.

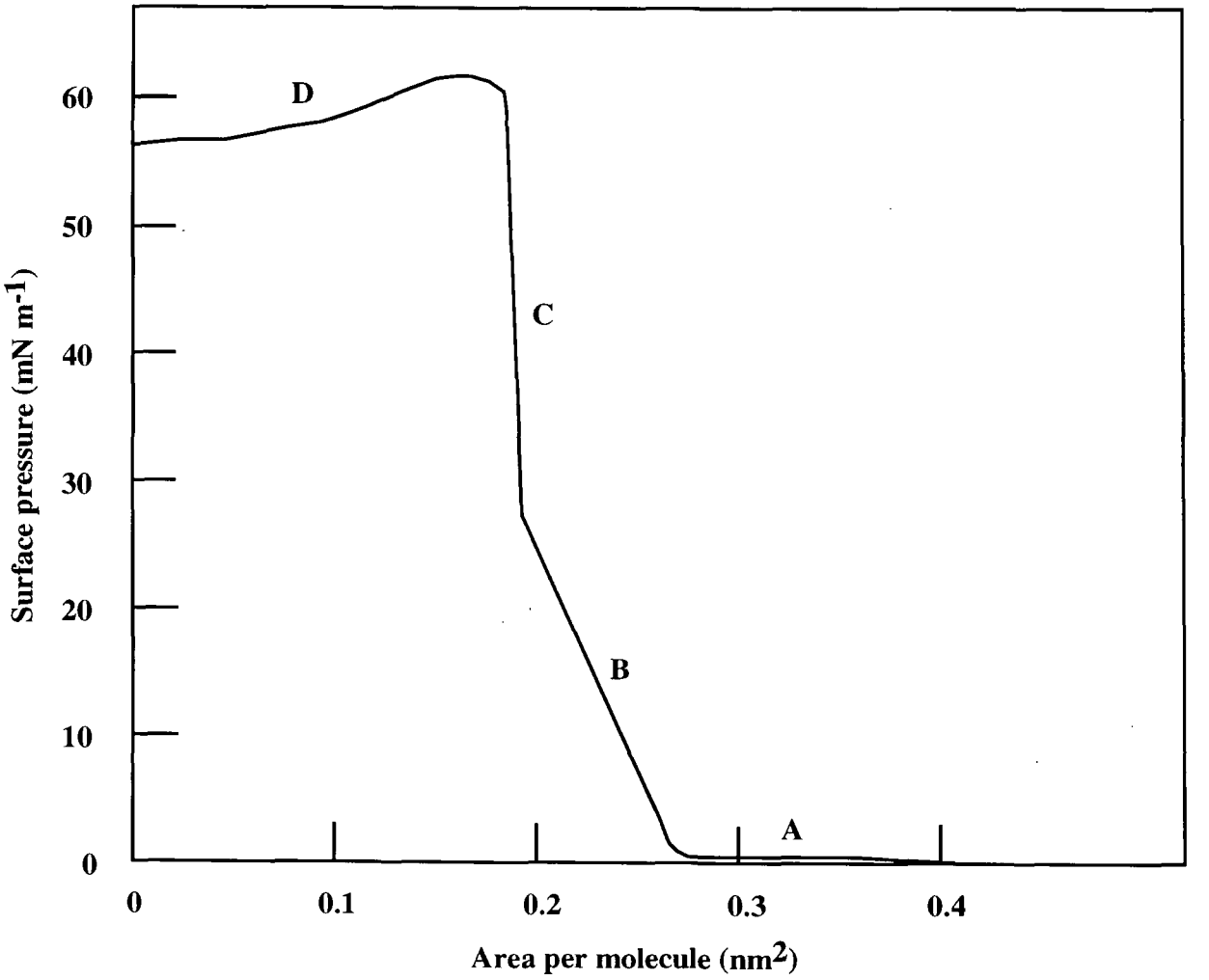

Fig. 3.3 Surface pressure/area isotherm of octadecanoic acid on an acidified water subphase.

layer is transferred during each traversal of the interface and these layers arrange in a head-to-head and tail-to-tail pattern. Two other dipping types are observed, known as X-type and Z-type. In the former, layers are deposited only as the substrate enters the subphase through the air/monolayer interface. No material is transferred during the upstroke. In the case of Z-type dipping, this situation is reversed and monolayers are only deposited as the substrate leaves the subphase. The expected arrangements of molecules obtained from the three types of deposition mode are illustrated schematically in Fig. 3.4. It should be noted, however, that it is possible for molecular reorganisation to occur on the substrate either during or after deposition. The surface of the substrate also has a bearing on the transfer of monolayers from the subphase. If the substrate is hydrophilic, the first layer tends to be transferred during the first upstroke, as the substrate emerges from the subphase. If, on the other hand the substrate is hydrophobic in nature, the first layer will be deposited on the first downstroke, as the substrate enters the subphase.

Using specialised deposition equipment, films may be prepared which consist of layers of different component molecules. For example, alternate-layer structures can be produced by dipping a substrate into the subphase through a monolayer of one material (monolayer A) and withdrawing it through a monolayer of a second substance (monolayer B). In this fashion, a multilayer structure of the form ABABAB can be built up, as illustrated in Fig 3.5. It is also possible to deposit complex monolayers in which the two components are spread as a mixture onto the surface of the subphase. In some cases, to improve the film transfer properties, a fatty acid is combined with a material which would normally be impossible to deposit reliably on its own. The components in complex monolayers may be completely miscible, as illustrated in Fig. 3.6(a) or immiscible, in which case the different molecules will aggregate (Fig. 3.6(b)).

There are two other techniques used for the deposition of multilayer organic films. The first was proposed by Langmuir and Schaefer[2], and is known as horizontal touching. In

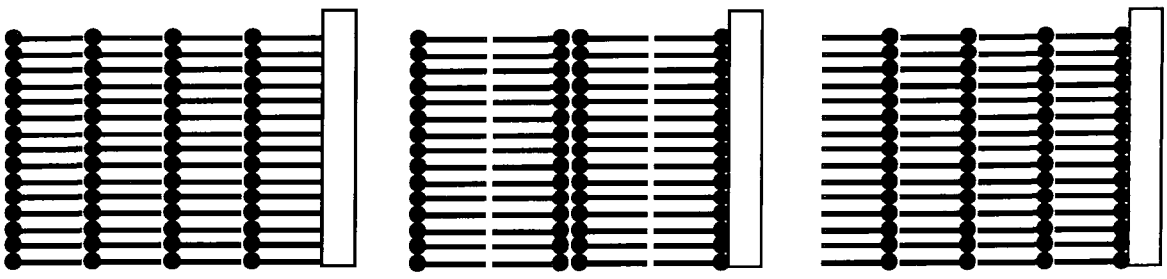

(a) (b) (c)

Fig 3.4 Schematic representation of the structures of multilayers deposited by the three different types of dipping.

(a) X-type.
(b) Y-type.
(c) Z-type.

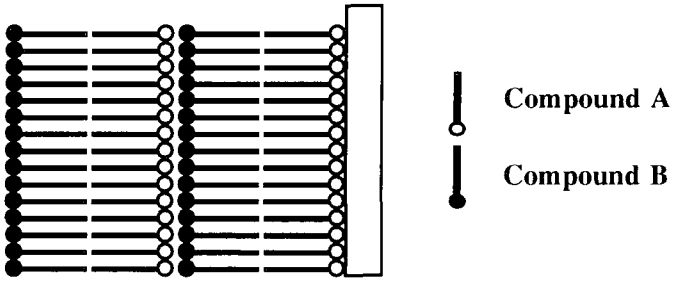

Fig. 3.5 Schematic illustration of an alternate-layer LB structure built up from compounds A and B.

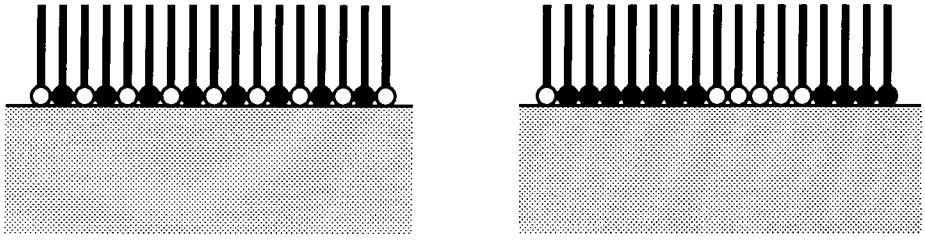

(a) (b)

Fig 3.6 Schematic diagram showing the two possible arrangements of molecules in a two-component monolayer.

(a) Miscible components.
(b) Immiscible components.

this method, the face of the solid substrate is held almost parallel to the surface of the subphase and then touched on to the monolayer which is held under constant surface pressure. If the substrate is now raised from the subphase surface, a second layer will be transferred giving a Y-type film.[3] X-type deposition can be achieved by removing the monolayer from the surface of the subphase (using a suitable barrier arrangement and/or an aspirator) before the substrate is raised to prevent the transfer of a second layer. In the second method, known as horizontal lifting, the first layer is deposited by lowering a substrate through a monolayer into the subphase. If Y-type transfer is required, the second layer is deposited by lifting the substrate back up through the interface. X- type deposition can be achieved by removing the monolayer before the substrate is raised so that no second layer is transferred. Alternate-layer films can be deposited by sequentially lowering the substrate through independent monolayers of different materials.[4]

3.2.2 Thermal evaporation

Thermal evaporation is a commonly used technique for the preparation of thin films of organic as well as inorganic materials. The process is carried out in a vacuum system. The use of low pressure serves to lower the evaporation temperature as well as reducing the amount of oxides and other impurities in the deposited film. In addition, under vacuum, straight line propagation of the evaporant is favoured, making it possible to reproduce finely defined patterns by the introduction of a shadow mask between the source and substrate. For best results, the vacuum chamber should be held at a pressure below 10^{-4} mbar for the duration of the process, with an ideal pressure for normal working of around 10^{-5} mbar. A variety of materials are suitable for use as substrates and the properties of the deposited film can be adjusted by heating or cooling the substrate. Deposition rates are variable over a wide range by control of the source temperature. An average value is 1 nm s^{-1}, but rates as high as 10^3 nm s^{-1} can be achieved. Deposition rate and overall film thickness can be monitored during the evaporation experiment by measuring the shift in the oscillation frequency of a quartz crystal which is also located in

the vacuum chamber and exposed to the evaporation source. Compound films can be produced by the co-evaporation of two or more components from separate sources. There are two common types of evaporation source: (a) wire filaments or metal foil boats which are directly heated by the passage of an electric current; and (b) non-metallic crucibles (oxides, nitrides etc) where heat can be supplied by a separate resistive heater or an RF coil wound around the crucible. Alternatively, the evaporant can be directly heated with a focused beam of electrons.

3.2.3 Spinning

Spinning is a quick and simple method for the production of uniform thin films which is widely used in the microelectronics industry for the production of photoresist layers. The technique involves the dissolution of the film material in a suitable solvent and deposition of a small amount of this solution onto the centre of the substrate to be coated. The latter is attached to the spindle of a motor using a vacuum chuck and then rapidly rotated at several thousand revolutions per minute for 10-60 seconds. During this spinning, the solution is spread over the surface of the substrate and excess material and solvent are thrown off at the edges. The resulting film, the thickness of which is determined by the viscosity of the solution and the speed and duration of spinning, is uniform to several nanometers.

3.3 Conductive LB films

There are four characteristic approaches used for the preparation of conducting LB film multilayer structures:

(i) Insulating films, prepared from organic donors or acceptors, suitably adapted for LB deposition, are chemically doped by exposure to a halogen vapour to achieve high conductivity.

(ii) Insulating films deposited onto a suitable conducting substrate are electrochemically doped to increase the electrical conductivity.

(iii) Intrinsically conducting films are prepared using mixtures of donors and acceptors, one of which has been suitably adapted for LB deposition.

(iv) Conducting films are deposited by alternating layers of amphiphilic donors and acceptors, both of which have been suitably adapted for LB transfer.

Before these methods are reviewed, it is important to note that there are two different methods used in the literature to calculate the in-plane dc conductivity of multilayer LB films from the measured current-voltage characteristics. In the first technique, used by Barraud *et al*[5], the value used for the thickness of the film neglects the hydrocarbon chain part of the molecule. This can result in a calculated conductivity up to an order of magnitude higher than the second method, employed by Nakamura and co-workers[6], in which the entire length of the charge-transfer system and hydrocarbon chain is used. This review will concentrate on the results of in-plane, dc conductivity studies, although it is possible to measure the conductivity perpendicular to the plane of the film.

3.3.1 Anion radical salts

The organic acceptor salts used most widely in LB studies are shown in Fig. 3.7. The first conductive LB films were produced by French workers[5] who prepared multilayer structures of the 1:1 stoichiometry anion-radical salt *N*-docosylpyridinium-TCNQ(**1**). In the as-deposited state, where there was full charge transfer between the pyridinium cation and TCNQ acceptor, these films were insulating. After iodine oxidation, a marked increase in conductivity was observed. A room temperature in-plane value of 0.1 S cm^{-1} was measured with semiconducting behaviour having a thermal activation energy of 0.15 eV. This increase in conductivity was not solely due to the formation of a mixed valence system however. Structural investigations by Richard *et al* [7] revealed that in the precursor

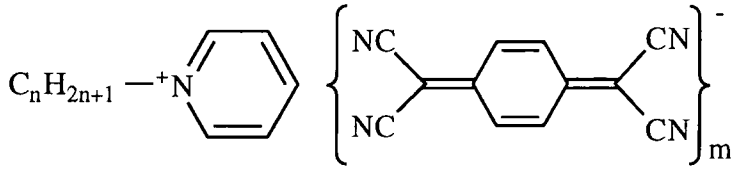

(**1**) n=22 m=1

(**2**) n=22 m=2

(**3**) n=18 m=1

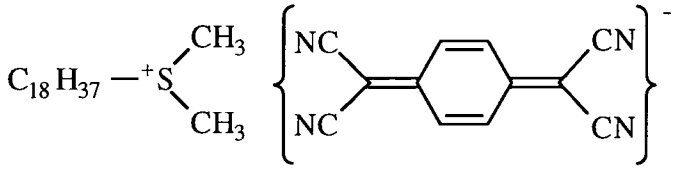

(**4**)

Fig. 3.7 Some organic acceptor complexes used in LB studies.

films, the TCNQ was present in sheets of dimers with the planes of the molecules almost parallel to the plane of the substrate. After careful oxidation of the films with iodine vapour diluted in a turbulent flow of dry nitrogen, it was discovered that the TCNQ molecules had re-orientated so that they now stood on edge with their molecular planes almost perpendicular to the substrate and their long axes roughly parallel to the substrate normal. This orientation would enhance the overlap between the molecular orbitals, favouring in-plane carrier transport and increased conductivity. Nakamura and co-workers, also working on the *N*-docosylpyridinium-TCNQ system,[6] found that although the films in the as-deposited state were not highly conducting, the deposition temperature would influence the orientation of the molecules on the substrate and hence the conductivity of the film. Multilayers deposited at 17°C were found to be more highly ordered than those produced at 3-5°C. Consequently, the structures transferred at high temperature were more conductive ($3x10^{-5}$ S cm^{-1}) than those deposited at low temperature ($7x10^{-7}$ S cm^{-1}). Matsumoto *et al*[8] prepared films having high electrical conductivity without the need for iodine doping by varying the ratio of the constituents. These workers discovered that films of the 1:2 stoichiometry salt *N*-docosylpyridinium-$(TCNQ)_2$(**2**) had a conductivity of 0.01 S cm^{-1} (calculated using the full molecular length) without any post-deposition treatment, the same as that of the 1:1 salt with iodine doping. The material was a semiconductor, with an activation energy of 0.3 eV. The conductivity of films of **2** were stable for at least two months when the samples were stored in air at room temperature. Dhindsa *et al* produced films of the 1:1 complex *N*-octadecylpyridinium-TCNQ[9](**3**) which were found to be conductive, with a room temperature conductivity of 0.02 S cm^{-1}, without the need for any post deposition oxidation. Unintentional doping by an anion such as OH^- during the deposition process was suggested as a reason for this high conductivity, which was found to depend exponentially on temperature. A thermal activation energy of 0.13 eV was measured (Fig. 3.8), a value similar to that of a doped inorganic semiconductor. The results of structural analysis suggested an interdigitated multilayer assembly with the long axes of

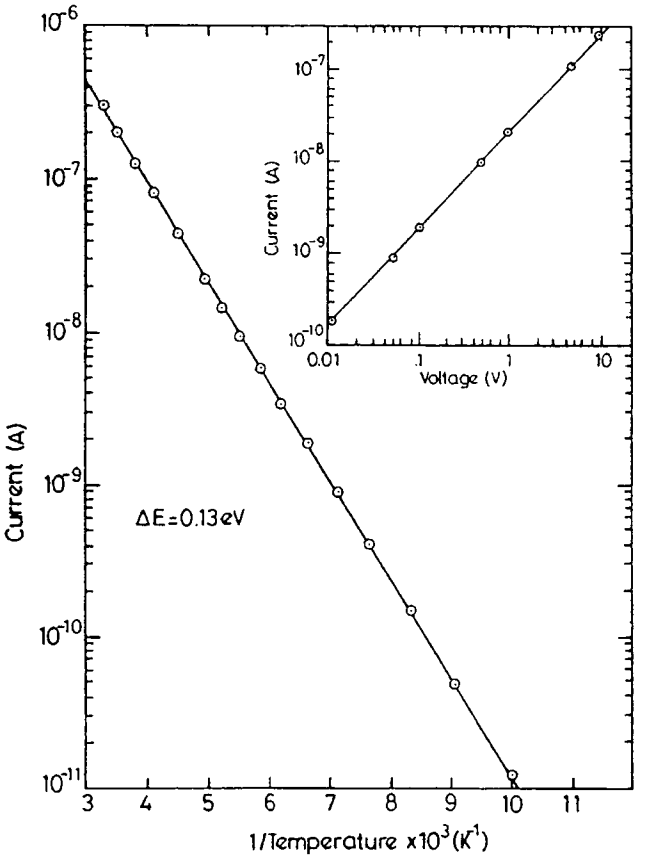

Fig. 3.8 **Semi-logarithmic plot of current (bias voltage 10V) versus reciprocal temperature for a 9-layer N-octadecylpyridinium-TCNQ LB film. The Ohmic current versus voltage characteristic at room temperature is shown inset.**

After Dhindsa *et al.*[9]

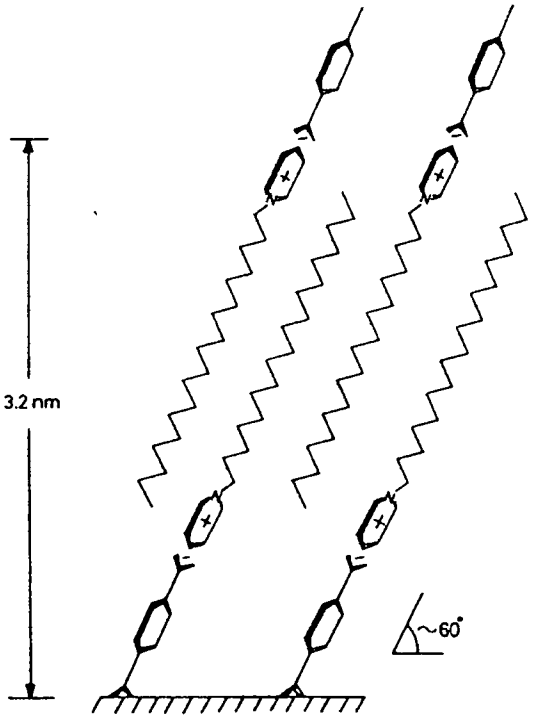

Fig. 3.9 **Proposed orientation of the molecules in an LB film of *N*-octadecylpyridinium-TCNQ.**

After Dhindsa *et al.*[11]

the molecules tilted at an angle of ~30° to the substrate normal (Fig 3.9).[10] Barraud *et al* have deposited multilayer structures of dimethyloctadecylsulphonium-TCNQ(**4**) which became conducting after iodine doping.[11] The electrical properties of LB films of the amphiphilic anion radical salts described above are summarised in Table 3.1.

Material	In-plane dc room temperature conductivity as-deposited ($S\ cm^{-1}$)	Activation energy as-deposited (eV)	In-plane dc room temperature conductivity after iodine doping ($S\ cm^{-1}$)	Activation energy after iodine doping (eV)	Reference
1	10^{-5}-10^{-7}		10^{-1}	0.15	5,7
2	10^{-2}	0.3			8
3	$2x10^{-2}$	0.13			9,10

Table 3.1. Summary of the electrical properties of LB films of anion radical salts. The numbers in the first column correspond to the labels in Fig. 3.7.

3.3.2 Cation radical salts

The various amphiphilic organic donor molecules that have been used in LB studies are shown in Fig. 3.10. LB films of these materials are usually formed from the neutral donor molecule and the transferred film is subsequently oxidised to produce a salt. This procedure yields high quality, regular films. The first compound to be studied was hexadecanoyl-TTF(**5**).[12] As-deposited, thin films of this material were found to be insulating, since no charge-transfer state existed. The films were oxidised using iodine or bromine vapour. On treatment with iodine vapour, by exposure to crystals of iodine in a sealed container, the system was oxidised to a full charge-transfer condition and as such remained insulating. After several hours in air, however, the release of excess iodine

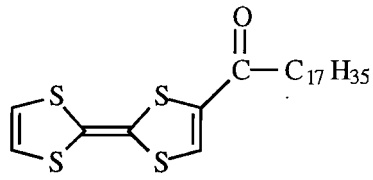

(5)

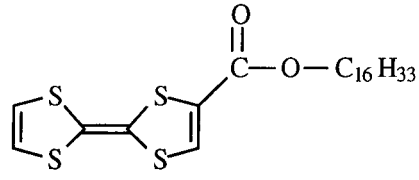

(6)

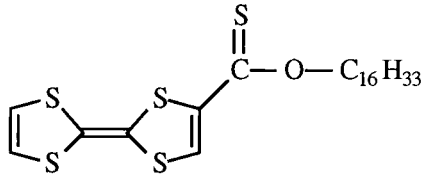

(7)

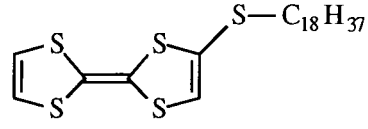

(8)

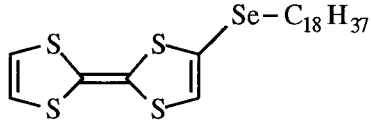

(9)

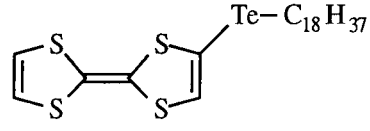

(10)

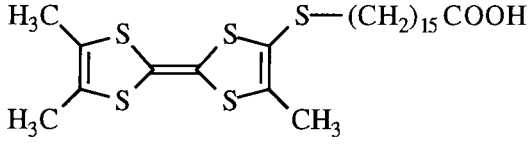

(11)

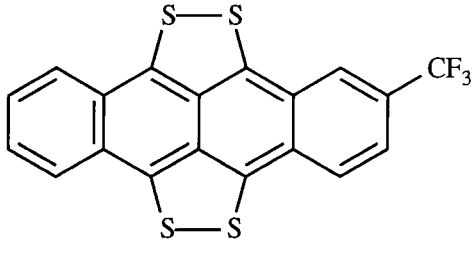

(12)

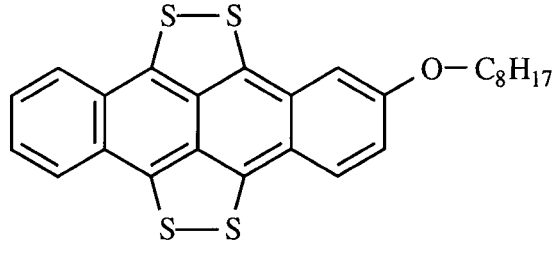

(13)

Fig. 3.10 Some organic donor molecules used in LB studies.

resulted in the formation of a conducting, mixed-valence state. Semiconducting behaviour was observed, with a room temperature conductivity of $1x10^{-2}$ S cm^{-1} and a thermal activation energy of 0.19 eV. This conductivity did not change when the samples were stored in air for two days. In contrast, films exposed to bromine vapour became insulating and even after removal from the vapour there was no increase in conductivity with time. The UV-visible-near IR absorption spectra of films of this material have been investigated.[13] Fig. 3.11 compares the spectra of three films: (a) 40 layers as-deposited (insulating); (b) 40 layers 20 hours after iodine-doping (conducting state); (c) 50 layers after bromine doping (insulating). The spectrum for the as-deposited film exhibits bands at *ca* 280 and 490 nm due to local excitations of the TTF molecule. After iodine doping, a charge-transfer band appears at 2100 nm. This band is absent in the case of the bromine doped film. Spectra have been recorded at various times after doping with iodine (Fig 3.12). Immediately after doping, an absorption appeared at 870 nm. This band has been attributed to the full charge-transfer state in TTF salts. As excess iodine left the film, the band at 870 nm reduced in intensity and was replaced by the absorption at 2100 nm. This band is characteristic of an organic conductor and is due to the charge-transfer transition resulting from the formation of a mixed-valence system. The intensity of this band reached a maximum several hours after doping, at a time corresponding to the maximum lateral dc conductivity in the layers. In the spectrum of the film doped with bromine, this charge-transfer band was absent. It was inferred that the bromine salt of HDTTF was more stable than that with iodine and no mixed-valence state developed. Consequently, the bromine doped films remained insulating. Low angle X-ray diffraction studies have been used to determine the arrangement of the molecules in these films. Before doping, the samples were found to consist of two phases. The dominant one (~90%) possesses a d-spacing of 6.1 nm. This corresponds to approximately twice the length of the hexadecanoyl-TTF molecule and is consistent with a head-to-head and tail-to-tail structure (Fig. 3.13(a)). The second phase present (~10%) had a smaller d-spacing of 4.1 nm, suggesting tilting and/or interdigitation of the molecules. After chemical doping, a single

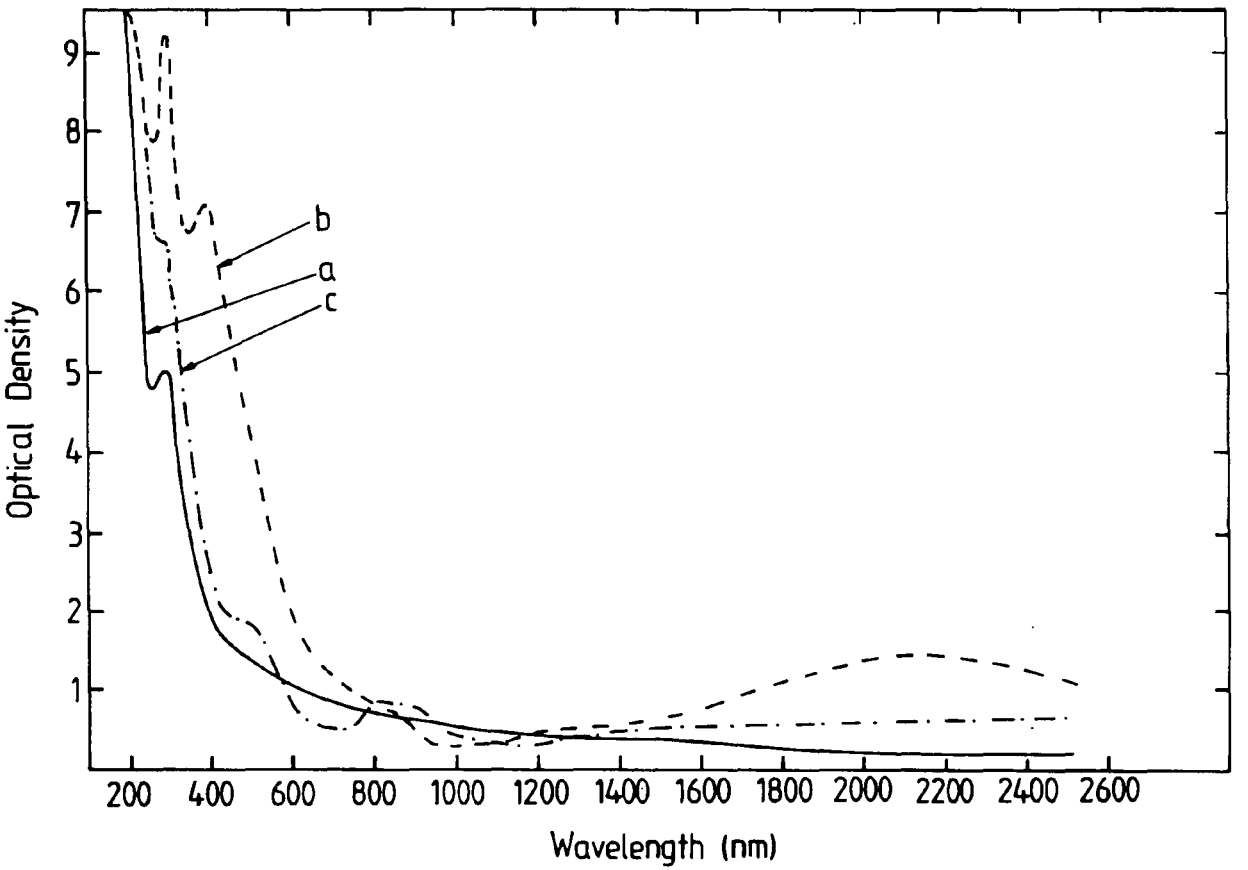

Fig. 3.11 **Optical absorption spectra for LB films of hexadecanoyl TTF.**

(a) **40-layer sample, as-deposited.**
(b) **40-layer sample, 20 hours after doping with iodine vapour.**
(c) **50-layer sample, 48 hours after doping with bromine vapour.**

After Dhindsa *et al.*[13]

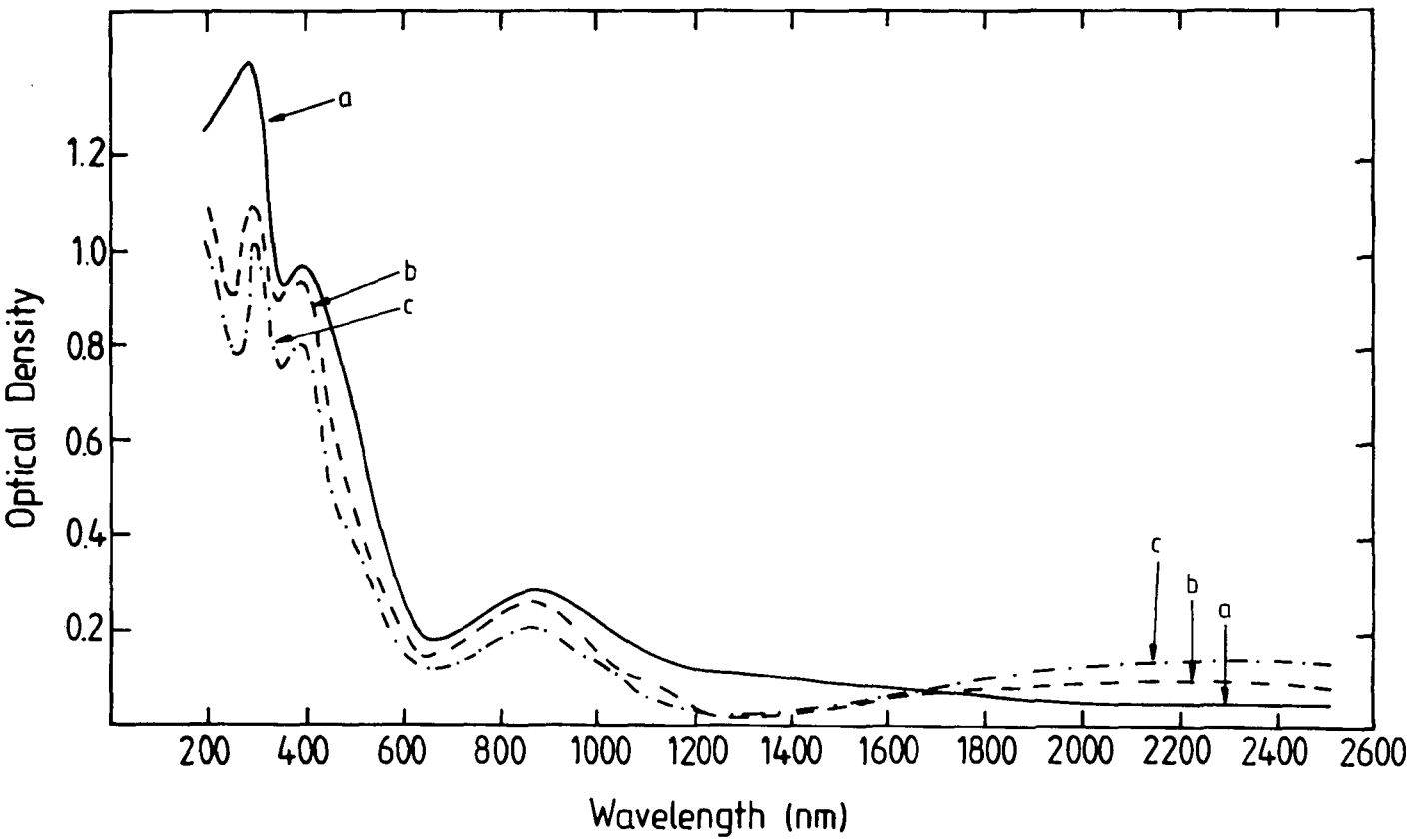

Fig. 3.12 **Optical absorption spectra for a 40-layer LB film of hexadecanoyl-TTF recorded at different times after doping with iodine.**

(a) 5 minutes after doping.
(b) 1 hour after doping.
(c) 2 hours after doping.

After Dhindsa *et al.*[13]

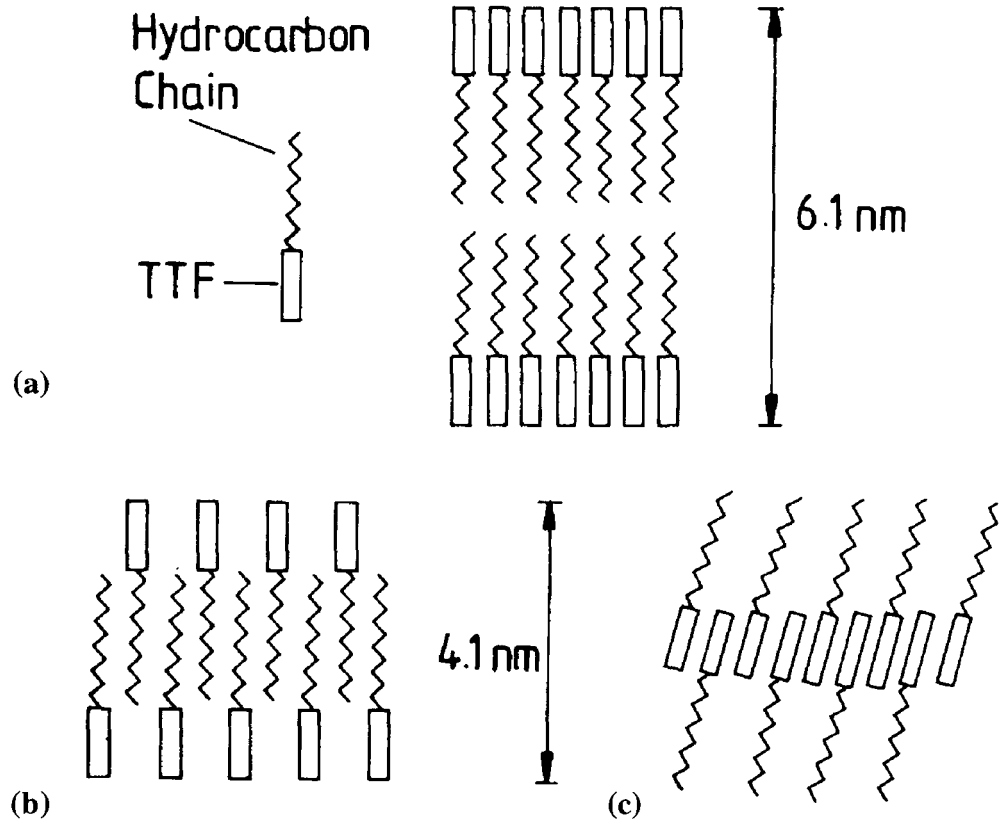

Fig. 3.13 **Schematic representation of the proposed arrangement of molecules in an LB multilayer of hexadecanoyl-TTF.**

(a) as-deposited.
(b) and (c) two alternative models for layers after iodine doping.

After Dhindsa *et al.*[13]

phase structure was observed with a d-spacing of ~4.1 nm. Again, this result implies tilting of the molecules or interdigitation of either the TTF head groups or the hydrocarbon chains. Two possible packing arrangements are illustrated schematically in Fig 3.13(b) and (c). Similar room temperature conductivity values were measured for multilayer films of the ester-derivative of TTF[14](**6**). After iodine doping, a room temperature conductivity of 10^{-2} S cm^{-1} was measured, with a thermal activation energy of 0.17 eV. LB multilayers of *O*-hexadecylthiocarboxy-TTF[15](**7**) were found to exhibit a similar structure and chemical doping characteristics to those of hexadecanoyl-TTF but had in-plane room temperature conductivity values two orders of magnitude higher after iodine doping. A maximum conductivity of 1.0 ± 0.2 S cm^{-1} was observed with a thermal activation energy of 0.09 eV. This conductivity was stable in air for several weeks. It was speculated that intermolecular S...S interactions might be responsible for the increased conductivity of this compound. Work on four new long-chain TTF derivatives, octadecylthio-TTF(**8**), octadecylseleno-TTF(**9**), octadecyltelluro-TTF(**10**) and 16(thiotrimethyltetrathiafulvalenyl) hexadecanoic acid(**11**), by Dhindsa *et al*[16] showed that these materials formed LB films with lower conductivity ($\sigma_{RT} \sim 10^{-3}$ S cm^{-1}) than those of hexadecanoyl-TTF and *O*-hexadecylthiocarboxy-TTF. It was concluded that the absence of the C=O or C=S group adjacent to the TTF ring resulted in less ordered films. As a consequence of this reduced quality, the structures exhibited lower conductivity. The LB film forming properties and electrical conductivity of transferred multilayer structures of two derivatives of tetrathiotetracene (TTT) were investigated by Tieke *et al* in 1989. Although the compounds 2-trifluoromethyl-5,6;11,12-bisepidithiotetracene(**12**)[17,18] and n-octyloxy-5,6,11,12-tetrathiotetracene (**13**)[18,19] are not classical amphiphiles (with a hydrophilic head and hydrophobic tail), they did form fairly stable monolayers on a water subphase. Film stability was increased by mixing the donor molecule with > 30 mole % of methylarachidate ($Me[CH_2]_{18}CO_2Me$) and Y-type films of more than 100 layers could be built up. As-deposited, these films were quite insulating with room temperature conductivities of 7.7×10^{-7} S cm^{-1} (**12**) and 2×10^{-8} S cm^{-1} (**13**). Several different doping

Material	In-plane dc room temperature conductivity as-deposited (S cm^{-1})	Activation energy as-deposited (eV)	In-plane dc room temperature conductivity after doping (S cm^{-1})	Activation energy after doping (eV)	Reference
5	$1x10^{-5}$	0.5 (230-300K) 0.05 (130-230 K)	$1x10^{-2}$	0.19 eV	12,13
6	10^{-5}		10^{-2}	0.17	14
7	$4x10^{-7}$		1.0	0.09 eV	15
8	$1x10^{-5}$		$8x10^{-2}$		16
9	$3x10^{-6}$		$6x10^{-3}$		16
10	$1x10^{-6}$		$1x10^{-3}$		16
11	$2x10^{-6}$		$8x10^{-3}$		16
12	$7.7x10^{-7}$		$1.2x10^{-4}$		17,18
13	$2x10^{-8}$		$1x10^{-2}$ (Iodine doped after exposure to KI_3 solution)		18,19

Table 3.2. Summary of the electrical properties of LB films of cation radical salts. The numbers in the first column correspond to the labels in Fig. 3.10.

methods were employed: (a) exposure to iodine vapour; (b) treatment with KI_3 solution (i) during or (ii) after film formation; (c) exposure to iodine vapour after treatment with KI_3 solution (i) during or (ii) after film formation; and (d) electrochemical oxidation in $LiClO_4$ solution during or after film formation.After doping, maximum conductivity values of $1.2x10^{-4}$ S cm^{-1} (compound (**12**) doped using method (a)) and $1x10^{-2}$ S cm^{-1} (compound (**13**) doped using method (c)(i)) were recorded. These values were seen to decrease gradually after doping, but could be restored by further exposure to iodine. The electrical properties of the cation radical salts described above are summarised in Table 3.2.

3.3.3 Donor-acceptor complexes

LB films containing both donor and acceptor derivatives have also been deposited. These systems are illustrated in Fig. 3.14. In this class of films, it is necessary to attach a hydrophobic tail to either the donor or the acceptor molecule or both components. The first films of this type were prepared by Japanese workers and were formed from the 1:1 complex tetramethyl-TTF(**14**)-octadecyl-TCNQ (**15**).[20,21] These layers were found to be semiconducting, with a thermal activation energy of 0.08 eV, and displayed an in-plane conductivity at room temperature of 0.1 S cm^{-1}, without the need for any post deposition treatment. This value was stable for at least three months when the samples were stored in air at room temperature. Later, the same group reported a bulk conductivity of 0.4 S cm^{-1} at room temperature for the 3:2 stoichiometry complex (tetramethyl-TTF)$_3$(**16**)-(tetradecyl-TCNQ)$_2$(**17**).[22] Dhindsa *et al* have studied LB films of the complex 1-tetrathiafulvalenyl-octadecan-1-ol(**18**)-TCNQ(**19**)[23] where a long hydrophobic chain was attached to the donor TTF molecule. As-deposited, a room temperature conductivity of 10^{-3} S cm^{-1} was measured, which was unaffected after leaving the samples in air for 2-3 weeks. Conduction was thermally activated with ΔE= 0.27 eV. The conductivity of these films was reduced considerably, down to 10^{-6} S cm^{-1}, by exposure to iodine vapour. Workers in France have studied the complex between the double alkyl chain TTF

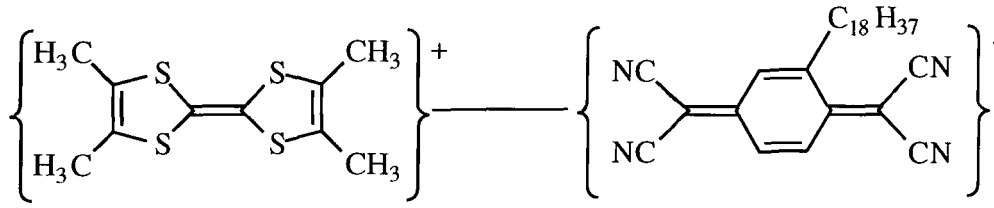

(14) (15)

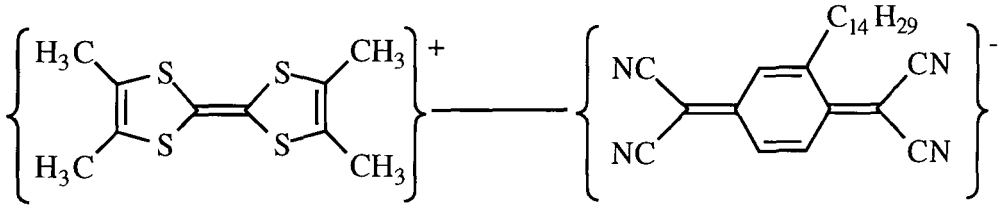

(16) (17)

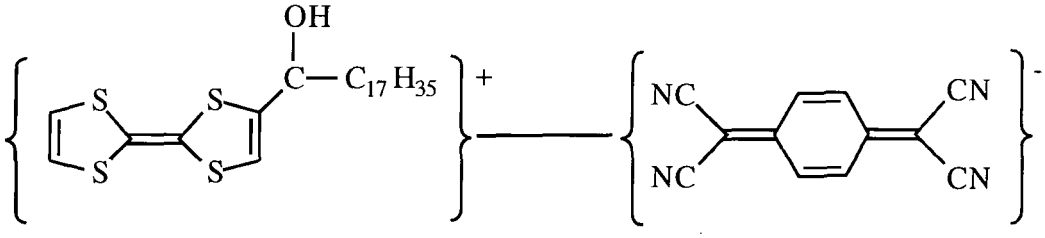

(18) (19)

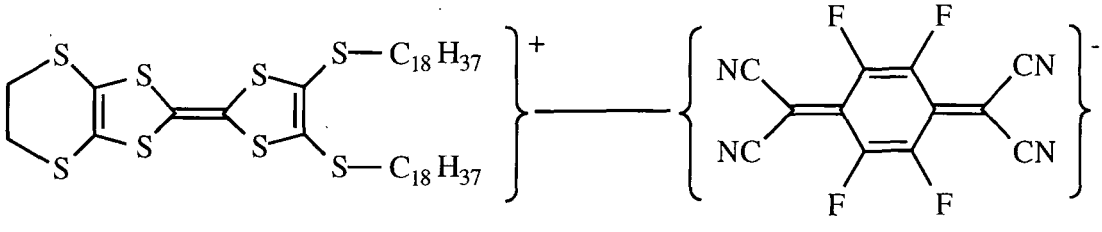

(20) (21)

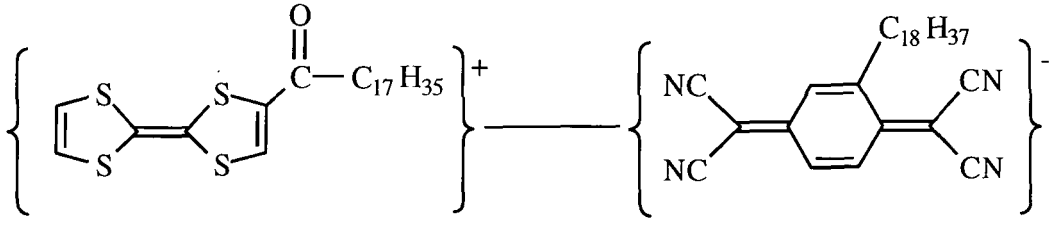

(22) (23)

Fig. 3.14 Some donor-acceptor complexes used in LB studies.

derivative ethylenedithiodioctadecylthio-TTF(**20**) and tetrafluoro-TCNQ(**21**).[24,25] As-deposited, these films were insulating but after doping with iodine, a semiconducting ternary mixed-valence complex was formed with a room temperature conductivity of $5x10^{-2}$ S cm^{-1} and an activation energy of 0.08 eV. In our laboratory, we have used a dual area LB deposition system to prepare alternated structures of the long chain TTF and TCNQ derivatives octadecanoyl-TTF(**22**) and octadecyl-TCNQ(**23**) (Fig. 3.15).[26] As-deposited, semiconducting properties were observed, with room temperature conductivity of $5x10^{-3}$ S cm^{-1} and an activation energy of 0.26 eV. Chinese workers have recently reported high conductivity (120 S cm^{-1}) in alternate layer films of long chain TTF and TCNQ derivatives.[27] The properties of the charge-transfer complexes described in this section are summarised in Table 3.3.

Donor	Acceptor	Ratio	In-plane dc room temperature conductivity as-deposited (S cm^{-1})	Activation energy as-deposited (eV)	In-plane dc room temperature conductivity after doping (S cm^{-1})	Activation energy after doping (eV)	Ref.
14	**15**	1:1	0.1	0.08			20,21
16	**17**	3:2	0.4				22
18	**19**	1:1	10-3	0.27	10^{-6}		23
20	**21**	1:1			$5x10^{-2}$	0.08	24,25
22	**23**	Alternate layers	$5 x10^{-3}$	0.26	$1x10^{-2}$	0.24	26

Table 3.3. Summary of the electrical properties of LB films of charge-transfer complexes.The numbers in the first two columns correspond to the labels in Fig. 3.14.

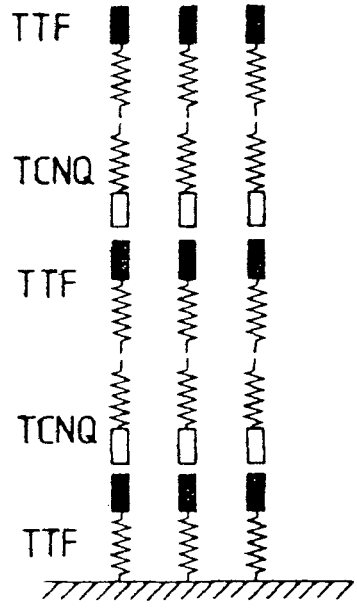

Fig. 3.15 **Schematic diagram illustrating the arrangement of molecules in a multilayer film of TTF and TCNQ built up by alternate-layer deposition.**

After Pearson *et al.*[26]

3.3.4 Organometallic systems

Conductive organic systems based on molecules like TTF and TCNQ are characterised by strong one-dimensional interactions. Organometallic donor molecules such as metal(dmit)$_2$ (where metal = Ni,Pd,Pt,Ag,Zn) have peripheral sulphur atoms which can participate in both inter- and intra-stack interactions and hence increase the dimensionality of the system. The chemical formulae of the organometallic systems used in LB work are illustrated in Fig. 3.16. Japanese workers have investigated the electrical properties of LB films of a variety of metal(dmit)$_2$ complexes with long chain ammonium or pyridinium cations. They reported that the conductivities of didecyldimethylammonium-Au(dmit)$_2$(**24**) and didecyldimethylammonium-Ni(dmit)$_2$(**25**) were of the order of 0.1 S cm^{-1} after bromine doping.[28] The films were semiconducting, with a thermal activation energy of 0.065 eV. These materials would not deposit in pure form and it was found necessary to mix the complexes with up to 50% (molar ratio) eicosanoic acid to stabilise the monolayer on the subphase. Also, since the resulting monolayer was quite rigid, it was necessary to transfer it to a solid substrate using a horizontal lifting technique rather than vertical deposition. Later, the same group produced films of the complex tridecylmethylammonium-Au(dmit)$_2$(**26**), also mixed with eicosanoic acid, which had room temperature conductivities that were significantly higher.[29] Conductivity values of around 10 S cm^{-1} after doping with bromine gas and 25 S cm^{-1} after electrochemical oxidation in aqueous $LiClO_4$ solution were reported. Also, after electrochemical doping, metallic behaviour was observed between room temperature and 200 K (fig. 3.17). Below this temperature, the films were semiconducting with an activation energy of 0.002 eV. Semiconducting films of the 2:1 complex (didecydimethylammonium)$_2$-Pd(dmit)$_2$(**27**) have also been prepared[30], with room temperature conductivity of 5.1 S cm^{-1} and activation energy of 0.05 eV. Taylor *et al* have investigated the monolayer behaviour and electrical characteristics of the monovalent and divalent dialkylammonium salts of M(dmit)$_2$ and M(mnt)$_2$ where M=Ni,[31-34]Pt[31,33]or Pd.[31,33] They found that the

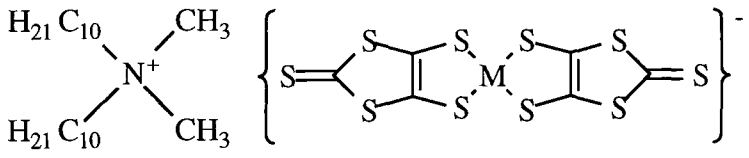

(**24**) M=Au

(**25**) M=Ni

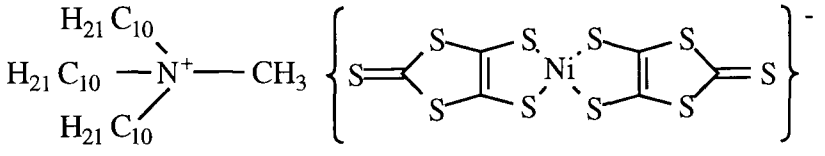

(**26**)

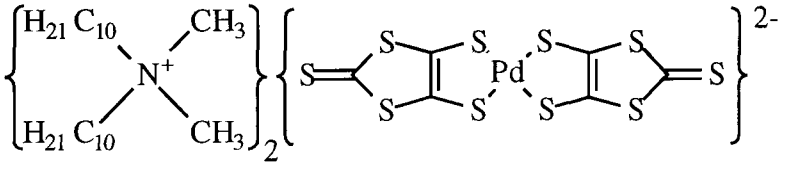

(**27**)

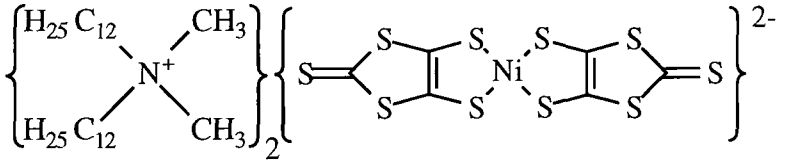

(**28**)

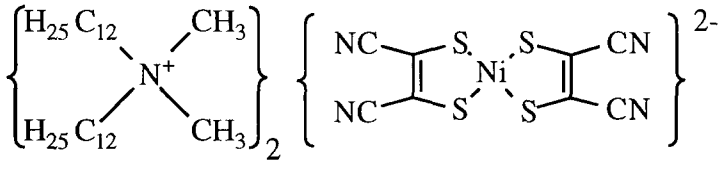

(**29**)

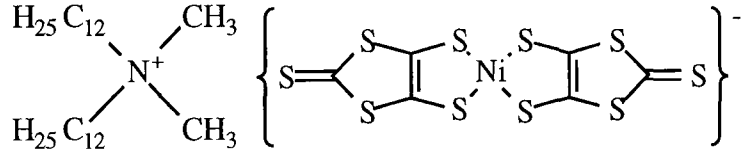

(**30**)

Fig. 3.16 Some organometallic complexes used in LB studies.

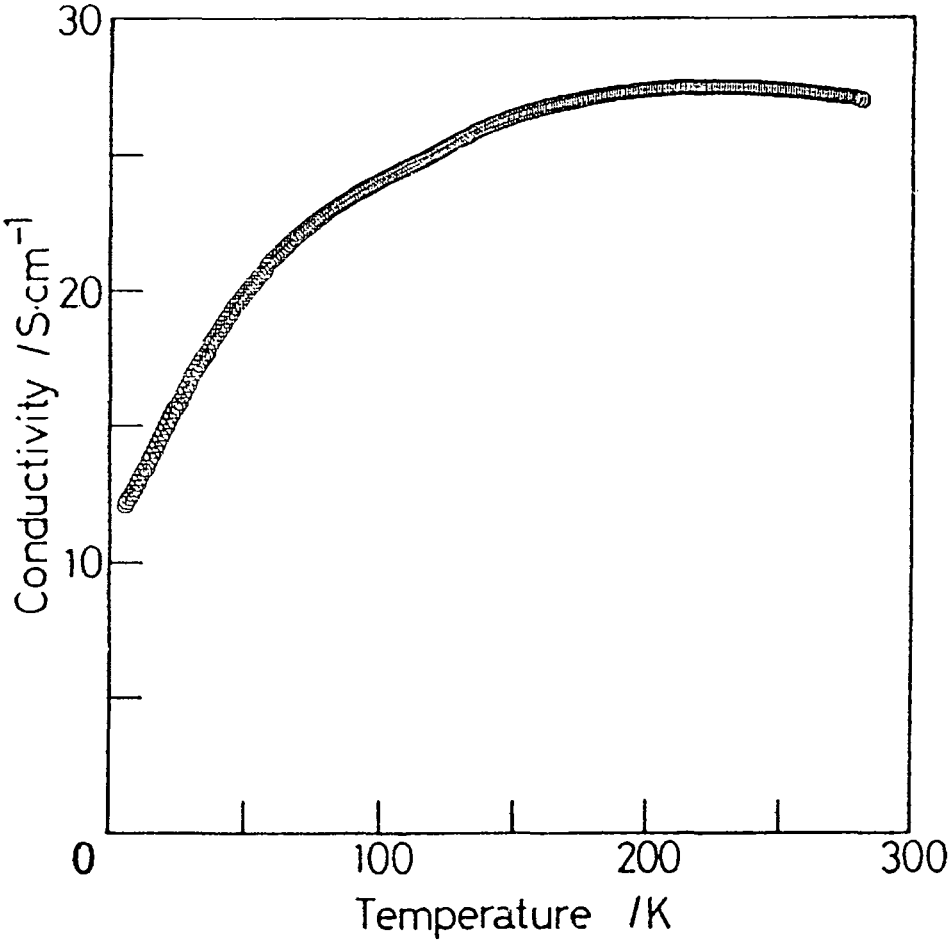

Fig. 3.17 **Temperature dependence of the conductivity of a 20-layer mixed film of tridecylmethylammonium-Au(dmit)$_2$ and eicosanoic acid after electrochemical oxidation with $LiClO_4$.**

After Nakamura *et al.*[28]

behaviour of these materials on the surface of a water subphase was dependent on a number of experimental variables including subphase temperature, spreading time and compression rate. Reproducible pressure-area isotherms and uniform deposition of multilayers by vertical dipping could only be obtained if monolayers were left fully expanded on the subphase for long periods of time. For transferred multilayer films which had been doped by exposure to bromine vapour, maximum conductivity values of

Complex	In-plane dc room temperature conductivity after doping ($S\ cm^{-1}$)	Activation energy after doping (eV)	Reference
24	0.12		28
25	1.0	0.065	28
26	10 (Bromine doped) 25 (Electrochemically doped in $LiClO_4$ solution	0.002 (50-200 K)	29
27	5.1	0.05	30
28	$2x10^{-2}$		31,32,33,34
29	$1x10^{-3}$		31,32,34
30	0.28		32,34

Table 3.4 Summary of the electrical properties of LB films of the organometallic systems described above. The numbers in the first column correspond to the labels in Fig. 3.16.

$2x10^{-2}$, $1x10^{-3}$ and $2.8x10^{-1}$ S cm^{-1} were recorded (for (didodecylmethyl-ammonium)$_2$-Ni(dmit)$_2$(**28**), (didodecylmethylammonium)$_2$-Ni(mnt)$_2$(**29**)and (didodecylmethylammonium)-Ni(dmit)$_2$(**30**), respectively). The results of the studies on the organometallic systems described in this section are listed in Table 3.4.

3.4 Summary

In this chapter, three different methods for the preparation of organic thin films were discussed: the LB technique; thermal evaporation and spinning. Most detail was included in the section regarding the LB technique, since this was the method used to produce the samples used in this project. A review of the work on conductive LB films of anion radical salts, cation radical salts, donor-acceptor charge-transfer complexes and organometallic molecules was included.

References

1. K.B. Blodgett, J. Am. Chem. Soc., 56 (1934) 495.
   K.B. Blodgett, J. Am. Chem. Soc., 57 (1935) 1007-1022.
2. I. Langmuir and V.J. Schaefer, J. Am. Chem. Soc., 60 (1938) 1351-1360.
3. M. Iwahashi, F. Naito, M. Watanabe, T. Seimiya, N. Morikawa, N. Nogawa, T. Ohshima, H. Kawakami, K. Ukai, I. Sugai, S. Shibata, T. Yasuda, Y. Shoji, T. Suzuki, T. Nagafuchi, H. Taketani, T. Matsuda, Y. Kukushima, M. Fujioka and K. Hisatake, Bull. Chem. Soc. Jpn., 58 (1985) 2093-2098.
4. T. Kato, Jpn. J. Appl. Phys., 27 (1988) L1358-L1360.
5. A. Ruaudel-Teixier, M. Vandevyver and A. Barraud, Mol. Cryst. Liq. Cryst., 120 (1985) 319-322.
6. T. Nakamura, M.Tanaka, T. Sekiguchi and Y. Kawabata, J. Am. Chem. Soc., 108 (1986) 1302-1303.
7. J. Richard, M. Vandevyver, P. Lesieur, A. Ruaudel-Teixier and A. Barraud, J. Chem. Phys., 86 (1987) 2428-2438.

8. T. Nakamura, M. Matsumoto, F. Takei, M. Tanaka, T. Sekiguchi, E. Manda and Y. Kawabata. Chem. Lett., (1986) 709-712.

M. Matsumoto, T Nakamura, F. Takei, M. Tanaka, T. Sekiguchi, M. Mizuno, E. Manda and Y. Kawabata, Synth. Met., 19 (1987) 675-680.

9. A.S. Dhindsa, M.R. Bryce, J.P. Lloyd and M.C. Petty, Synth. Met., 22 (1987) 185-189.

R.J. Ward, A.S. Dhindsa, M.R. Bryce, M.C. Petty and H.S. Munro, Thin Solid Films, 198 (1991) 363-367.

10. A. Barraud, M. Lequan, R.M. Lequan, P. Lesieur, J. Richard, A Ruaudel-Teixier and M. Vandevyver, J. Chem. Soc., Chem. Commun., (1987) 797-798.

11. A.S. Dhindsa, G.H. Davies, M.R. Bryce, J. Yarwood, J.P. Lloyd, M.C. Petty and Y. M. Lvov, J. Molec. Electron., 5 (1989) 135-142.

12. A.S. Dhindsa, M.R. Bryce, J.P. Lloyd and M.C. Petty, Thin Solid Films, 165 (1988) L97-L100.

13. A.S. Dhindsa, R.J. Ward, M.R. Bryce, Y.M. Lvov, H.S. Munro and M.C. Petty, Synth. Met., 35 (1990) 307.

14. G. Cooke, A.S. Dhindsa, Y.P. Song, G. Williams, A.S. Batsanov, M.R. Bryce, J.A.K. Howard, M.C. Petty and J. Yarwood, Synth. Met., 55-57 (1993) 3871-3878.

15. A.S. Dhindsa, J.P. Badyal, M.R. Bryce, M.C. Petty, A.J. Moore and Y. M. Lvov, J. Chem. Soc. Chem. Commun., (1990) 970-972.

16. A.S. Dhindsa, G Cooke, K. Lerstrup, K. Bechgaard, M.R. Bryce and M.C. Petty, Chem. Mater., 4 (1992) 720-723.

17. A. Wegmann, B. Tieke, C.W. Mayer and B. Hilti, J.Chem. Soc., Chem. Commun., (1989) 716-717.

18. B.Tieke and A. Wegmann, Thin Solid Films, 179 (1989) 109-120.

19. B. Tieke, A. Wegmann, W. Fischer, B. Hilti, C.W. Myer and J. Pfeiffer, Thin

Solid Films, 179 (1989) 233-238.

20. T. Nakamura, F. Takei, M. Tanaka, M. Matsumoto, T. Sekiguchi, E. Manda, Y. Kawabata and G. Saito, Chem. Lett., (1986) 323-324.

21. Y. Kawabata, T. Nakamura, M. Matsumoto, M. Tanaka, T. Sekiguchi, H. Komizu, E. Manda and G. Saito, Synth. Met., 19 (1987) 663-668.

22. M. Matsumoto, T. Takayoshi, E. Manda ,Y. Kawabata, K. Ikegami, S. Kuroda, M. Sugi and G. Saito, Thin Solid Films, 160 (1988) 61-66.

23. A.S. Dhindsa, C. Pearson, M.R. Bryce and M.C. Petty, J. Phys. D: Appl. Phys., 22 (1989) 1586-1590.

24. J. Richard, M. Vandevyver, A. Barraud, J.P. Morand, R. Lapouyade, P. Delhaes, J.F. Jacquinot and M. Roulliay, J. Chem. Soc., Chem. Commun., (1988) 754.

25. J. P. Morand, R. Lapouyade, P. Delhaes, M. Vandevyver, J. Richard and A. Barraud, Synth. Met., 27 (1988) B569-B574.

26. C. Pearson, A.S. Dhindsa, M.R. Bryce and M.C. Petty, Synth. Met., 31 (1989) 275-279.

27. Y.Q. Liu, Y. Xu and D.B. Zhu, Proceedings of the Seventh International Conference on Organised Molecular Films, (1995) In Press.

28 T. Nakamura, H. Tanaka, M. Matsumoto, H. Tachibana, E. Manda and Y. Kawabata, Synth. Met., 27 (1988) B601-B608.

T. Nakamura, H. Tanaka, K. Kojima, M. Matsumoto, H. Tachibana, M. Tanaka and Y. Kawabata, Thin Solid Films, 179 (1989) 183-189.

29. T. Nakamura, K. Kojima, M. Matsumoto, H. Tachibana, M. Tanaka, E. Manda and Y. Kawabata, Chem. Lett., (1989) 367-368.

30. Y.F. Miura, M. Takenaga, A. Kasai, T. Nakamura, Y. Nishio, M. Matsumoto and Y. Kawabata, Thin Solid Films, 210/211 (1992) 306-308.

31. D.M. Taylor. A.E. Underhill, S.K. Gupta and C.E. Wainwright, Makromol. Chem. Macromol. Symp., 46 (1991) 199-203.

32. D. M. Taylor, S.K. Gupta, A.E. Underhill and C.E. Wainwright, Thin Solid Films, 210/211 (1992) 287-289.

33. S.K. Gupta, D.M. Taylor, P. Dynarowicz, E. Barlow, C.E.A. Wainwright and A.E. Underhill, Langmuir, 8 (1992) 3057-3062.

34. S.K. Gupta, D.M. Taylor, A.E. Underhill and C.E.A. Wainwright, Synth. Met., 58 (1993) 373-382.

Chapter 4

The Thin Film Transistor

4.1 Introduction

The most common field-effect transistor (FET) is the metal-insulator-semiconductor FET (MISFET). A schematic diagram of an p-channel silicon MISFET is shown in Fig. 4.1. The source and drain contacts are two p-n junctions and if a negative voltage of sufficient magnitude is applied to the gate contact, an inversion layer (p-type surface layer) will form which provides a channel between the source and drain. Thus, a conventional MISFET is a minority carrier device since the current in an n-type semiconductor is carried by holes in a p-type channel. Fig. 4.2 illustrates schematically two alternative structures used in the fabrication of organic thin film transistors (TFTs). Structure (a) is preferred by LB workers since no further processing is required after deposition of the organic layer. In both cases, the source and drain form Ohmic contacts to, and majority carriers are injected into, the semiconducting organic layer. As a consequence, organic MISFETs operate by the modulation of the concentration of majority carriers, in a channel between the source and drain contacts, by a gate voltage of suitable polarity. The equations describing the operation of a classical inversion MOSFET must therefore be modified to provide a model for a MISFET operating in accumulation mode. Additionally, in an organic TFT no p-n junctions exist between the source and drain contacts and the organic layer. Consequently, an Ohmic current flows in the bulk of the semiconductor in parallel with the channel current.

4.2 Thin film transistor theory

Horowitz *et al* have developed a model accounting for the operation of organic MISETs in the accumulation regime.[1] A schematic view of an organic TFT is given in Fig. 4.3(a). The channel has width (source to drain distance) W, length L and the gate insulator oxide

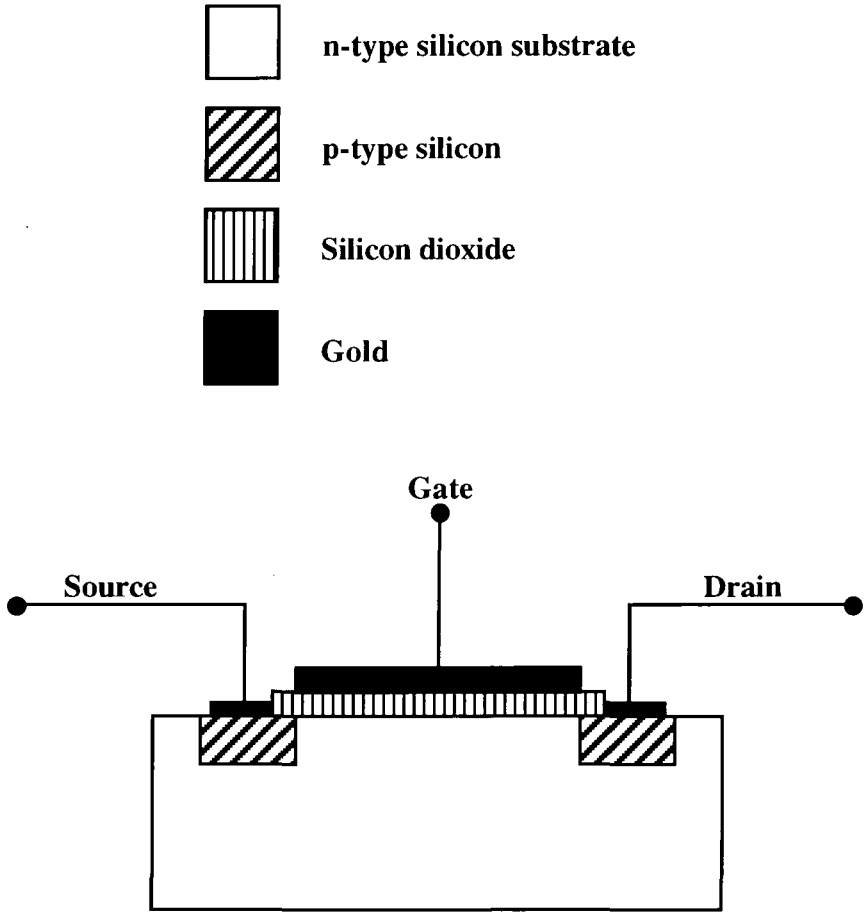

Fig. 4.1 Schematic diagram of a conventional p-channel silicon metal-insulator-semiconductor field-effect transistor (MISFET).

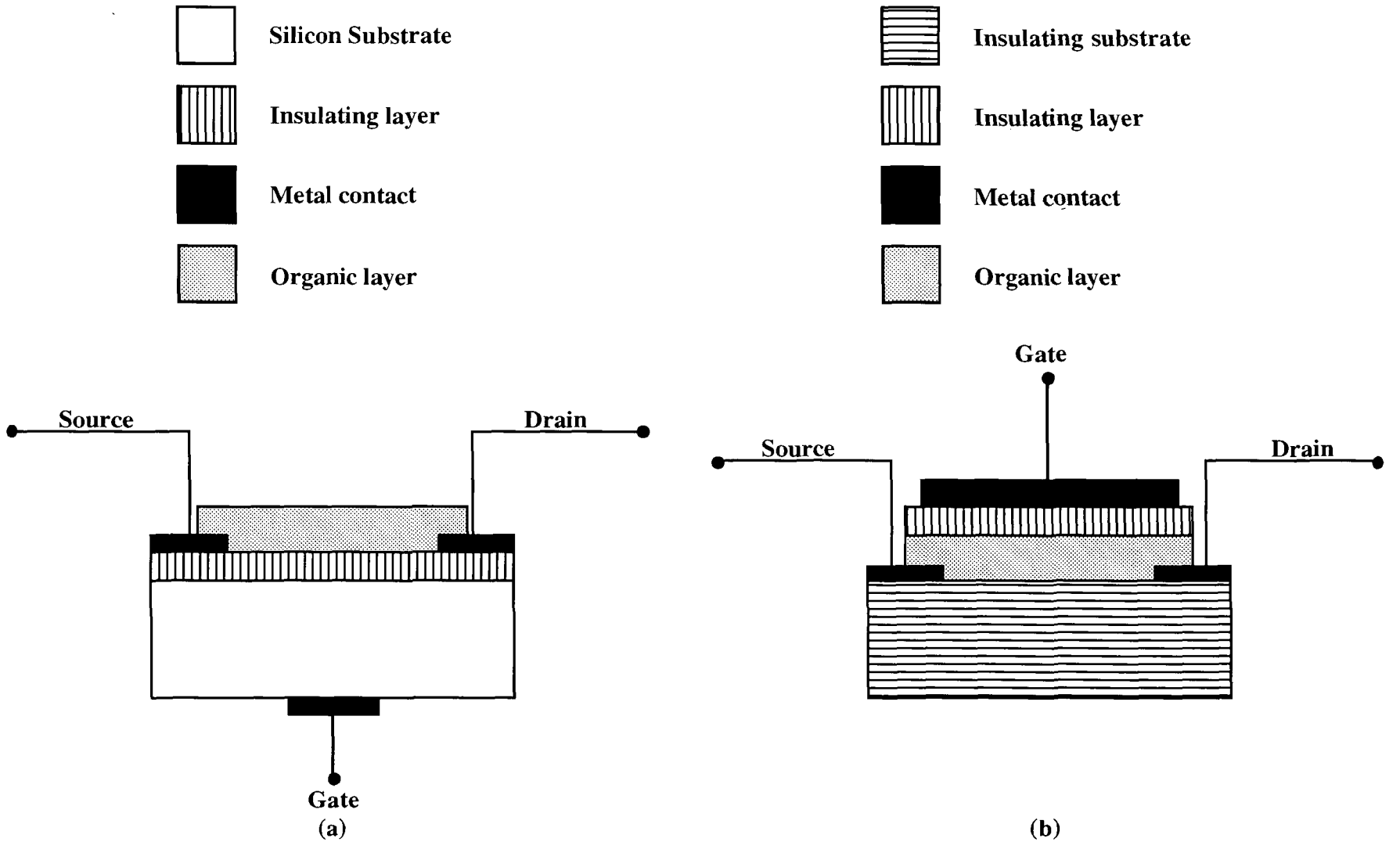

Fig. 4.2 Two alternative structures used for organic thin-film field-effect transistors.

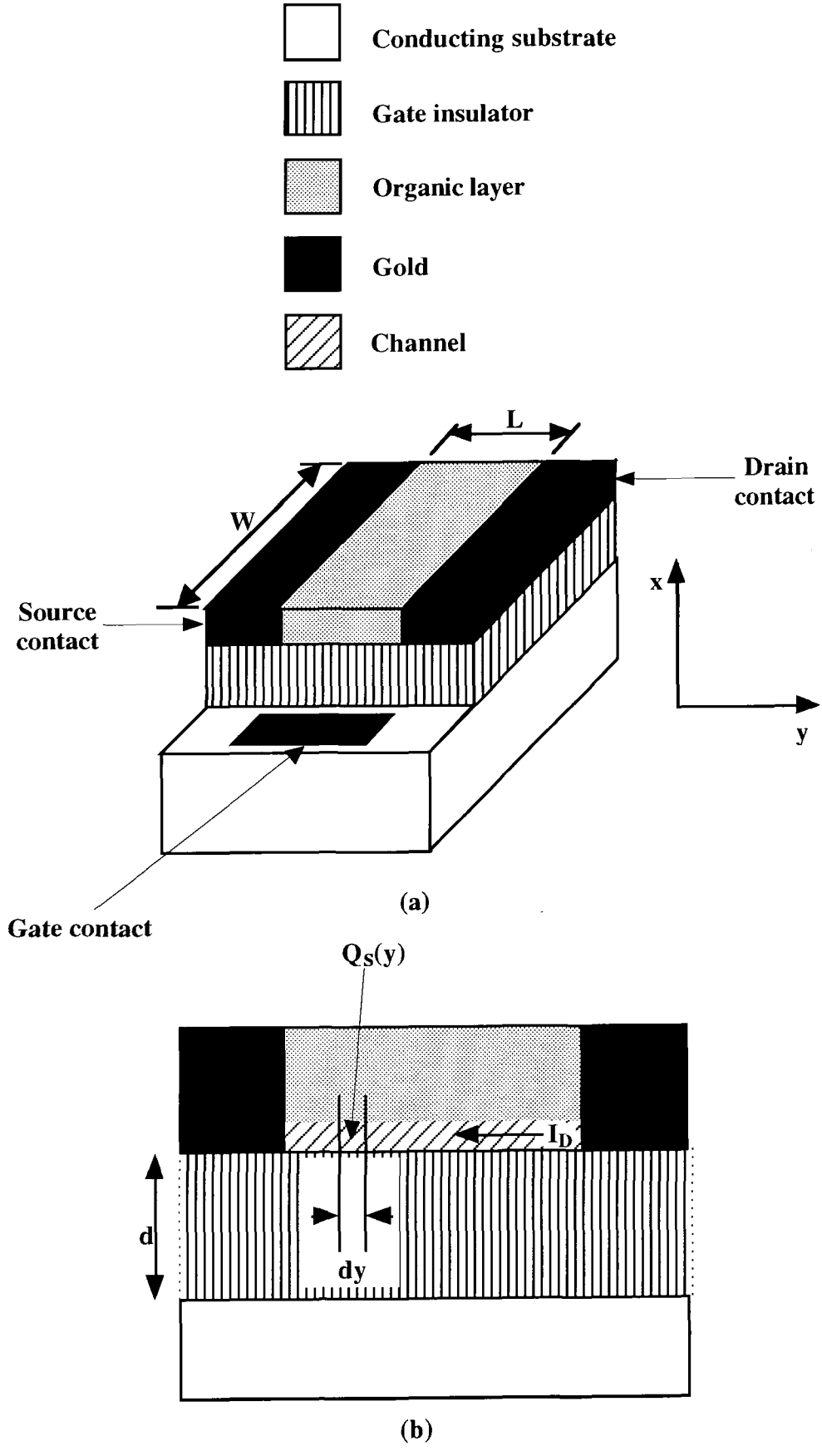

Fig. 4.3 (a) Schematic diagram of an organic thin film transistor. (b) Close up schematic view of the channel region of an organic thin film transistor.

has thickness d. Fig. 4.3(b) is a close up schematic diagram of the channel region in this structure. Here the x-axis is directed from the source to the gate and the y-axis from the source to the drain. The total charge per unit area induced in the channel at distance y from the source by the gate voltage V_G is given by

$$Q_s(y) = -\left[V_G - \psi_s(y)\right] C_i \qquad 4.1$$

where $\psi_s(y)$ is the surface potential, and the capacitance per unit area of the gate insulator, having permittivity ε_i, is $C_i = \varepsilon_i/d$.

Assuming that

$$\psi_s(y)=V(y)+V_t \qquad 4.2$$

where V(y) is the bias between point y and the grounded source and V_t is a voltage to be defined later, then

$$Q_s(y) = -\left[V_G - V(y) - V_t\right]C_i \qquad 4.3$$

The conductivity of the channel can be approximated by

$$\sigma(x) = q\, n(x)\, \mu(x) \qquad 4.4$$

where q is the charge, n(x) the number and $\mu(x)$ the mobility of the charge carriers. The conductance of the channel is given by

$$g = \frac{W}{L}\int_0^{x_a} \sigma(x)\, dx \qquad 4.5$$

where x_a is the thickness of the channel.

Then, assuming a constant mobility in the accumulation layer, this becomes

$$g = \frac{W}{L} q\mu \int_0^{x_a} n(x)\, dx \qquad 4.6$$

The integral

$$\int_0^{x_a} n(x)\, dx \qquad 4.7$$

is equal to the total charge per unit area in the accumulation layer and hence equal to $|Q_S|$. Therefore

$$g = \frac{W}{L} q\mu |Q_S| \qquad 4.8$$

The channel resistance dR of an elemental section dy is given by

$$dR = \frac{dy}{gL} = \frac{dy}{W \mu |Q_S(y)|} \qquad 4.9$$

and the voltage drop dV across the elemental section is

$$dV = I_D dR = \frac{I_D dy}{W \mu |Q_S(y)|} \qquad 4.10$$

where I_D is the drain current which is independent of y.

Substituting from equations (4.9) and (4.3)

$$dV = \frac{I_D dy}{W\mu[V_G - V(y) - V_t]C_i} \qquad 4.11$$

Integrating from the source (y=0 and V=0) to the drain (y=L and V= V_D)

$$W\mu C_i \int_0^{V_D} [V_G - V(y) - V_t]dV = I_D \int_0^L dy \qquad 4.12$$

gives

$$I_D = \frac{W\mu C_i}{L}\left((V_G - V_t)V_D - \frac{V_D^2}{2}\right) \qquad 4.13$$

Typical current-voltage characteristics for a MISFET are shown in Fig. 4.4. For a given value of V_G, the drain current first increases linearly with the drain voltage. This is the linear region, and equation 4.13 reduces to

$$I_D \approx \frac{W}{L}\mu C_i (V_G - V_t)V_D \quad \text{for } V_D << (V_G - V_t) \qquad 4.14$$

When $Q_S(L) = 0$ or, from equations 4.1 and 4.2 when $V_D = V_G - V_t = V_{D,sat}$, the channel becomes pinched off near the drain contact. Thus, for $V_D > V_G - V_t$, I_D becomes saturated. The value of this saturated drain current $I_{D,sat}$ is given by

$$I_{D,sat} = \frac{W\mu C_i}{2L}(V_G - V_t)^2 \qquad 4.15$$

where V_t appears to play the same role as the threshold voltage in conventional inversion MOSFETs. In an inversion MOSFET, this threshold voltage arises from the requirement that a substantial gate voltage must be applied before an inversion layer will form. In an ideal accumulation MISFET, this requirement does not exist and V_t should be zero. The term must be included to take account of the pseudo threshold voltage observed in actual organic devices. Several explanations are possible, e.g. charge in the insulator layer or at the semiconductor-gate insulator interface.

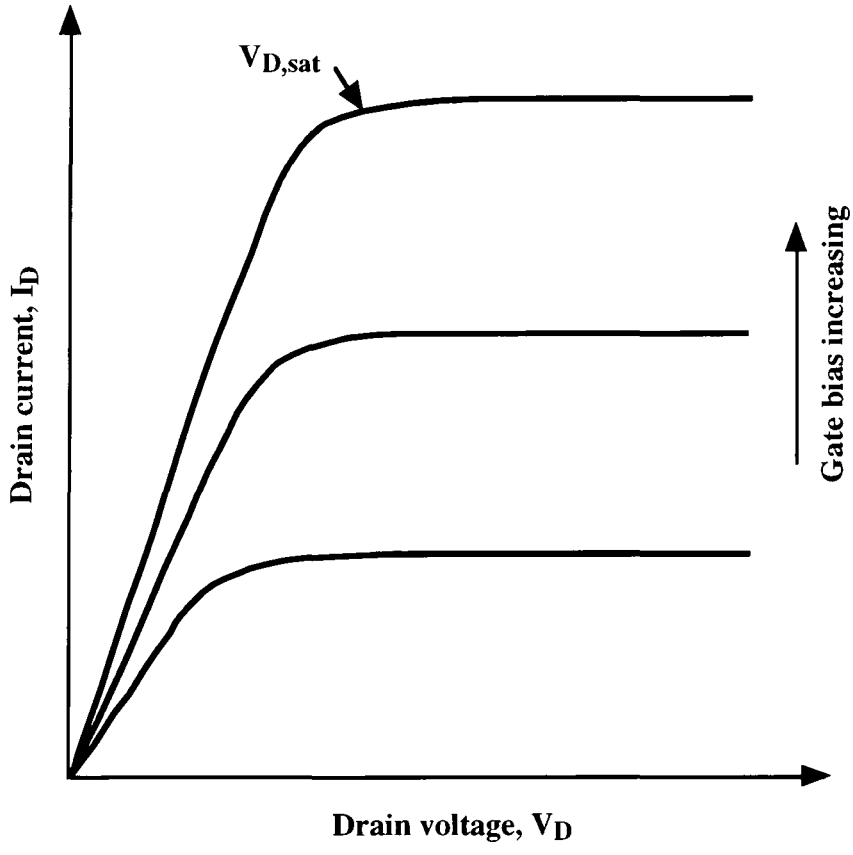

Fig. 4.4 Typical current-voltage characteristics for a thin film MISFET based on the theoretical treatment given in the text.

4.3 Gate insulator capacitance

The gate insulator can be characterised by incorporating the layer in an MIS capacitor structure, as illustrated in Fig. 4.5, and measuring the capacitance versus voltage (CV) behaviour. A typical high frequency capacitance versus voltage plot for a structure consisting of an oxide layer on p-type silicon is shown in Fig. 4.6. The curve can be divided into three regions known as accumulation, depletion and inversion. In accumulation, majority carriers are attracted to the silicon/oxide interface by a bias voltage of opposite sign, and form a thin layer which acts like a capacitor plate of equal area to the top electrode. The capacitance is therefore due to the geometry of the device and is defined by the area of the top electrode and the thickness of the oxide. The central region of the CV curve, where the capacitance changes rapidly with dc bias is known as the depletion region. Here, charge in the semiconductor is repelled by the voltage on the top electrode, and a depletion region is created under the electrode. This region is insulating, effectively increasing the distance between the plates of the capacitor and decreasing the device capacitance. This trend of decreasing capacitance is limited by the onset of inversion. This occurs when the voltage applied to the top electrode is sufficient to pull minority carriers away from neutral semiconductor atoms and towards the interface. When these minority carriers outnumber the majority carriers, a so called inversion layer forms at the surface of the semiconductor. To add or remove charge to this layer, slow thermal generation/recombination processes have to occur. Consequently, at high frequency, the minority carriers cannot exchange charge in response to the test signal, the measured capacitance is due only to the majority carriers and is much lower than that in accumulation.

4.4 The organic thin film transistor

The materials used in the fabrication of organic thin-film field-effect transistors and the properties of the resulting devices are collated in Table 4.1. In some of the devices that were investigated, drain current saturation was not observed. These cases are indicated in

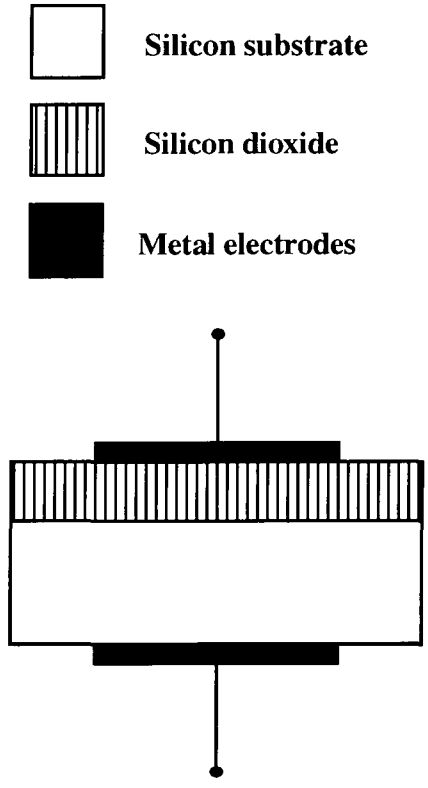

Fig. 4.5 The metal oxide semiconductor (MOS) capacitor structure used to measure capacitance versus voltage (CV) characteristics.

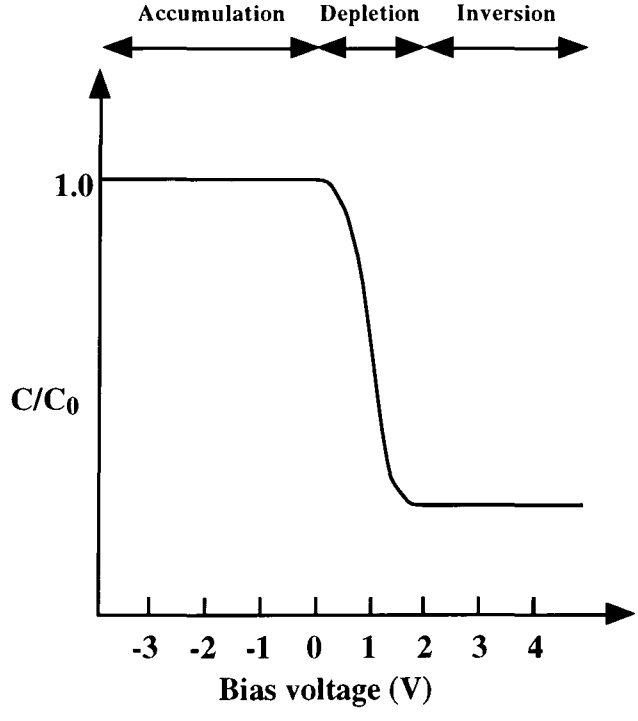

Fig. 4.6 Ideal high frequency CV characteristic for a p-type MOS capacitor.

the table by an asterisk adjacent to the reference number.

Material Deposition technique	Substrate/ gate insulator	Conductivity (S cm^{-1})	Mobility (cm^2 V^{-1} s^{-1})	Reference
Polyacetylene Direct synthesis from C_2H_2 gas	glass/ polysiloxane	1.8×10^{-5}		2*
Spin coating	Si/SiO_2		10^{-4}	3*
Poly (N-methylpyrrole) Chemical polymerisation	Si/SiO_2	2×10^{-5}	10^{-2}	4*
Polythiophene Electrochemical synthesis	Si/SiO_2	10^{-8} - 10^{-6}	10^{-5} - 10^{-3}	5,6,7
Lutetium bisphthalocyanine on top of zinc phthalocyanine Vacuum evaporation	Si/SiO_2	10^{-5}		8*
Scandium diphthalocyanine on top of nickel phthalocyanine Vacuum evaporation	Si/SiO_2	10^{-6}	10^{-3}	9
Poly (3-hexylthiophene) Spin coating	Si/SiO_2	10^{-8}	10^{-5} - 10^{-4}	10

Material Deposition technique	Substrate/ gate insulator	Conductivity (S cm^{-1})	Mobility (cm^2 V^{-1} s^{-1})	Reference
α-sexithienyl Vacuum evaporation	Si/SiO_2	10^{-7} - 10^{-6}	10^{-4} - 10^{-3}	11
	Glass/ polyvinylalcohol		9.3×10^{-4}	12
	Glass/ cyanoethylpullulan		3.4×10^{-2}	12
	poly (-parabanic acid) resin/ cyanoethylpullulan		4.6×10^{-1}	13
	Si/SiO_2		10^{-5} - 10^{-4}	14
Poly (3-hexylthiophene) arachidic acid (40%) LB deposition	Si/SiO_2	4×10^{-7}	7×10^{-7}	15
Quinquethiophene arachidic acid (40%) LB deposition	Si/SiO_2	3×10^{-7}	1×10^{-5}	15
Poly (3-butylthiophene) Spin coating	Si/SiO_2		2×10^{-4}	16
Poly (3-hexylthiophene) Spin coating	Si/SiO_2		1×10^{-4}	16
Poly (3-octylthiophene) Spin coating	Si/SiO_2		3×10^{-6}	16

Material Deposition technique	Substrate/ gate insulator	Conductivity (S cm^{-1})	Mobility (cm^2 V^{-1} s^{-1})	Reference
Poly (3-decylthiophene) Spin coating	Si/SiO_2		6×10^{-7}	16
Lead phthalocyanine Vacuum evaporation	Si/SiO_2 or Si_3N_4			17*
Poly (thienylenevinylene) Spin coating	Si/SiO_2 Si/Si_3N_4	10^{-5} - 10^{-6} 2×10^{-6}	2.2×10^{-1} 10^{-4}	18 20
α,ω-di(hexyl) sexithiophene Vacuum evaporation	Adhesive tape/polyethylene terephthalate		6×10^{-2}	19
Ethylenedithio tetrathiafulvalene- $(SC_{18})_2$ LB deposition	Si/SiO_2	0.06 - 0.2	$5 - 7 \times 10^{-3}$	21*
Pentacene Spin coating	Si/Si_3N_4	10^{-5}	10^{-3}	20

Table 4.1 Properties of organic thin film field effect transistors. Saturation of the drain current was not observed in those devices where the reference number is marked with an asterisk

From this table, it can be seen that in general, the mobilities observed for the carriers in these devices lie in the range 10^{-6} to 10^{-2} cm^2 V^{-1} s^{-1}. These mobilities are small compared to those seen for the carriers in conventional single crystal inorganic

semiconductors e.g.2900 $cm^2\ V^{-1}\ s^{-1}$ (1900 $cm^2\ V^{-1}\ s^{-1}$), 1350 $cm^2\ V^{-1}\ s^{-1}$ (480 $cm^2\ V^{-1}\ s^{-1}$) and 8600 $cm^2\ V^{-1}\ s^{-1}$ (250 $cm^2\ V^{-1}\ s^{-1}$) for intrinsic electrons (holes) in germanium, silicon and gallium arsenide, respectively. Work with α-sexithienyl has shown that the field effect mobility can be varied over five orders of magnitude by changing the material used to form the gate insulator. The conducting channel in an organic TFT is formed at the semiconductor/insulator interface and this plays a key role in the operation of the device. The highest mobility observed in a polymer TFT was 4.6 x 10^{-1} $cm^2\ V^{-1}\ s^{-1}$ for a device with α-sexithienyl as the semiconductor, cyanoethylpullulan as the gate insulator and poly(-parabanic acid) resin as the substrate.[13] This mobility is comparable to that of the carriers in amorphous silicon devices i.e. 10^{-1} - 1 $cm^2\ V^{-1}\ s^{-1}$.

Fig. 4.7(a) shows the drain characteristics, reported by Paloheimo *et al*,[15] of a device using 35 LB layers of the conducting polymer quinquethiophene mixed with arachidic acid as the active layer. The characteristics were due to modulation of the conductivity of the organic channel and indicated that the material was a p-type conductor. A mobility value of $1x10^{-5}$ $cm^2\ V^{-1}\ s^{-1}$ was calculated. Hesto *et al*[21] fabricated devices incorporating ethylenedithiotetrathiafulvalene-$(SC_{18})_2$. The characteristics of a device having a channel consisting of 10 LB layers are shown in Fig. 4.7(b). Here, the drain characteristics did not resemble those of the theoretical model for a conventional thin film transistor, and the observed modulation in this case was attributed to the variation of the height of a barrier at the source-channel contact by a voltage applied to the gate. A carrier mobility of $5x10^{-3}$ $cm^2\ V^{-1}\ s^{-1}$ was calculated.

4.5 Summary

In this chapter, the operation of organic thin film transistors was described. A review of the work on field effect transistors incorporating organic thin films as the active layer was included.

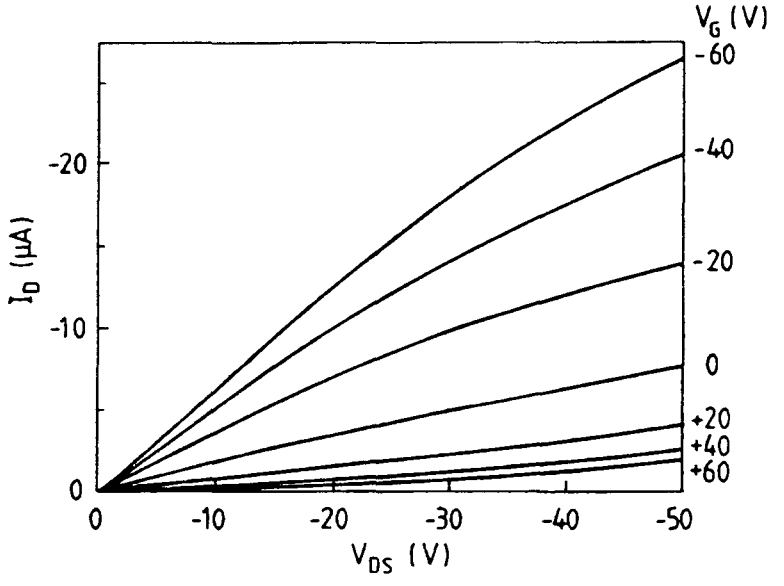

(a)

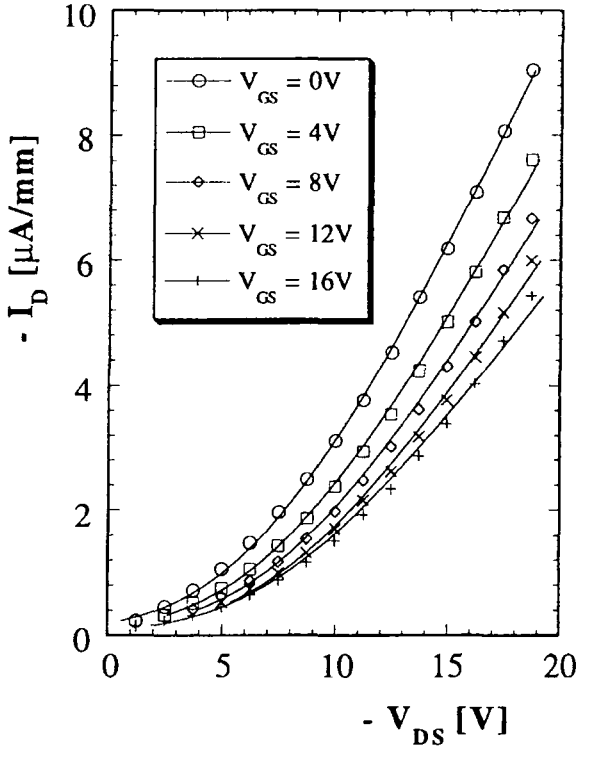

(b)

Fig. 4.7 **Experimental drain characteristics of two organic field effect transistors**

(a) **35 LB layers of quinquethiophene mixed with arachidic acid as the active layer.**

After Paloheimo *et al.*[15]

(b) **10 LB layers of ethylenedithiotetrathiafulvalene-$(SC_{18})_2$ as the active layer.**

After Hesto *et al* .[21]

References

1. G. Horowitz, X. Peng, D. Fichou and F. Garnier, J. Appl. Phys., 67 (1990) 528-532.
2. F. Ebisawa, T. Kurokawa and S. Nara, J. Appl. Phys., 54 (1983) 3255-3259.
3. J.H. Burroughes, C.A. Jones and R.H. Friend, Nature, 335 (1988) 137-141.
4. A. Tsumura, H. Koezuka, S. Tsunoda and T. Ando, Chem. Lett., (1986) 863-866.
5. A. Tsumura, H. Koezuka and T. Ando, Appl. Phys. Lett., 49 (1986) 1210- 1212.
6. H. Koezuka, A. Tsumura and T. Ando, Synth. Met., 18 (1987) 699-704.
7. A. Tsumura, H. Koezuka and T. Ando, Synth. Met., 25 (1988) 11-23.
8. M. Madru, G. Guillaud, M. AlSadoun, M. Maitrot, C. Clarisse, M. LeContellec, J.-J. André and J. Simon, Chem. Phys. Lett., 142 (1987) 103-105.
9. C. Clarisse, M.T. Riou, M. Gauneau and M. Le Contellec, Electron. Lett., 24 (1988) 674-675.
10. A. Assadi, C. Svensson, M. Willander and O. Inganäs, Appl. Phys. Lett., 53 (1988) 195-197.
11. G. Horowitz, D. Fichou, X. Peng, Z. Xu and F. Garnier, Solid State Commun., 72 (1989) 381-384.
12. X. Peng, G. Horowitz, D. Fichou and F. Garnier, Appl. Phys. Lett., 57 (1990) 2013-2015.
13. F. Garnier, G. Horowitz, X. Peng and D. Fichou, Adv. Mater. 2, (1990) 592-594.
14. P. Ostoja, S. Guerri, S. Rossini, M. Servidori, C. Taloani and R. Zamboni, Synth. Met., 54 (1993) 447-452.
15. J. Paloheimo, P. Kuivalainen, H. Stubb, E. Vuorimaa and P. Yi-Lahti, Appl. Phys. Lett., 56 (1990) 1157-1159.

16. J. Paloheimo, H. Stubb, P. Yli-Lahti and P. Kuivalainen, Synth. Met., 41-43 (1991) 563-566.

17. C. Hamann, M. Müller, A. Mrwa, M. Starke and W. Vollmann, Synth. Met., 41-43 (1991) 1081-1086.

18. H. Fuchigama, A. Tsumura and H. Koezuka, Appl. Phys. Lett., 63 (1993) 1372-1374.

19. F. Garnier, R. Hajlaoui, A. Yassar and P. Srivastava, Science, 265 (1994) 1684-1686.

20. A.R. Brown, A. Pomp, C.M. Hart and D.M. de Leeuw, Science, 270 (1995) 972-974.

21. P. Hesto, L. Aguilhon, G. Tremblay, J.P. Bourgoin, M. Vandevyver and A. Barraud, Thin Solid Films, 242 (1994) 7-10.

Chapter 5

Experimental Methods

5.1 Introduction

This chapter is concerned with the experimental techniques used in the course of the work. The equipment and methods used in the deposition of thin organic films are described including the preparation of spreading solutions, measurement of pressure versus area isotherms, substrate cleaning and LB deposition. Film thickness measurement by ellipsometry and surface profiling techniques, and the investigation of film morphology and composition by optical and electron microscopy and electron probe microanalysis are all explained. The measurement of the electrical properties of the multilayer structures is also described. In particular, in-plane conductivity (at room temperature and low temperature) and capacitance. Finally, the fabrication and characterisation of organic thin film transistor structures are considered .

5.2 Langmuir-Blodgett Film Deposition

5.2.1 The LB trough

Surface pressure versus area studies and LB film deposition were carried out in a class 10,000 microelectronics clean room using constant perimeter barrier LB troughs which were designed and built in Durham.[1] A schematic diagram of the constant perimeter LB deposition system is shown in Fig. 5.1. The barrier tape, which was made from glass fibre coated with polytetrafluoroethylene (PTFE), was supported by six PTFE rollers. Two of these rollers were fixed and the other four attached to movable metal arms driven by a variable speed dc motor and toothed rubber belt system. By moving these arms, the area inside the barrier could be varied between maximum and minimum values (Fig. 5.1 inset (a) and (b), respectively). The limits of travel of the arms were set by microswitches connected to the control electronics.

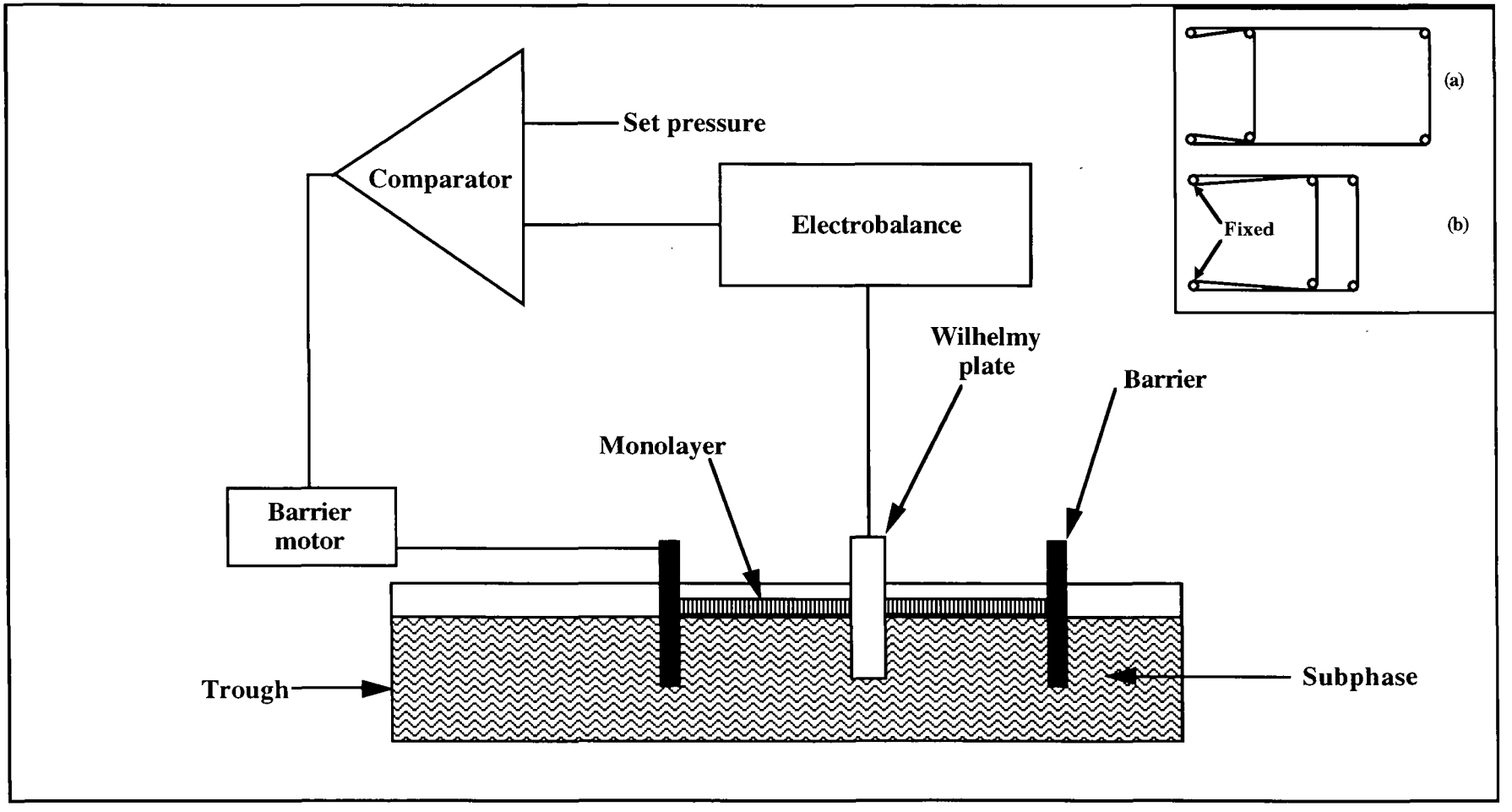

Fig. 5.1 Schematic diagram of the feedback system used to allow the control of monolayer surface pressure. The constant perimeter barrier system is shown inset.

A subphase consisting of ultrapure water was used. Subphase purity was very important since any contaminants were likely to affect the monolayer properties. Hence, mains tap water was very carefully purified by pre-filtering, reverse osmosis, carbon filtration, two stages of de-ionisation, UV sterilisation and 0.2 μm particulate filtration. Water quality was monitored using an Anatel Total Organic Carbon (TOC) analyser which indicated a resistivity of > 17.5 MΩ cm and TOC content of < 5 ppb. The trough which held the subphase was constructed from glass or PTFE and mounted on a hand-operated mechanical jack. This allowed the trough to be lowered to a position below the bottom of the barrier tape support rollers to facilitate removal for cleaning as well as adjustment of the water level relative to the barrier tape. Trough cleaning consisted of washing the glass with Analar grade propan-2-ol and rinsing with ultra-pure water. Cleaning of the barrier tape and rollers was achieved by removing these items from the trough and refluxing them in propan-2-ol.

Surface pressure was measured by the Wilhelmy plate method.[2] The Wilhelmy plate consisted of a piece of chromatography paper (3 cm long by 1 cm wide) partially immersed in the subphase and linked to a CI microbalance head by a thread. Changes in the force on the plate due to variations in surface tension were transmitted to the balance and converted to an electrical signal. This signal was used, via a feedback loop, to adjust the area enclosed by the barrier tape and hence control the surface pressure during film deposition.

The dipping head consisted of a micrometer screw driven by a variable speed dc electric motor. The sample, onto which monolayers were to be transferred, was clamped into a suitable holder which could be fixed onto the front of the dipping head.

High precision linear potentiometers were attached to the barrier system to allow measurement of the monolayer area and to the dipping mechanism to facilitate control of

the positions of the upper and lower deposition limits. An electronic counter was included in the control electronics so that the required number of dipping cycles could be set and the trough left to dip automatically. Two chart recorders were connected to the system: a Bryans 2000 X-Y recorder to allow for the plotting of pressure versus area isotherms and a W+W 312 2Y-T chart recorder to provide a permanent record of surface pressure and trough area against time throughout an experiment. The latter could be used to calculate the transfer ratio of the monolayer to the substrate, given by

$$\tau = \frac{\Delta A}{A_S} \qquad 5.1$$

where ΔA is the decrease in area of the monolayer during a dipping cycle and A_S is the coated area of the substrate. For good Y-type film transfer, τ should have a value of unity for deposition on the downstroke and upstroke of the dipping cycle.

5.2.2 Solution preparation

The organic compounds used in the course of this work were synthesised by Dr. A.S Dhindsa and Dr. A.J. Moore in the Department of Chemistry at the University of Durham. The required amount of solid material was weighed into a volumetric flask using an Oertling digital balance with a resolution of 0.1 mg. An accurately measured amount of a suitable solvent was then added to give a solution of the required concentration (the flasks used were marked with a line to give the stated volume with an accuracy of 1%). In some cases it was necessary to use ultrasonic agitation for a period of up to 30 minutes to assist dissolution of the solid. A variety of different organic materials were used as spreading solvents, either pure or as multi-component mixtures, depending on the solubility of the monolayer material.

5.2.3 Isotherm measurement

A plot of surface pressure versus trough area, undertaken at constant temperature, is

known as an isotherm.[3] It is the most sensitive indicator of the properties of a monolayer. A precisely measured amount of spreading solution was applied to the surface of the subphase, drop by drop, from a Hamilton microlitre syringe. To aid spreading of the organic material, the drops were distributed evenly over the entire subphase area. A length of time was then allowed for the solvent to evaporate. This time ranged from as little as one minute up to tens of hours, depending on the volatility of the solvent in use and the spreading characteristics of the monolayer material. Isotherms were recorded at a compression rate of $2.5\pm2.0\times10^{-3}$ nm^2 $molecule^{-1}$ s^{-1}. The plot obtained was examined and used to select a suitable pressure for film deposition, usually on the steepest part of the trace

5.2.4 Substrate preparation

All substrates, except those for thin film transistor fabrication, were cleaned using a standard technique. First, the surface was scrubbed with detergent (Decon 90) on a polishing pad. This would remove any large pieces of dirt. The samples were then arranged in a slotted holder and treated in an ultrasonic bath for 30 minutes in a 10% detergent solution. After rinsing with ultrapure water another treatment in the ultrasonic bath was carried out, this time with the substrates immersed in ultrapure water for 30 minutes. Finally the clean substrates were dried in a stream of nitrogen from a blow gun. A variety of different substrate types were used, depending on the specific application. For in-plane conductivity measurements, Chance Propper microscope slides were used. To perform capacitance measurements, a 130 nm thick layer of gold undercoated with a thin layer of chromium (a few tenths of a nm to improve adhesion) was deposited onto the glass by thermal evaporation in an Edwards 306A vacuum coating system. This metal layer acted as a bottom electrode. For ellipsometric measurements, single crystal silicon wafers were used. In some cases, after cleaning, the pieces of silicon were treated with a 2% solution of dimethyldichlorosilane ($(CH_3)_2SiCl_2$) in 1,1,1-trichloroethane. This is known as silanising solution and it creates a hydrophobic surface on silicon. The

surface of bare silicon has OH groups bonded to it. Exposure to a silanising solution results in a chemical reaction, as illustrated in Fig 5.2. The hydrogen atoms at the substrate surface are replaced by $(CH_3)_2Si$. This hydrophobic surface can improve LB film transfer. To carry out silanising treatment, the silicon substrates were immersed in silanising solution in an ultrasonic bath for a period of 10 minutes. On removal, the substrates were rinsed with ultrapure water to remove any traces of HCl before being dried in a stream of nitrogen.

5.2.5 Deposition conditions

Films were transferred from a pure water subphase at a temperature of 18 ± 2 °C and pH of 5.8 ± 0.2. The dipping speed was dependent on the specific material, as was the time between dipping cycles to allow for drying of the deposited film.

5.3 Film thickness measurement

5.3.1 Ellipsometry

Ellipsometry has been used to determine the thickness of LB layers.[4] When a light beam with a known polarisation state is reflected from a specular surface, the amplitude and phase of the parallel and perpendicular components of the electric field of the beam are modified. If a thin film is present on the reflecting surface, the resulting change in the polarisation state of the light beam caused by the film can be measured. The thickness and refractive index of the film may then be calculated, provided that the optical constants of the substrate are known. In this work, the thickness of thermally grown oxides and LB multilayers on silicon substrates were measured using ellipsometry.

A Rudolph Research AutoEL-IV nulling ellipsometer capable of operating at three different wavelengths i.e. 405.0, 546.1 and 632.8 nm was used. This equipment contained a dedicated computer to control measurements and perform all calculations. This computer had a number of built-in programs applicable to different types of sample.

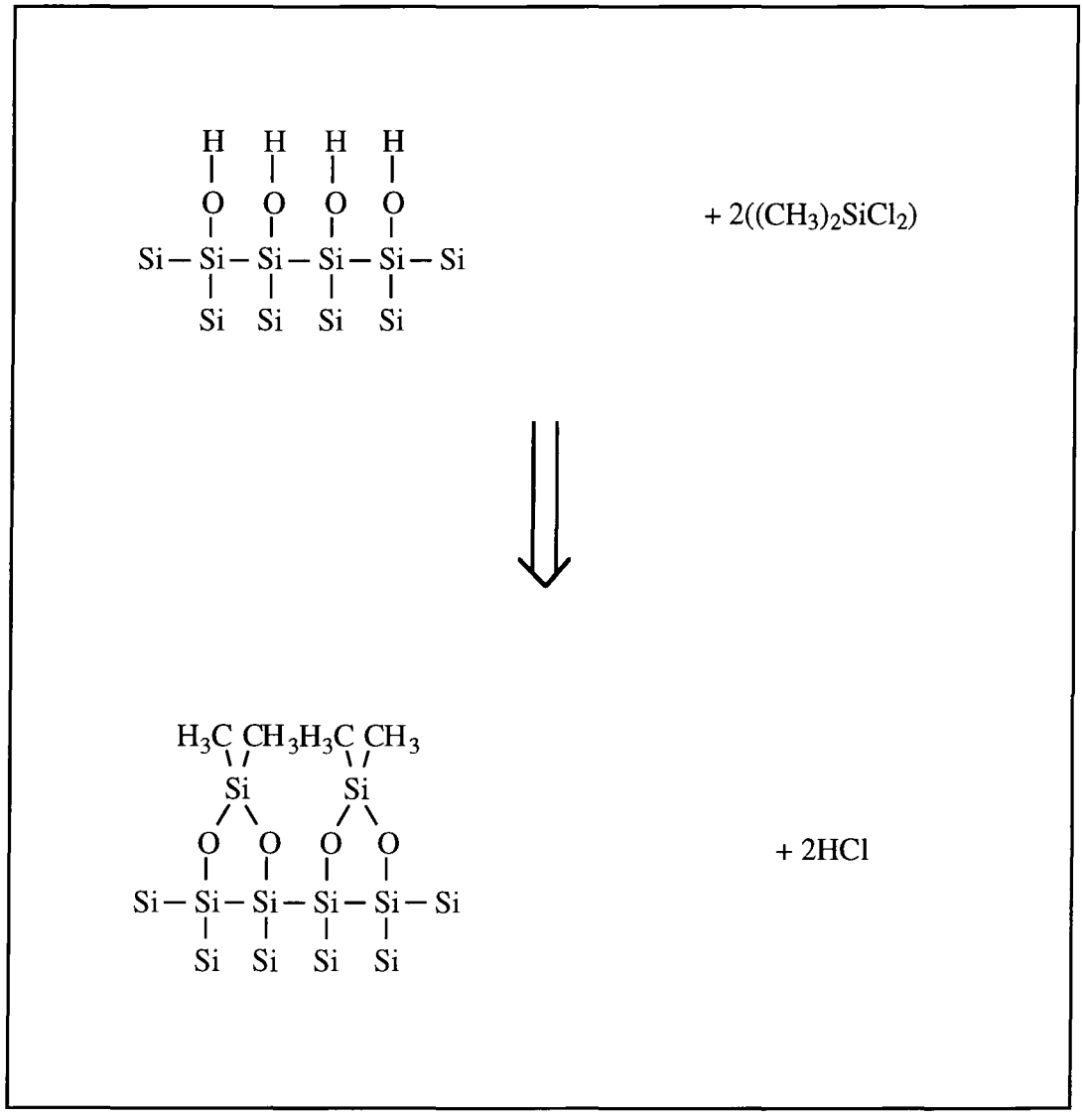

Fig 5.2 **The treatment of a silicon substrate with dimethyldichlorosilane to create a hydrophobic surface.**

The most suitable one for this study assumed an isotropic, non-absorbing film on an isotropic substrate. Although this model does not accurately represent the situation for an ideal LB film, den Engelsen[5] calculated that the thickness of a cadmium eicosanoate monolayer was 2.68 ± 0.02 nm using an anisotropic model, compared to 2.70 ± 0.03 nm when an isotropic model was used. Cresswell[6], working with 22-tricosenoic acid layers, found a layer thickness of 2.89 ± 0.01 nm whichever model was used.

For the ellipsometric measurement of LB layers, silicon substrates cleaned by the method described earlier were used. A stepped LB film structure e.g. 20, 40, 60 layers was deposited, leaving part of the silicon uncoated. It was necessary to measure the optical constants of the substrate and subsequently input these values into the program used to calculate the thickness and refractive index of the LB overlayers. The results obtained by ellipsometry are cyclic, with many possible thickness values calculated during a single measurement. In the Auto-EL IV, a multi-wavelength program was available which would perform measurements using two different wavelengths at the same spot on a sample. The thickness of the LB layer was independent of wavelength and by comparing the possible values obtained from the calculation routine at the two wavelengths used, the program could select any results which matched. A graph of thickness versus number of layers could be plotted and used to determine accurately the thickness per layer of the LB structures.

5.3.2 Surface profiling

The stylus profilometer is a mechanical instrument which has been used to measure the thickness of fatty acid salts.[7] In this technique, a stylus is moved slowly across the surface of the sample under test. The upward force on the stylus varies with the height of the surface and therefore a graph of the pressure, measured electronically, against stylus position provides a profile of the surface which can be calibrated to give height measurements. Since the profilometer detects changes in height, a step must be provided

in the film. For the measurement of the thickness of LB films using this method, multilayer structures were deposited onto polished silicon substrates and a step created by carefully wiping away a portion of the film using a tissue soaked in a suitable organic solvent, usually chloroform. Additionally, to prevent the stylus from penetrating the surface of the film, a layer of aluminium ~ 150 nm thick was deposited by thermal evaporation over the step between the film and the area of cleaned substrate.

The stylus profilometer used was a Tencor Instruments Alpha-step 200. A stylus force of 11±1 mg was used, together with a scan length of 1-2 mm and a sample frequency of 1 per micron.

5.4 Microscopy

5.4.1 Optical microscopy

Film morphology was assessed using a Vickers optical microscope. The microscope was used in reflection mode without polarisation. Objective lenses with magnification factors of 2.5, 4, 10, 400 and 800 times were available. Optical micrographs were recorded using a 35 mm camera.

5.4.2 Electron microscopy

LB multilayers of amphiphilic TCNQ compounds have been studied using scanning electron microscopy.[8] The technique was used here to allow detailed investigation of film morphology. A Cambridge Instruments Stereoscan 600 scanning electron microscope (SEM) was used, where the electron beam accelerating voltage was variable and could be set at 1.5, 7, 15 or 25 kV. A 35 mm camera was available for the recording of electron micrographs.

5.4.3 Electron probe microanalysis

Material characterisation using an electron microprobe (EMP) to excite X-rays

characteristic of the elements present in the sample under investigation is called electron probe microanalysis (EPMA).[9] EPMA makes use of the electron beam, focusing lenses and deflection coils of a scanning electron microscope, with the addition of an X-ray detector. Two types of detector are used, giving energy-dispersive spectrometers (EDS) which are useful for rapid sample analysis and wavelength-dispersive spectrometers (WDS) for high resolution measurements. The EDS has the ability to analyse all energies simultaneously, the detector can be positioned very close to the sample resulting in high detection efficiency. In this work, a Link systems 860 series 2 EDS fitted to a Cambridge Instruments Stereoscan 600 SEM was used. X-rays emitted from the sample passed through a thin beryllium window onto a liquid nitrogen cooled reverse biased Si(Li) detector. The charge pulses (generated by X-rays absorbed by the detector) were converted to voltage pulses which were amplified and passed to a multi-channel analyser (MCA). The MCA sorted the pulses and assigned these to the appropriate channel of the display, with the channel number calibrated to correspond to X-ray photon energy. The energy spectrum was displayed on a CRT and the software of the analyser allowed for the positioning of cursors corresponding to the characteristic X-rays of different elements to aid in the identification of the components in the sample. Hard copy of spectra and raw data were available from a dot matrix printer.

5.5 Optical absorption spectroscopy

The optical absorption spectra of multilayer LB films deposited onto microscope glass slides was measured over the range 300-2500 nm in 1 nm steps using a Perkin-Elmer Lambda 19 UV-VIS-NIR dual beam spectrophotometer. A baseline was recorded with two identical glass slides as samples, one in the path of each beam. One of these was then removed and replaced by a slide with an LB coating (making sure that the beam was incident on the coated area of the slide). The other remained as a reference while the spectrum was recorded.

5.6 Electrical measurements

5.6.1 Two probe dc conductivity

The sample geometry for the two probe measurement of the in-plane conductivity of a thin film is shown in Fig 5.3. For contacts of length l cm distance d cm apart on a film of thickness t cm, the conductivity of the film in S cm^{-1} is given by the relationship

$$\sigma = \frac{I}{V}\frac{d}{t\,l} \qquad 5.2$$

where I is the current in amps flowing due to an applied bias of V volts. Hence, by careful measurement of the dimensions of the electrodes and if the thickness of the film is known, the conductivity can be calculated.

The experimental circuit for the two probe measurement of the current versus voltage characteristics of thin film samples is shown in Fig 5.4. The measurements were made under vacuum in a sealed and electrically grounded metal sample chamber. Contacts to the sample under test were made using gold ball probes. All electrical connections between the sample chamber, the variable voltage source and picoammeter were screened to minimise noise interference. Voltages were supplied by a Time Electronics type 2003S voltage calibrator and 10 x dc-dc converter giving a maximum bias of 100 V. Current flow was measured using a Keithley Instruments 410A picoammeter.

Schematic representations of the three contact types employed for two probe conductivity measurements are shown in Fig 5.5. These were (a) Acheson Colloids Electrodag 915 high conductivity silver paint or Leit-C conductive carbon cement applied after deposition of the LB layers, (b) gold deposited after the LB film and (c) gold undercoated with chromium deposited before the LB film. Silver paint and carbon cement were applied with a thin wire and 10 minutes were allowed for the paint or cement to dry before measurements were made. Gold and chromium/gold contacts were deposited by thermal

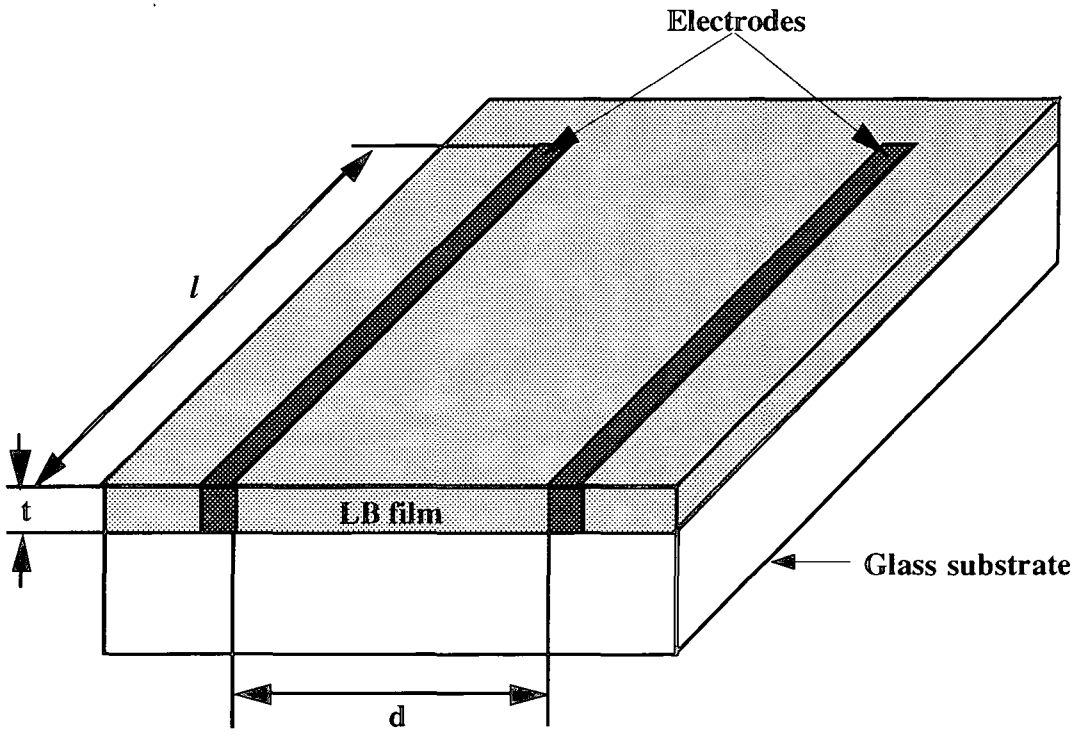

Fig. 5.3 Sample geometry for two-probe conductivity measurement.

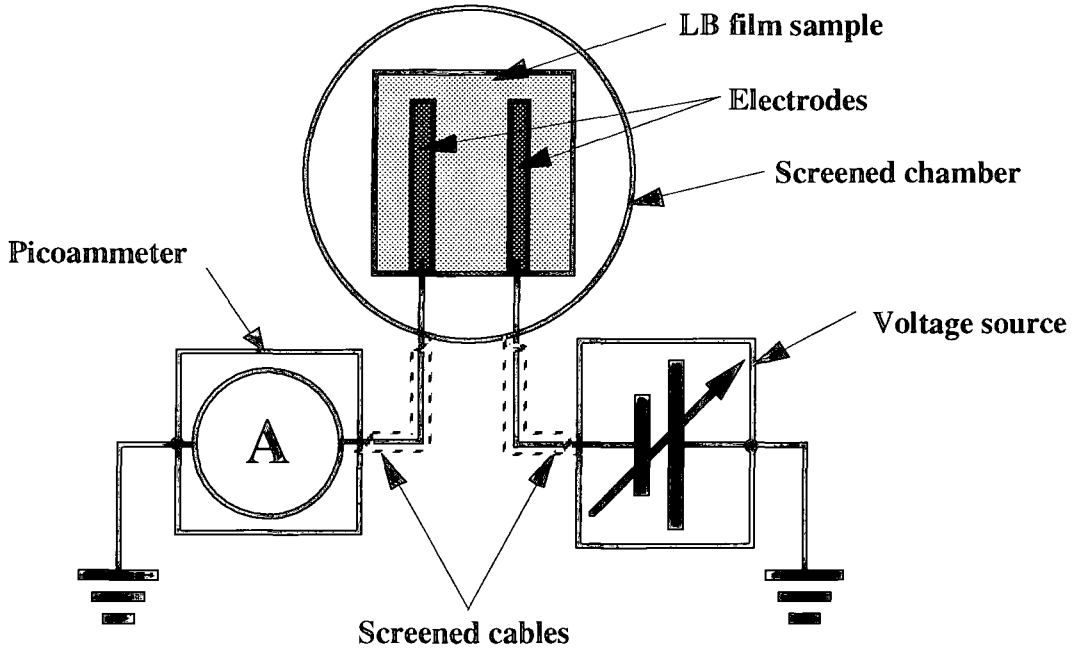

Fig. 5.4 Electrical circuit for two-probe conductivity measurement.

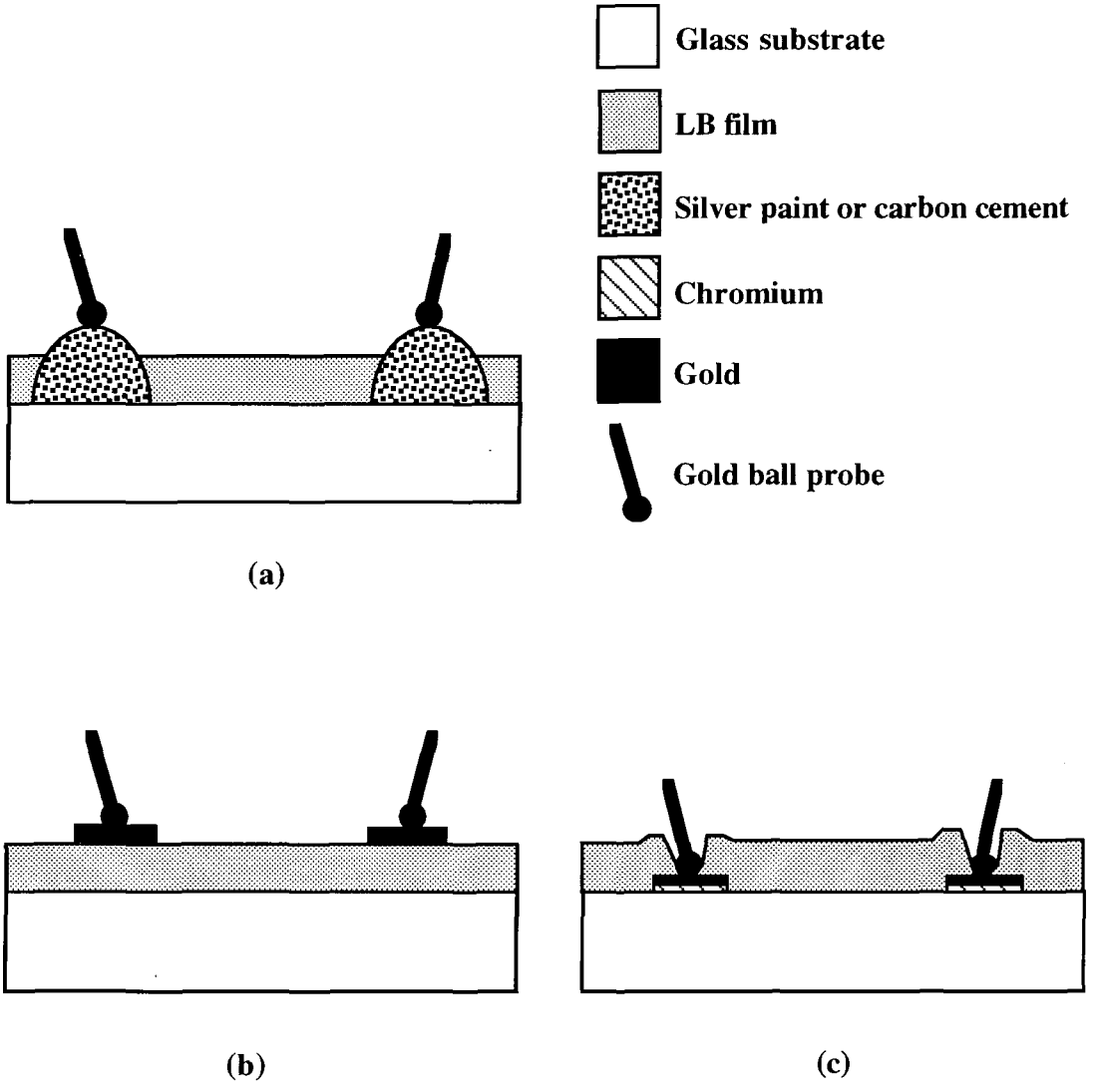

Fig. 5.5 Contact types for two-probe conductivity measurement.

(a) Silver paint or carbon cement.
(b) Gold top contacts.
(c) Gold (undercoated with chromium) bottom contacts.

evaporation. In all cases, the distance between the contacts was varied and a plot of resistance versus distance used to determine the contact resistance.

5.6.2 Low temperature conductivity

To investigate temperature induced variations in the dc electrical conductivity of samples, an Oxford Instruments liquid nitrogen exchange gas cryostat was used. The unit was constructed around a sample tube with an internal diameter of 20 mm to which a copper heat exchanger was attached. This heat exchanger was cooled with liquid nitrogen fed from a stainless steel reservoir vessel via a supply tube. Nitrogen gas leaving the heat exchange block could exit from the cryostat through an exhaust valve in the top plate. The reservoir vessel was regularly topped up during the course of an experiment to ensure a continuous supply of coolant. A vacuum system consisting of a rotary vane backing pump and an oil vapour diffusion high vacuum pump was used for evacuation of the equipment. Also, an activated charcoal 'sorb' which would cryopump when cooled was incorporated in the equipment ensuring a good insulating vacuum for the liquid nitrogen in the reservoir.

The samples were cut to a size of approximately 1 cm^2 and held in position on the sample holder with air drying silver paint. Electrical contact to the film was made using evaporated gold, air drying silver paint or conductive carbon cement. 10 minutes were allowed for the paint or cement to dry before measurements were made. The exchange gas was helium and after insertion of the sample, the tube was evacuated and flushed out with gas to ensure removal of any water vapour before closing off.

The heat exchange block was fitted with a platinum resistance thermometer and a 39 Ω resistive heater, allowing the temperature to be measured and controlled. Temperature variation was achieved by balancing the heat input against the cooling power available, which could be regulated by opening and closing the exhaust valve. The required

temperature was set and held constant by an Oxford Instruments DCT2 precision temperature controller.

Current versus voltage characteristics could be measured over the temperature range 77 K to 300 K. Sample current was monitored on a Linseis chart recorder and allowed to stabilise before results were recorded.

5.6.3 Capacitance

A schematic diagram of the structure used for the measurement of the capacitance of multilayer LB films is shown in Fig 5.6. Glass slides cleaned by the standard technique and then coated by thermal evaporation with gold (undercoated with chromium to assist adhesion of the gold to the glass) were used as substrates. A base layer consisting of 40 layers of 22-tricosenoic acid was deposited onto this, followed by a stepped thickness structure of the charge transfer complex. Finally silver dots of diameter 1 mm and thickness 400 nm were carefully evaporated on top of this to act as top electrodes. A Boonton 72BD digital capacitance meter operating at 1 MHz was used to make the capacitance measurements.

5.7 Device fabrication

A schematic diagram of the thin film transistor (TFT) structure used in this work is shown in Fig. 5.7. Devices were fabricated on p-type silicon slices, with a resistivity of 14 Ω cm. This substrate also served as the gate electrode for the device. Three inch wafers with 100 orientation were used. These were cut into four pieces by cleaving along the crystal plane after first scribing with a diamond tipped cutting tool.

5.7.1 Substrate preparation

The processing of silicon slices for use as substrates was undertaken in a class 1000 microelectronics clean room. Several pieces of silicon were processed simultaneously.

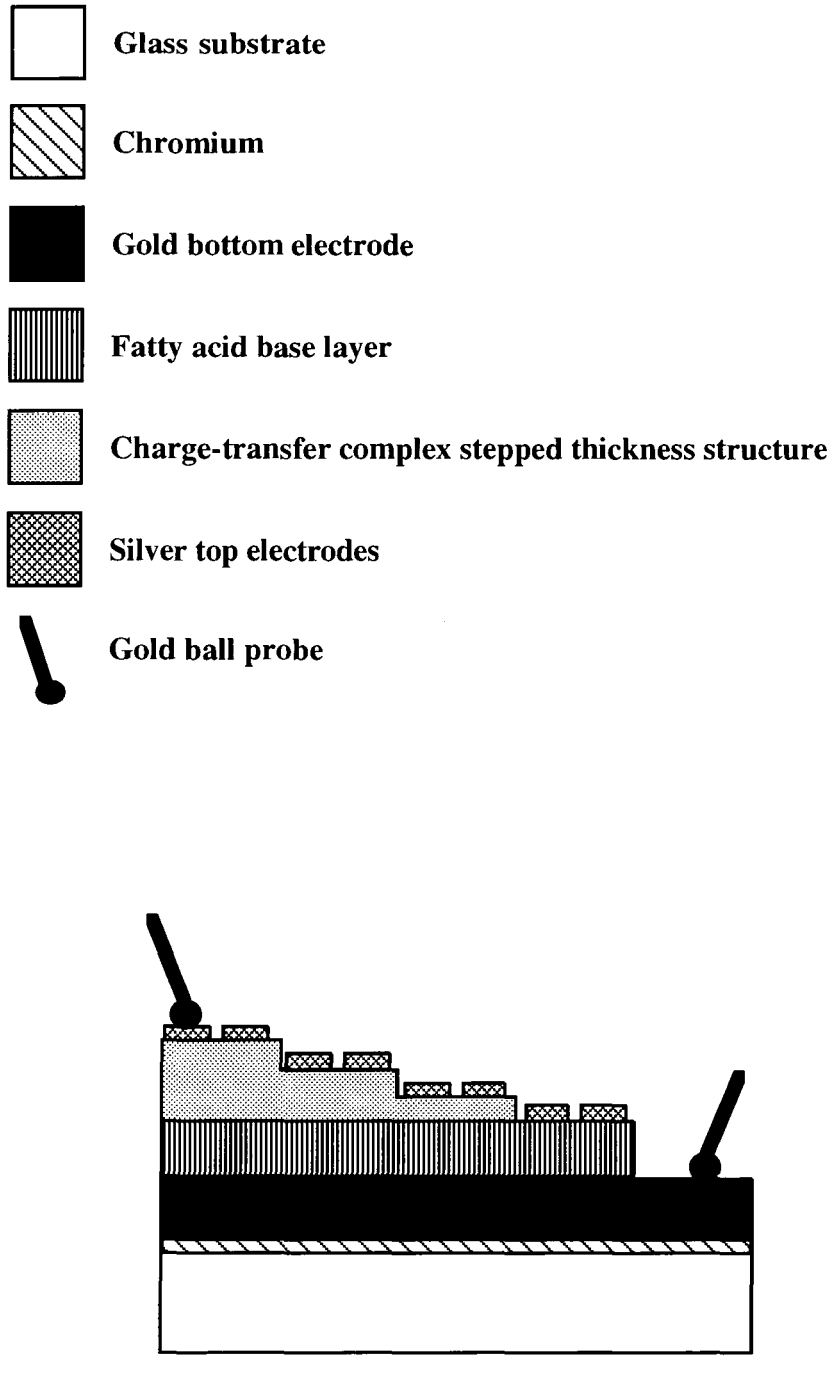

Fig. 5.6 Sample structure for the measurement of the capacitance of LB layers.

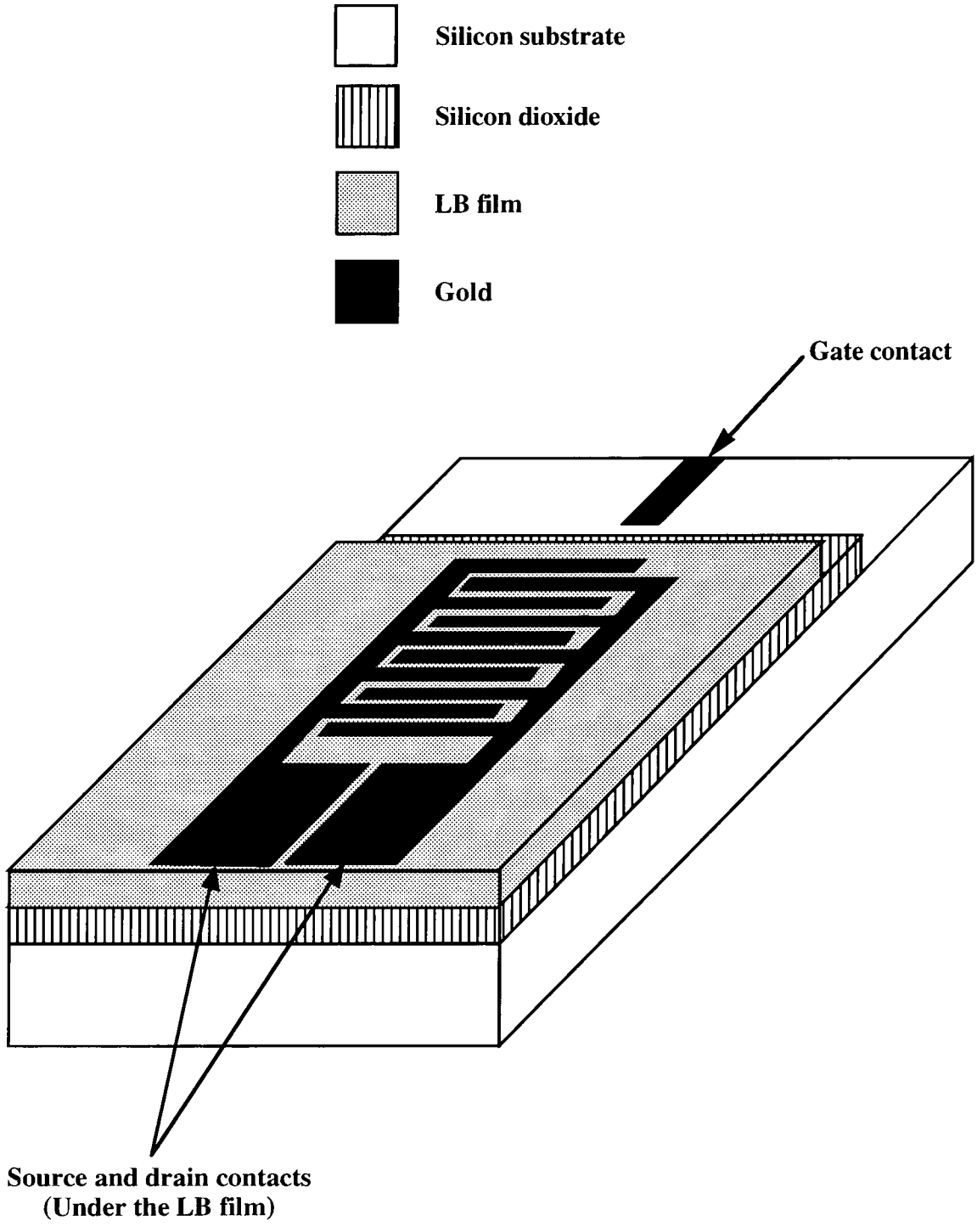

Fig.5.7 Schematic diagram of a TFT structure.

These were supported in a glass jig throughout the cleaning procedure. First, to remove any grease, the samples were immersed in boiling Aristar grade 1,1,1-trichloroethane on an electric hotplate for five minutes. This step was repeated using fresh solvent and the second cycle was followed by agitation in an ultrasonic bath for one minute. The slices were then rinsed, firstly with Aristar grade propan-2-ol and then with ultrapure water before being boiled in a solution consisting of one part concentrated sulphuric acid to one part 100 volumes hydrogen peroxide, for a period of thirty minutes. This solution simultaneously oxidised and etched the silicon surface. Consequently, the first few microns of the surface were removed, along with any scratches or other physical damage. Following a wash in ultrapure water, the slices were etched in a 10% hydrofluoric acid solution for two minutes to remove any residual oxide layer. A further rinse in ultrapure water was carried out and finally the jig containing the slices was transferred to a recirculating wash bath containing ultrapure water. This bath was fitted with a meter to measure the resistivity of the recirculating water and give an indication of the cleanliness of the slices. A resistivity value of 10^7 Ω cm was considered to be high enough to indicate that the substrates had been rinsed for long enough and were now clean.

5.7.2 Oxide growth

Gate oxides were grown in a dry oxidation furnace at a temperature of approximately 1000 °C. The oxide thickness obtained could be set by varying the oxidation time or temperature. The clean silicon slices were transferred from the ultrapure water wash bath into a beaker of Aristar grade propan-2-ol and agitated in an ultrasonic bath for thirty seconds before being dried in a stream of nitrogen gas and placed in a glass boat. The boat containing the samples was placed in the mouth of the furnace for 10 minutes in a nitrogen flow of one litre min^{-1} and then pushed to the centre of the temperature 'flat zone' of the furnace and left there for a further ten minutes. The nitrogen was then turned off and replaced by an oxygen flow of a one litre min^{-1} for the required duration of the oxidation. When the correct length of time had elapsed, the oxygen flow was removed

and the nitrogen flow restored. The samples were left at the centre of the furnace for a further ten minutes and then pulled back to the mouth to cool before removal. The oxide thicknesses were measured by ellipsometry in order to obtain an exact value.

5.7.3 Metallisation

After oxidation, the silicon slices were coated with a 40 nm thick layer of gold undercoated with a thin layer of chromium (included to improve adhesion of the gold to the substrate) by thermal evaporation in an Edwards 306A vacuum coating system. The gold was evaporated at a rate of ~ 2 nm s^{-1}.

5.7.4 Mask fabrication

To create the required interdigitated electrode pattern in the chromium/gold metal film, a mask was required. This was fabricated using a photographic technique. Initially, the pattern was cut into a sheet of 'Stabilene Cut 'n' Strip' film. This material consisted of clear acetate coated with a red film which could be cut with a sharp blade and then peeled away allowing unwanted areas to be removed. The pattern created is shown at 0.5 x actual size in Fig 5.8. This original pattern was attached to a light box and exposed onto a Kodak 1A high resolution plate using a large format Sinar camera. After development, a negative, reduced by a factor of 13 from the original, was produced. This was then used in a Watson 'step and repeat' camera to create a 5 x 5 matrix of patterns on a second photographic plate. A further reduction of 10 times was introduced at this stage giving a final gap of 20 μm with a channel width of 4 cm.

5.7.5 Photolithography

The steps involved in the photolithographic patterning of a thermally evaporated metallisation on an oxidised silicon substrate are illustrated in Fig 5.9. The samples were processed directly from the evaporator to ensure that no moisture was present on the

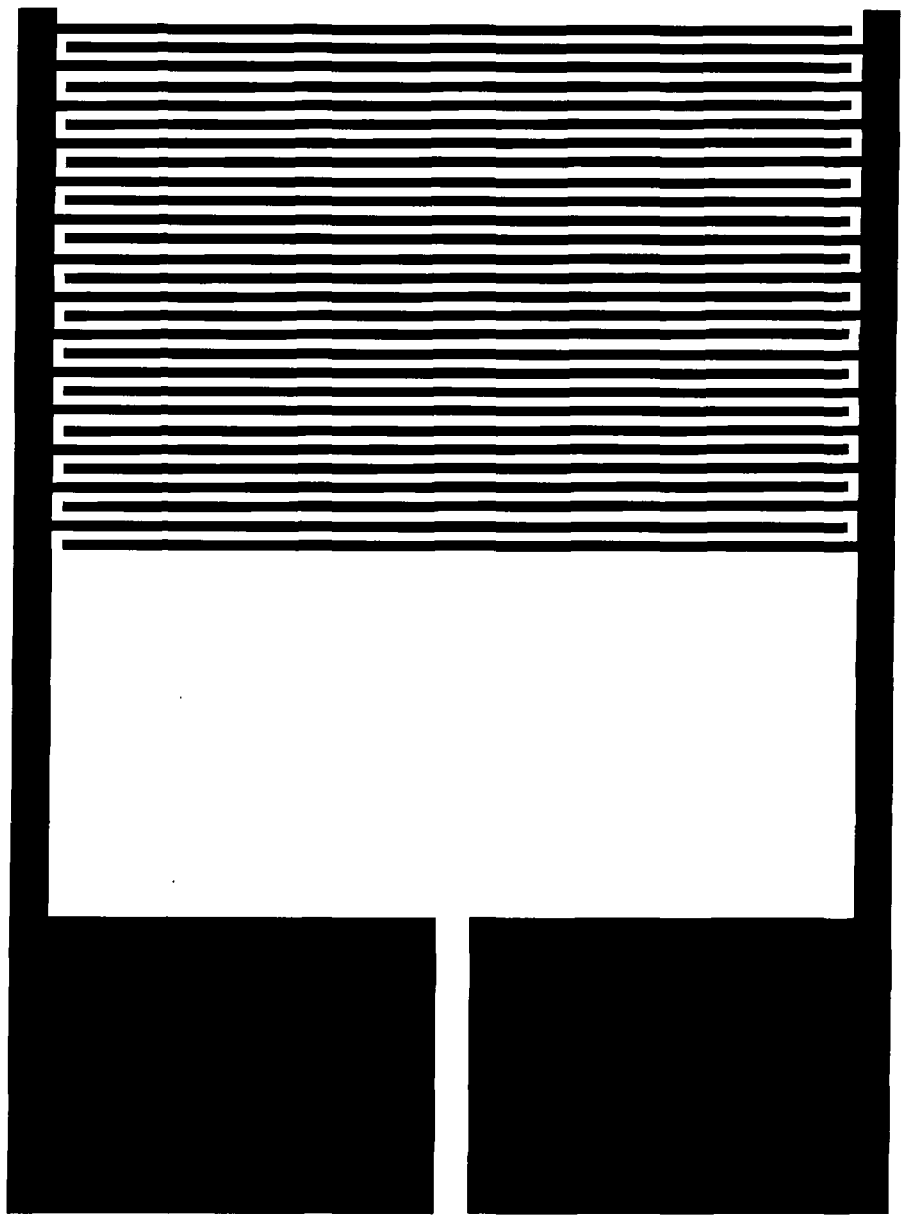

Fig. 5.8 **Original pattern for the production of the interdigitated electrode mask shown at one half of actual size.**

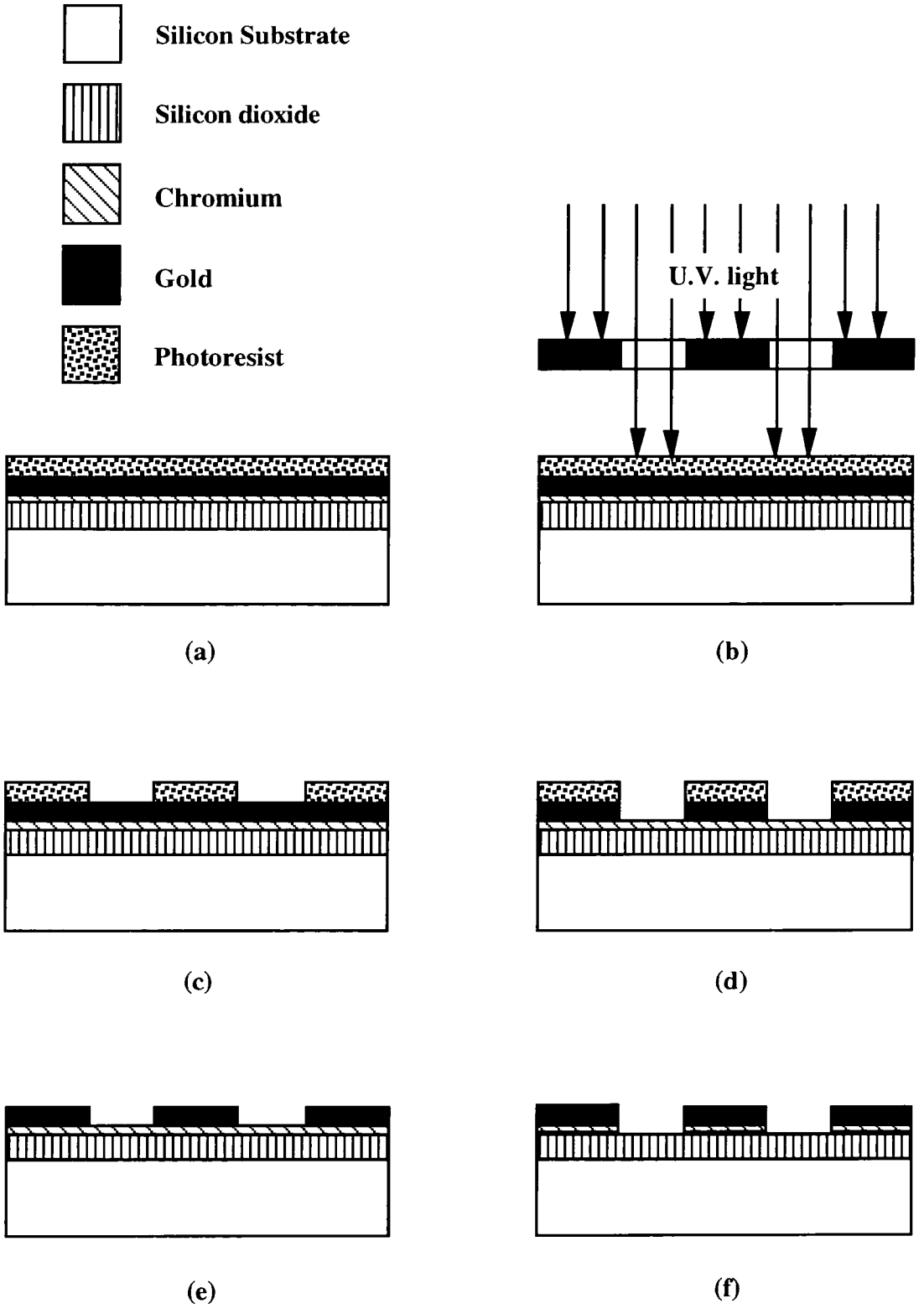

Fig. 5.9 Steps in the photolithograpic patterning of gold, undercoated with chromium, to produce interdigitated electrode structures

(a) Metallised wafer with resist layer.
(b) Unwanted resist regions are exposed to U.V. light through a shadow mask.
(c) Exposed resist regions are dissolved away.
(d) Unwanted gold regions are etched away.
(e) Resist layer is dissolved away.
(f) Unwanted chromium regions are etched away.

surface. Each slice was placed in turn onto the turntable of a spinner, and held in position by a vacuum chuck. A small amount of liquid photoresist (Shipley Microposit S1813) was applied to the centre of the slice and the turntable spun at a speed of ~ 1000 r.p.m. for 30 seconds to evenly distribute the resist across the surface (Fig 5.9(a)). This resist film was baked on a hotplate at 80 °C for 30 minutes to evaporate the solvent. A Kasper Instruments mask aligning machine was used to expose the samples to U.V. radiation (Fig 5.9 (b)) from a high pressure mercury vapour lamp through the photographic mask prepared earlier. The exposed resist became soluble in Shipley Microposit MF312 developer and could be washed away leaving the electrode patterns behind (Fig 5.9 (c)). A solution consisting of 4 g of potassium iodide and 1 g of iodine in 40 ml of ultrapure water was used to etch away the unwanted gold areas (Fig 5.9 (d)). The resist patterns were dissolved away with Aristar grade Acetone, and finally, the unwanted chromium film was etched away using solutions of potassium hexacyanoferrate (1g per 3ml water) and sodium hydroxide (1g per 2ml water) mixed in the ratio 3:1 (Fig 5.9 (f)).

5.7.6 Gate contact

The thermally grown gate oxide was etched away using a 10% solution of HF carefully applied using a small paintbrush before metallic contacts to the silicon substrate (to allow application of a gate bias voltage) were deposited by thermal evaporation.

5.7.7 LB coating

The silicon wafer substrates with their electrode patterns were coated with a stepped thickness structure of organic semiconductor material by the LB technique. A schematic diagram of the finished TFT array with LB overlayers is shown in Fig. 5.10.

5.8 Device characterisation

5.8.1 Gate oxide capacitance

A parallel plate MOS capacitor structure (using the gate oxide as the dielectric) was made

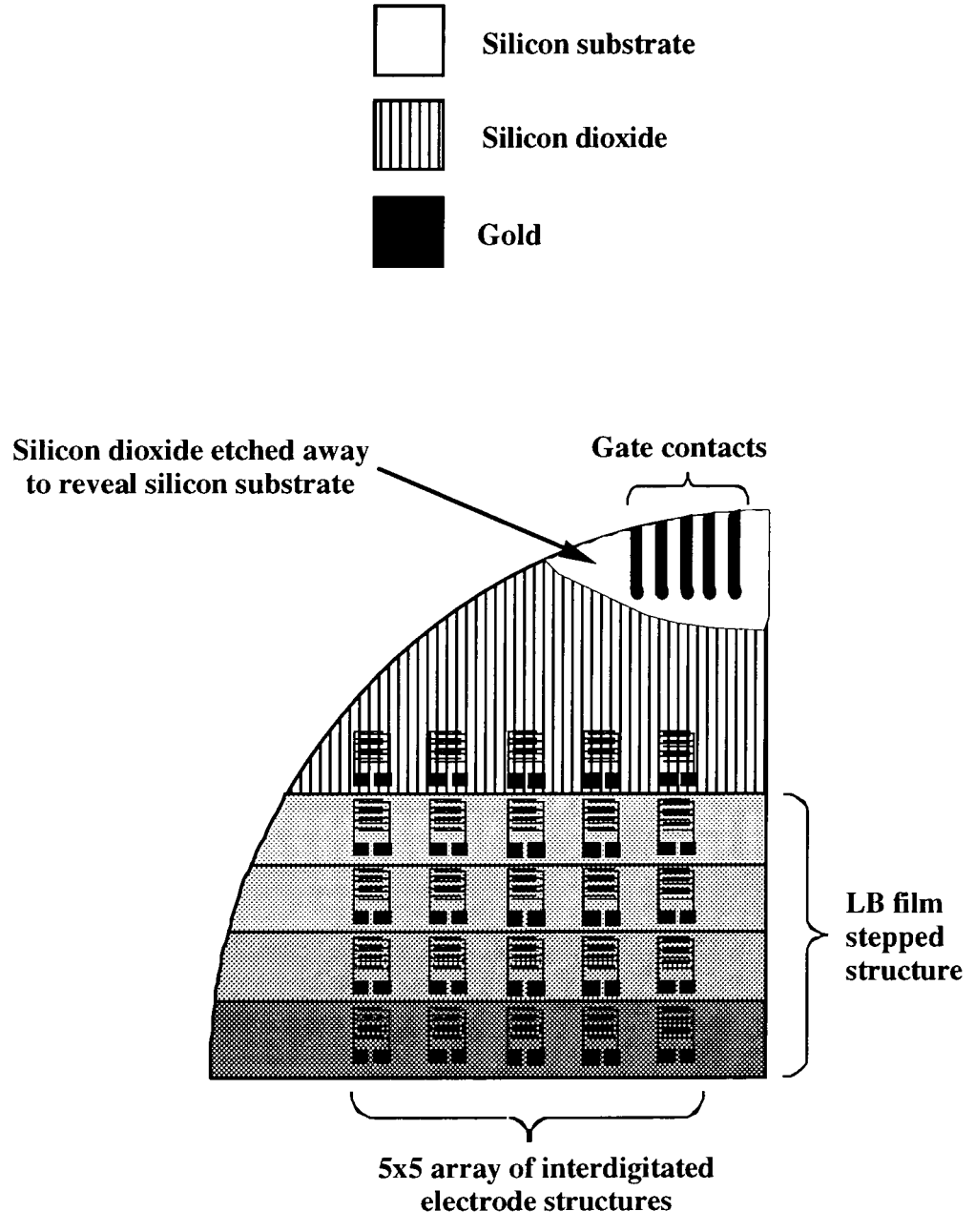

Fig. 5.10 Schematic diagram of a completed array of thin film transistors complete with LB layers of an organic semiconductor.

by thermally evaporating gold dot electrodes *ca* 100 nm thick and 1 mm in diameter on top of the oxide. Gold ball probes were used to make contact to the gate contact and the top contact. Capacitance versus voltage measurements were made in a screened metal sample chamber. A Boonton 72BD digital capacitance meter operating at 1 MHz was used, together with a Time Electronics type 2003S voltage calibrator to provide dc bias.

5.8.2 Electrical characteristics

A diagram of the equipment used for the investigation of device characteristics is shown in Fig. 5.11. Electrical measurements were performed under vacuum in an electrically screened metal sample chamber. Electrical contacts to the source, drain and gate were made using gold ball probes. The electrical circuit used is illustrated in Fig. 5.12. Drain-source and gate voltages were provided by Time Electronics type 2003S voltage calibrators. In the case of the gate voltage, a 10 x dc-dc converter was employed to give a maximum potential of 100 V. The drain current was displayed on a Keithley Instruments 410A picoammeter.

5.9 Summary

Details of the methods used for the characterisation of floating organic layers and the deposition of LB films on solid substrates have been described. The measurement of the thickness of transferred multilayer films using ellipsometry and surface profiling and the observation of film morphology and composition using optical and scanning electron microscopy and energy dispersive spectroscopy were included. The techniques used to measure the room temperature and low temperature conductivity and the capacitance of LB structures were explained. The stages in the fabrication of organic thin film transistors and the subsequent electrical measurement procedures to determine device characteristics were also described.

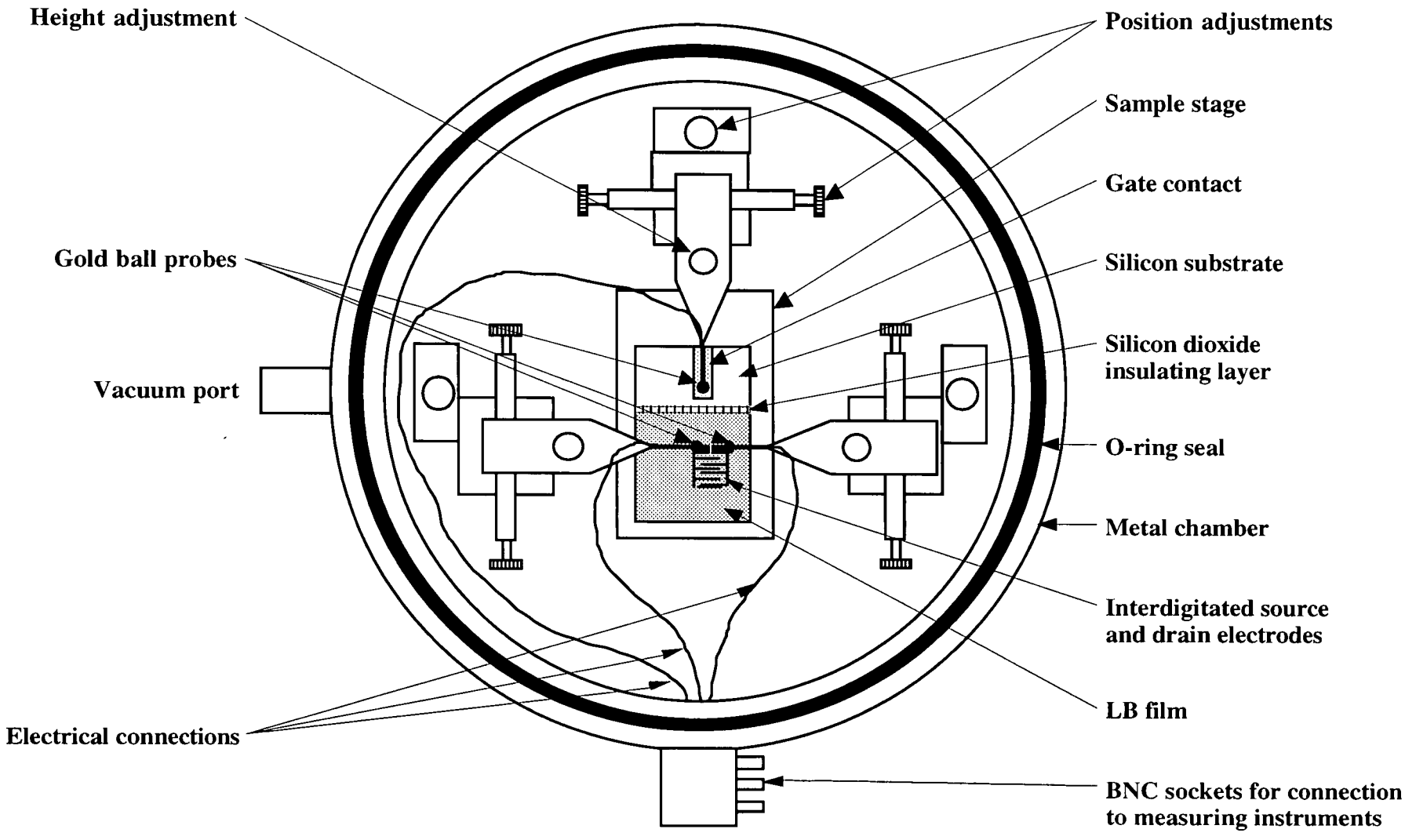

Fig. 5.11 Sample chamber for electrical measurements.

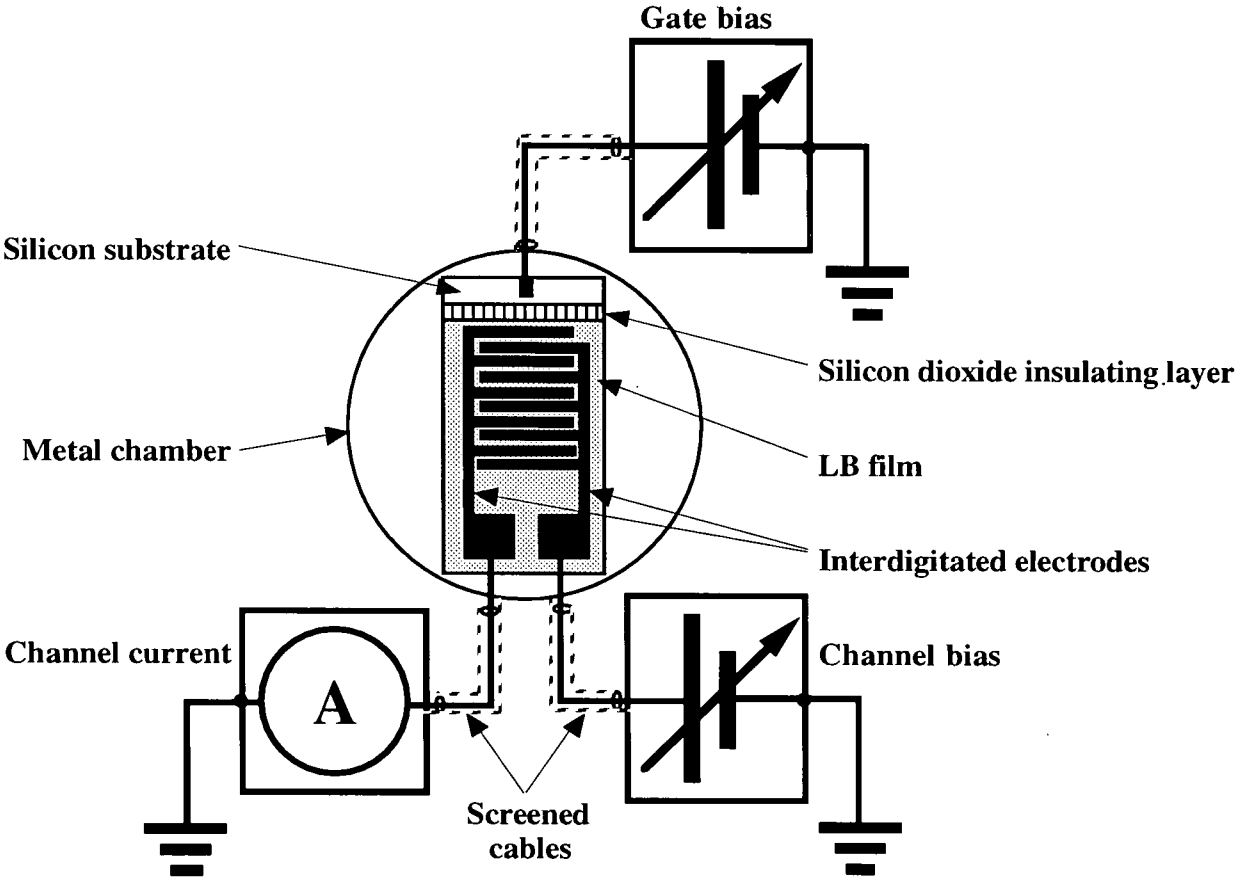

Fig. 5.12 Electrical circuit used for the measurement of TFT characteristics.

References

1. M. C. Petty and W. A. Barlow in *'Langmuir-Blodgett Films'* ed. G.G. Roberts, Plenum Press, New York (1990) p. 93.
2. W. D. Harkins and T. F. Anderson. J. Am. Chem. Soc., 59 (1937) 2189-2197.
3. R.A. Hann in *'Langmuir-Blodgett Films'* ed. G.G. Roberts, Plenum Press, New York (1990) p. 17.
4. R. Steiger, Helv. Chim. Acta., 54 (1971) 2645-2658.
5. D. den Engelsen, J. Opt. Soc. Amer., 61 (1971) 1469-1466
6. J.P. Cresswell, PhD Thesis, University of Durham, UK (1992)
7. L. M. Walpita and C.W. Pitt, Electron. Lett., 13 (1977) 210-212.
8. A. Barraud, J. Richard, A. Ruaudel-Teixier and M. Vandevyver, Thin Solid Films, 159 (1988) 413-419.
9. D. K. Schroder, *'Semiconductor Material and Device Characterisation'* John Wiley and Sons Inc. (1990) p. 521.

Chapter 6

Preparation and Characteristics of Films Containing Octadecanoyl-TTF

6.1 Introduction

In this chapter, the LB film forming properties and characteristics of multilayer films containing the long chain TTF derivative octadecanoyl-TTF (ODTTF) are described. The conditions for LB deposition are discussed, and pressure versus area isotherms presented. Thickness measurements have been performed (using ellipsometry and surface profiling) with multilayer structures on single crystal silicon, and a possible arrangement for the molecules in these films is suggested. The room temperature and low temperature dc electrical characteristics are shown, and a model for the bulk conductivity is described, supported by optical micrographs giving structural information. Film morphology has been studied using the SEM, and compositional information obtained from EDS analysis. Optical absorption spectra are included, and the observed absorption bands related to the behaviour of the electrical conductivity.

6.2 Monolayer forming properties

The chemical structure and space-filling model of ODTTF are shown in Fig 6.1 (a) and (b), respectively. The dimensions of the molecule, obtained from the standard CPK molecular model, are marked on the figure. This material could not be reliably transferred to a solid substrate in pure form, so it was necessary to mix it with a quantity of octadecanoic acid (OA) or pentacosa-10,12-diynoic acid (PA) (1:10 to 1:0.14; acid:ODTTF) to aid the deposition of multilayer films. The chemical structure of OA and PA are shown in Fig 6.2 (a) and (b), respectively. Separate solutions of ODTTF and fatty acid were prepared to a concentration of ~ 1 gl^{-1}, in a pair of volumetric flasks, using chloroform to dissolve the solid material. The amount of each solution required to give the desired molar ratio was then accurately measured into a third flask using a

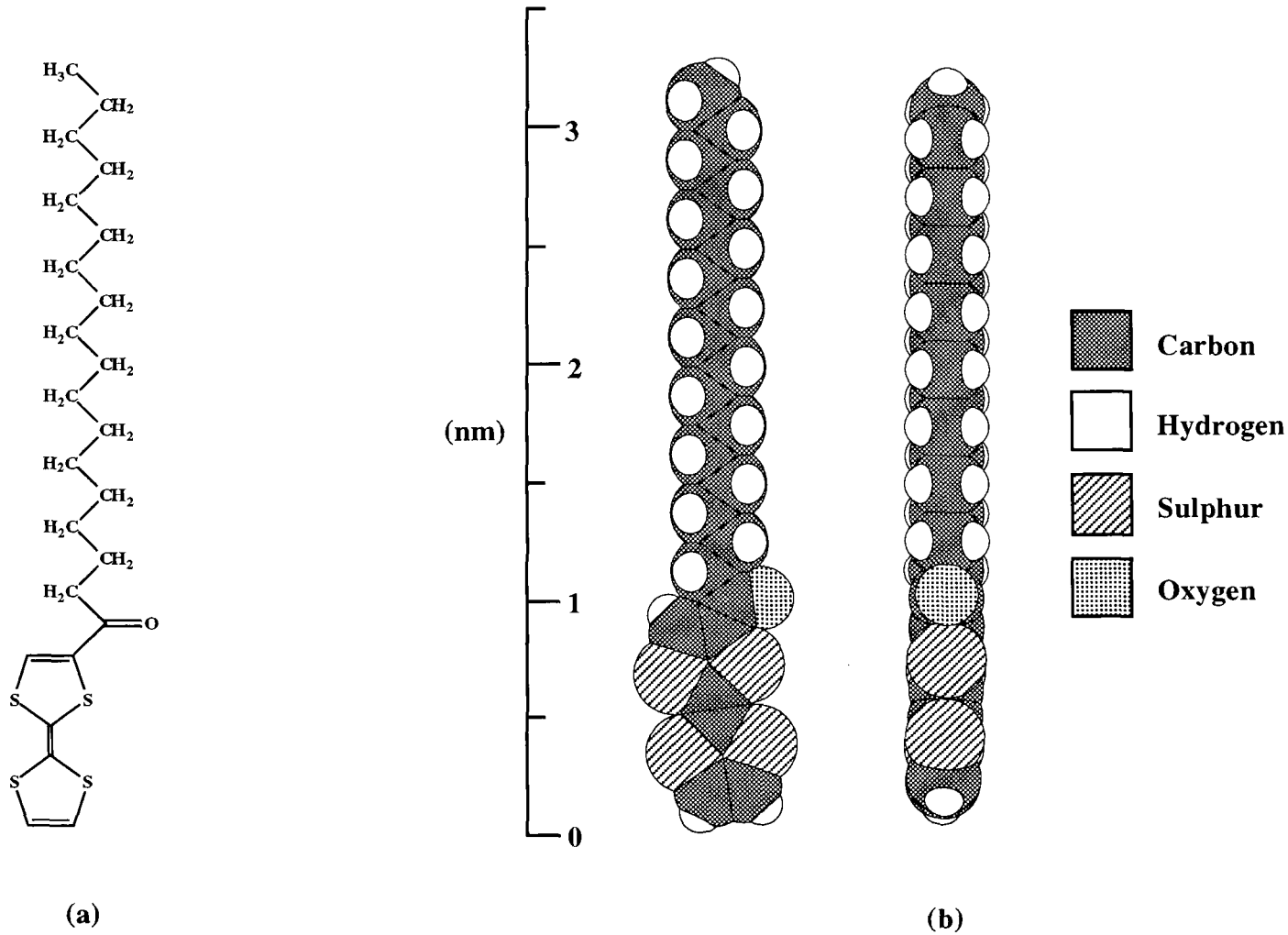

Fig. 6.1 **(a) Chemical structure and (b) space-filling molecular models of ODTTF.**

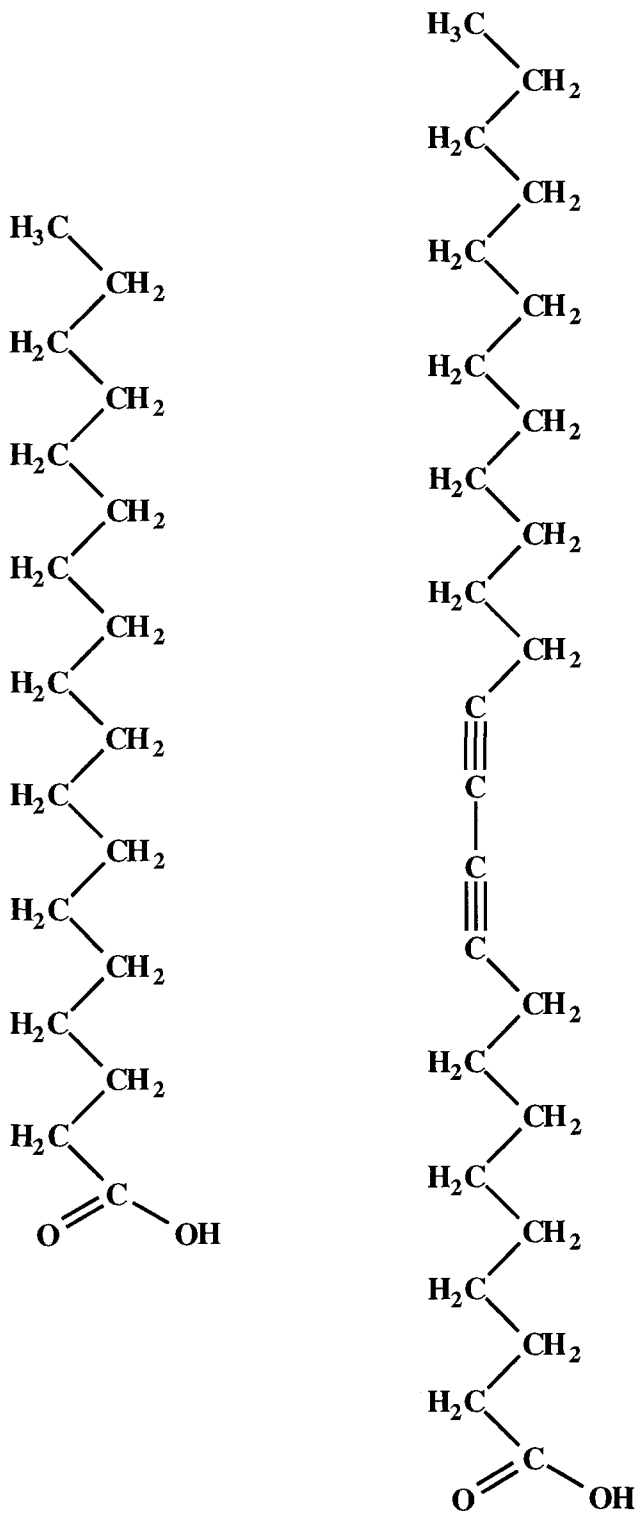

Fig. 6.2 Molecular formulae of (a) OA and (b) PA.

transferpettor. A suitable volume of this mixture (50-200 μl) was distributed over the surface of a pure water subphase. A time was then allowed for evaporation of the chloroform solvent. Pressure versus area isotherms were recorded at a compression speed of 2.6±1.9 x 10^{-3} nm^2 $molecule^{-1}$ s^{-1}. Fig. 6.3(a) shows an isotherm plot for a monolayer of pure ODTTF. The isotherm is quite condensed and the limiting area per molecule, obtained by extrapolating the steepest portion of the isotherm back to zero surface pressure, is approximately 0.25±0.02 nm^2. This is in close agreement with the cross sectional area of the molecule obtained from the space filling model (0.26±0.05 nm^2), indicating that the molecules are probably arranged with their alkyl chains almost perpendicular to the subphase surface. Fig 6.3(b) is a pressure versus area isotherm measured for a mixed monolayer of OA:ODTTF in the ratio 1:2.3. Here, it was assumed that the cross sectional area of each OA molecule in the film was 0.2 nm^2 and the x-axis scale was adjusted, by subtracting the total area of the OA in the monolayer, to indicate the area occupied by each ODTTF molecule. It can be seen that the limiting area per molecule in this case is 0.27±0.02 nm^2, again suggesting that the molecules were arranged with their long axes normal to the plane of the subphase. Fig 6.3(c) shows a pressure versus area isotherm obtained from a mixed monolayer of PA:ODTTF in the ratio 1:3. Again, the area scale has been adjusted, by subtracting the area occupied by the PA in the film, to show area per ODTTF molecule. An area per ODTTF molecule of 0.25±0.02 nm was measured for the condensed floating film. In all of these cases, the material was allowed to stand uncompressed on the surface of the water for 10 minutes before the isotherm was recorded. Changes were negligible when the layers were expanded and subsequently re-compressed, and there was no difference when the material was left on the subphase for times greater than 10 minutes before the initial compression.

6.3 LB film deposition

Mixed monolayers of ODTTF and either OA or PA were compressed to a surface

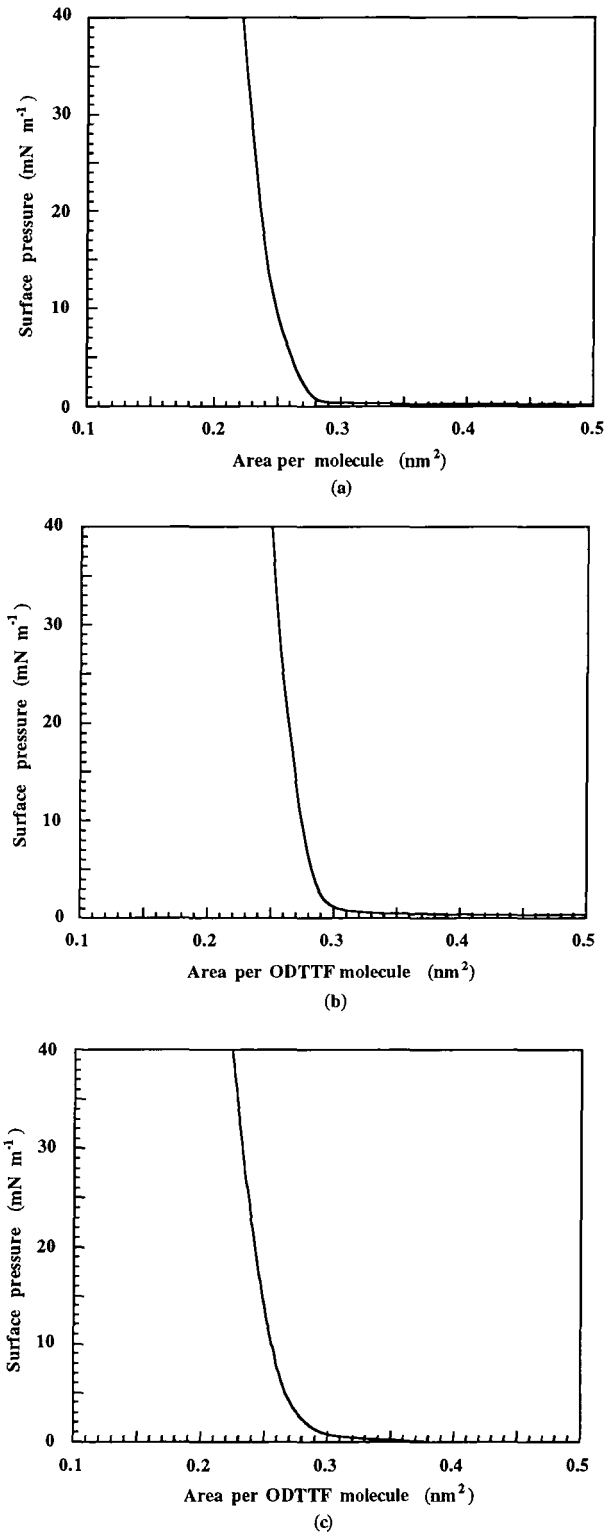

Fig. 6.3 **Pressure versus area isotherms of**

(a) pure ODTTF
(b) OA : ODTTF in the ratio 1 : 2.3
(c) PA : ODTTF in the ratio 1 : 3

In (b) and (c), the x-axis has been adjusted to represent the area per ODTTF molecule.

pressure of 30 mN m^{-1} for transfer to solid substrates - microscope glass slides and single crystal silicon wafers. Both types of substrate were cleaned by the standard technique and in some cases treated with silanising solution to produce a hydrophobic surface. Dipping was started with the substrates positioned in air above the surface of the subphase, and deposition was carried out at a speed of 2 mm min^{-1}, allowing the substrates to stand in air for 10 minutes to enable the transferred layers to dry between cycles. Transfer ratios of 1.0 ± 0.1 were recorded for both hydrophilic and hydrophobic substrates.

6.4 Film properties:octadecanoic acid mixed with octadecanoyl-TTF

6.4.1 Thickness measurements

Ellipsometric and surface profiling studies were carried out using multilayer structures on silicon substrates. For ellipsometry, a multi-wavelength program was used, operating at 632.8 and 546.1 nm, which would select matching thickness values from the results of two measurements performed at the different wavelengths.

A plot of thickness versus number of layers for as-deposited films of OA:ODTTF, in the ratio 1:2.3, on hydrophilic and hydrophobic silicon substrates, is shown in Fig. 6.4. The data points lie on a straight line, confirming the reproducible nature of monolayer transfer. The layer thickness of these samples was found to vary with the ratio of the components. A plot of average layer thickness (measured using ellipsometry) versus ODTTF content, obtained for 19-layer films on hydrophilic silicon substrates, is shown in Fig. 6.5. The straight line fit, extrapolated between x=0 and x=1, intercepts the y-axis at thickness values of 2.55 ± 0.03 nm and 3.45 ± 0.05 nm, respectively. These values compare well with the lengths of the OA and ODTTF molecules, i.e. 2.5 ± 0.1 nm and 3.3 ± 0.1 nm, respectively, obtained from the molecular models. The measured layer thickness is equal to the weighted average of the lengths of the two component molecules. One possible arrangement in these films, in which the molecules are

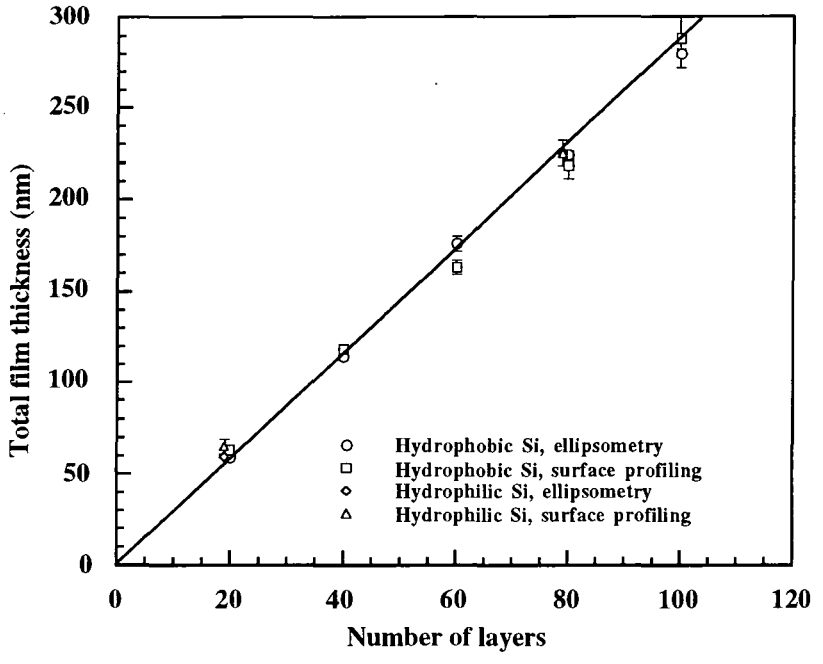

Fig. 6.4 Total thickness vesus number of layers for as-deposited films of OA:ODTTF in the ratio 1:2.3.

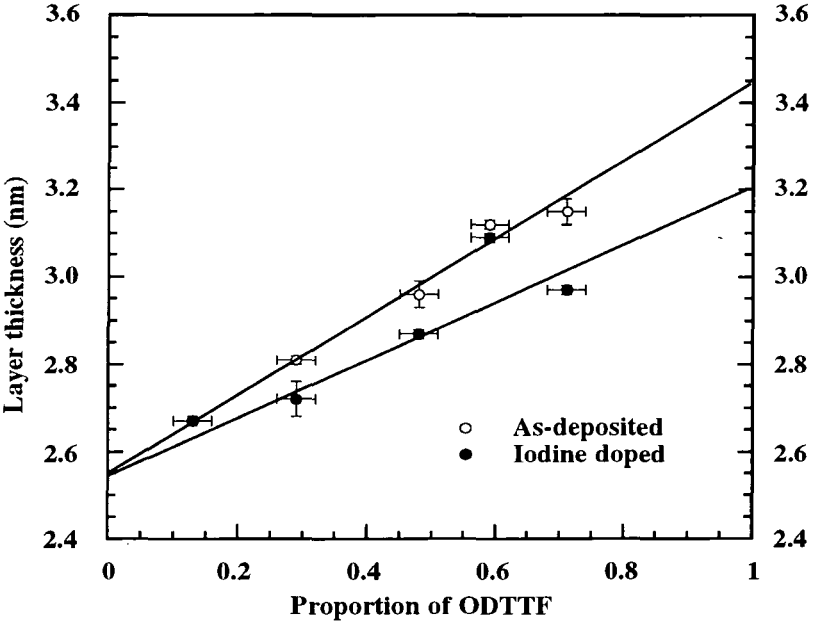

Fig.6.5 Average layer thickness, obtained from ellipsometry measurements, plotted against the proportion of ODTTF contained in 19-layer films of OA:ODTTF.

interdigitated, is illustrated in Fig. 6.6.

The effect of chemical doping with iodine on the thickness of multilayer films of OA:ODTTF was monitored using ellipsometry. The layer thickness, obtained for the same 19-layer films on hydrophilic silicon substrates after exposure to iodine vapour for 22 hours is also plotted in Fig. 6.5. For samples containing a high proportion of ODTTF, a reduction in the layer thickness was observed after doping. Similar behaviour has been reported for LB multilayer films of the related amphiphilic TTF compound, hexadecanoyl-TTF, measured using low angle X-ray diffraction.[1] Here, the d-spacing (the thickness of a bilayer for a Y-type LB multilayer film) was found to contract from 6.1 ± 0.1 nm to 4.2 - 4.4 nm after doping with iodine or bromine. This change was attributed to a combination of tilting of the molecules and interdigitation of the TTF head groups and/or the alkyl chains. In the present work, a much smaller thickness change was observed. It is possible that the presence of the OA reduces the ability of the ODTTF molecules to reorganise.

6.4.2 Room temperature conductivity

Conductivity measurements with multilayer LB films of C_{18}Py-Pd(dmit)$_2$ revealed that evaporated gold electrodes did not provide reliable contact through the whole thickness of the sample (Chapter 7, section 7.5.3). Therefore, the in-plane room temperature dc conductivity of LB samples containing ODTTF was measured using silver paint or carbon cement to establish contacts to the multilayer films. After doping, it was found that the measurements were more consistent if new contacts were prepared after the iodine exposure was completed. Measurements were performed with contacts parallel and perpendicular to the dipping direction, and no anisotropy of the conductivity was observed. Plots of sample resistance versus distance between contacts, after iodine doping and desiccation, for silver paint and carbon cement contacts to a 19-layer film of OA:ODTTF (molar ratio 1:2.3) are presented in Fig. 6.7 (a) and (b), respectively. The

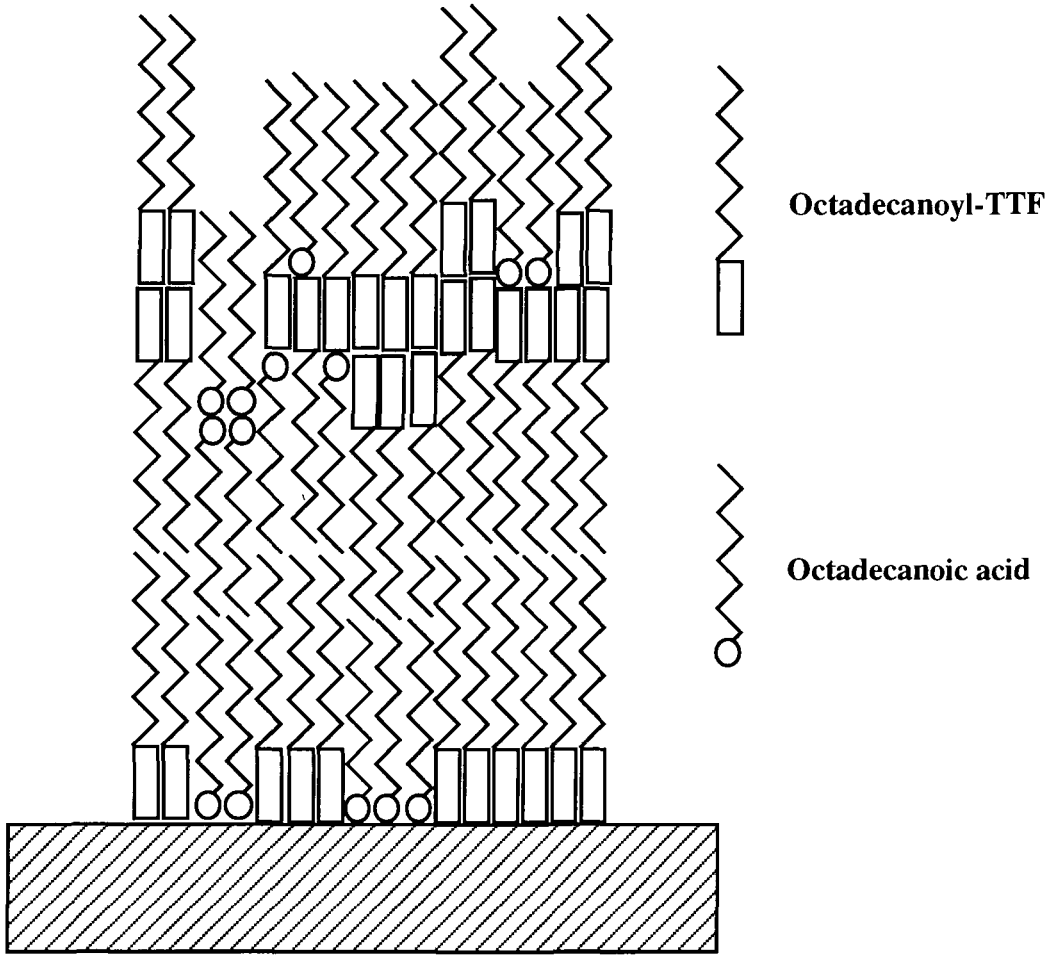

Fig. 6.6 A possible arrangement of the molecules in mixed LB layers of OA:ODTTF.

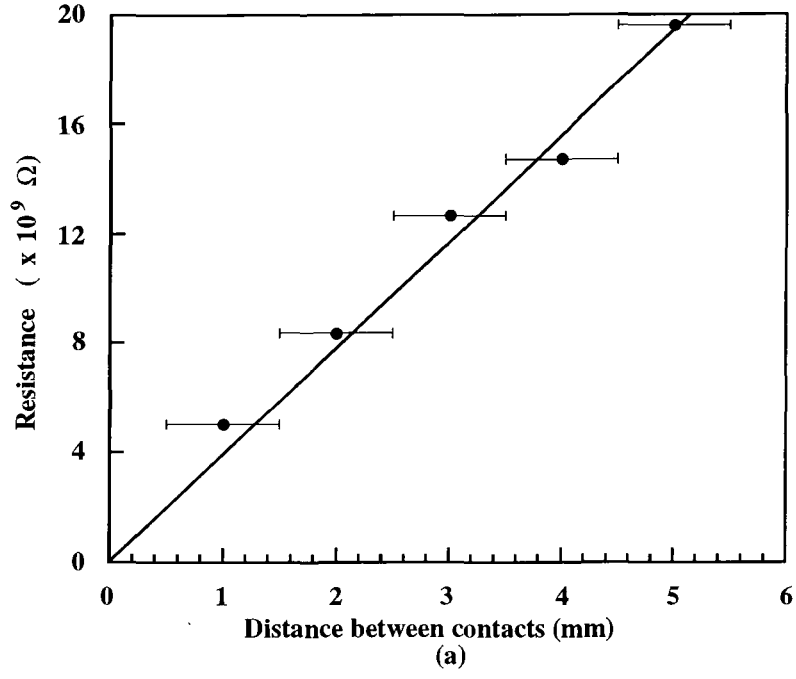

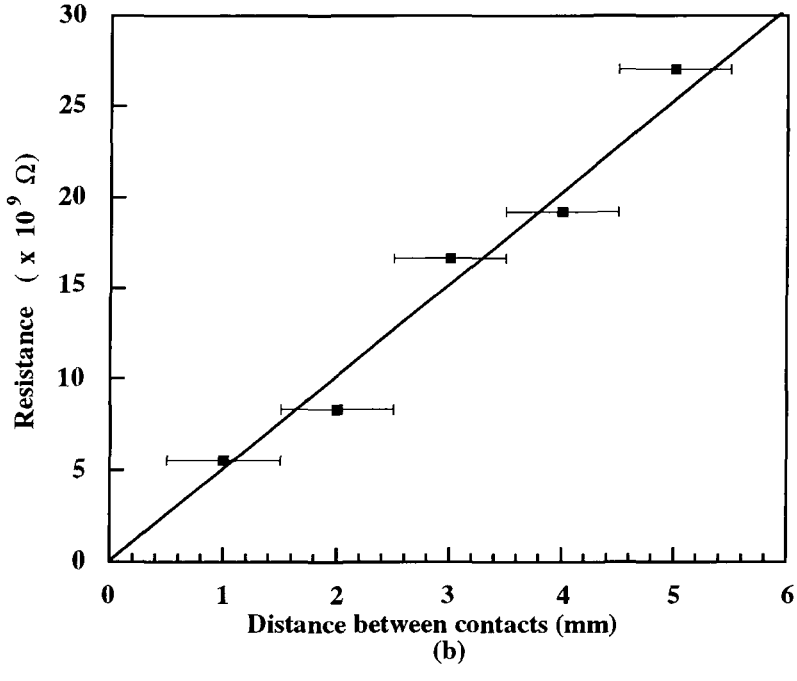

Fig 6.7 Sample resistance versus distance betweencontacts for 19-layer films of OA:ODTTF in the ratio 1:2.3

(a) silver paint contacts.
(b) carbon cement contacts.

straight line fit passes through the origin on both graphs, indicating that the contact resistance was negligible.

The current versus voltage characteristics for a 19-layer film of OA:ODTTF (molar ratio 1:2.3) with silver paint contacts are shown in Fig 6.8. Under all conditions, Ohmic behaviour was observed. As-deposited, the sample possessed a conductivity of $2.0 \pm 0.2 \times 10^{-3}$ S cm^{-1}. The reason for this high conductivity without any post-deposition treatment is not known. It is possible that inadvertent doping with some unidentified ion during the deposition process may be responsible. Desiccation to remove any residual water from the film reduced the conductivity to $1.0 \pm 0.1 \times 10^{-3}$ S cm^{-1}. After chemical doping, by exposing the sample to iodine vapour for 6 minutes, the film initially became more insulating (conductivity *ca.* 2×10^{-5} S cm^{-1}). With time, the conductivity was seen to rise, reaching a maximum value after *ca.* 3 hours. This behaviour is illustrated in Fig 6.9. The data shown here were measured at a constant bias of 0.1 V. For this sample, a maximum conductivity value (after doping) of $2.4 \pm 0.1 \times 10^{-2}$ S cm^{-1} was observed.

Over the duration of the project, a large variation in the dc conductivity of multilayer films containing the same proportion of fatty acid was noted. The current versus voltage characteristics for two samples of OA:ODTTF (1:5) with silver paint contacts are shown in Fig 6.10 (a) and (b). Samples A and B consisted of 19 and 21 LB layers, respectively. The films were prepared at different times, but the experimental conditions were the same on both occasions. For sample A, the conductivity was $1.1 \pm 0.1 \times 10^{-5}$ S cm^{-1} and $1.2 \pm 0.1 \times 10^{-3}$ S cm^{-1} before and after doping, respectively. In the case of sample B, the values recorded were $1.2 \pm 0.1 \times 10^{-3}$ S cm^{-1} and $1.6 \pm 0.4 \times 10^{-2}$ S cm^{-1}.The reason for this variability is not understood. Again, it is possible that some unknown agent present in the spreading solvent or the subphase was responsible. The amount of organic material used in each experiment was so small that a very low concentration of any contaminant could have a significant effect on the film properties.

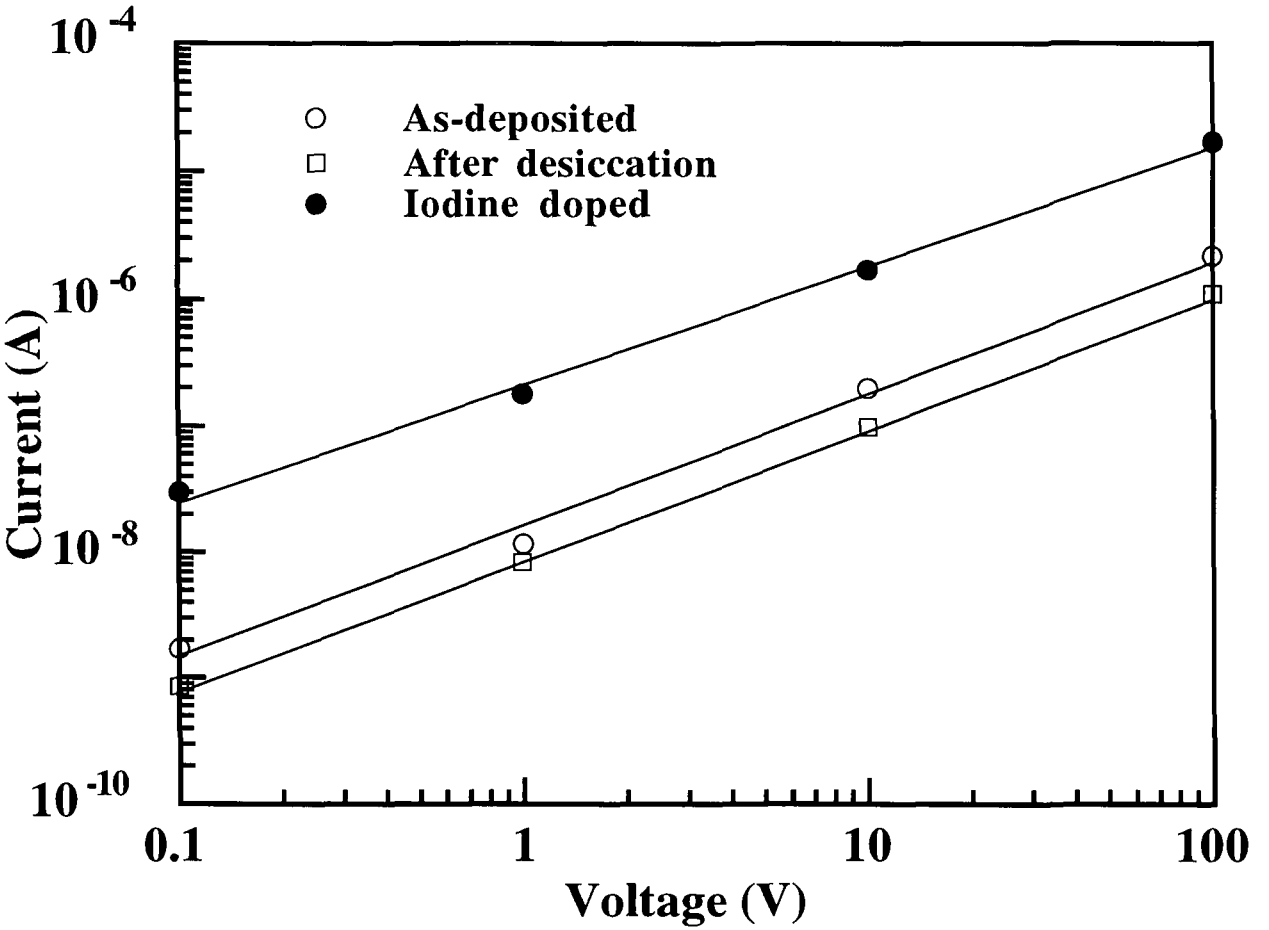

Fig. 6.8 Room temperature dc current versus characteristics for a 19-layer film of OA:ODTTF in the ratio 1:2.3, as-deposited and after iodine doping. Silver paint contacts were used.

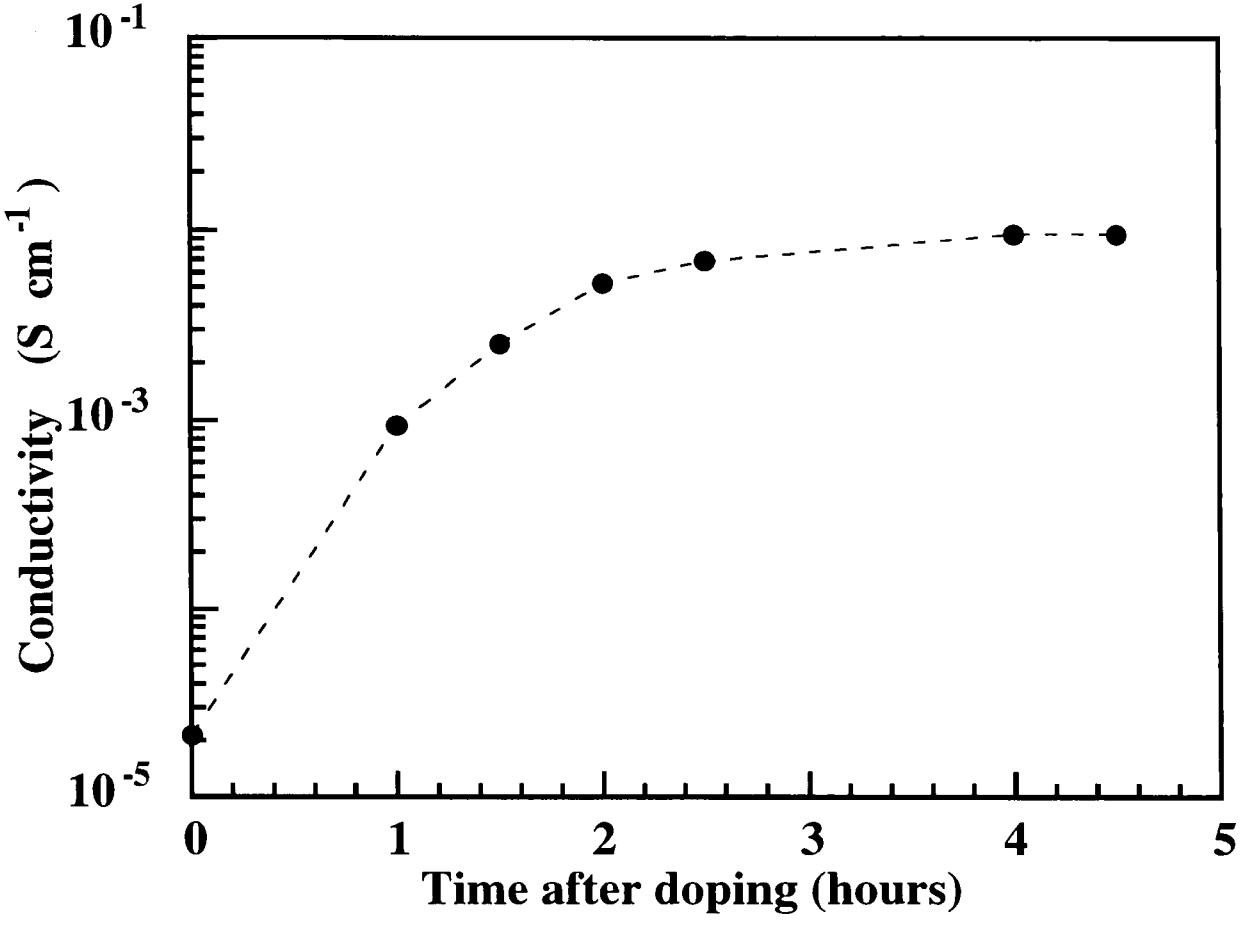

Fig 6.9 **Conductivity versus time after doping for a 19-layer film of OA:ODTTF in the ratio 1:2.3. Silver paint contacts were used with a constant bias voltage of 0.1 V applied.**

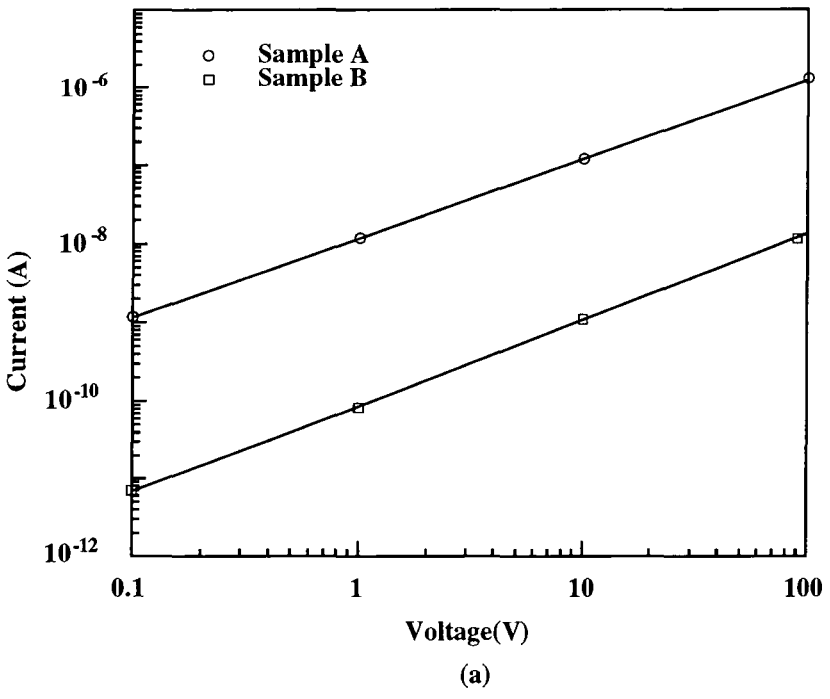

(a)

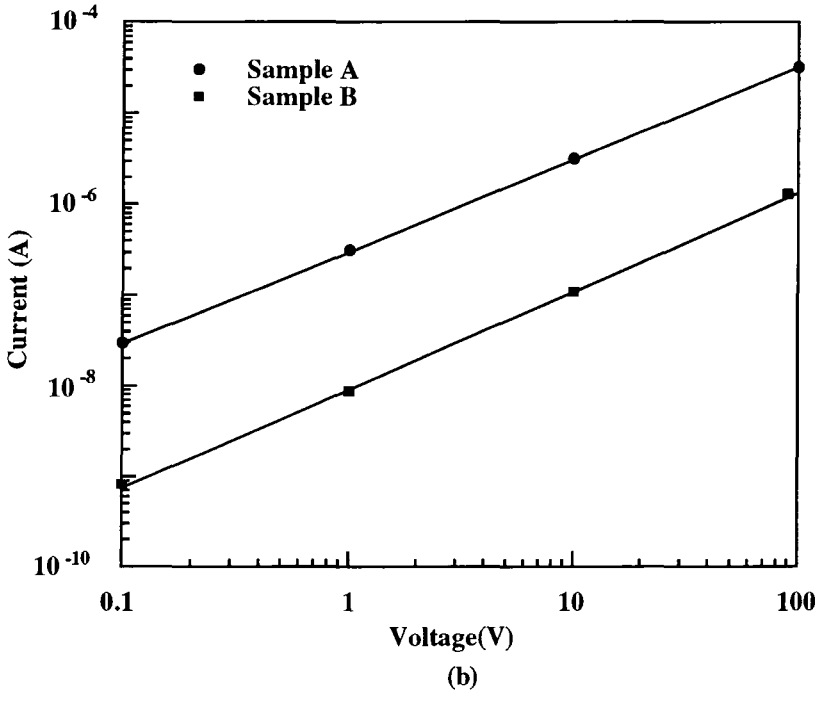

(b)

Fig. 6.10 **Room temperature dc current versus voltage characteristics, with silver paint contacts, for two samples of OA:ODTTF in the ratio 1:5. Sample A, 19-layers; sample B, 21-layers**

(a) As-deposited.
(b) Iodine doped.

6.4.3 Percolation effects

The value of the room temperature conductivity of these films was found to be strongly dependent on the proportion of fatty acid contained in the film. The conductivity versus proportion of ODTTF present in mixed films of OA:ODTTF, after doping with iodine, is shown in Fig. 6.11. The samples used here were all prepared at a similar time in order to avoid any variation in conductivity due to changes in experimental conditions. The data points were obtained by calculating the average conductivity with four different voltages applied to four separate pairs of silver paint contacts on each sample. Two conductivity regimes are evident. When the proportion of ODTTF in the film is low, the conductivity is also low, with a value (for a film with an ODTTF content of 0.13) of *ca.* 1.5×10^{-7} S cm^{-1}. This value represents an "effective" conductivity, since when the film conductivity was low, the measured current would contain a component due to the glass substrate. As the amount of ODTTF was increased, the conductivity also increased, reaching a plateau at *ca.* $2 \pm 1 \times 10^{-2}$ S cm^{-1} for films with a proportion of ODTTF of 0.6 or more.

Tasaka *et al*[2] have developed two-site two-dimensional (2D) and three-dimensional (3D) percolation models to explain the behaviour of LB films of α-quinquethiophene in cadmium stearate-stearic acid. These were subsequently used by Dourthe *et al*[3] in their studies of LB samples of (ethylenedithio)bis(octadecylthio)tetrathiafulvalene in behenic acid. The 2D model, referred to as the monolayer model, consists of an infinite two-dimensional array of hexagonal cells, as shown in Fig. 6.12(a). Each cell can be occupied either by a phase with low conductivity, σ_a (with a probability of $1-\phi$), or a highly conductive phase, σ_b (with a probability of ϕ). The 3D model, referred to as the bulk model, consists of a stack of layers, each containing an infinite array of hexagonal cells, depicted in Fig. 6.12(b). Once again, a cell may be occupied by the phase with high conductivity or that with low conductivity. For the monolayer model, the following equations were derived

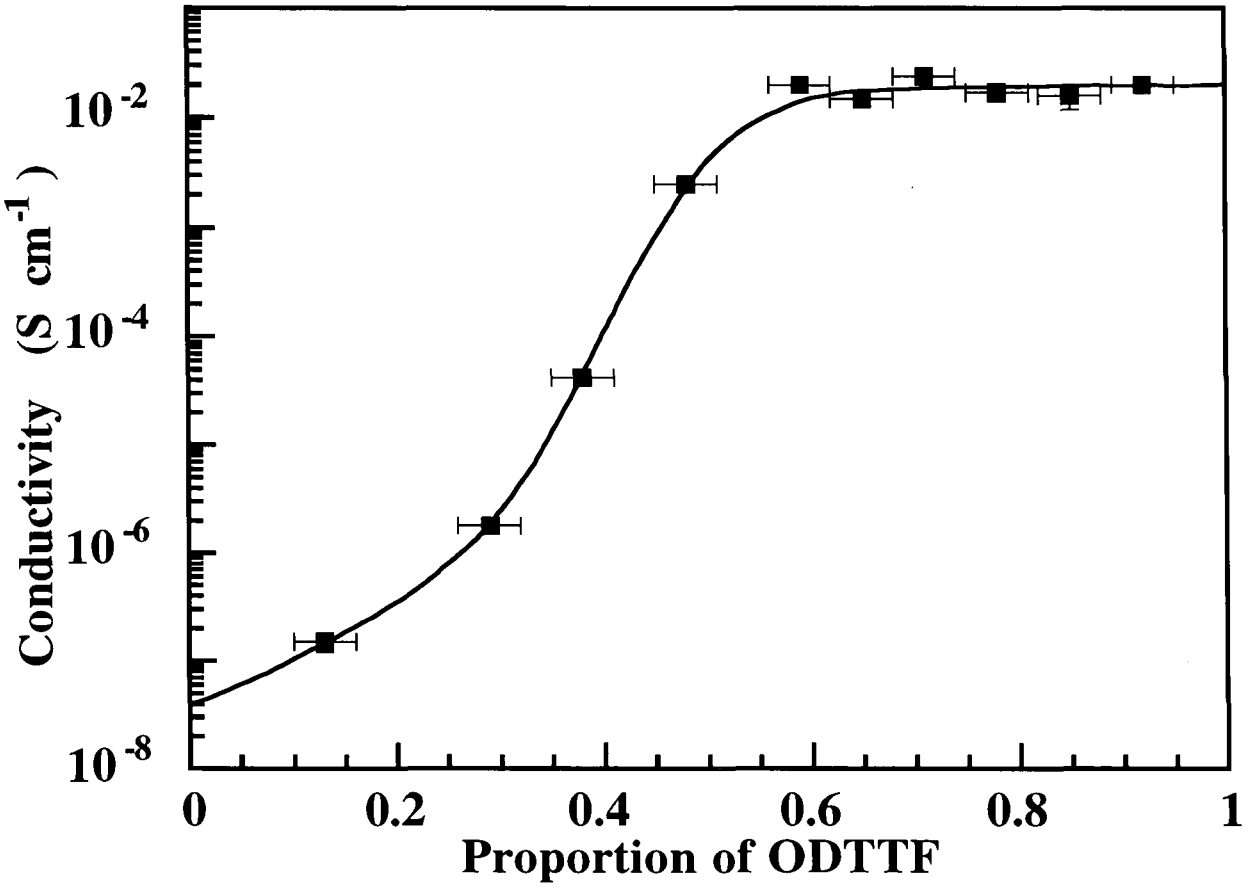

Fig. 6.11 Room temperature dc conductivity versus proportion of ODTTF present in iodine-doped mixed films of OA:ODTTF.

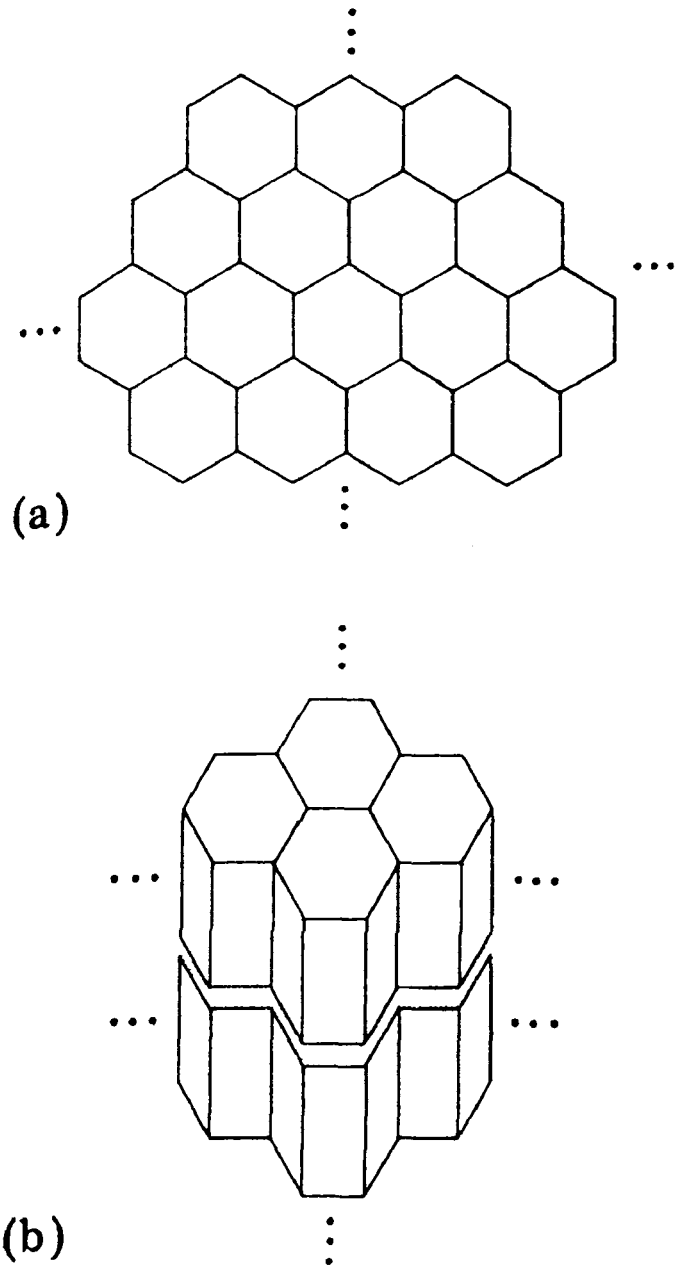

Fig. 6.12 The 2D and 3D percolation models

(a) The 2D model consists of an array of space-filling hexagons.
(b) The 3D model consists of a stack of layers, each one an array of hexagonal cells

$$\phi(n+1) = \phi^3(n) + 3\phi^2(n)[1-\phi(n)] \qquad 6.1$$

$$\sigma_a(n+1) = \exp\left[\frac{[1-\phi(n)]\ln\sigma_a(n) + 3\phi(n)\ln\left[\frac{\sigma_a(n)}{2} + \frac{\sigma_a(n)\,\sigma_b(n)}{\sigma_a(n)+\sigma_b(n)}\right]}{1 + 2\phi(n)}\right] \qquad 6.2$$

$$\sigma_b(n+1) = \exp\left[\frac{\phi(n)\ln\sigma_b(n) + 3[1-\phi(n)]\ln\left[\frac{\sigma_b(n)}{2} + \frac{\sigma_a(n)\,\sigma_b(n)}{\sigma_a(n)+\sigma_b(n)}\right]}{3 - 2\phi(n)}\right] \qquad 6.3$$

where $\sigma_a(0) = \sigma_a$, $\sigma_b(0) = \sigma_b$ and $\phi(0) = \phi$. For a specific set of σ_a,σ_b and ϕ, and with n (the number of iterations) large enough to give the required accuracy, these relations can be iterated to convergence. Equation 6.1 has a fixed point at $\phi^* = 0.5$, and for starting values of ϕ greater than ϕ^*, $\sigma_b(n+1)$ is used as an estimate of the effective conductivity, while if ϕ (0) is less then ϕ^*, $\sigma_a(n+1)$ is used.

For the 3D model, the following relationships were derived

$$\phi\,(n+1) = [\phi^3(n) + 3\phi^2(n)(1-\phi\,(n))][2 + 2\phi^3(n) - 3\phi^2(n)] \qquad 6.4$$

$$\begin{aligned}\sigma_a(n+1) = \exp[\{&[1 - \phi\,(n)]^2 \ln\sigma_a(n) + 6[1 - \phi\,(n)]\phi\,(n)\ln[(3\sigma_a(n) + \sigma_{ab})/4] \\ &+ 9\phi^2(n)\ln[(\sigma_a(n) + \sigma_{ab})/2]\}\{[1 - \phi\,(n)]^2 + 6[1 - \phi\,(n)]\phi\,(n) \\ &+ 9\phi^2(n)\}^{-1}]\end{aligned} \qquad 6.5$$

$$\begin{aligned}\sigma_b(n+1) = \exp[\{&\phi^4(n)\ln\sigma_b(n) + 6\phi^3(n)[1 - \phi\,(n)]\ln[(3\sigma_b(n) + \sigma_{ab})/4] \\ &+ 9\phi^2(n)[1 - \phi\,(n)]^2\ln[(\sigma_b(n) + \sigma_{ab})/2] \\ &+ 6\phi^2(n)[1 - \phi\,(n)]^2\ln[(2\sigma_b(n) + \sigma_a(n) + \sigma_{ab})/4] \\ &+ 2\phi\,(n)[1 - \phi\,(n)]^3\ln[(\sigma_a(n) + \sigma_b(n))/2] + 18\phi\,(n)[1-\phi\,(n)]^3 \\ &\text{x}\ln[(\sigma_a(n) + \sigma_b(n) + 2\sigma_{ab})/4] + 6[1 - \phi\,(n)]^4\ln[(2\sigma_a(n) \\ &+ \sigma_b(n) + \sigma_{ab})/4]\}\{6 - 4\phi\,(n) - 9\phi^2(n) + 12\phi^3(n) - 4\phi^4(n)\}^{-1}]\end{aligned} \qquad 6.6$$

where

$$\sigma_{ab} = \frac{2\sigma_a(n)\,\sigma_b(n)}{\sigma_a(n) + \sigma_b(n)} \qquad 6.7$$

Equation 6.4 has a fixed point at $\phi^* = 0.2038$ and, as before, $\sigma_a(n+1)$ is used to estimate the effective conductivity when $\phi(0) > \phi^*$ and $\sigma_b(n+1)$ when $\phi(0) < \phi^*$.

The numerical solutions of the 2D and 3D percolation equations, together with the experimental conductivity values obtained from the multilayer LB film samples, are presented in Fig. 6.13. Values of $\sigma_a(0) = 4 \times 10^{-8}$ S cm^{-1} and $\sigma_b(0) = 2 \times 10^{-2}$ S cm^{-1} were used in the models, which were obtained by extrapolating the experimental curve back to $\phi = 0$ and $\phi = 1$, respectively. It can be seen that the percolation threshold exhibited by the experimental data matched that of the 2D model. Below $\phi = 0.5$, however, σ did not fall sharply as predicted by classical percolation, and the transition between high and low conductivity was smeared out. This result can be explained if the proposed film structure is considered (Fig. 6.6). The structural model consists of parallel planes of conducting TTF head groups, separated from each other by relatively insulating alkyl chains. Charge transport will be favoured in the in-plane direction, parallel to the substrate ($\sigma_{//}$), but there will also be a conductivity in the perpendicular direction ($\sigma_{\perp}$). The conductivity anisotropy, $\sigma_{//}/\sigma_{\perp}$, of a 39-layer film of OA:ODTTF with ratio 1:0.8, was found to be $6.7 \pm 0.7 \times 10^3$ after doping with iodine. As the in-plane conductivity value was reduced by the addition of increasing quantities of fatty acid, it would approach that in the orthogonal direction, and, as a consequence, the system would become more three-dimensional in nature.

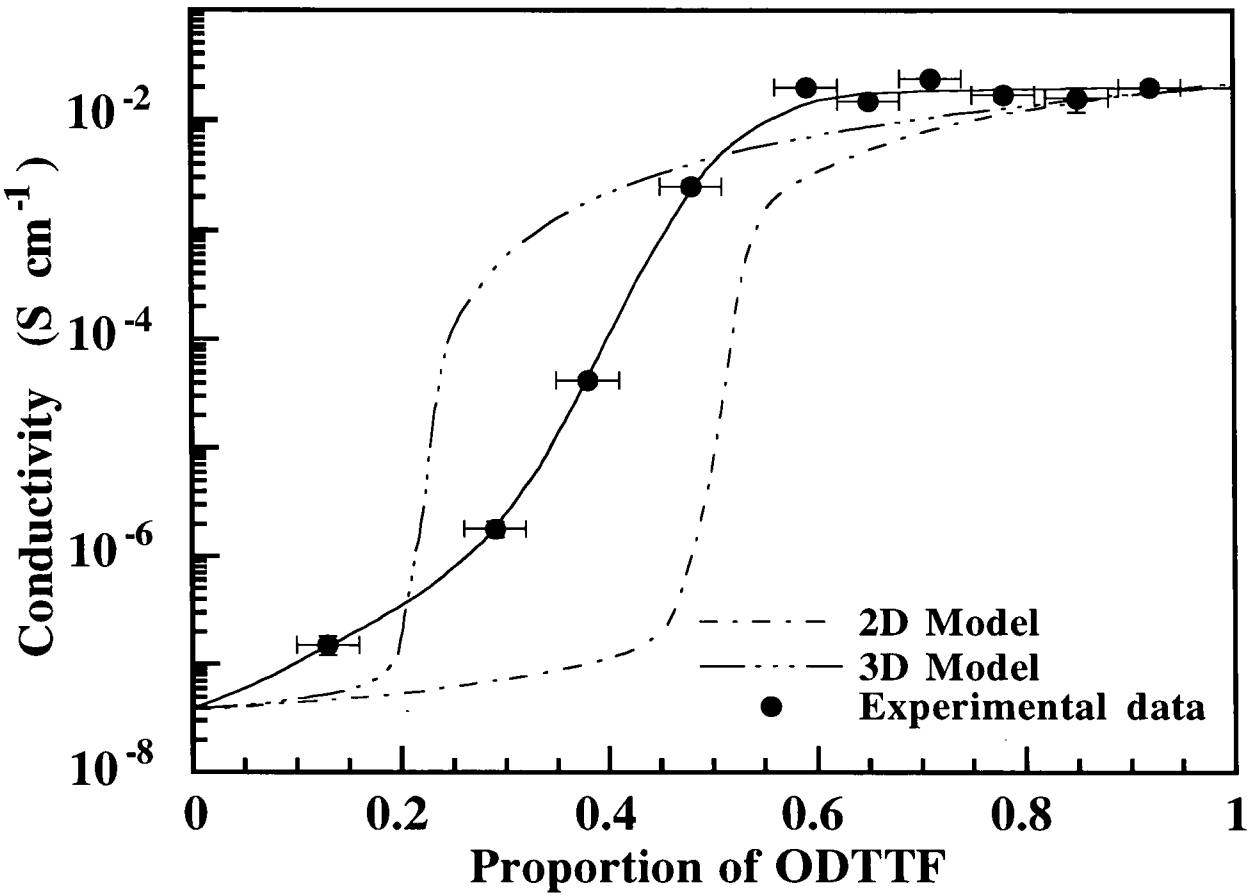

Fig. 6.13 The numerical solutions of the 2D and 3D percolation equations, together with the experimental conductivity values obtained from iodine-doped multilayer LB films of OA mixed with ODTTF.

6.4.4 Low temperature conductivity

The semi-logarithmic plots of current versus reciprocal temperature for two 79-layer samples of OA:ODTTF (in the ratio 1:2.3) over the temperature ranges 190 - 295 K for the as-deposited film and 140 - 310 K for a sample after iodine doping are shown in Figs. 6.14(a) and (b), respectively. Contacts to the films were established using carbon cement. The current versus voltage characteristics were Ohmic over the temperature range studied, as illustrated inset to Fig. 6.14(a) and (b). In both cases, the conductivity followed an exponential dependence on temperature, T, of the form

$$\sigma = A \exp\left(-\frac{\Delta E}{kT}\right) \qquad 6.8$$

where A is a constant and ΔE is a thermal activation energy. This indicates semiconducting behaviour. From the slopes of the graphs, activation energies for conductivity of 0.45 ± 0.02 eV and 0.25 ± 0.02 eV were calculated, for the as-deposited and iodine doped samples, respectively. These values are comparable with those previously reported for LB layers of HDTTF.[4] Warmack *et al* have measured the room temperature dc conductivity and the variation of the conductivity at low temperature of single crystal samples of TTF-I_2.[5] They reported a conductivity at 300 K of between 1 x 10^{-3} S cm^{-1} and 2 x 10^{-3} S cm^{-1}. The temperature dependence showed constant exponential behaviour below 250 K, with an activation energy of 0.24 eV, in close agreement with the value measured for these LB layers after iodine doping.

6.4.5 Stability with time

The currents versus time, with a bias of 100 V applied to silver paint contacts on 9-layer films of OA:ODTTF in the ratio 1:2.3, as-deposited and after doping with iodine, are plotted in Fig. 6.15. After multilayer transfer, the films were desiccated to remove any residual water before the contacts were applied. The samples were stored in air between measurements. After doping, the conductivity reached a peak value after ~ 3 hours (cf

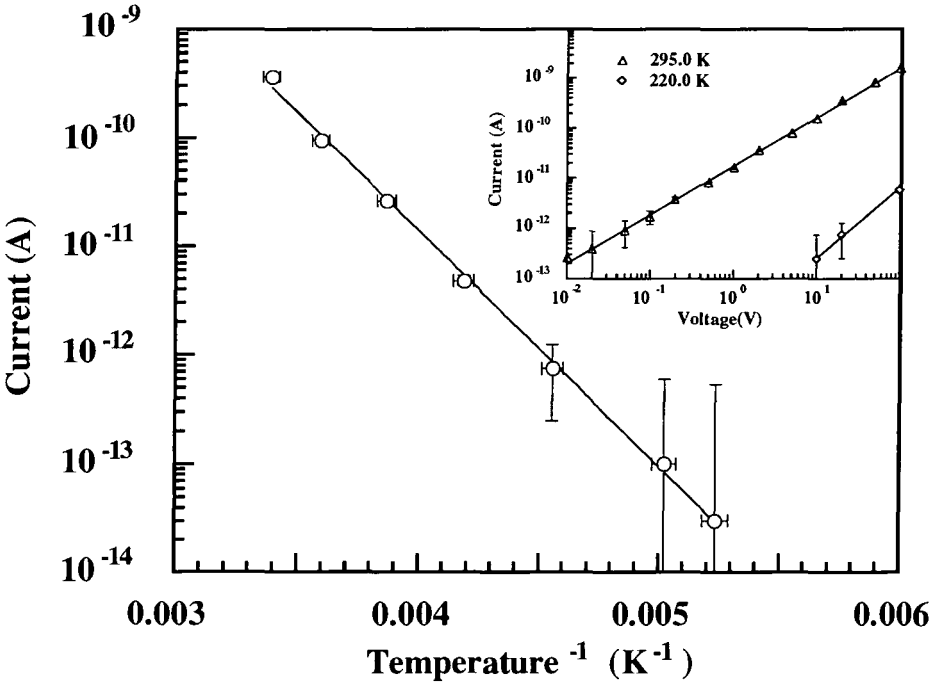

(a)

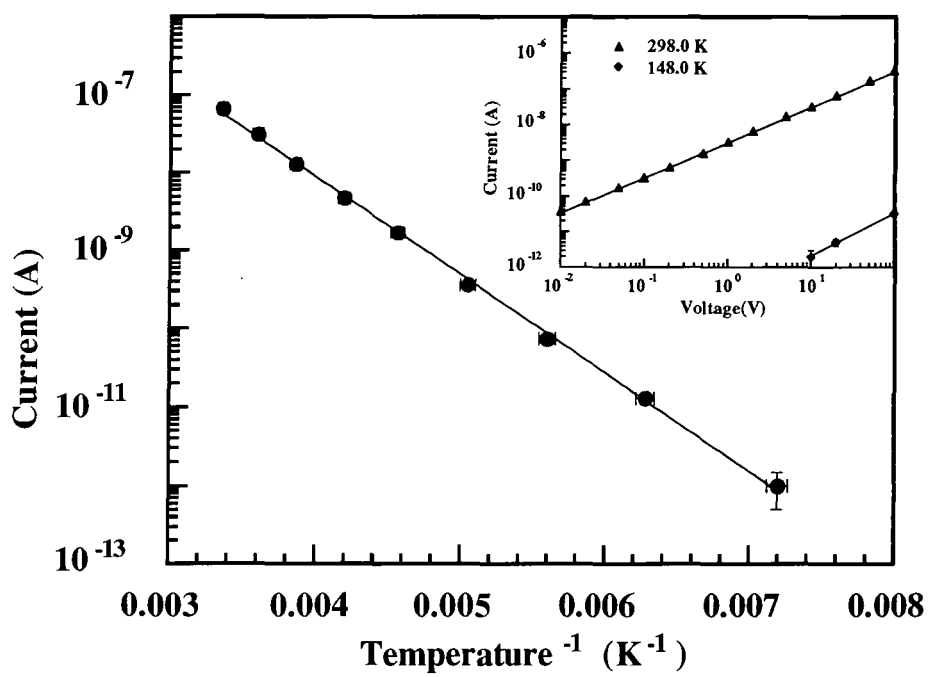

(b)

Fig. 6.14 **Semi-logarithmic plots of current versus reciprocal temperature for two 79-layer samples of OA : ODTTF in the ratio 1:2.3**

(a) As-deposited.
(b) Iodine doped.

In both cases, the current versus voltage characteristics at the extremes of the temperature range studied are shown inset.

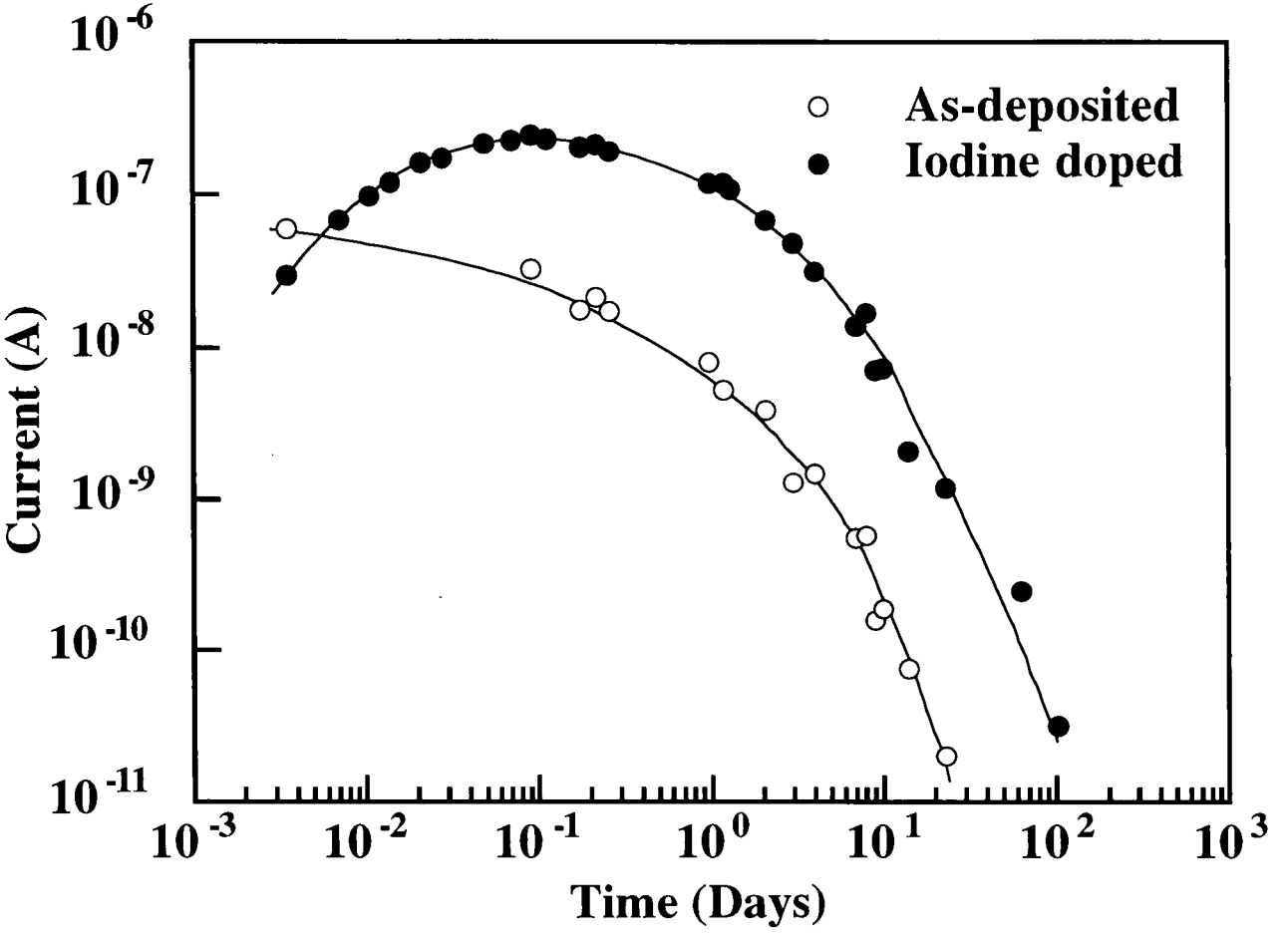

Fig. 6.15 Current versus time (with a bias of 100V) for 9-layer films of OA:ODTTF in the ratio 1:2.3 before and after iodine doping. Silver paint contacts were used and the samples were stored in air between measurements.

Fig. 6.9) before beginning to decline. This fall in conductivity was also seen in the as-deposited sample. The high conductivity could not be restored by making new contacts or by additional iodine doping, indicating that decomposition of the organic material in the sample was responsible for the instability. This feature of these ODTTF films would tend to make them unsuitable for use in device applications.

6.4.6 Optical absorption

The optical absorption spectra for 79-layer LB films of OA:ODTTF in the ratio 1:2.3, are presented in Fig. 6.16. In Fig. 6.16(a), the solid curve was measured for a film in the as-deposited state and the broken line was obtained from the same sample, 4 hours after doping with iodine. For the undoped sample, an absorption band was seen in the visible region, with a maximum at *ca.* 480 nm. In the related HDTTF LB system, this band has been attributed to the excitation of a lone-pair nonbonding electron to a π^* molecular orbital,[1] known as the n-π^* transition. After doping with iodine, new absorption bands at *ca.* 380, 850 and 2200 nm were seen. The band at 380 nm was due to an intramolecular local excitation of the $ODTTF^{+\bullet}$ radical cation, and the two absorptions at 850 and 2200 were intermolecular charge-transfer bands.[6,7] The absorption spectra for the same sample at various times after exposure to iodine are shown in Fig. 6.16(b). The data were recorded immediately after doping and then after an additional 0.5, 4 and 28 hours. It can be seen that the magnitude of the peaks at 380 and 850 nm decreased with time, whereas that at 2200 nm increased in intensity. A parallel can be drawn between the behaviour of these absorption bands and the electrical conductivity of these films. The broad charge-transfer band at 2200 nm increased in intensity with the same time dependence as the in-plane electrical conductivity, behaviour which was in agreement with the observations of Dhindsa *et al* for films of HDTTF.[1] Also, the energy corresponding to the wavelength of the 2200 nm band was calculated to be 0.56 ± 0.05 eV, which was similar to the value of $2\Delta E$ (the band gap for an intrinsic semiconductor or the depth of an impurity level for an extrinsic semiconductor) obtained from low temperature dc conductivity measurements

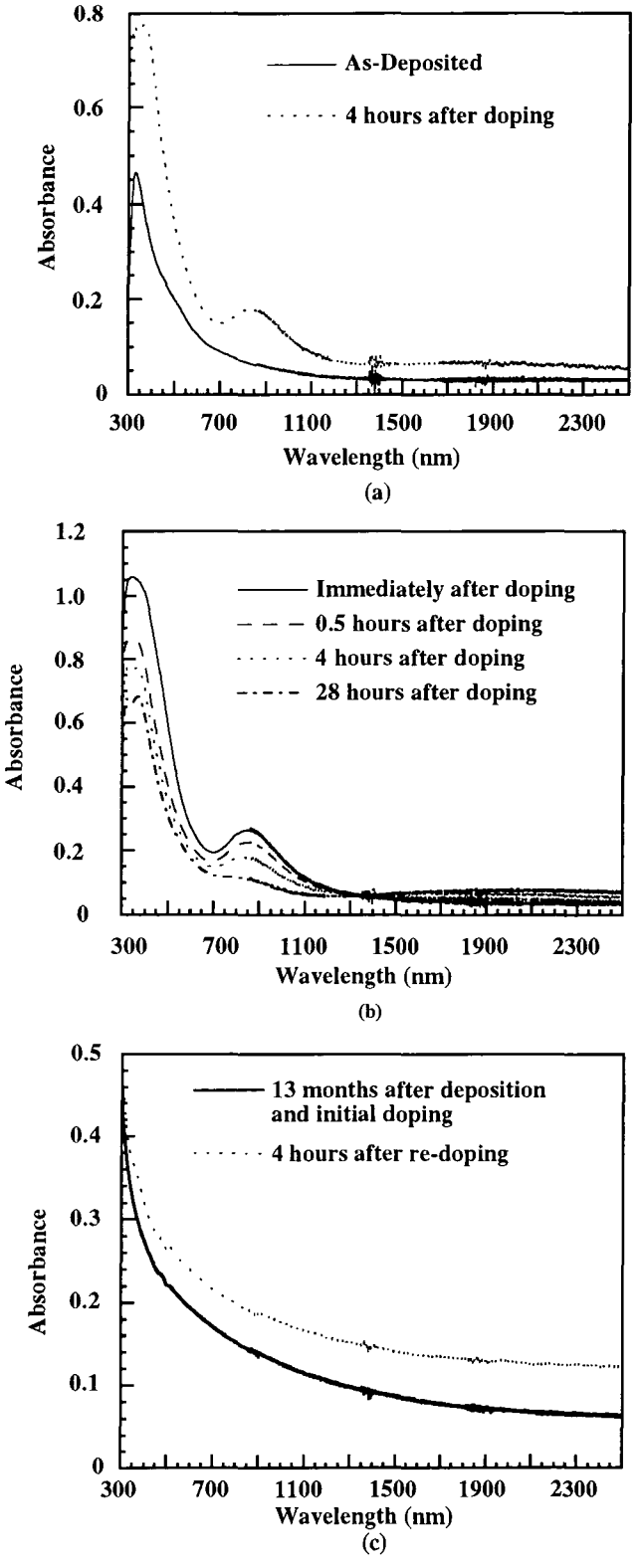

Fig. 6.16 **Optical absorption spectra for 79-layer films of OA:ODTTF in the ratio 1:2.3**

(a) As-deposited and four hours after iodine doping.
(b) Immediately and 0.5, 4 and 28 hours after iodine doping.
(c) 13 months after deposition and initial doping and 4 hours after re-doping.

on films doped with iodine vapour, i.e 0.50 ± 0.04 eV.

The optical absorption spectra for the same sample, 13 months after deposition and initial doping are shown in Fig. 6.16(c). The sample was stored in air between measurements. The solid line was obtained for the film without any additional treatment and the data for the broken line were recorded 4 hours after re-doping of the film with iodine. It can be seen that the spectrum for the film without any additional treatment exhibited none of the absorption bands displayed by the freshly deposited sample, and after re-doping, the charge transfer bands still did not appear. This behaviour is again in agreement with the significant decrease in electrical conductivity with time.

6.4.7 Electron microscopy

Fig. 6.17 is an scanning electron micrograph of an iodine doped 79-layer film of OA:ODTTF in the ratio 1:2.3. An accelerating voltage of 15 kV was used, and the sample was coated with a thin layer of silver to prevent charging by the electron beam. The film consisted of two phases, with bright, flake-like crystallites distributed in a darker matrix. It is thought that ODTTF in the film existed as flakes in a background of OA.

6.4.8 Energy dispersive spectroscopy

The characteristic X-ray spectra of the same 79-layer sample pictured in Fig. 6.17, after doping with iodine, are shown in Fig. 6.18. The spectra were recorded with the electron probe directed at points A and B on the film. Penetration of the LB layers by the beam resulted in a peaks due to the silicon which was present in the glass substrate (this was confirmed by recording the spectra from a piece of glass without any LB coating), and a signal due to the silver overlayer was also recorded. The peaks due to sulphur and iodine were higher when the beam was incident on point A on the micrograph, corresponding to one of the flake-like crystallites, rather than point B, the background matrix. This observation strengthened the hypothesis that the films were made up from clusters of

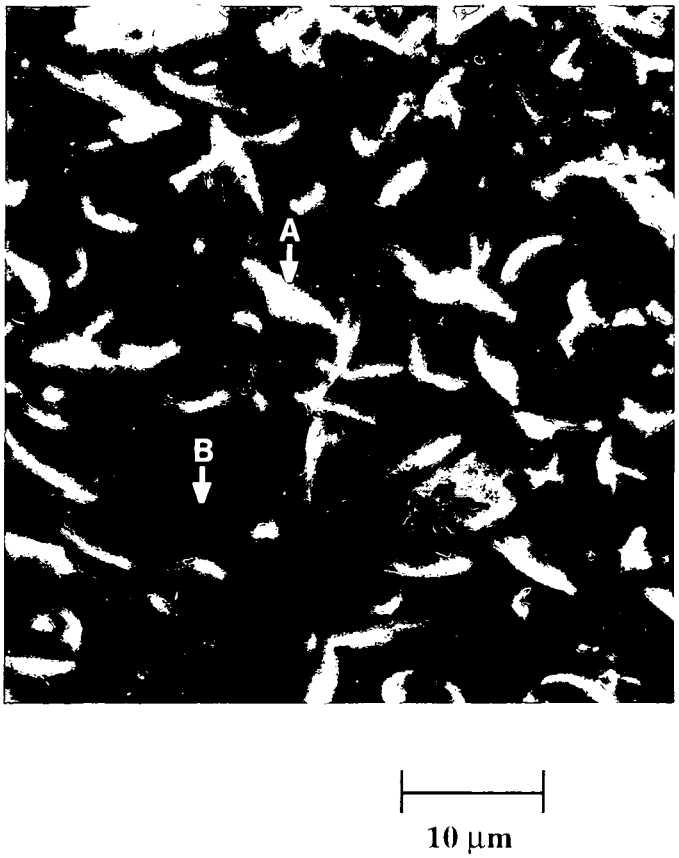

Fig. 6.17 Scanning electron micrograph of an iodine doped 79-layer film of OA:ODTTF in the ratio 1:2.3. The sample was coated with silver to prevent charging by the electron probe.

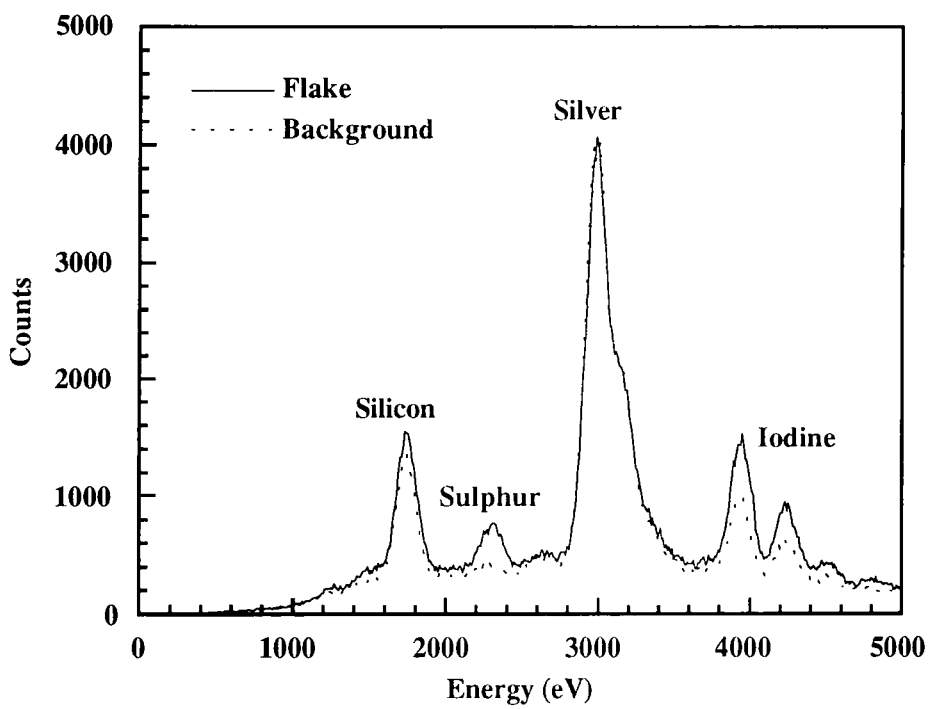

Fig. 6.18 EDS spectra recorded from a 79-layer film of OA:ODTTF in the ratio 1:2.3. The electron probe was directed at point A on the micrograph shown in Fig. 6.17 when the solid line was recorded and point B for the data represented by the dotted line.

ODTTF in a background of fatty acid.

6.5 Film properties:Pentacosa-10,12-diynoic acid mixed with octadecanoyl-TTF

6.5.1 Thickness measurements

Fig 6.19 is a plot of layer thickness versus ODTTF content for 19-layer films of PA:ODTTF. The data were obtained, using ellipsometric measurements, from samples deposited on hydrophilic silicon substrates. The length of the PA molecule, measured from a standard molecular model, was 3.4±0.1 nm. This value was similar to that of the ODTTF molecule (3.3 ± 0.1 nm). Consequently, the thickness per layer for these as-deposited films, did not depend on the ratio of the component molecules. The measured value was lower than expected, i.e. 3.20 ± 0.02 nm. This result indicates interdigitation and/or tilting of the molecules with respect to the plane of the substrate. After doping with iodine, a reduction in the layer thickness of films with a high proportion of ODTTF was observed. By extrapolation of a straight line fit to the y-axis, a reduction in the thickness per layer of a pure ODTTF film of *ca.* 0.8 nm was predicted. This is similar to the change in the layer thickness of pure HDTTF films observed by Dhindsa *et al*[1] after doping with either bromine or iodine, where a change in the d-spacing of approximately 2 nm was seen.

6.5.2 Room temperature conductivity

The current versus voltage characteristics for an 11-layer film of PA:ODTTF (molar ratio 1:3) with silver paint contacts are shown in Fig. 6.20. Ohmic behaviour was observed over the range of bias voltage studied. As-deposited, the conductivity for this sample was $2.3 \pm 0.6 \times 10^{-5}$ S cm^{-1}. Desiccation to remove any residual water from the film reduced this value to $2.1 \pm 0.6 \times 10^{-6}$ S cm^{-1}. After iodine doping, the conductivity increased to a maximum value of $8.4 \pm 0.4 \times 10^{-4}$ S cm^{-1}.

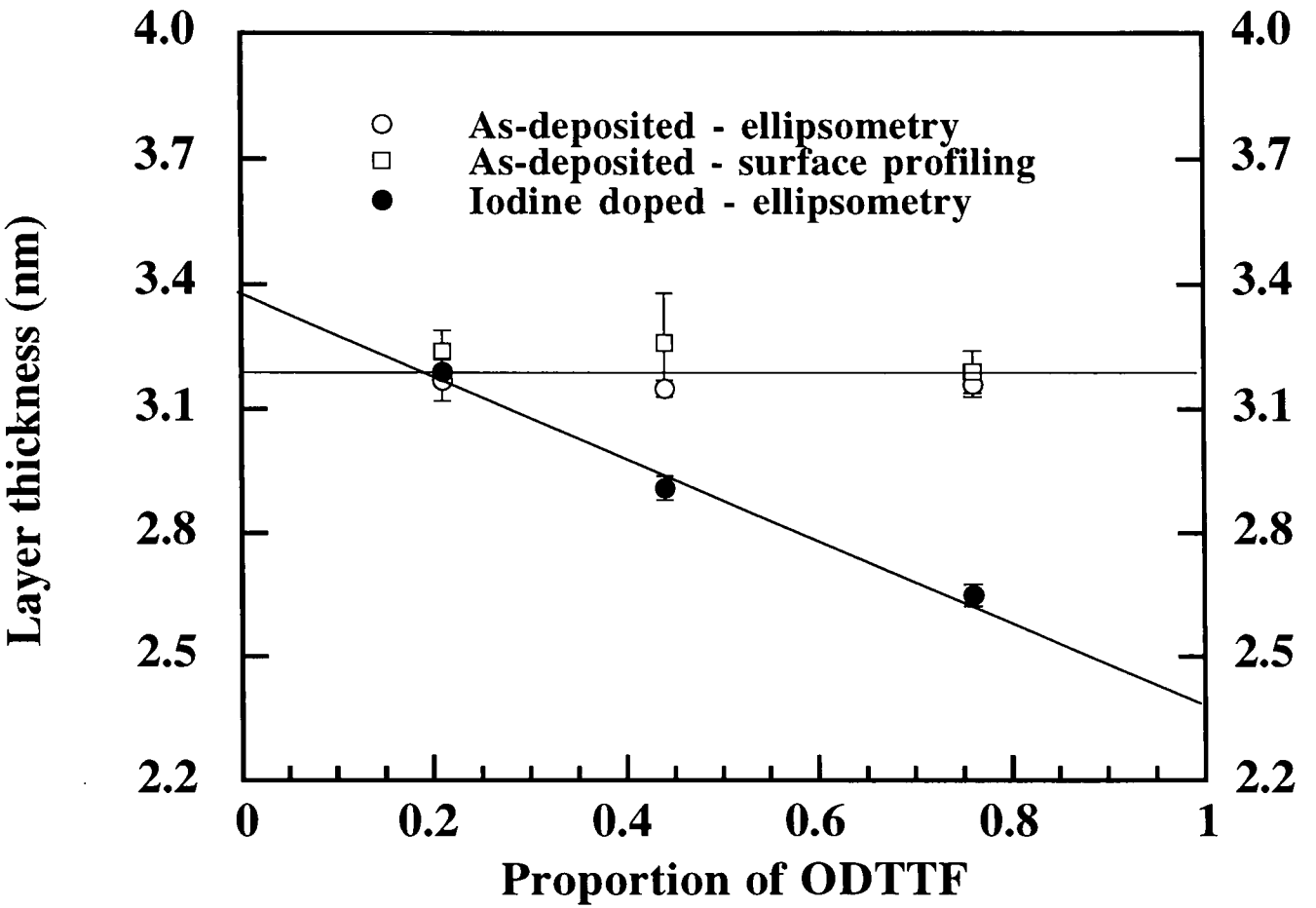

Fig. 6.19 Average layer thickness versus proportion of ODTTF contained in 19-layer films of PA:ODTTF.

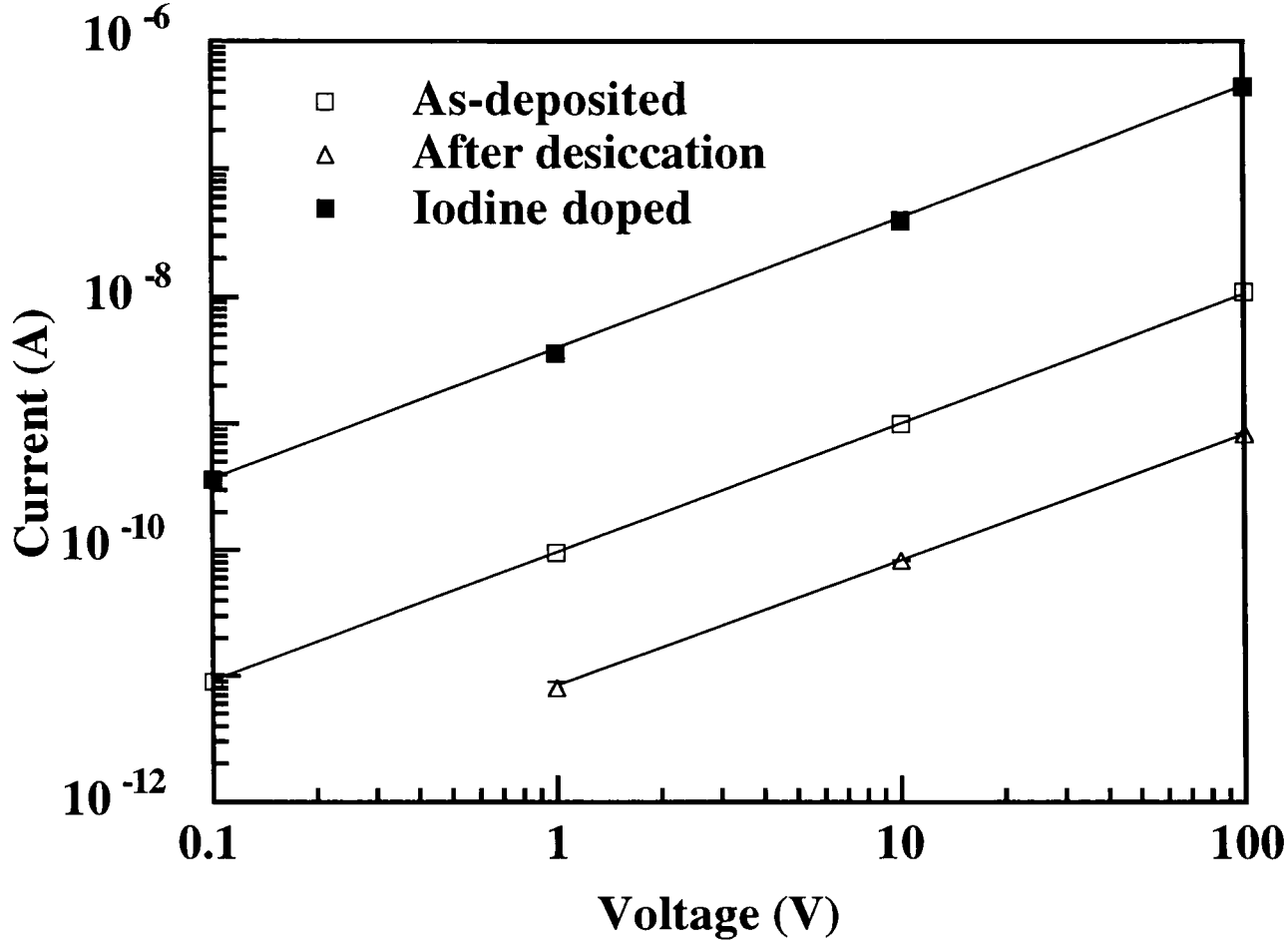

Fig. 6.20 Room temperature dc I/V characteristic with silver paint contacts for an 11-layer film of PA:ODTTF in the ratio 1:3.

6.5.3 Percolation effects

The conductivity versus proportion of ODTTF present in mixed multilayer films of PA:ODTTF, after doping with iodine, is shown in Fig. 6.21 together with the solutions to the 2D and 3D classical percolation equations. The experimental data were obtained from samples which were prepared in the same series of experiments to remove the possibility of variation due to changes in the experimental conditions with time. The percolation equations were solved using values of $\sigma_a(0) = 4 \times 10^{-8}$ S cm^{-1} and $\sigma_b(0) = 2 \times 10^{-3}$ S cm^{-1}, obtained by extrapolating the fit to the experimental data to $\phi = 0$ and $\phi = 1$, respectively. Again, the conductivity exhibited a strong dependence on the ratio of the components in the film, with a percolation threshold at 0.5. In this case, however, the experimental data more closely followed the 2D classical percolation model, suggesting lower conductivity perpendicular to the plane of the substrate in this case compared to films of OA:ODTTF. Sugi *et al* have investigated the through-plane dc conductivity of LB multilayers of the cadmium salts of fatty acids with various chain lengths.[8] They discovered an exponential dependence of conductivity on monolayer thickness, with an increase in chain length of two carbon atoms causing a downward shift of the conductivity by an order of magnitude or more. Here, when the proportion of ODTTF present was 0.3, films containing PA were *ca.* 0.4 nm per layer thicker than those containing OA. Also, the layer thickness was seen to decrease with increasing proportion of OA, but increase with higher PA content. Hence, $\sigma_\perp$ would be expected to be lower in films diluted with PA rather than OA. An attempt was made to record the anisotropy of the conductivity of an iodine doped film of PA:ODTTF in the ratio 1:0.8, but short circuits between the electrodes made the through-plane measurement impossible.

6.5.4 Optical microscopy

PA molecules can be cross-linked by exposure to UV light. This polymerisation is accompanied by a colour change,[9] making the material visible under an optical microscope. Samples were exposed to UV radiation, at a wavelength of 253.7 nm, in an

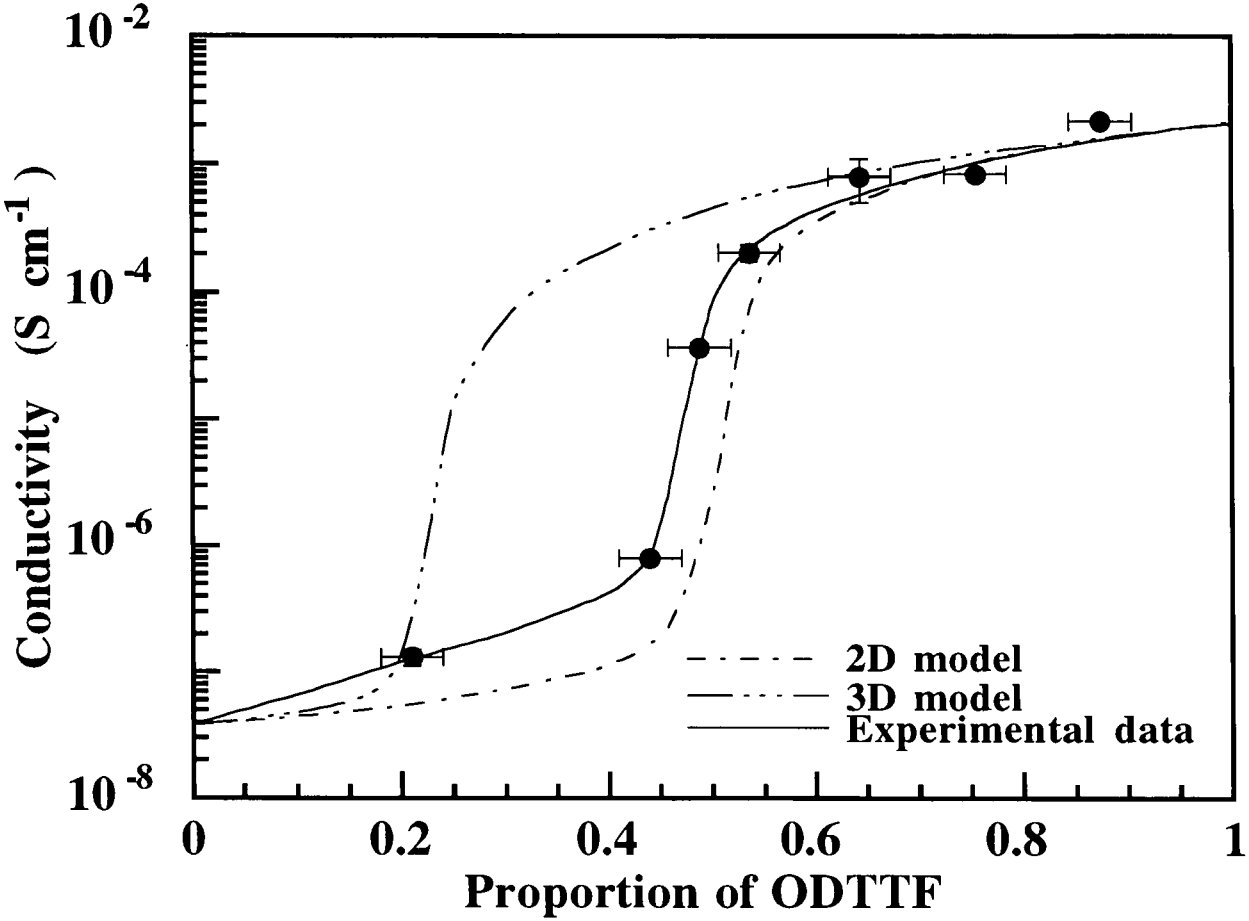

Fig. 6.21 The numerical solutions of the 2D and 3D percolation equations, together with the experimental conductivity values obtained from multilayer LB films of PA mixed with ODTTF.

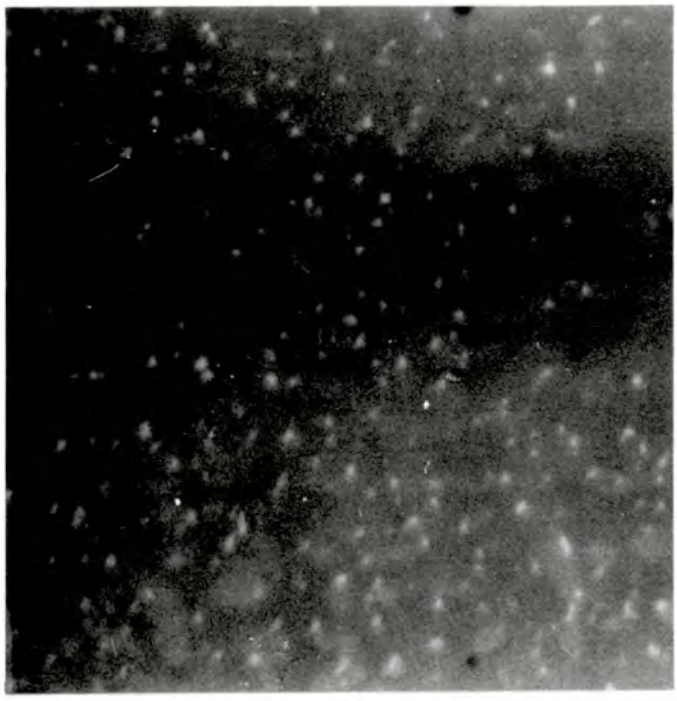

(a)

100 μm

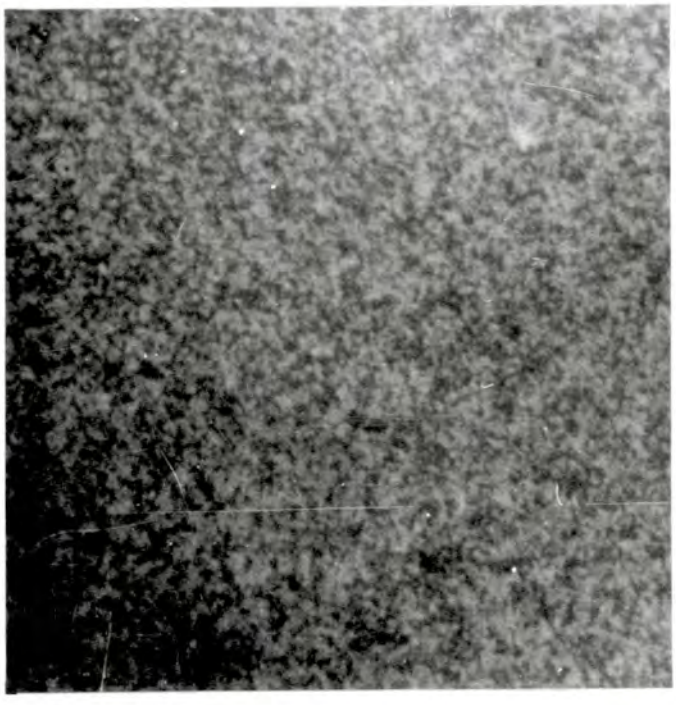

(b)

Fig 6.22 **Optical micrographs of UV polymerised PA:ODTTF films**

(a) Ratio 1:3.1.
(b) Ratio 1:0.5.

EPROM eraser. Optical micrographs of two UV polymerised PA:ODTTF films, with ratios 1:3.1 and 1:0.5, are shown in Fig. 6.22(a) and (b), respectively. In Fig. 6.22(a), clusters of PA in the film can be seen as light areas, *ca.* 10 μm in size, in a dark background of ODTTF. Here, a continuous path remained through the ODTTF phase and around the PA clusters allowing for uninterrupted charge transport. The electrical conductivity was therefore high. When the PA content was increased, as in Fig. 6.22(b), it can be seen that the dark ODTTF areas became isolated in a background of PA. Consequently, there was no simple path for carrier transport and the conductivity was much reduced.

6.6 Summary

LB multilayer films of octadecanoyl-TTF mixed with a fatty acid (either octadecanoic acid or pentacosa-10,12-diynoic acid) to aid film transfer have been deposited. The thickness of the films, measured using ellipsometry and surface profiling, depended on the ratio of the component molecules, and was reduced by iodine doping. Room temperature and low temperature dc conductivity measurements revealed semiconducting behaviour with Ohmic current versus voltage behaviour, before and after iodine doping. An increase in conductivity was observed after doping. The level of the conductivity was found to depend strongly on the amount of fatty acid contained in the sample, and this behaviour has been modelled by a two-site percolation theory. Film morphology was investigated using optical and electron microscopy and EDS, revealing a structure in which the two components were not completely miscible, and existed as two separate phases. Optical absorption spectra were recorded, and the behaviour of the observed absorption bands with time after doping with iodine has been related to the corresponding increase in the electrical conductivity.

References

1. A.S Dhindsa, R.J. Ward, M. R. Bryce, Y.M. Lvov, H.S. Munro and M.C.

Petty, Synth. Met., 35 (1990) 307-318.

2. S. Tasaka, H.E. Katz, R.S. Hutton, J. Orenstein, G.H. Fredrickson and T.T. Wang, Synth. Met., 16 (1986) 17-30.
3. C. Dourthe, M. Izumi, C. Garrigou-Lagrange, T. Buffeteau, B. Desbat and P. Delhaes, J. Phys. Chem., 96 (1992) 2812-2820.
4. A.S Dhindsa, M.R. Bryce, J.P. Lloyd and M.C. Petty, Synth. Met., 27 (1988) B563-B568.
5. R.J. Warmack, T.A. Callcott and C.R. Watson, Phys. Rev. B, 12 (1975) 3336-3338
6. T. Sugano, K. Yakushi and H. Kuroda, Bull. Chem. Soc. Jpn., 51 (1978) 1041-1046.
7. J.B. Torrance, B.A. Scott, B. Welber, F.B. Kaufman and P.E. Seiden, Phys. Rev. B, 19 (1979) 730-741.
8. M. Sugi, T. Fukui and S. Iizima, App. Phys. Lett., 27 (1975) 559-561.
9. G. Lieser, B. Tieke and G. Wegner, Thin Solid Films, 68 (1980) 77-90.

Chapter 7

Multilayer Films of *N*-octadecylpyridinium-Pd(dmit)$_2$

7.1 Introduction

This chapter concerns the LB deposition and subsequent characterisation of transferred multilayer films of *N*-octadecylpyridinium-Pd(dmit)$_2$ (C_{18}Py-Pd(dmit)$_2$), as-deposited and after iodine doping. The effect of spreading time (the time that the material was allowed to age on the surface of the subphase before the first compression) on the properties of the floating film and the transferred layers is investigated, using isotherms, surface profiling and electron microscopy with EDS. Changes in optical absorption and electrical conductivity, at room temperature and over the temperature range 77-300 K, are also reported.

7.2 Monolayer forming properties

The chemical structure and space filling models of *N*-octadecylpyridinium-Pd(dmit)$_2$ (C_{18}Py-Pd(dmit)$_2$) are shown in Fig. 7.1. This material could be deposited in pure form, but the behaviour of the floating layer was solvent dependent. The solid was only slightly soluble in chloroform. It dissolved completely when dichloromethane was used, but this solvent evaporated quickly and consequently spreading of the layer on the surface of the subphase was poor. To aid spreading, a mixed solvent consisting of dichloromethane:benzene in the volume ratio 3:2 was used. To prepare the solution, 3 ml of dichloromethane was added to ~ 1 mg of solid material in a volumetric flask. This mixture was agitated in an ultrasonic bath for 10 minutes before 2 ml of benzene was added to give a final concentration of ~ 0.2 g l^{-1}. A suitable amount of this (0.5-3 ml) was distributed over the surface of a pure water subphase using a micro syringe. This material was left uncompressed on the surface of the subphase for between 1 minute and 21 hours. Pressure versus area isotherms were plotted at a compression speed of 2.3±1.7

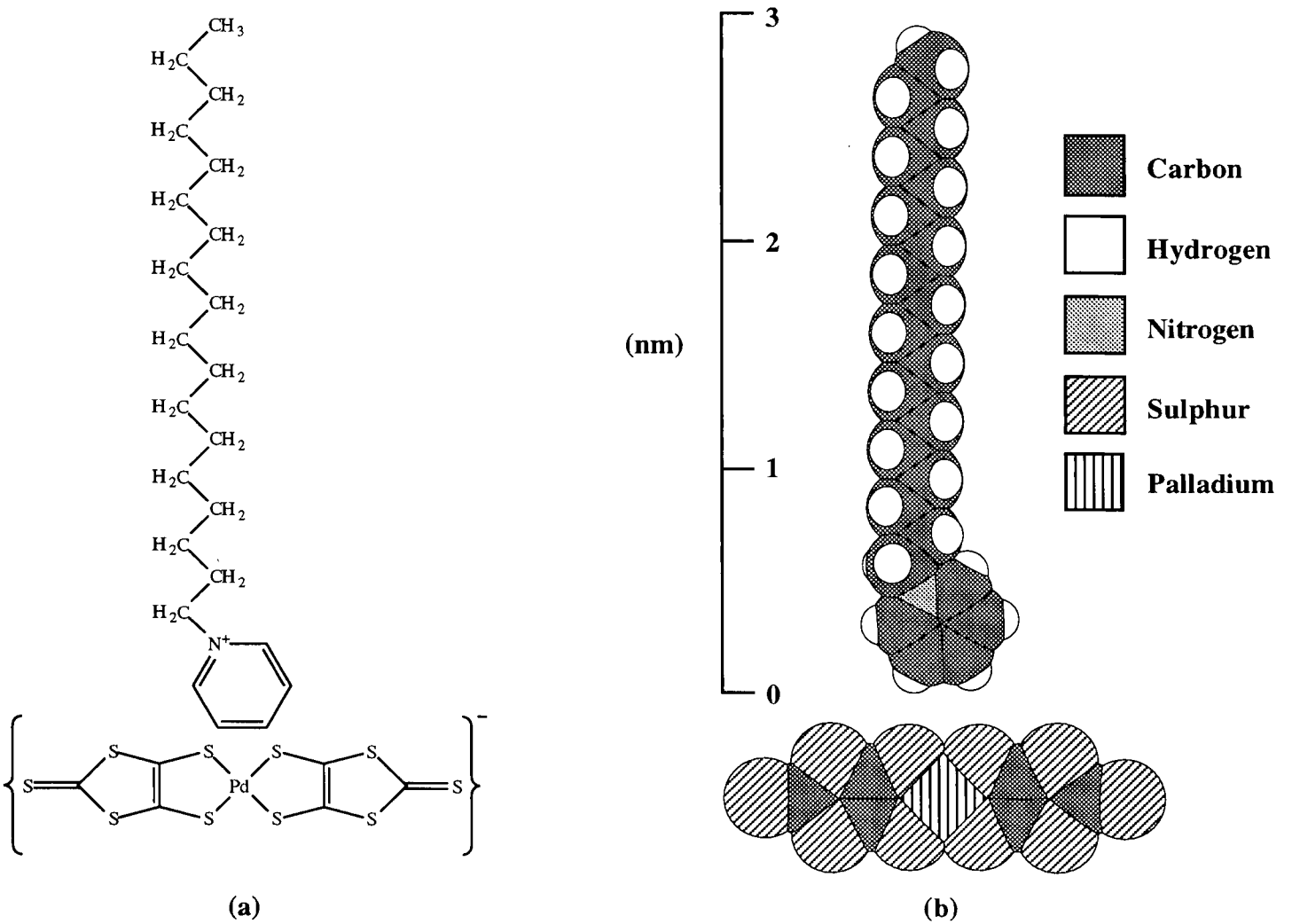

Fig. 7.1 (a) Chemical structure and (b) space filling molecular model of $C_{18}Py\text{-}Pd(dmit)_2$.

x 10^{-3} nm^2 $complex^{-1}$ s^{-1}. Condensed isotherms were recorded, but, in common with floating layers of the related compound C_{18}Py-Ni(dmit)$_2$ (chapter 8, section 8.2), the shape of the plot was found to have a strong dependence on the time that the layer was left on the surface of the subphase before compression, as well as on the amount of solution spread. In Fig. 7.2(a), examples of isotherms recorded at different times after the application of 1 ml of C_{18}Py-Pd(dmit)$_2$ solution to the subphase surface are shown. After 1 minute before compression, the area per complex, measured at a surface pressure of 30 mN m^{-1} was *ca.* 0.12 nm^2, and a plateau region was evident in the plot, thought to be associated with reorganisation of the floating layer. A significant increase in the area per complex was observed if the floating film was left uncompressed for longer times. After 10 minutes, for example, the area per complex at 30 mN m^{-1} was *ca.* 0.26 nm^2, increasing to *ca.* 0.36 nm^2 after 18 hours. Also, for longer times, the plateau region disappeared from the curve. Taylor *et al* have observed similar behaviour in the isotherms of the 2:1 salts bis(didodecyldimethylammonium)-M(dmit)$_2$ (M=Ni[1],Pd,Pt).[2] Significant changes in the isotherm of the Ni complex were observed during the first hour after spreading with the area per complex moving to higher values with increasing time on the subphase before the first compression. The isotherms of the Pd complex also changed with time, but to a lesser degree, and those of the Pt salt exhibited an even smaller time dependence.

Fig. 7.3 compares isotherms recorded 10 minutes after the spreading of 1 ml and 2 ml of C_{18}Py-Pd(dmit)$_2$ solution. When a large volume of solution was spread, a small area per complex at 30 mN m^{-1} of *ca.* 0.15 nm^2 was observed, with a plateau at *ca.* 27 mN m^{-1}. When the volume of solution spread was reduced to 1 ml, spreading was improved, and an increased area per complex of *ca.* 0.26 nm^2 at 30 mN m^{-1} was recorded. Gupta *et al* [2] observed the same behaviour in their divalent M(dmit)$_2$ salts with didodecyldimethylammonium. They found that increasing the amount of material applied to the surface of the subphase shifted the isotherm to lower areas, and implied that this

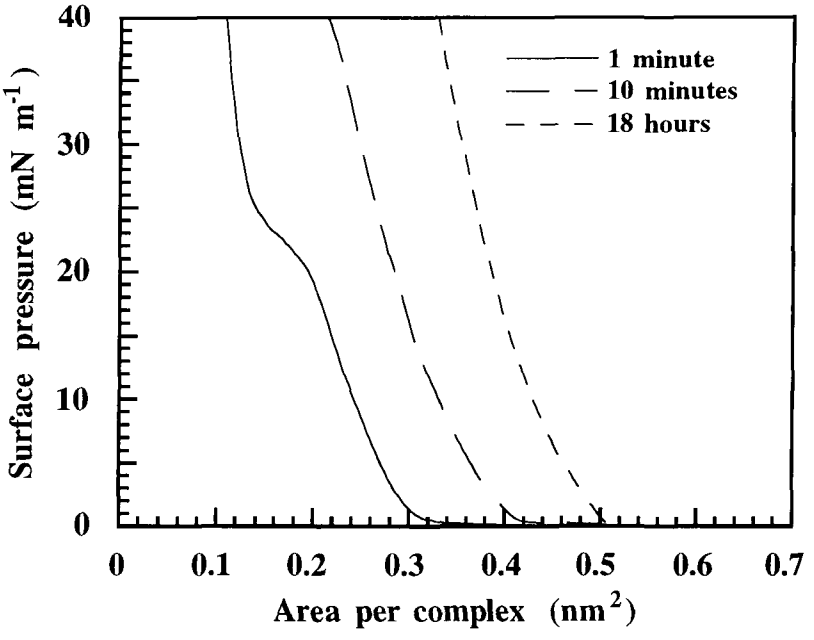

Fig. 7.2 Surface pressure versus area isotherm plots for C_{18}Py-Pd(dmit)$_2$ films, 1 minute, 10 minutes and 18 hours after the spreading of 1 ml of solution on a pure water subphase.

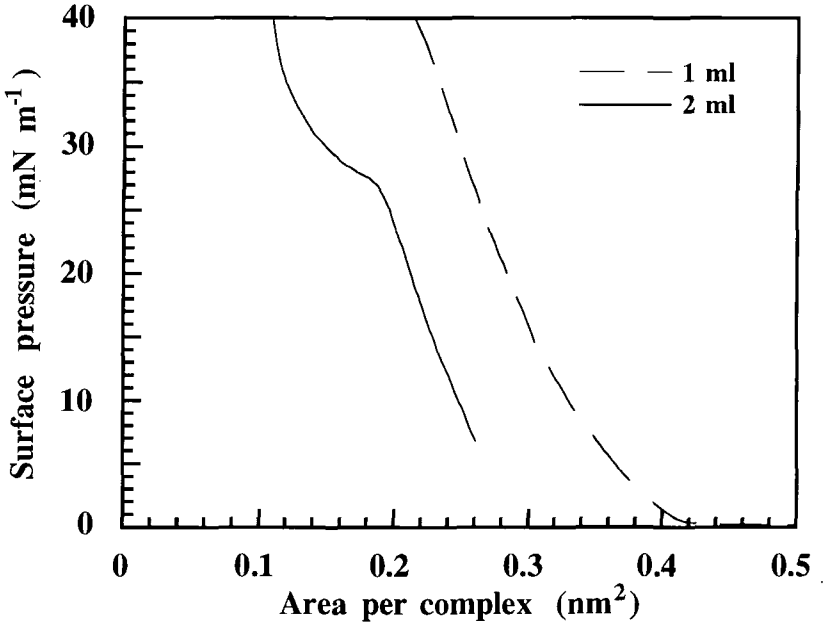

Fig. 7.3 Surface pressure versus area isotherm plots for C_{18}Py-Pd(dmit)$_2$ films, 10 minutes after the spreading of 1 ml and 2 ml of solution on a pure water subphase.

was due to poor spreading of the complexes. Fig 7.4 is a plot of area per complex, measured at a surface pressure of 30 mN m^{-1}, versus the time that uncompressed films of C_{18}Py-Pd(dmit)$_2$ were aged on the subphase surface. Data obtained for various different volumes of spreading solution are plotted on the same graph. It is evident that for short times, aggregation or multilayer formation occurred, and the area per complex was correspondingly small. After extended times, the molecules rearranged, and the area occupied by each complex increased. Gupta *et al*[3] have used microscopy to examine LB multilayers of the monovalent salt didodecyldimethylammonium-Ni(dmit)$_2$. They found that a 9-layer film deposited after a spreading time of 20 minutes was composed of a mass of microcrystallites. After a spreading time of 1 hour, the number of microcrystallites contained in another 9-layer film was significantly reduced.

Spreading of C_{18}Py-Pd(dmit)$_2$ was improved, accompanied by a relatively large area per complex, if the volume of solution applied was small. From space filling molecular models, the dimensions of the *N*-octadecylpyridinium cation were found to be 0.8±0.1 nm x 0.3±0.1 nm x 2.9±0.1 nm and those of the Pd(dmit)$_2$ molecule were 1.6±0.1 nm x 0.6±0.1 nm x 0.4±0.1 nm. The maximum area per complex measured here, i.e *ca* 0.33 nm^2, when a small amount of solution was spread and allowed to stand uncompressed for a long time, was lower than that expected for a film in which both components were in contact with the subphase, i.e. 0.24 nm^2 for the *N*-octadecylpyridinium cation and a minimum of 0.24 nm^2 for the Pd(dmit)$_2$ molecule, giving a total of 0.48 nm^2. A proposed model for the arrangement of the molecules in these films is discussed later. When a large amount of material was spread and left for a long time before compression, the area per complex was smaller still. Observation of these layers on the subphase surface revealed the existence of large particles. Using atomic force microscopy, Japanese workers have observed μm sized plate-like crystallites present in monolayer and multilayer LB films of tridecylmethylammonium-Au(dmit)$_2$ mixed with eicosanoic acid.[4] It was thought that these platelets formed at the air-water interface and were

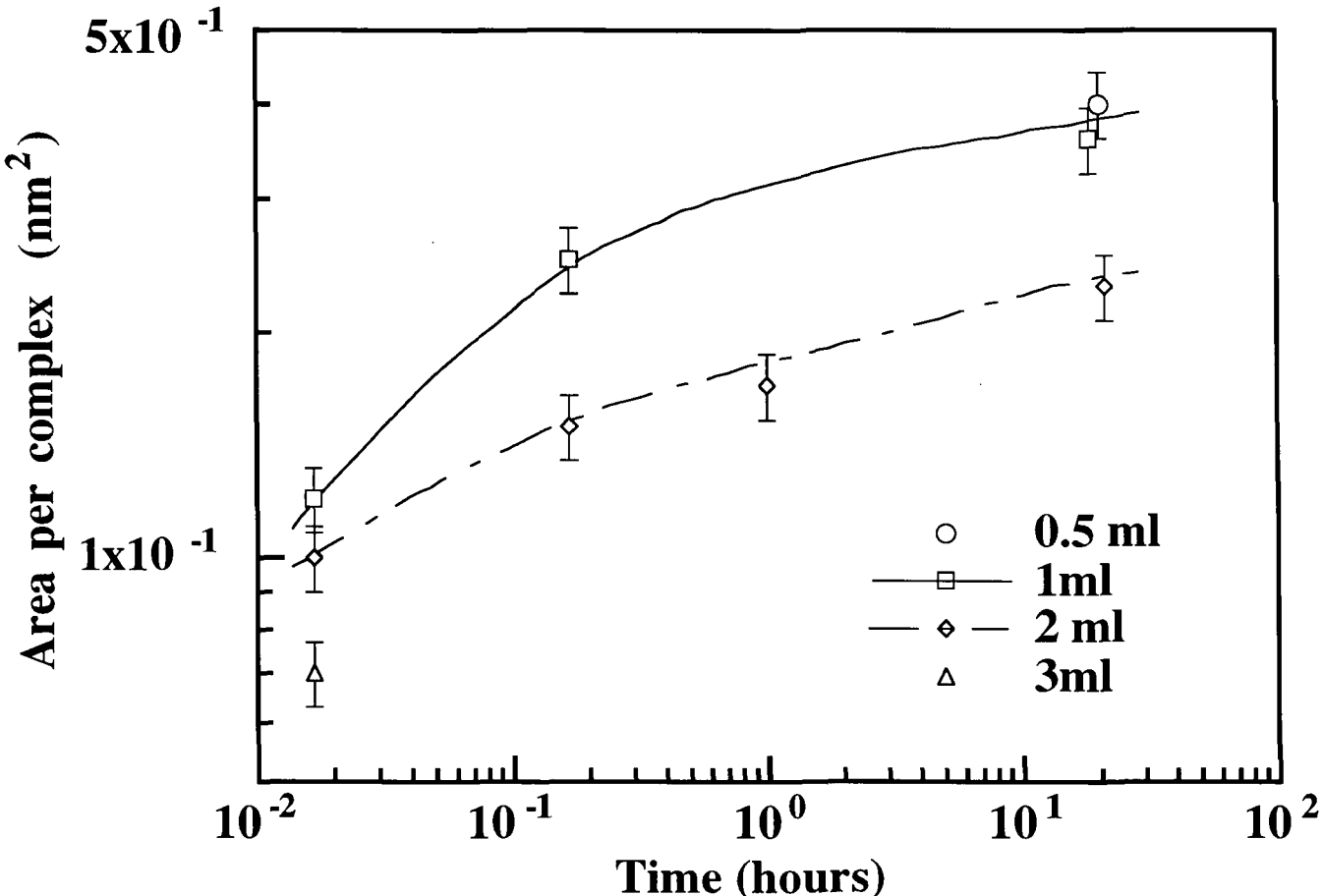

Fig. 7.4 Area per complex, measured at a surface pressure of 30 mN m^{-1}, versus the time that C_{18}Py-Pd(dmit)$_2$ molecules were allowed to remain on the surface of a pure water subphase before isotherms were recorded. The data measured for four different volumes of solution are plotted on the same graph.

subsequently transferred to the substrate during monolayer transfer. This structure was consistent with the small area per molecule which had been obtained by surface pressure versus area measurements.[5]

7.3 LB film deposition

In experiments where an isotherm with no plateau was recorded, a deposition pressure of 30 mN m^{-1} was used. When a plateau was observed, a surface pressure of 38 mN m^{-1} (above the plateau) was substituted. Dipping was started with the substrates in air above the surface of the subphase and was undertaken at a speed of 6 mm min^{-1}, allowing 15 minutes of drying time between cycles. The substrates used were hydrophilic glass slides, and consequently the first cycle exhibited Z-type transfer. The transfer ratio, τ, recorded was dependent on the exact experimental conditions. The values measured are listed in Table 7.1.

Amount of solution spread (ml)	Time on the subphase before compression	Number of layers deposited	Transfer ratio on 2nd cycle down/up (±0.1)	Transfer ratio on final cycle down/up (±0.1)
1	10 minutes	19	0.5/1.1	0.9/1.1
1	18 hours	19	0.5/1.1	0.8/1.1
2	10 minutes	19	1.1/1.1	1.1/1.1
2	21 hours	39	1.1/1.1	1.1/1.1

Table 7.1 Transfer ratios for LB deposition of C_{18}Py-Pd(dmit)$_2$ onto hydrophilic glass substrates.

7.4 Film properties

7.4.1 Thickness measurements

The thicknesses of multilayer films deposited from layers formed from different amounts of solution which had been allowed to stand uncompressed on the subphase for different lengths of time were measured using surface profiling. A typical scan, obtained for a 19-layer film which had been transferred from a floating layer formed from 1 ml of solution compressed after 10 minutes on the subphase is shown in Fig. 7.5. The film was continuous up to a thickness of *ca.* 90 nm, but the surface was very undulating, and a number of regions up to 200 nm thick and 50 μm in diameter were recorded, as well as a 'giant' peak close to the edge of the film. This peak was attributed to physical damage caused as the step was formed by wiping away a portion of the film with a tissue soaked in dichloromethane. This resulted in an accumulation of organic material at the edge of the step. The variation of the thickness per layer with amount of material spread and the time that the floating layer was aged before compression was similar to that observed with C_{18}Py-Ni(dmit)$_2$ films. The results of four experiments are listed in Table 7.2

Amount of solution spread. (ml)	Time before compression.	Thickness per layer. (nm)
1	10 minutes	4.7±0.2
1	18 hours	2.5±0.3
2	10 minutes	11.4±0.2
2	21 hours	5.7±0.3

Table 7.2 The variation of layer thickness with the amount of C_{18}Py-Pd(dmit)$_2$ solution spread and the length of time allowed before compression.

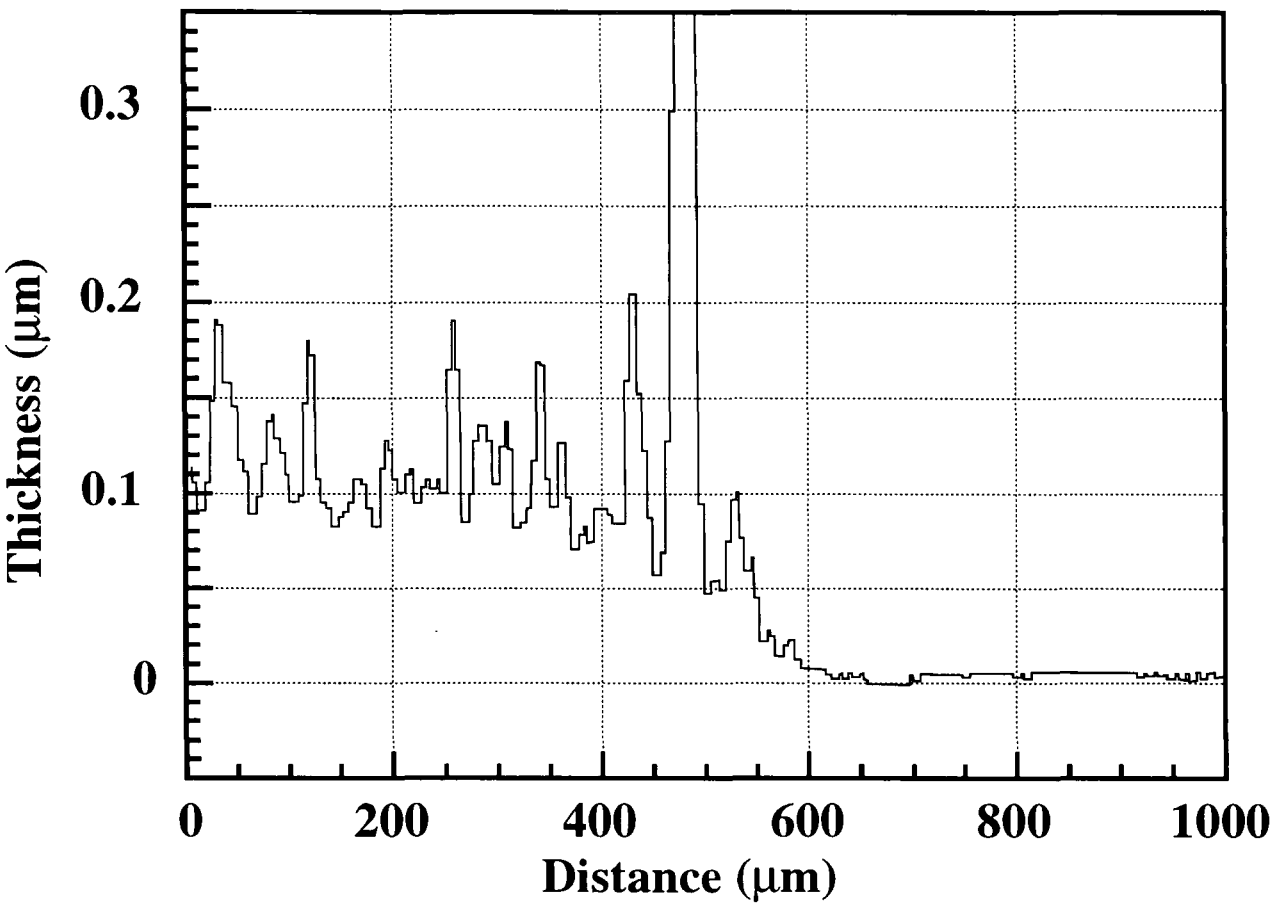

Fig. 7.5 A typical surface profiling Alpha-Step trace, recorded from a 19-layer film of C_{18}Py-Pd(dmit)$_2$. The sample was deposited from a floating layer formed from 1 ml of solution that had been allowed to stand on the surface of the subphase for 10 minutes before compression.

The best spreading characteristics, and hence the thinnest layers, were observed when 1 ml of solution was spread and the film left on the subphase for 18 hours before compression. Thicker layers were deposited if the film was compressed earlier or if more solution was spread. The relationship between layer thickness, t, and area per complex at the surface pressure used for deposition, A_0, is illustrated in Fig. 7.6. From the slope of the graph, the relationship

$$t \propto A_0^{-1.0\pm0.1} \qquad 7.1$$

was deduced.

In the following sections, the results of experiments are reported that were carried out on films prepared using the four different spreading conditions described above: 1 ml of solution aged for 10 minutes; 1 ml of solution aged for 18 hours; 2 ml of solution aged for 10 minutes and 2 ml of solution aged for 21 hours.

7.4.2 Electron microscopy and energy dispersive spectroscopy

Fig 7.7 shows a scanning electron micrograph obtained from a 19-layer film deposited onto a glass substrate from a film formed from 1 ml of solution which had been allowed to stand on the subphase uncompressed for 10 minutes. Irregularly shaped aggregates can be seen, tens of microns in size, i.e. having similar dimensions to the thick regions seen in previous surface profiling scans (Fig. 7.5). Fig. 7.8 shows the results of EDS measurements for the two electron probe positions marked on the micrograph, corresponding to one of the aggregates (position A) and the background (position B). Sulphur and palladium were predominantly detected when the aggregate was probed, although traces of these elements were also seen in the background spectrum, revealing the presence of $Pd(dmit)_2$. Using this technique it was not possible to detect the presence

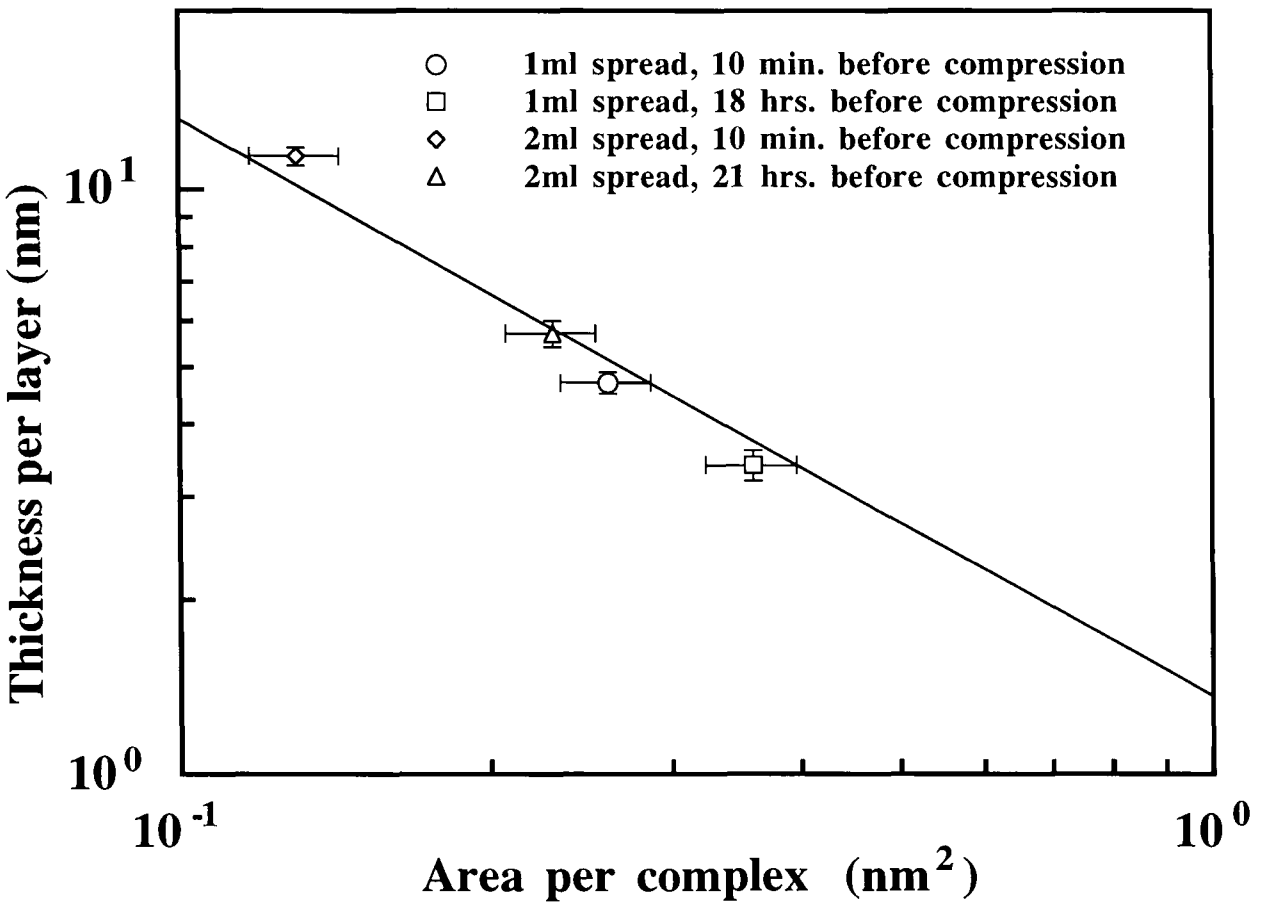

Fig. 7.6 Thickness per layer in transferred films of C_{18}Py-Pd(dmit)$_2$, obtained using surface profiling, versus area per complex on the surface of a pure water subphase at the pressure used for deposition.

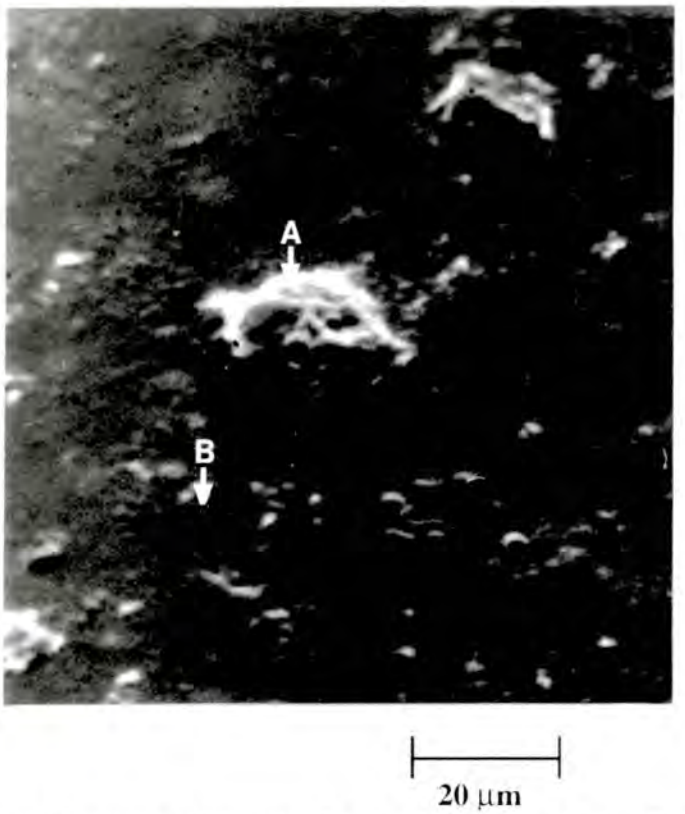

Fig. 7.7 **Scanning electron micrograph of an as-deposited 19-layer film of C_{18}Py-Pd(dmit)$_2$. The sample was transferred from a layer formed from 1 ml of solution that had been allowed to stand on the surface of the subphase for 10 minutes before compression.**

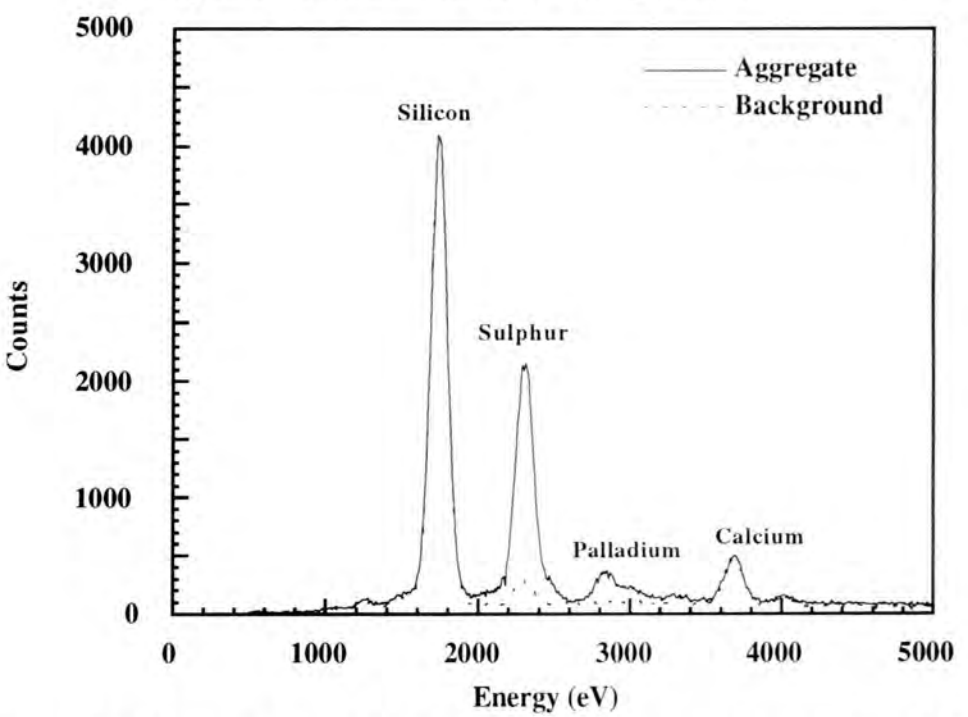

Fig. 7.8 **EDS spectra recorded from an as-deposited 19-layer film of C_{18}Py-Pd(dmit)$_2$. The sample was transferred from a layer formed from 1 ml of solution that had been allowed to stand on the surface of the subphase for 10 minutes before compression. The electron probe was directed at point A on the micrograph shown in Fig. 7.7 when the solid line was recorded and at point B for the data represented by the dashed line.**

of the long chain pyridinium cation. The strong signals due to silicon and calcium seen in the spectra were due to the substrate, confirmed by an EDS measurement on an uncoated piece of glass. The result of leaving the same amount of solution on the subphase for 18 hours before compression can be seen in Fig. 7.9. Here, no large aggregates were found, and the film contained only small features, a few microns in size. It is therefore suggested that when 1 ml of solution was spread, large crystallites containing $Pd(dmit)_2$ were immediately formed. It would seem that these crystallites dissociated with time, however, giving a more uniform LB film. This observation is similar to that of Gupta *et al* [3] for films of didodecyldimethylammonium-$Ni(dmit)_2$.

When 2 ml of solution was spread and compressed after 10 minutes on the subphase, a higher density of crystallites was observed, as shown in the micrograph of Fig. 7.10, which was taken from a 19-layer as-deposited film. After ageing, much larger aggregates formed which were hundreds of microns in size. These clusters could be observed in the layer on the surface of the subphase and were subsequently transferred to the substrate. A micrograph recorded from a 39-layer film which was deposited from a film formed from 2 ml of solution which had been allowed to stand uncompressed for 21 hours is shown in Fig. 7.11, where one of the large particles can clearly be seen. EDS scans, performed at the two positions marked on the figure (position A corresponding to the particle and position B to the background) are shown in Fig. 7.12. The scan at position A contained large signals due to sulphur and palladium, revealing the presence of $Pd(dmit)_2$. The peaks due to these elements were much lower when position B, in the background, was probed. Peaks due to the silicon and calcium in the glass substrate were again seen, but these were much reduced when the particle was probed, reflecting the increased thickness of this feature.

7.4.3 Optical absorption

The optical absorption spectra for as-deposited films of $C_{18}Py$-$Pd(dmit)_2$ transferred

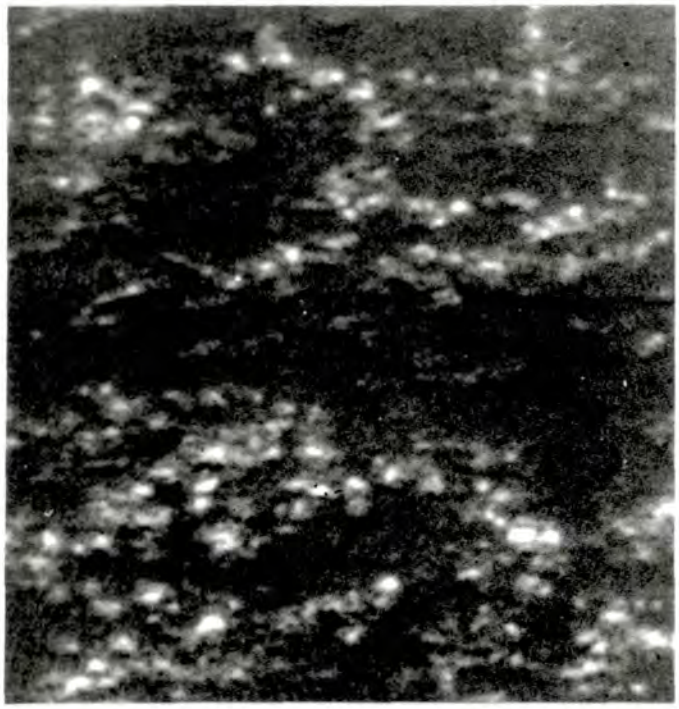

Fig. 7.9 **Scanning electron micrograph of an as-deposited 19-layer film of C_{18}Py-Pd(dmit)$_2$. The sample was transferred from a layer formed from 1 ml of solution that had been allowed to stand on the surface of the subphase for 18 hours before compression.**

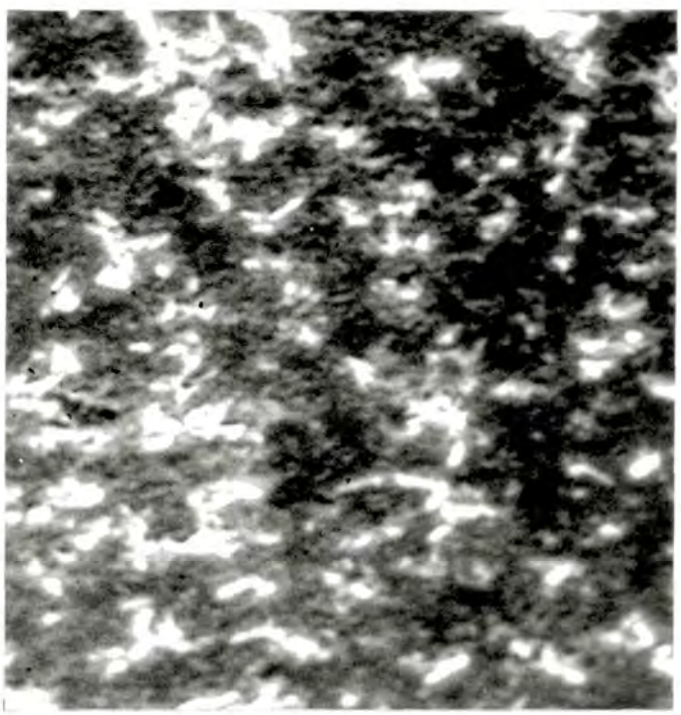

Fig. 7.10 **Scanning electron micrograph of an as-deposited 19-layer film of C_{18}Py-Pd(dmit)$_2$. The sample was transferred from a layer formed from 2 ml of solution that had been allowed to stand on the surface of the subphase for 10 minutes before compression.**

Fig. 7.11 **Scanning electron micrograph of an as-deposited 39-layer film of C_{18}Py-Pd(dmit)$_2$. The sample was transferred from a layer formed from 2 ml of solution that had been allowed to stand on the surface of the subphase for 21 hours before compression.**

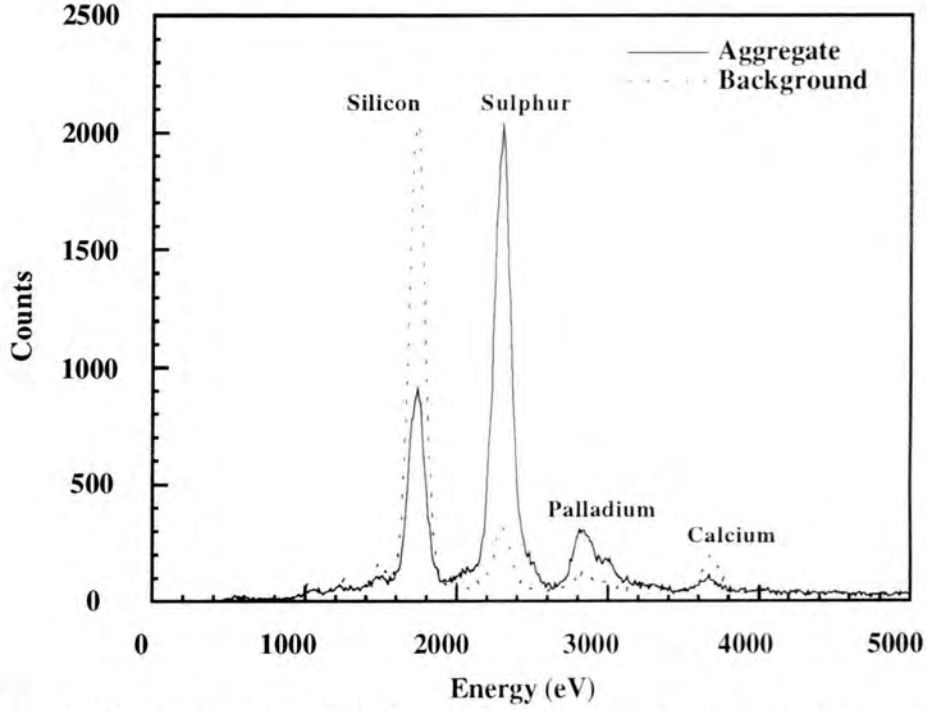

Fig. 7.12 **EDS spectra recorded from an as-deposited 39-layer film of C_{18}Py-Pd(dmit)$_2$. The sample was transferred from a layer formed from 2 ml of solution that had been allowed to stand on the surface of the subphase for 21 hours before compression. The electron probe was directed at point A on the micrograph shown in Fig. 7.11 when the solid line was recorded and at point B for the data represented by the dashed line.**

from floating layers formed from different amounts of solution which had been left on the subphase for different times are shown in Fig. 7.13. The following samples were used: 19-layers deposited from a floating layer formed from 1 ml of solution that had been aged for (a) 10 minutes and (b) 18 hours, (c) 19-layers and (d) 39-layers transferred from a floating layer formed from 2 ml of solution that had been aged for 10 minutes and 21 hours, respectively. The absorption bands which were observed at 330, 380 and 480 nm are probably due to intramolecular transitions within the $Pd(dmit)_2$ molecules. Additionally, broad bands were seen at 800 and 1400 nm. Absorptions in the near infrared have been associated with intermolecular charge-transfer transitions by Underhill *et al*[5] in single crystals of $Cs[Pd(dmit)_2]$ and Miura *et al* for LB multilayers of tridecylmethylammonium-$Au(dmit)_2$ mixed with eicosanoic acid and deposited by the horizontal lifting method.[6] The variation in the intensity of the absorption bands reflects the different LB film thicknesses, and a plot of absorption, measured at 800 nm, versus film thickness, measured using surface profiling, is shown inset to Fig 7.13. The graph indicates a linear relationship between the two quantities.

Spectra recorded for the same films after chemical doping are shown in Fig 7.14. After treatment with iodine vapour, the bands at 380 and 480 nm and the broad absorption in the infra red were significantly reduced, whereas the band at *ca* 800 nm remained. The band was strongest in spectra recorded for samples with high bulk conductivity, i.e. those deposited from floating monolayers that had been aged on the surface of the subphase for a short time (see section 7.5). Two peaks were observed, at a similar wavelength, in the spectra of conductive iodine-doped films of C_{18}Py-$Ni(dmit)_2$ (chapter 8, section 8.4.4). It seems likely that some (or all) of these absorptions are associated with a charge-transfer band arising from the formation of a mixed valence complex.

7.5 Room temperature conductivity

During the measurement of the electrical properties of LB multilayers of C_{18}Py-

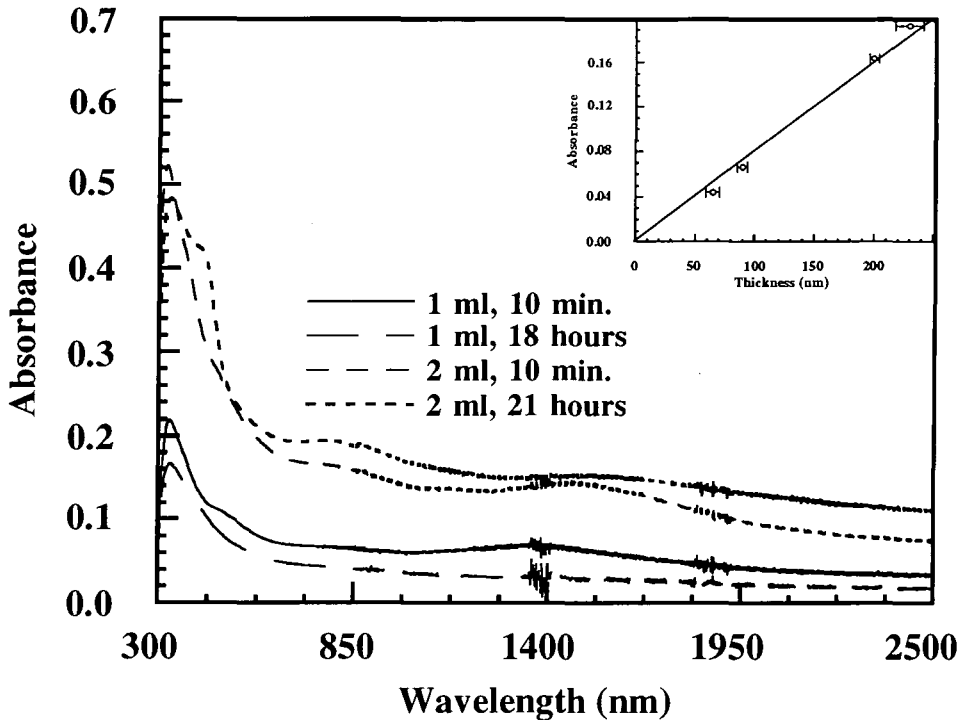

Fig. 7.13 Optical absorption spectra for 19-layer as-deposited LB films of C_{18}Py-Pd(dmit)$_2$ prepared from floating films that had been allowed to age on the subphase for different lengths of time. The absorbance at 800 nm versus measured film thickness is shown inset.

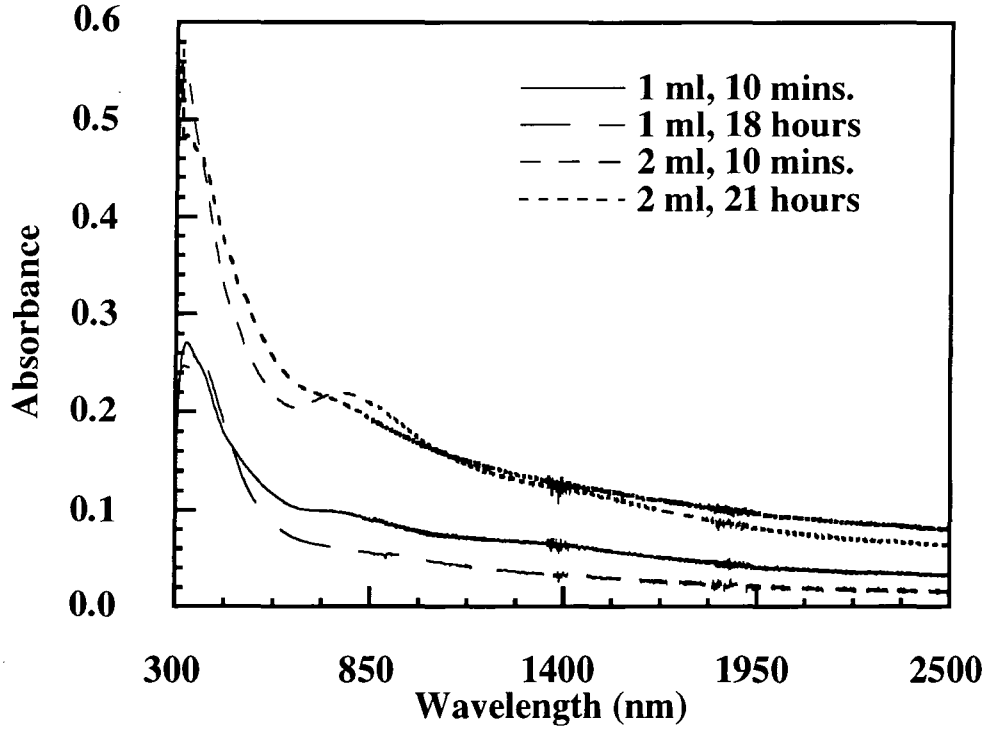

Fig. 7.14 Optical absorption spectra for 19-layer iodine doped LB films of C_{18}Py-Pd(dmit)$_2$ prepared from floating films that had been allowed to age on the subphase for different lengths of time.

$Ni(dmit)_2$, the reproducibility of results was dependent on the electroding material, with instability observed when silver paint was used (chapter 8, section 8.5.1). To avoid this problem, the dc conductivities of $C_{18}Py$-$Pd(dmit)_2$ films were measured using carbon cement or, in some cases, a thin film of evaporated gold to provide contacts. These materials were found to remain stable for at least twelve months after application. The conductivity was found to be strongly dependent upon the conditions used to prepare the organic film.

7.5.1 One ml of solution spread and 10 minutes allowed before compression.

The current versus voltage characteristics for a 19-layer film of $C_{18}Py$-$Pd(dmit)_2$ which was deposited from a layer formed from 1 ml of solution which had been allowed to stand uncompressed on the subphase for 10 minutes are shown in Fig. 7.15. These measurements were performed under vacuum at a pressure of *ca* 10^{-2} mbar. The film had carbon cement contacts with different spacings, and was found to be conducting without the need for any post-deposition doping treatment. This behaviour is consistent with the presence of a band at *ca.* 800 nm in the optical absorption band of these films, which has been attributed to an intermolecular charge transfer transition in single crystals of $Cs[Pd(dmit)_2]$.[5] A room temperature in-plane dc conductivity of $3.5\pm2.5 \times 10^{-3}$ S cm^{-1} at a bias of 1V was calculated using the thickness of the film obtained from surface profiling measurements. This value was much higher than that measured for as-deposited films of $C_{18}Py$-$Ni(dmit)_2$ (chapter 8, section 8.5). The reason for this high conductivity without any post deposition doping treatment is not understood. A conductivity of 10^{-2} S cm^{-1} was reported by Ward *et al*[7] for LB films of the 1:1 salt *N*-octadecylpyridinium-TCNQ. It was suggested that inadvertent doping with an anion (such as OH^-) during the deposition procedure may have been responsible. The current versus voltage characteristics for as-deposited $C_{18}Py$-$Ni(dmit)_2$ did not follow a simple straight line over the entire bias range studied, and a super-Ohmic region was observed at high bias. In this super Ohmic region, current saturation was slow, and a few tens of minutes were

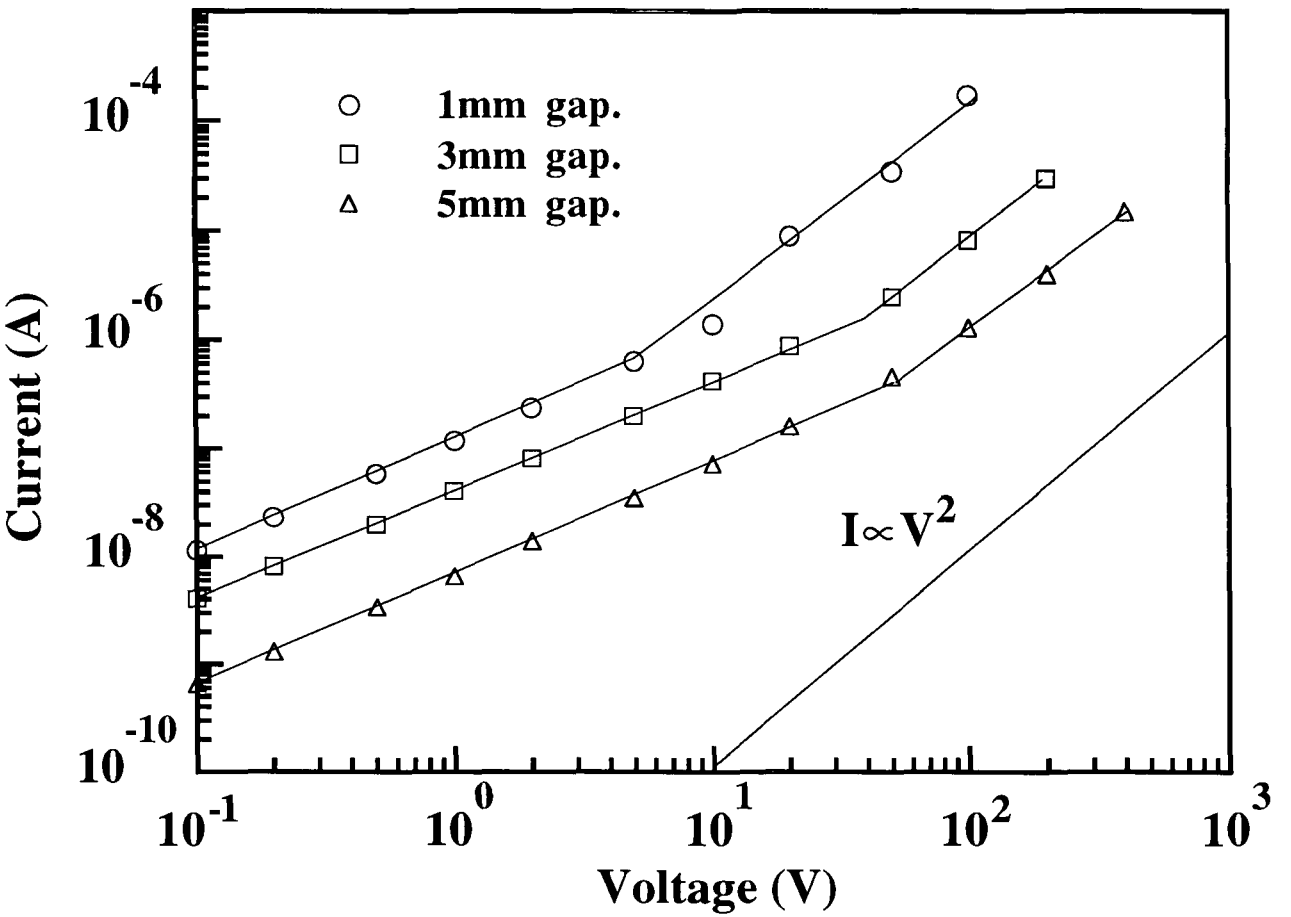

Fig. 7.15 Current versus voltage characteristics for a 19-layer LB film of C_{18}Py-Pd(dmit)$_2$ with carbon cement contacts 1 mm, 3 mm and 5 mm apart. The sample was deposited from a floating layer formed from 1 ml of solution that had been allowed to stand uncompressed on the surface of the subphase for 10 minutes.

required for the current to reach its peak value. Fig. 7.16 shows the change in current with time after the application of a bias of 100 V to a pair of carbon cement contacts with a gap of 1.0±0.5 mm, on a 19-layer film, under vacuum. Under high bias, the peak sample current was found to be proportional to the square of applied voltage. Taylor *et al* [8] have observed super Ohmic current versus voltage behaviour in films of bis(didodecyldimethylammonium)-Pt(dmit)$_2$, bis(octadecylpyridinium)-Pd(dmit)$_2$ and octadecylpyridinium-Au(dmit)$_2$ with evaporated gold contacts, and the same effect was seen in multilayers of the 2:1 complex (*N*-octadecylpyridinium)$_2$-Ni(dmit)$_2$.[9] This behaviour may indicate space charge limited conductivity (SCLC)[10], which is described by the general law

$$J \propto L\left(\frac{V}{L^2}\right)^n \qquad 7.2$$

where J is the current density, V the bias voltage, L the thickness of the sample and n is a constant. For single carrier injection, (electrons or holes) n=2 whereas for double injection, (electrons and holes) n=3. A graph of sample current at high bias (100V) versus the distance between contacts, L, is shown in Fig. 7.17. The best fit to this data, represented by the dashed line, has a slope of -2.9±0.2. Hence, equation 7.2 is satisfied with n=2. From the same model, the threshold voltage $V_{\Omega c}$, where the Ohmic current crosses over into the SCL regime is given by

$$V_{\Omega c} = \frac{8}{9}\frac{enL^2}{\varepsilon\theta_n} \qquad 7.3$$

where e is the electronic charge, n is the concentration of conduction electrons, ε is the permittivity and θ_n the fraction of total carriers which are free. From this equation, it can be seen that for SCL conductivity, $V_{\Omega c}$ should be proportional to the square of the thickness of the sample. By fitting straight lines to the Ohmic and super Ohmic portions

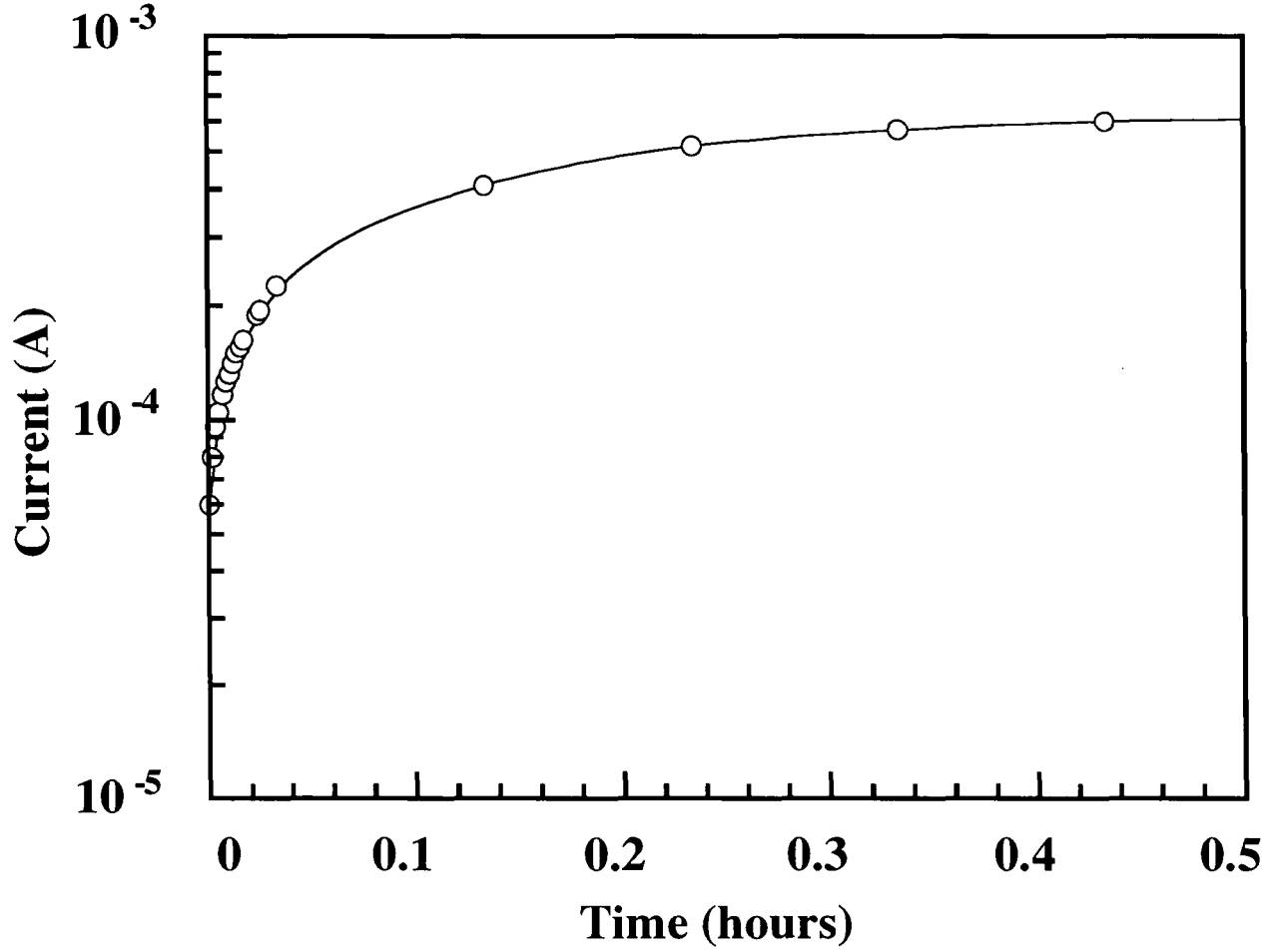

Fig. 7.16 Change of current with time after application of a bias voltage of 100 V to a pair of carbon cement contacts 1.0±0.5 mm apart on a 19-layer as-deposited film of C_{18}Py-Pd(dmit)$_2$. The film was transferred from a floating layer prepared from 1 ml of solution that had been allowed to stand on the surface of the subphase for 10 minutes before compression.

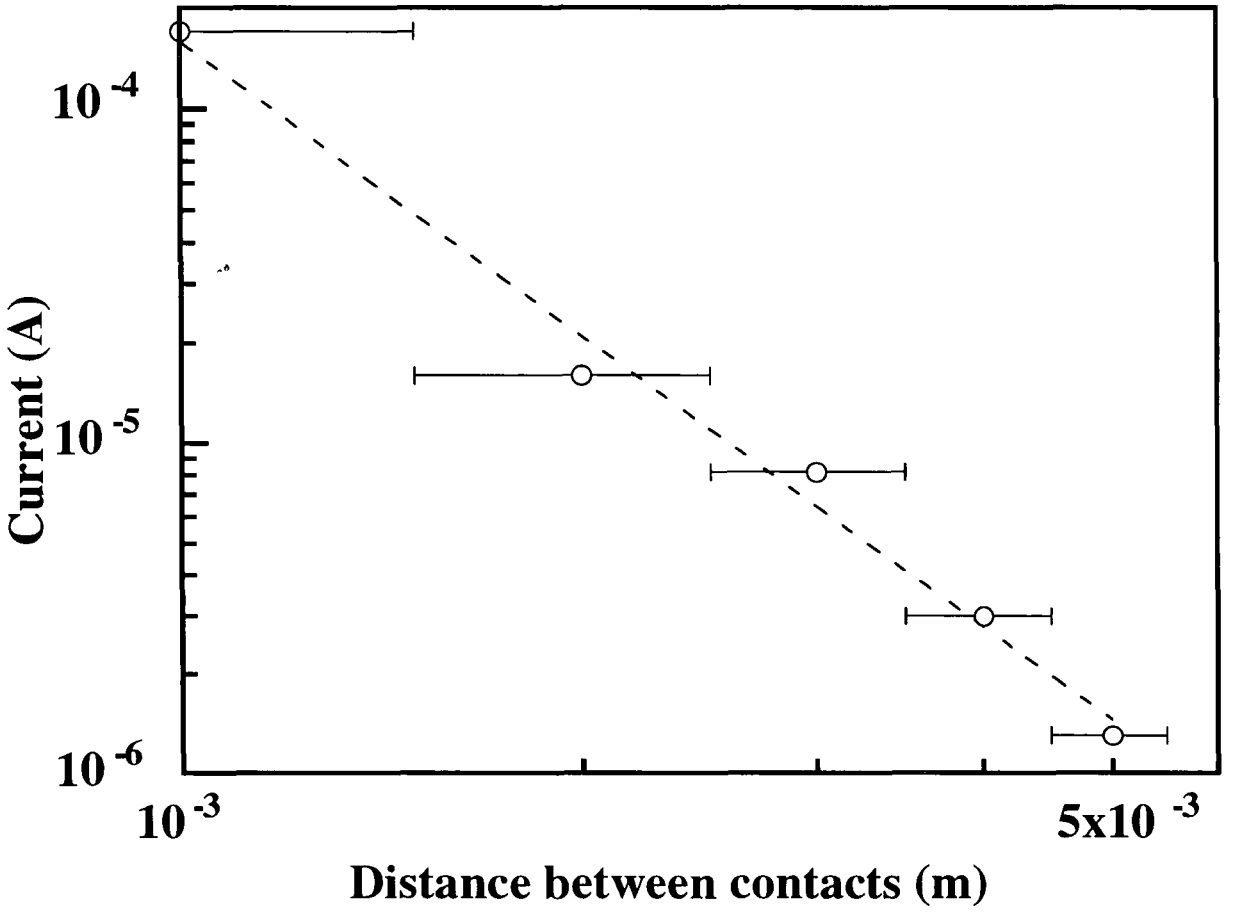

Fig. 7.17 **Current, with a bias of 100 V applied to carbon cement contacts, versus the distance between the contacts. The dashed line represents the best fit to the data, and has a slope of -2.9±0.2.**

of the experimental current versus voltage characteristics, this threshold voltage has been obtained for the different distances between contacts, L. A plot of $\sqrt{V_{\Omega c}}$ versus L is shown in Fig 7.18. The points lie on a straight line, indicating agreement with equation 7.3. These results strongly suggest that the observed super-Ohmic characteristics are caused by single carrier space charge injection.

High conductivity was retained after the removal of bias in the SCLC region. It has been reported that the accumulation of charge can affect current readings in materials where SCLC is observed.[11] Fig. 7.19 shows the variation of the conductivity of a 19-layer film, with carbon cement contacts 2.5±0.5 mm apart, as the voltage was cycled from 10^{-1} V to $5x10^{2}$ V and back again. The conductivity increased with increasing bias, and the high value was retained as the voltage was reduced. This high conductivity remained for a considerable time after the removal of bias in the SCLC regime. For example, Fig. 7.20 shows the variation of current with time when a bias of 10 V was applied to carbon cement contacts 1.0±0.5 mm apart on a 19-layer LB sample, after a voltage of 100 V had previously been applied until current saturation occurred. The conductivity returned to a level close to the value recorded before application of high bias only after several months.

If air was admitted to the sample chamber with simultaneous application of a high bias voltage to a sample, a sudden decrease in current was seen, as illustrated in Fig. 7.21. Here, 100 V was applied to carbon cement contacts with a gap of 1.0±0.5 mm until current saturation was observed. Air was then admitted to the sample chamber at the point indicated on the time scale. The conductivity was rapidly reduced to one fifth of the initial value. It is possible that in the presence of atmospheric moisture or oxygen, a barrier is formed at one (or both) of the electrodes which limits the flow of current.

Films that had been chemically doped with iodine vapour exhibited no super-Ohmic region in their current versus voltage characteristic. Fig. 7.22 is an I versus V plot for a

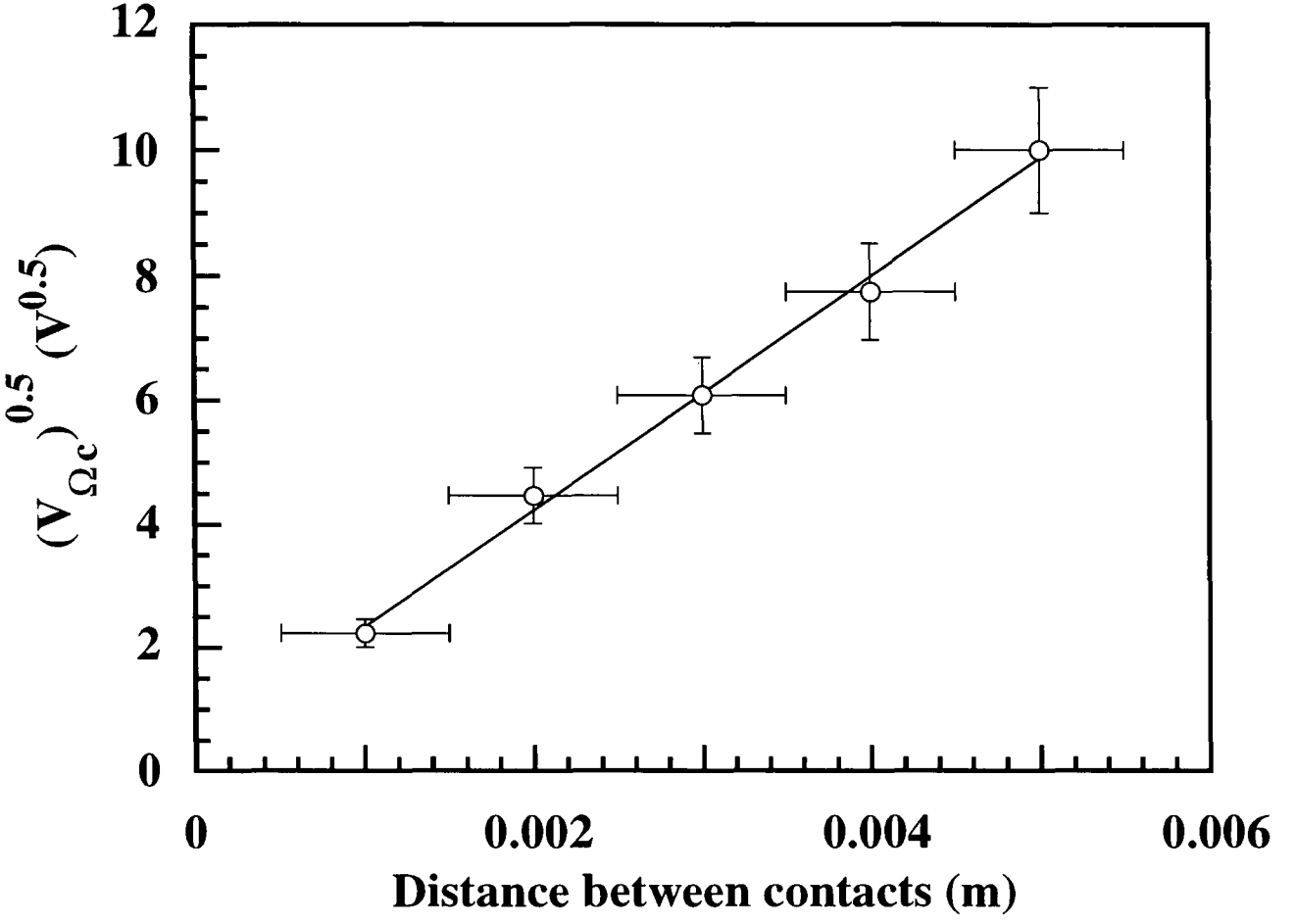

Fig. 7.18 $(V_{\Omega c})^{0.5}$ versus the distance between carbon cement contacts on a 19-layer as-deposited film of C_{18}Py-Pd(dmit)$_2$. The film was transferred from a floating layer prepared from 1 ml of solution compressed 10 minutes after spreading.

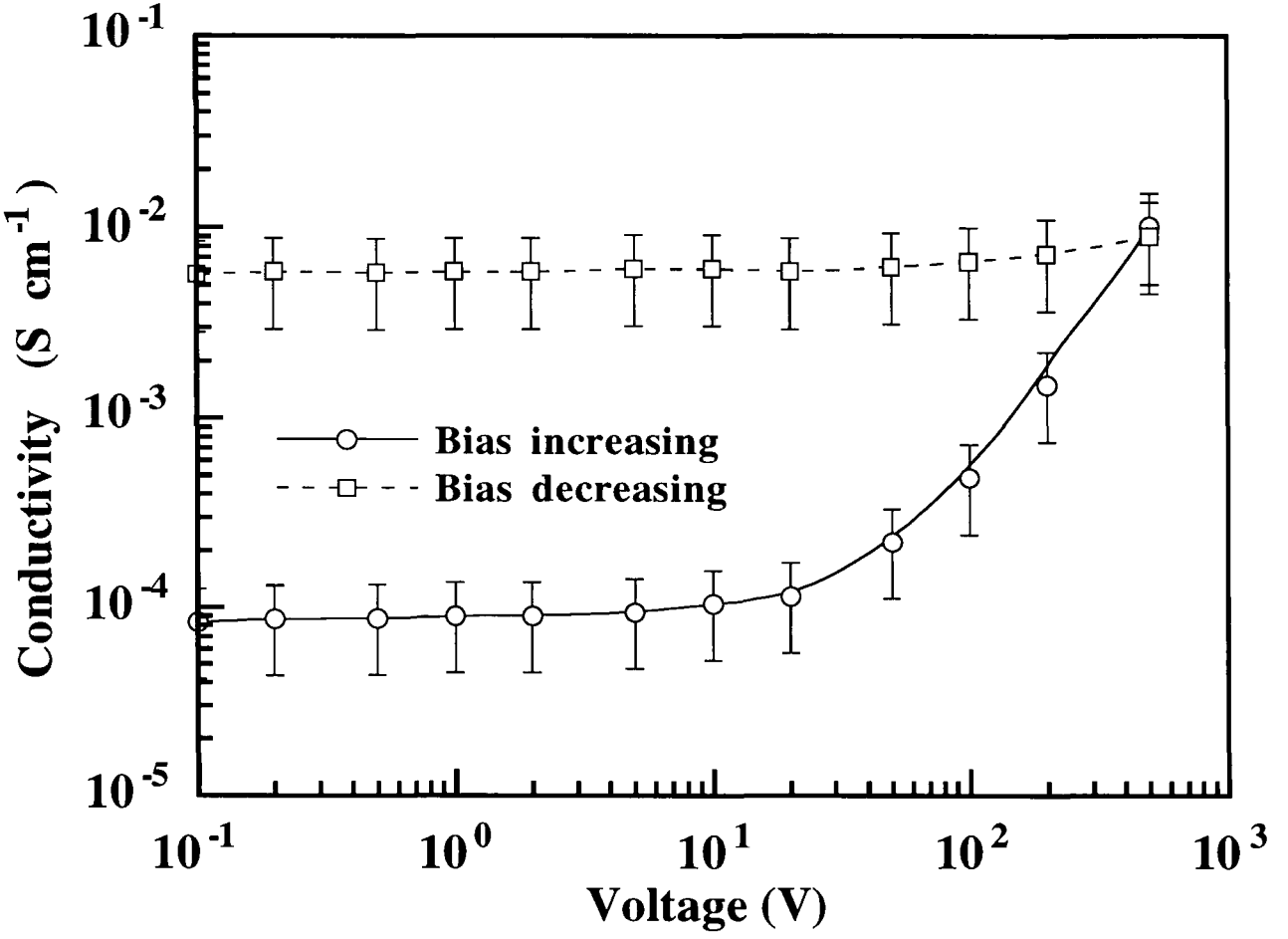

Fig. 7.19 Variation of the conductivity of a 19-layer as-deposited film of C_{18}Py-Pd(dmit)$_2$ with bias voltage. The film was deposited from a floating layer formed from 1 ml of solution that was aged for 10 minutes before compression. Contacts 1.0±0.5 mm apart were established using carbon cement.

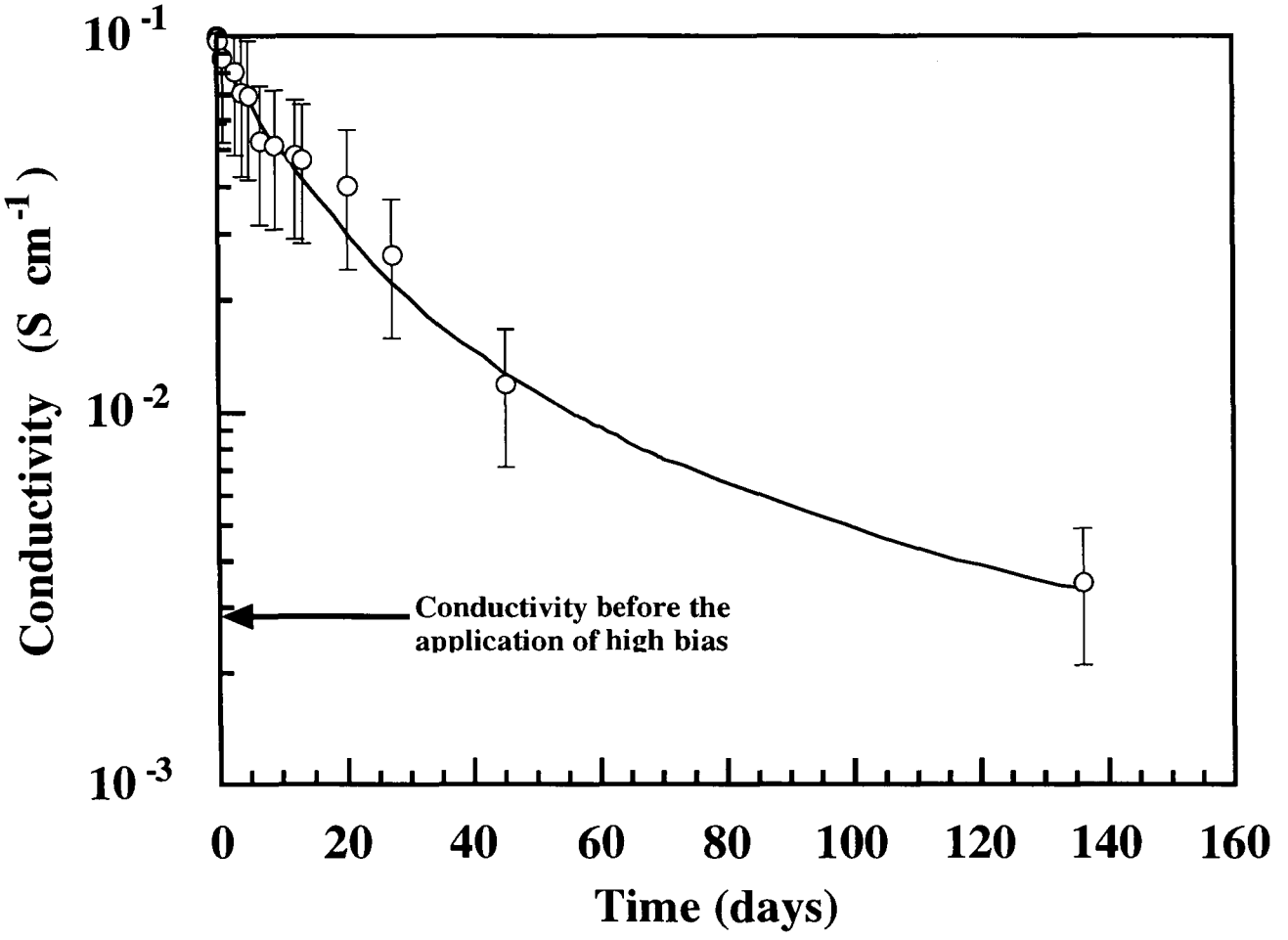

Fig. 7.20 Variation of the conductivity with time (with a bias of 10 V applied to carbon cement contacts 1.0±0.5 mm apart) of a 19-layer as-deposited film of C_{18}Py-Pd(dmit)$_2$. The film was transferred from a floating layer formed from 1 ml of solution aged for 10 minutes before compression. The sample was pre-treated by the application of 100 V until current saturation occurred.

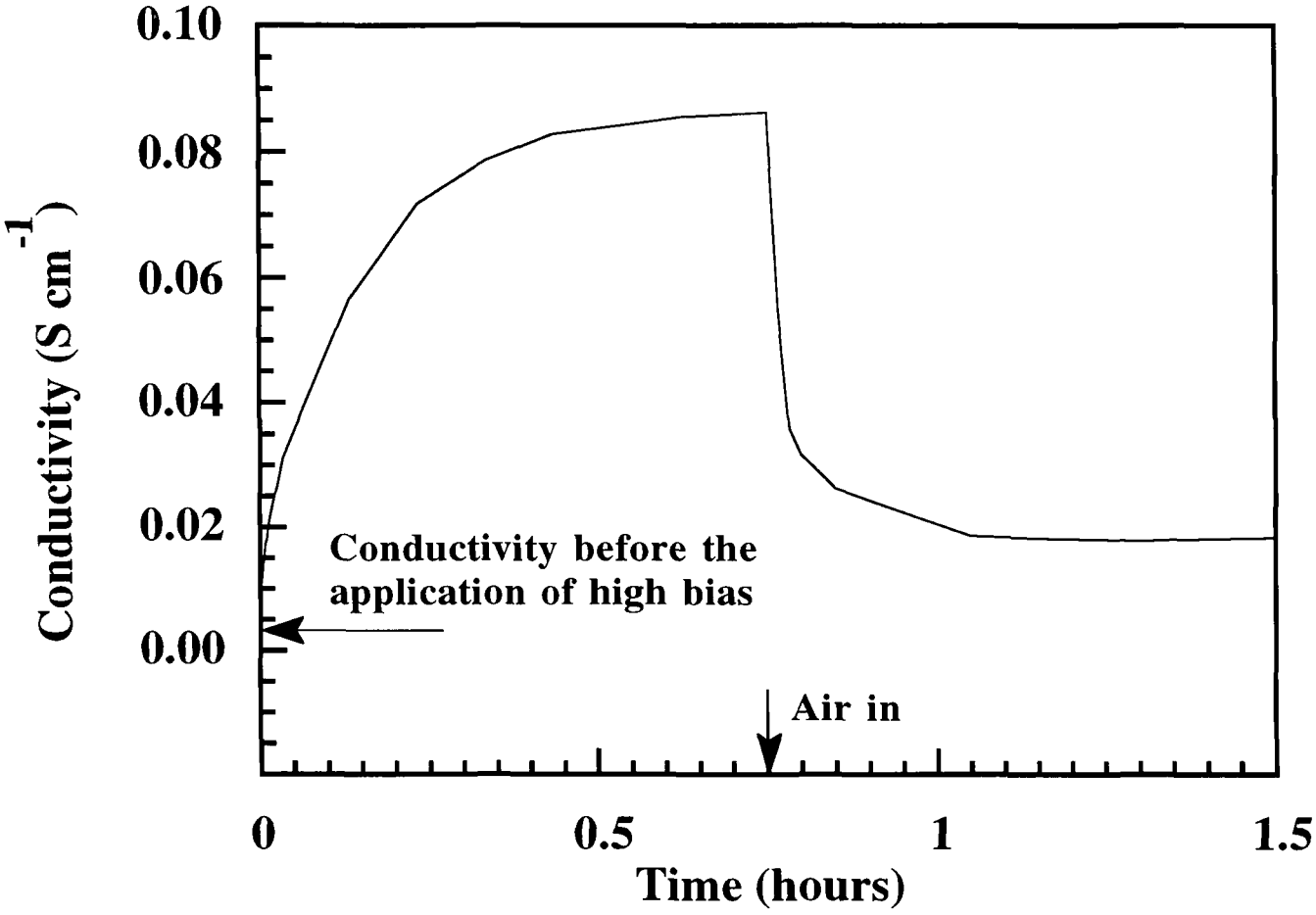

Fig. 7.21 The effect of admitting air to the sample chamber with simultaneous application of 100 V (on the super-Ohmic part of the current versus voltage characteristic) to contacts 1.0±0.5 mm apart on a 19-layer as-deposited sample of C_{18}Py-Pd(dmit)$_2$. The film had been transferred from a floating layer formed from 1 ml of solution that had been aged on the surface of the subphase for 10 minutes. The point at which air was admitted and the conductivity at low bias are marked on the x and y axes, respectively.

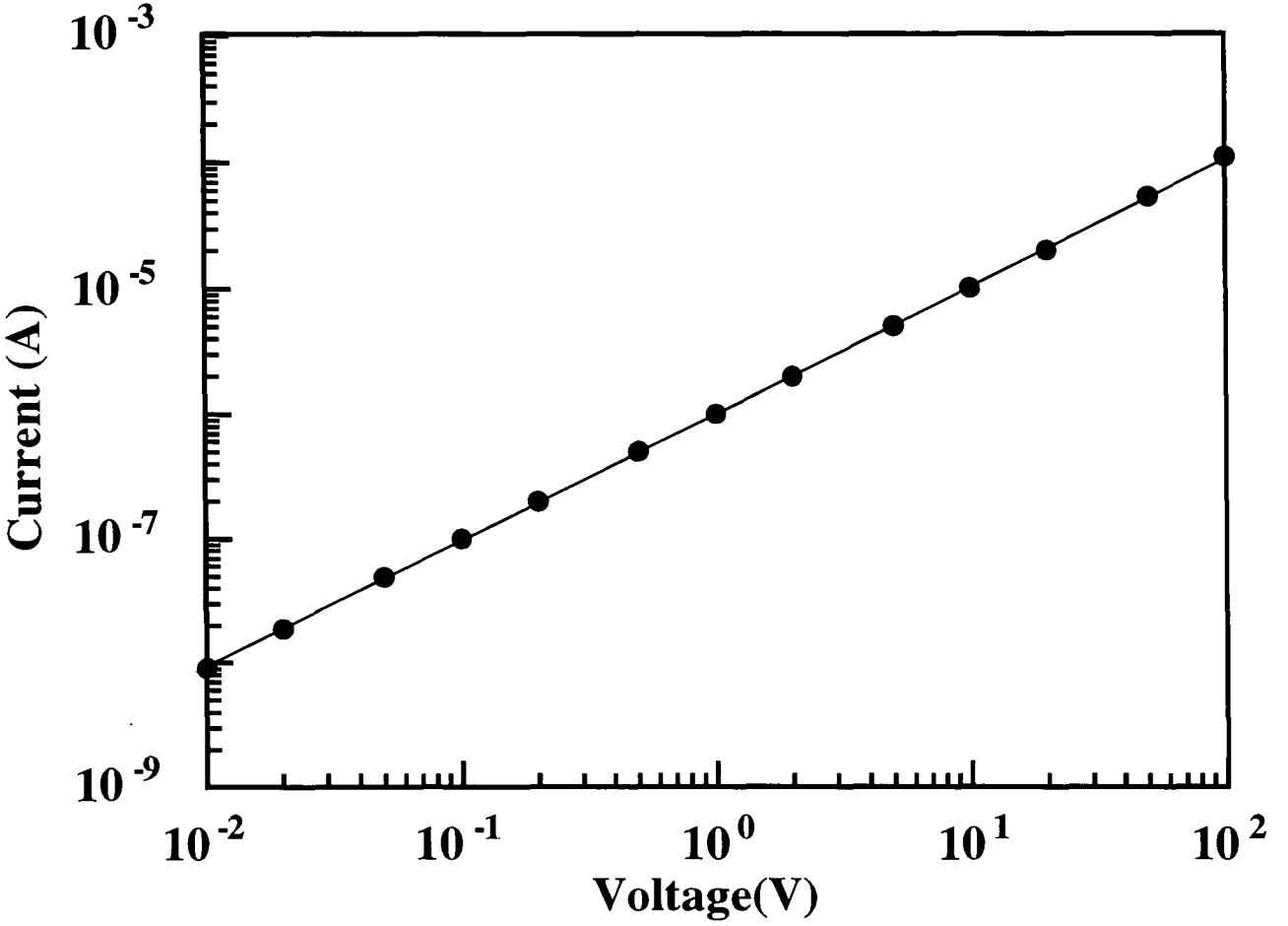

Fig. 7.22 Current versus voltage characteristic for a 19-layer film of C_{18}Py-Pd(dmit)$_2$ after doping with iodine. The sample was deposited from a floating layer formed from 1 ml of solution that was aged for 10 minutes before compression.

19-layer iodine doped film, having carbon cement contacts 1.0±0.5 mm apart. From this graph, a conductivity value of $2.6\pm1.7\times10^{-2}$ S cm^{-1} was calculated. This figure was higher than that measured for the as-deposited sample, and smaller than the values measured for multilayer films of C_{18}Py-Ni(dmit)$_2$ (chapter 8, section 8.5) and (*N*-octadecylpyridinium)$_2$-Ni(dmit)$_2$[9] after iodine doping.

7.5.2 One ml of solution spread and 18 hours allowed before compression.

Samples deposited from floating films formed from 1 ml of solution that was allowed to age on the subphase for 18 hours, in common with films transferred from aged layers of C_{18}Py-Ni(dmit)$_2$, were non-conductive (<10^{-8} S cm^{-1}) in the as-deposited state. After exposure to iodine vapour the conductivity measured using carbon cement contacts was seen to rise to 10^{-5}-10^{-4} S cm^{-1} initially, but rapidly fall back to the as-deposited value on application of vacuum. Optical absorption experiments have revealed the presence of Pd(dmit)$_2$ in these samples, so the absence of conductivity must be related to the physical structure of the films. Fig 7.23 shows one possible molecular arrangement. Here, the Pd(dmit)$_2$ anions are interdigitated between the long-chain pyridinium cations, which are tilted at an angle to the substrate normal. A tilt angle of about 30°, a value similar to that found in LB layers of *N*-octadecylpyridinium-TCNQ[12], would give a monolayer thickness of 2.5±0.1 nm, in agreement with the results of surface profiling measurements. Additionally, using the dimensions obtained from molecular modelling, an area per complex of around 0.3±0.1 nm^2 would be expected for this structure, close to the maximum value recorded for these floating films i.e. 0.36±0.04 nm^2. With this arrangement, the Pd(dmit)$_2$ molecules are prevented from packing closely in either direction which would prevent high in-plane conductivity. This structure is similar to that proposed by Taylor *et al*[13] for their 1:1 and 2:1 salts of didodecyldimethylammonium and Ni(dmit)$_2$, based on the measurement of limiting area per complex values. These writers suggested a structure for their floating layers in which close packed cations were interspersed with vertically stacked anions with their long axes either parallel or

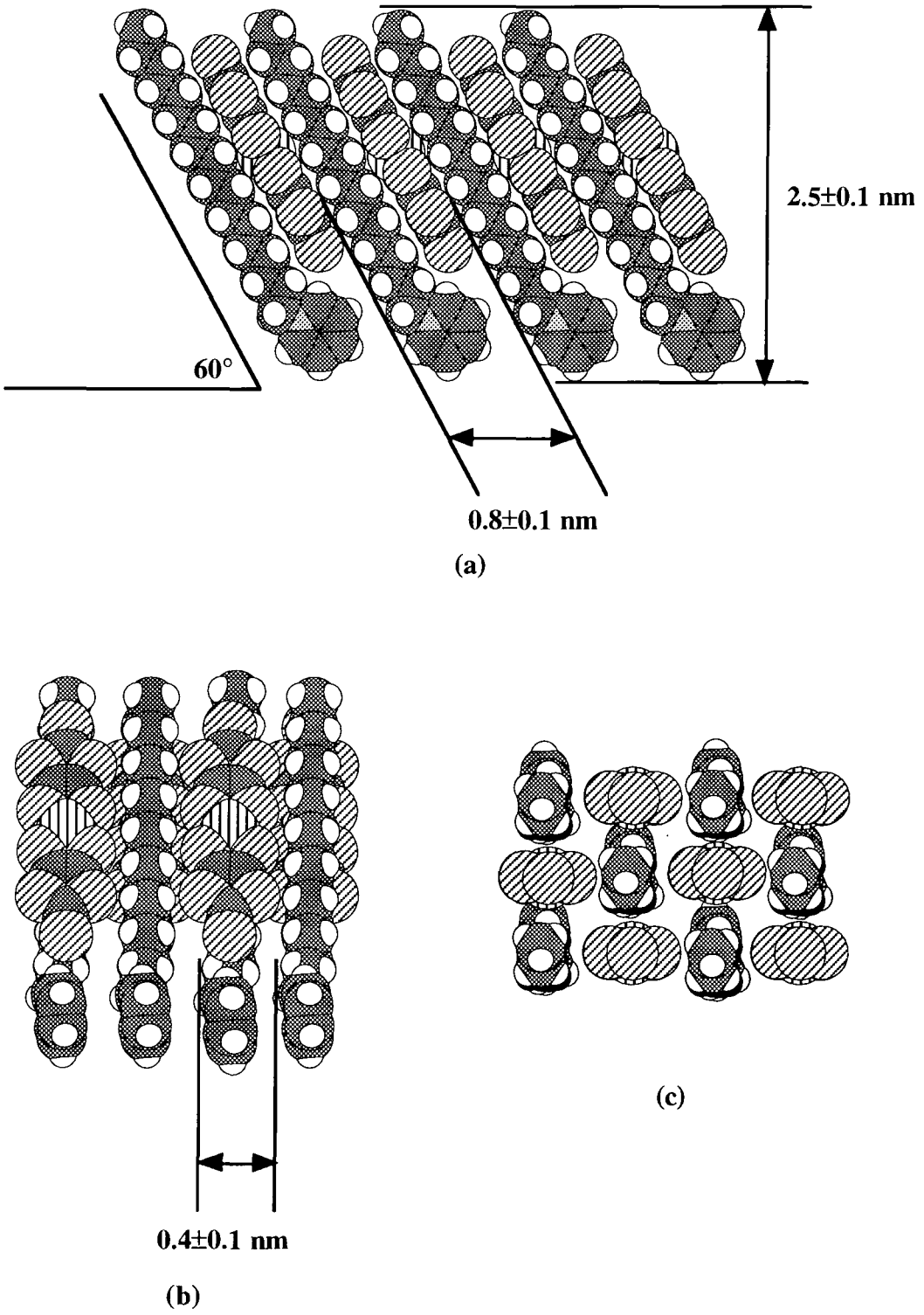

Fig. 7.23 One possible arrangement of the molecules in LB films of C_{18}Py-Pd(dmit)$_2$ deposited from floating layers that have been aged on the surface of the subphase for a long time before compression.

(a) View from the side, parallel to the plane of the substrate.
(b) View parallel to the substrate, orthogonal to (a).
(c) View along the long molecular axis.

perpendicular to the surface of the subphase.

7.5.3 Two ml of solution spread and 10 minutes allowed before compression.

When samples were prepared from a floating layer formed from 2 ml of solution that had been allowed to stand on the surface of the subphase for 10 minutes before compression, high conductivity was once again observed without any post deposition doping. The current versus voltage behaviour of a 17-layer film, with carbon cement contacts that were 1.0±0.5 mm apart, before doping with iodine, is shown in Fig. 7.24. The characteristic was Ohmic over most of the bias range studied, with a slight departure from linear behaviour seen only at the upper voltage limit. A conductivity of 1.5±1.0 x 10^{-1} S cm^{-1} was calculated from this characteristic, a value similar to that of C_{18}Py-Ni(dmit)$_2$ films after iodine doping (chapter 8, section 8.5). After chemical doping of the same 17-layer film with iodine, the behaviour was again predominantly Ohmic, as shown in Fig. 7.25. The conductivity was lower after doping within the limits of the experimental errors, with a value of 6.0±4.0 x 10^{-2} S cm^{-1} calculated. Plots of resistance versus the distance between carbon cement contacts for 19-layer films are shown in Fig. 7.26(a) and Fig. 7.26(b) for as-deposited and iodine doped samples, respectively. In both cases, some of the points lie on a straight line through the origin, indicating negligible contact resistance. The resistance measured for some pairs of contacts was much higher than expected, however, indicating that for these devices, the contact resistance was significant. The conductivity values quoted above were calculated from the measurements recorded for those samples where the resistance of the contacts was seen to be negligible, i.e. where the overall resistance of the device was relatively small. Evaporated gold was also used to provide contacts to these films. Two plots representing sample resistance versus the distance between gold electrodes that were evaporated onto one glass slide before the deposition of 19 LB layers of C_{18}Py-Pd(dmit)$_2$ and on top of an identical organic film on a second glass slide are shown in Fig. 7.26(c). The data sets lie on straight lines through the origin indicating that in both cases the contact resistance was

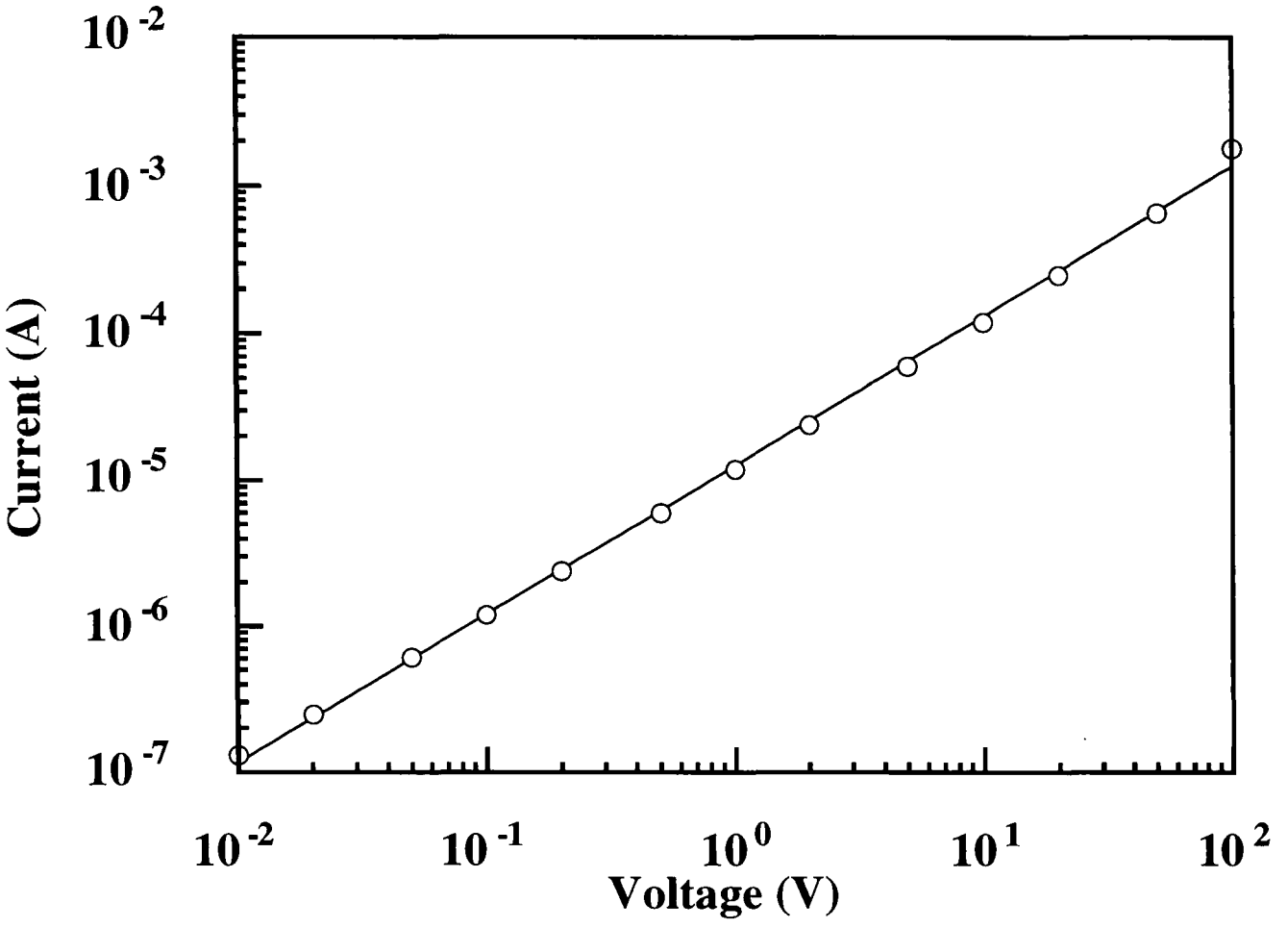

Fig. 7.24 Current versus voltage characteristics for a 17-layer as-deposited LB film of C_{18}Py-Pd(dmit)$_2$ with carbon cement contacts 1.0±0.5 mm apart. The sample was deposited from a floating layer formed from 2 ml of solution that had been allowed to stand uncompressed on the surface of the subphase for 10 minutes.

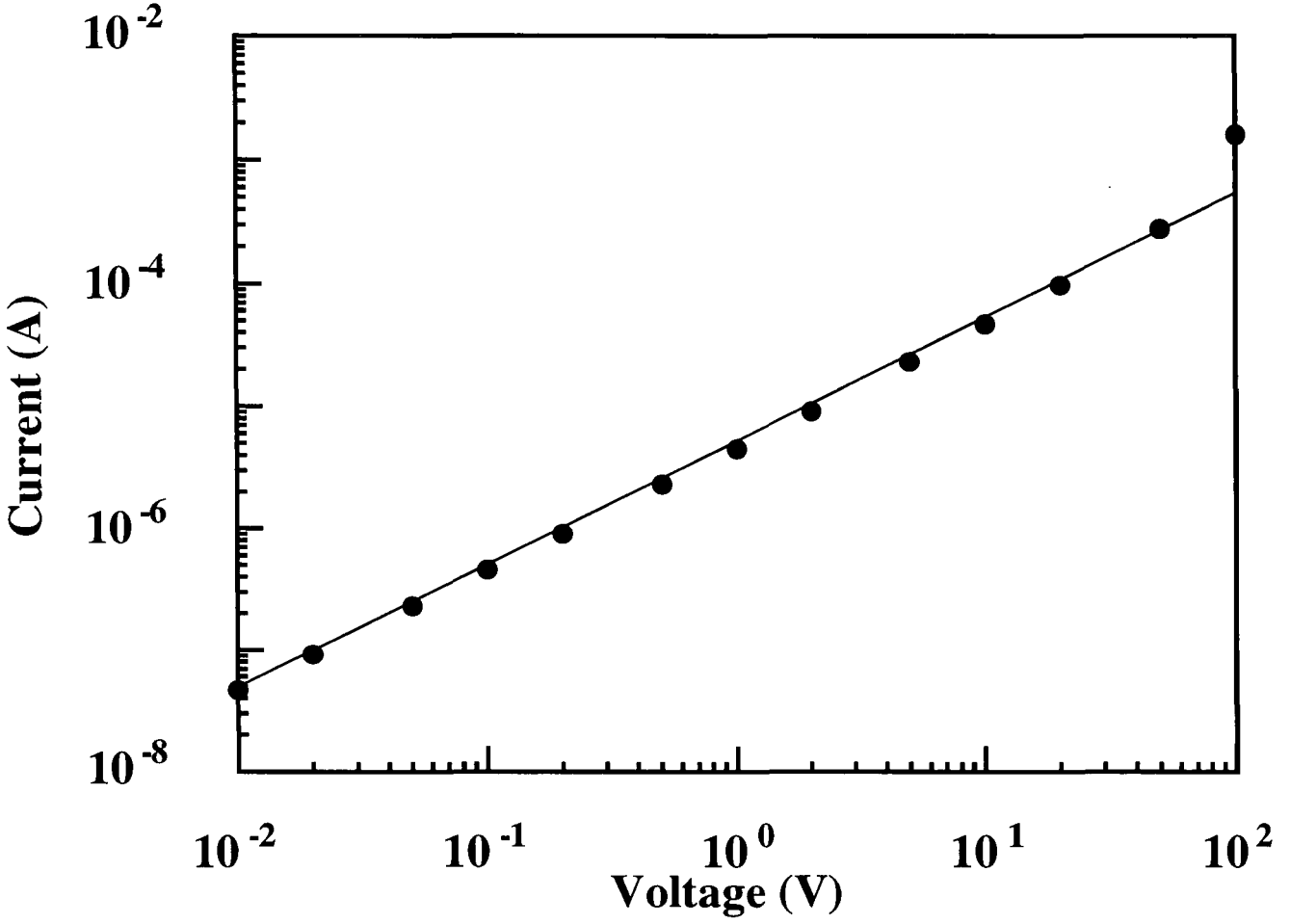

Fig. 7.25 Current versus voltage characteristics for a 17-layer iodine doped LB film of C_{18}Py-Pd(dmit)$_2$ with carbon cement contacts 1.0±0.5 mm apart. The sample was deposited from a floating layer formed from 2 ml of solution that had been allowed to stand uncompressed on the surface of the subphase for 10 minutes.

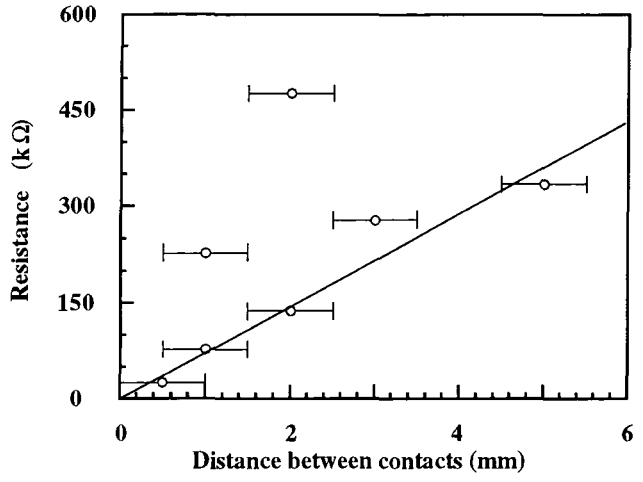

(a)

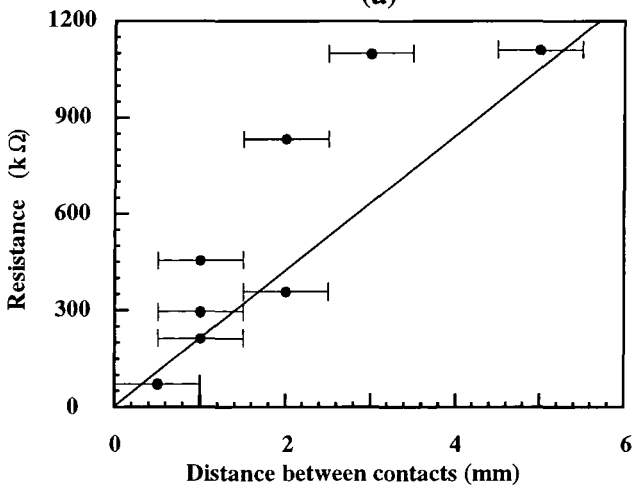

(b)

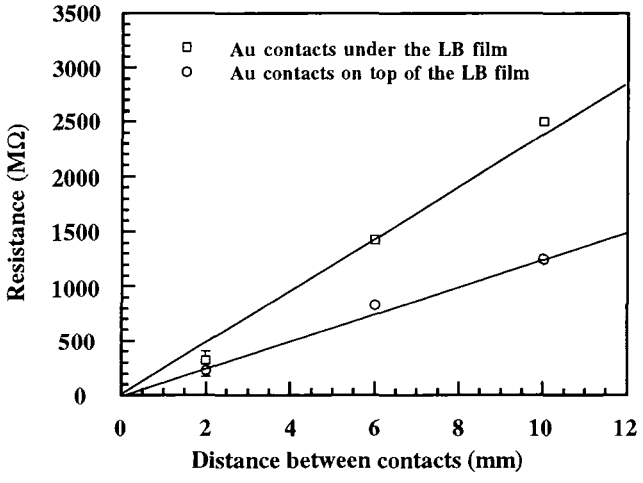

(c)

Fig. 7.26 **Resistance versus the distance between contacts for a 19-layer LB films of $C_{18}Py\text{-}Pd(dmit)_2$.**

(a) Carbon cement contacts, as-deposited.
(b) Carbon cement contacts, iodine doped.
(c) Evaporated gold contacts, as-deposited.

The films were transferred from a floating layer formed from 2 ml of solution aged for 10 minutes before compression.

negligible. In these experiments, however, the sample resistance was significantly higher than that observed when carbon cement contacts were used. Consequently, the conductivity values that were calculated using the measured film thickness, i.e. $2.5\pm1.5\times10^{-5}$ S cm^{-1} and $3.7\pm2.0\times10^{-5}$ S cm^{-1} for contacts under and on top of the organic film, respectively, were much lower than that obtained using carbon cement electrodes. Carbon cement was applied using an organic solvent, and it seems likely that this would dissolve through the LB layers and make contact through the whole thickness of the film. Gold evaporated before or after transfer of the LB film would contact only the lower or upper layers, respectively. If any insulating alkyl chains existed between the layers, these would partially isolate adjacent layers from each other. A conductivity value calculated using the measured film thickness would therefore contain a large error.

7.5.4 Two ml of solution spread and 21 hours allowed before compression.

In common with multilayer samples transferred from 1 ml of solution that had been aged before compression, films deposited from floating layers formed from 2 ml of solution which had been allowed to stand uncompressed on the subphase for 21 hours exhibited bulk conductivity which was too low to measure, either in the as-deposited state or after doping with iodine. Visible crystallites were present in these films, however, and by carefully making contact to these with carbon cement, and recording a current versus voltage characteristic, these were found to be electrically conductive. Fig.7.27 is an electron micrograph of one such aggregate contained in a 39-layer film. The contacts to the cluster can be seen as dark areas at the sides of the micrograph. Fig. 7.28 is a surface profiling scan taken across the aggregate, which reveals that the feature is ~500 μm long and 1-2 μm thick. The results of current versus voltage measurements for this crystallite, before and after doping with iodine, are shown in Fig. 7.29. From these data and the dimensions of the aggregate, obtained from the micrograph and surface profiling scan, conductivity values of $1.2\pm1.0\times10^{-1}$ S cm^{-1} and $4.0\pm3.3\times10^{-2}$ S cm^{-1} were calculated, before and after doping, respectively. These values are similar to those obtained for the

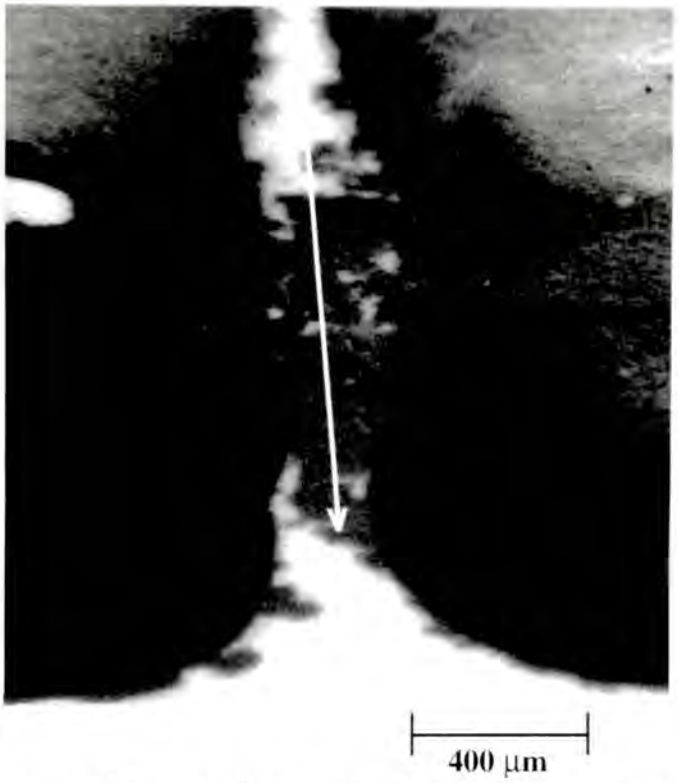

Fig. 7.27 **Scanning electron micrograph of a visible aggregate contained in a 39-layer LB film of C_{18}Py-Pd(dmit)$_2$. The film was transferred from a floating layer formed from 2 ml of solution aged for 21 hours before compression. The dark regions at the sides of the micrograph are the carbon cement contacts. The arrow indicates the direction of the surface profiling scan used to obtain the trace shown in Fig. 7.28.**

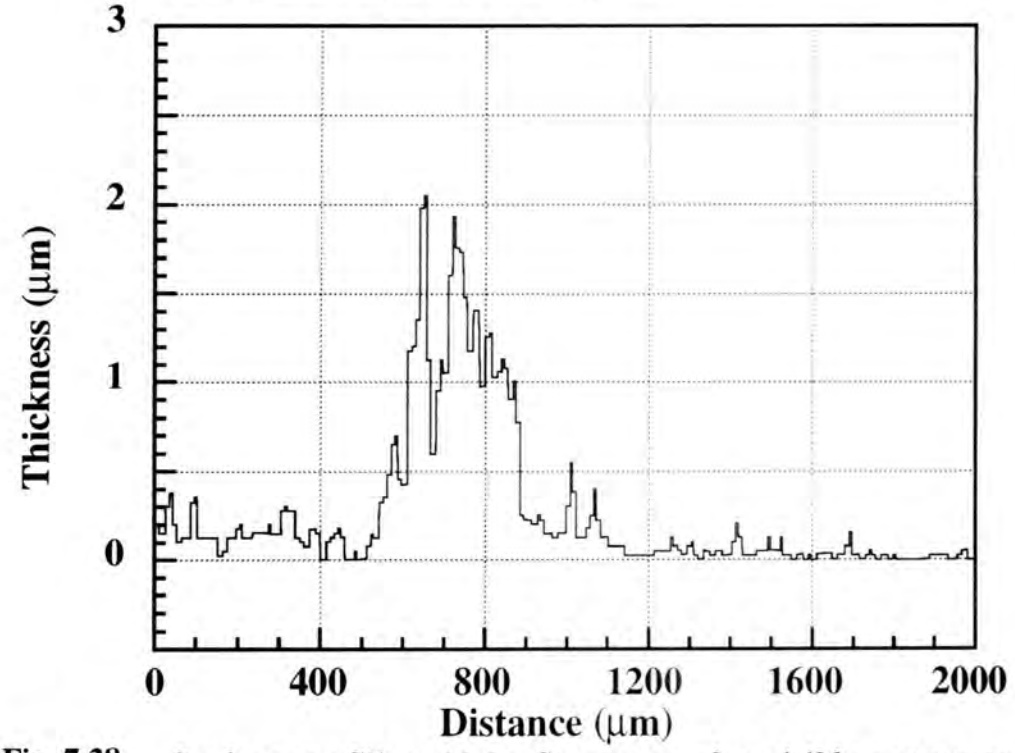

Fig. 7.28 **Surface profiling Alpha-Step scan of a visible aggregate contained in a 39-layer film of C_{18}Py-Pd(dmit)$_2$. The sample was deposited from a layer formed from 2 ml of solution that had been allowed to stand on the surface of the subphase for 21 hours before compression.**

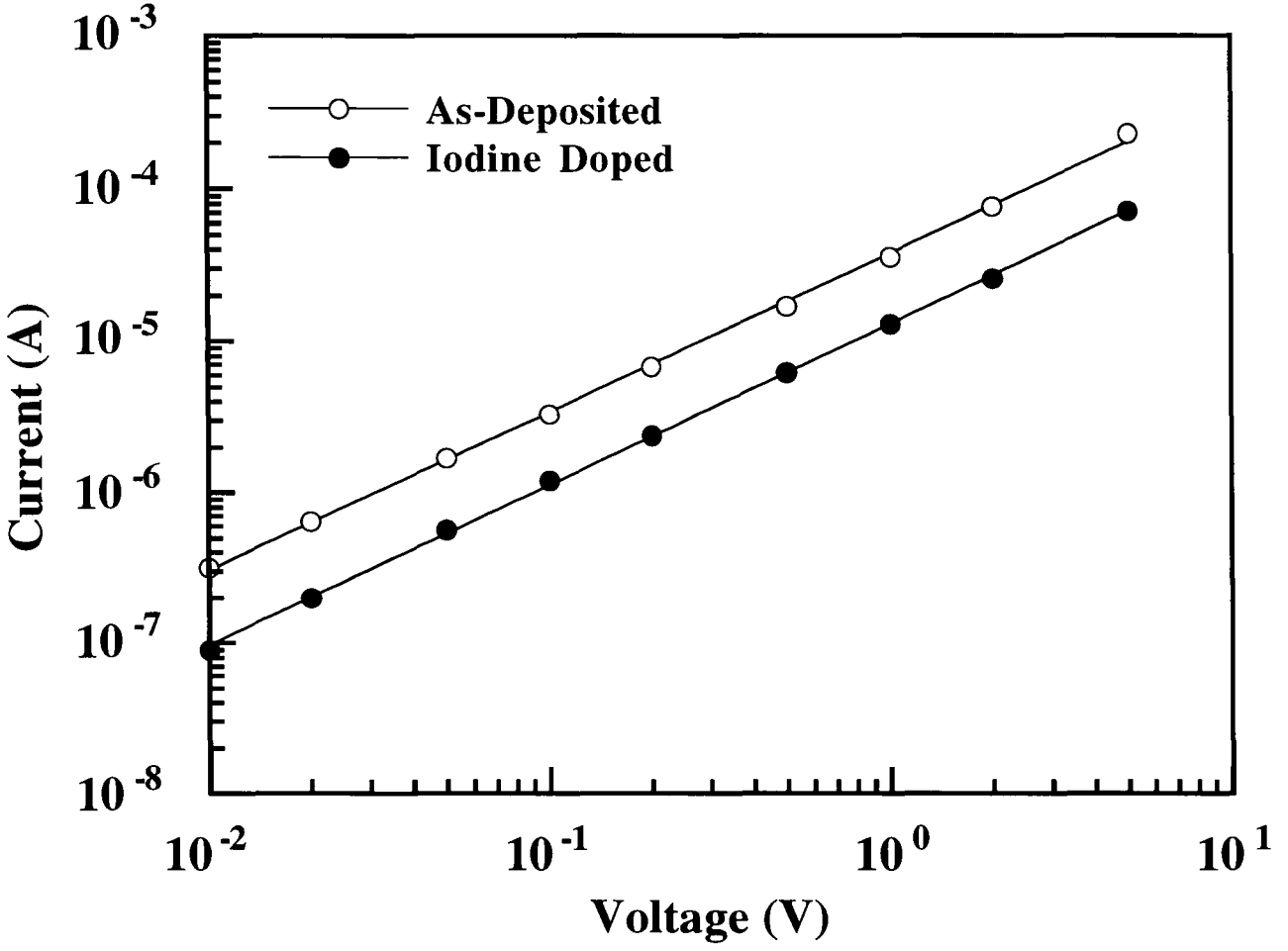

Fig. 7.29 Current versus voltage characteristics for a conducting crystallite contained in a 39-layer film of C_{18}Py-Pd(dmit)$_2$ which was deposited from a floating layer formed from 2 ml of solution that had been allowed to age uncompressed on the surface of the subphase for 21 hours. Carbon cement contacts were used.

bulk conductivity of samples deposited from films formed from 2 ml of solution compressed after 10 minutes floating on the surface of the subphase.

The room temperature dc electrical properties for the films described above are summarised in table 7.3

Amount of solution spread (ml)	Time before compression	Doping state	Conductivity ($S\ cm^{-1}$)
1	10 minutes	As-deposited	$3.5\pm2.5\times10^{-3}$
		Iodine doped	$2.6\pm1.7\times10^{-2}$
1	18 hours	As-deposited	Unmeasurable
		Iodine doped	Unmeasurable
2	10 minutes	As-deposited	$1.5\pm1.0\times10^{-1}$
		Iodine doped	$6.0\pm4.0\times10^{-2}$
2	21 hours	As-deposited Bulk	Unmeasurable
		Iodine doped	Unmeasurable
		As-deposited Aggregate	$1.2\pm1.0\times10^{-1}$
		Iodine doped	$4.0\pm3.3\times10^{-2}$

Table 7.3 The conductivity of films of C_{18}Py-Pd(dmit)$_2$ deposited under different experimental conditions.

When a small amount of solution was applied to the surface of the subphase, the spreading of the organic molecules was more effective. Consequently, after transfer to a

solid substrate, the average thickness per layer of a multilayer film was relatively small. Observation using electron microscopy and EDS revealed large, thick, isolated regions containing a high proportion of $(dmit)_2$ in a uniform background matrix with a lower $(dmit)_2$ content. It is thought that the conductivity was lower in these films due to the relatively low conductivity of this background matrix. It is possible that that chemical doping with iodine increased the conductivity of the background and hence the overall conductivity of the film. When longer times were allowed before compression, the large isolated regions disappeared and were replaced by much smaller clusters. These films were insulating, even after chemical doping with iodine. It is thought that extended times on the subphase with the film uncompressed allowed a reordering of the molecules into a structure where the $(dmit)_2$ moieties were unable to pack close enough together to facilitate carrier transport (Fig. 7.23).

When a large amount of solution was distributed, the spreading characteristics were poorer, and transferred films relatively thick. After a short time before compression, a high density of crystallites was observed in the multilayer structure, in close proximity to each other, and well distributed throughout the film. Conductivity was high, before and after doping with iodine. After longer times, these crystallites were seen to aggregate together into a smaller number of much larger clusters. Bulk conductivity was low, but the conductivity of the clusters was found to be high, before and after iodine doping. The conductivity values recorded here are similar to the values reported by Nakamura *et al*[6] for bromine doped multilayers of alkylammonium-$M(dmit)_2$ salts (M=Ni,Au,Pd,Pt) mixed with eicosanoic acid, Taylor *et al*[13] for pure films of bis(didodecydimethylammonium)-$Ni(dmit)_2$, again after chemical doping with bromine, and Xiao *et al*[14] for mixed films of tetrabenzylthiotetrathiafulvalene-$Zn(dmit)_2$ and octadecanoic acid, after iodine doping.

7.6 Low temperature conductivity

Low temperature dc conductivity was measured using carbon cement contacts 1.0±0.5 mm apart and 4.0±0.5 mm long. Current versus voltage characteristics were recorded at the extremes of the temperature range studied, which was between liquid nitrogen temperature and room temperature.

7.6.1 One ml of solution spread and 10 minutes allowed before compression.

Two semi-logarithmic current versus reciprocal temperature plots recorded for a 19-layer sample prepared from a film formed from 1 ml of solution allowed to stand on the subphase for 10 minutes before compression are shown in Fig. 7.30. The current versus voltage characteristics at the extremes of temperature are shown inset. To make the current measurements, bias voltages of 1V and 200 V (in the linear and super-Ohmic parts of the current versus voltage characteristics) were applied. These data deviate from the simple straight line relationship predicted by equation 6.8 at low temperature. The temperature dependence of the electrical conductivity of a semiconductor involves the contributions due to (a) changes in carrier concentration, from (i) the activation energy, ΔE (ii) the density of states in the transport band, which varies as $T^{3/2}$, and (b) fluctuating carrier mobility, μ, (due to scattering), which typically varies as T^n with $-3 \leq n \leq 3/2$. If the temperature dependence of the mobility is dominated by lattice scattering, then $\mu \propto T^{-3/2}$, and a weak temperature dependence would be expected from the product of mobility and density of states. If, however, mobility is controlled by impurity scattering, $\mu \propto T^{-3/2}$, and the product of mobility and state density has a T^3 dependence. Epstein *et al* [15] have used an equation of the form

$$\sigma = \sigma_0 T^{\alpha} \exp\left(-\frac{\Delta}{T}\right) \qquad 7.4$$

where $\Delta = \Delta E/k$, to describe the temperature dependence of the conductivity of some organic single crystals (such as NMP-TCNQ) where there is a thermally activated carrier

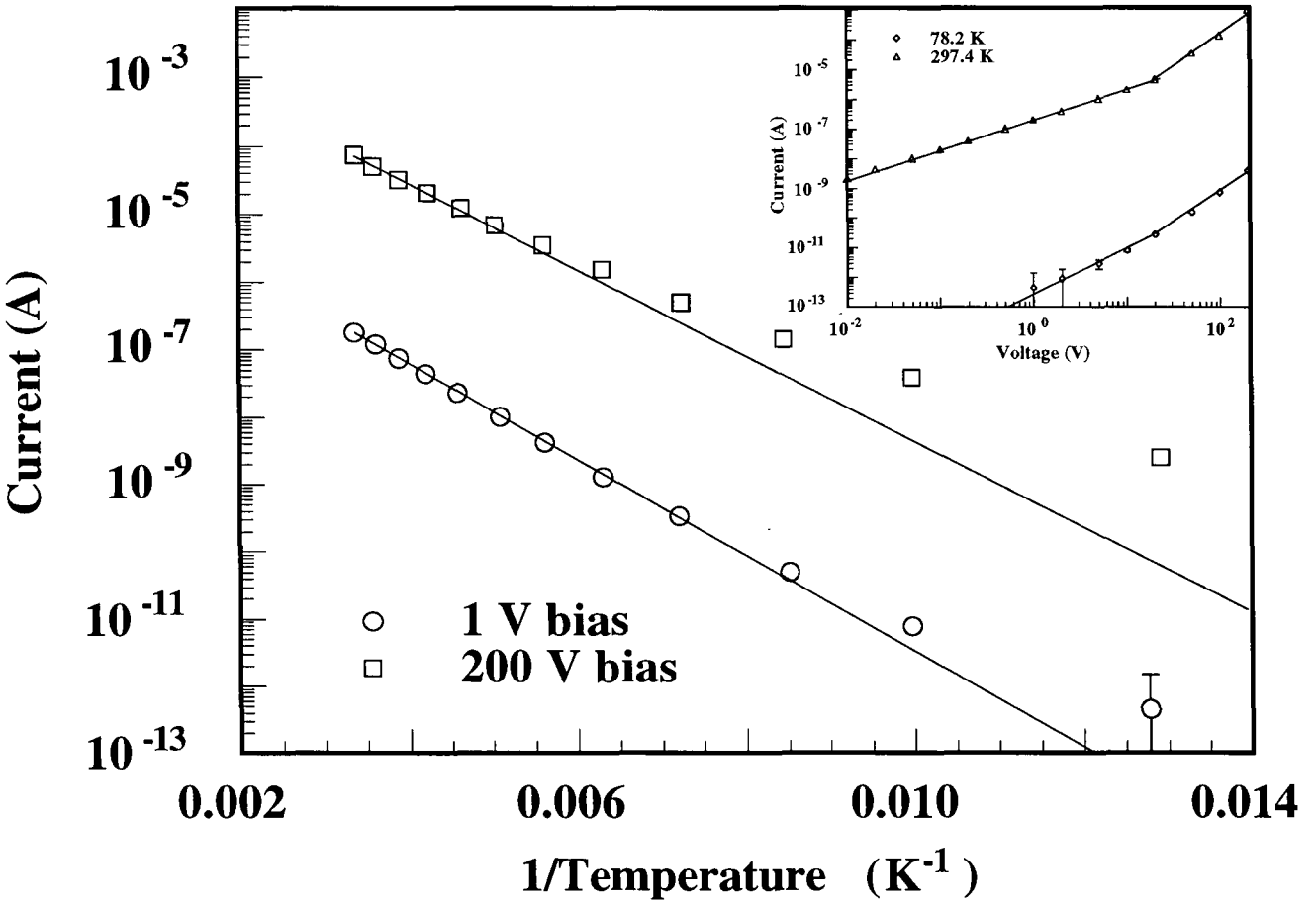

Fig. 7.30 **Semi logarithmic plots of current (with bias voltages of 1 V and 200 V) versus reciprocal temperature for a 19-layer as-deposited LB sample of C_{18}Py-Pd(dmit)$_2$. The film was deposited from a floating layer formed from 1 ml of solution that was aged on the subphase for 10 minutes before compression. The current versus voltage characteristics at the extremes of the temperature range studied are shown inset.**

concentration, $n \propto \exp(-\Delta/T)$ and a temperature dependent mobility, $\mu \propto T^{\alpha}$. They measured α values in the range -3 to -4 for a range of TCNQ systems, attributed to the interaction of charge carriers with molecular vibrations. In this situation, a graph of $\log_e(I/T^{\alpha})$ versus 1/T would be expected to yield a straight line. Good linear fits to the experimental data for the LB films of C_{18}Py-Pd(dmit)$_2$, at bias voltages of 1V and 200V were obtained when $\log_e(I/T^{\alpha})$ versus 1/T was plotted with $\alpha = 4.0$ and 3.4, respectively, as shown in Fig. 7.31. This suggests a power law temperature dependence of conductivity, with contributions from the state density and a carrier mobility variation dominated by impurity scattering. Activation energies which were the same within the limits of the experimental error, i.e. 0.07±0.01 eV and 0.05±0.01 eV, were calculated from the slopes of these graphs for low and high bias voltages, respectively. Nakamura *et al*[16] have measured a similar activation energy of 0.065 eV for LB films of didecyldimethylammonium-Ni(dmit)$_2$, and Miura *et al*[17] have reported a value of 0.05 eV for LB films of didecyldimethylammonium-Pd(dmit)$_2$. Roberts *et al*[10] have shown that identical activation energies for Ohmic and SCL conduction is indicative of extrinsic behaviour with ΔE equal to the depth of the dominant trap.

The current versus reciprocal temperature graph for a 19-layer LB sample after iodine doping is plotted in Fig. 7.32. The current versus voltage characteristics, recorded at the highest and lowest temperatures in the range are shown inset to the figure. Once again, the data deviate from a simple straight line relationship, and are replotted in Fig. 7.33 after correction for a power law temperature dependence. A value of α=1.4, probably due to the temperature variation of the density of states, gave the best straight line fit. From the slope of the graph, an activation energy slightly higher than that of the as-deposited sample, i.e. 0.09±0.01 eV, was calculated.

7.6.2 One ml of solution spread and 18 hours allowed before compression.

LB multilayers deposited from floating films formed from 1 ml of solution that had been

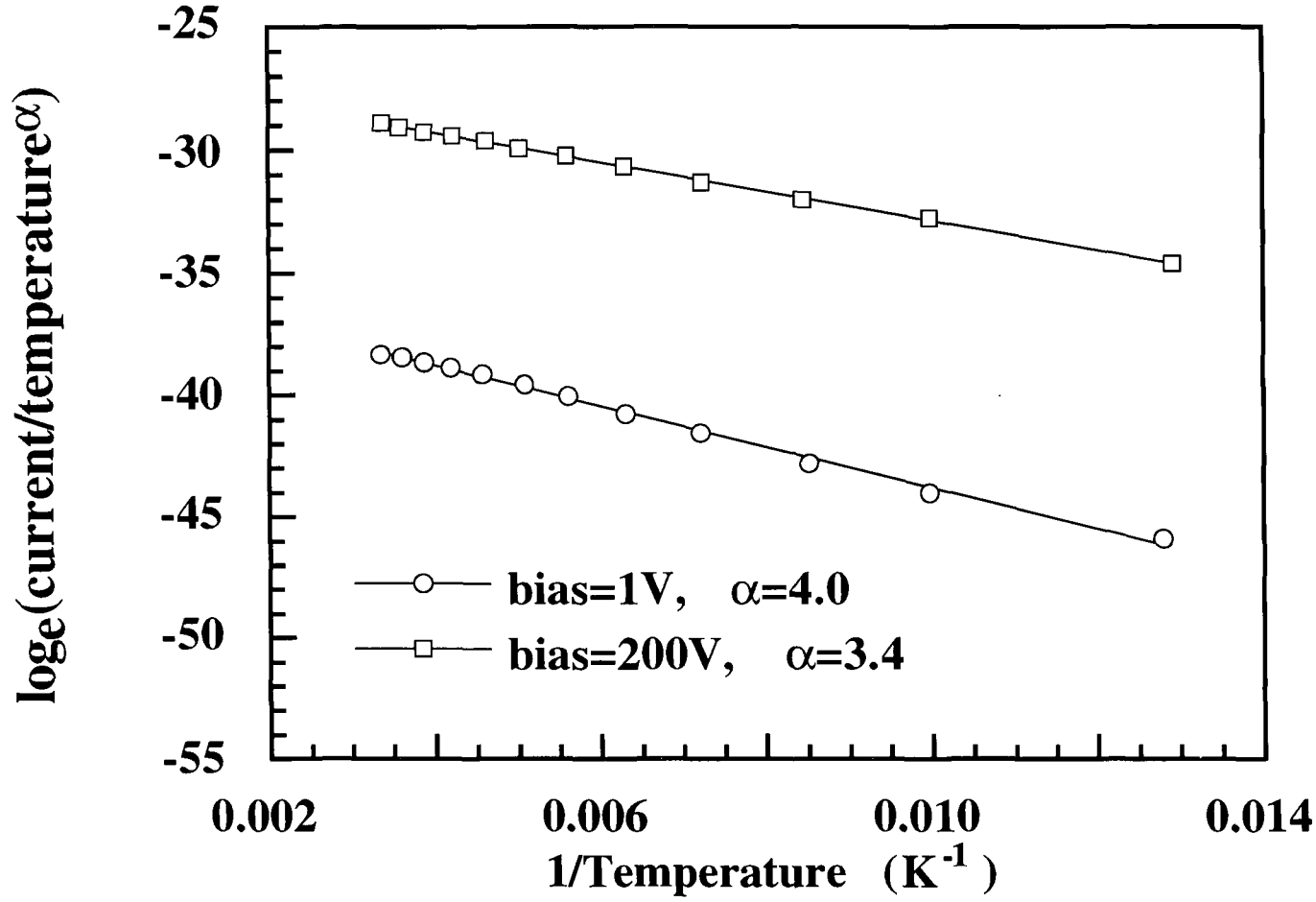

Fig. 7.31 The current versus reciprocal temperature data of Fig. 7.30 corrected for the effect of a temperature dependent carrier mobility. The 19-layer sample of C_{18}Py-Pd(dmit)$_2$ was deposited from a floating layer formed from 1 ml of solution that had been allowed to age on the surface of the subphase for 10 minutes before compression.

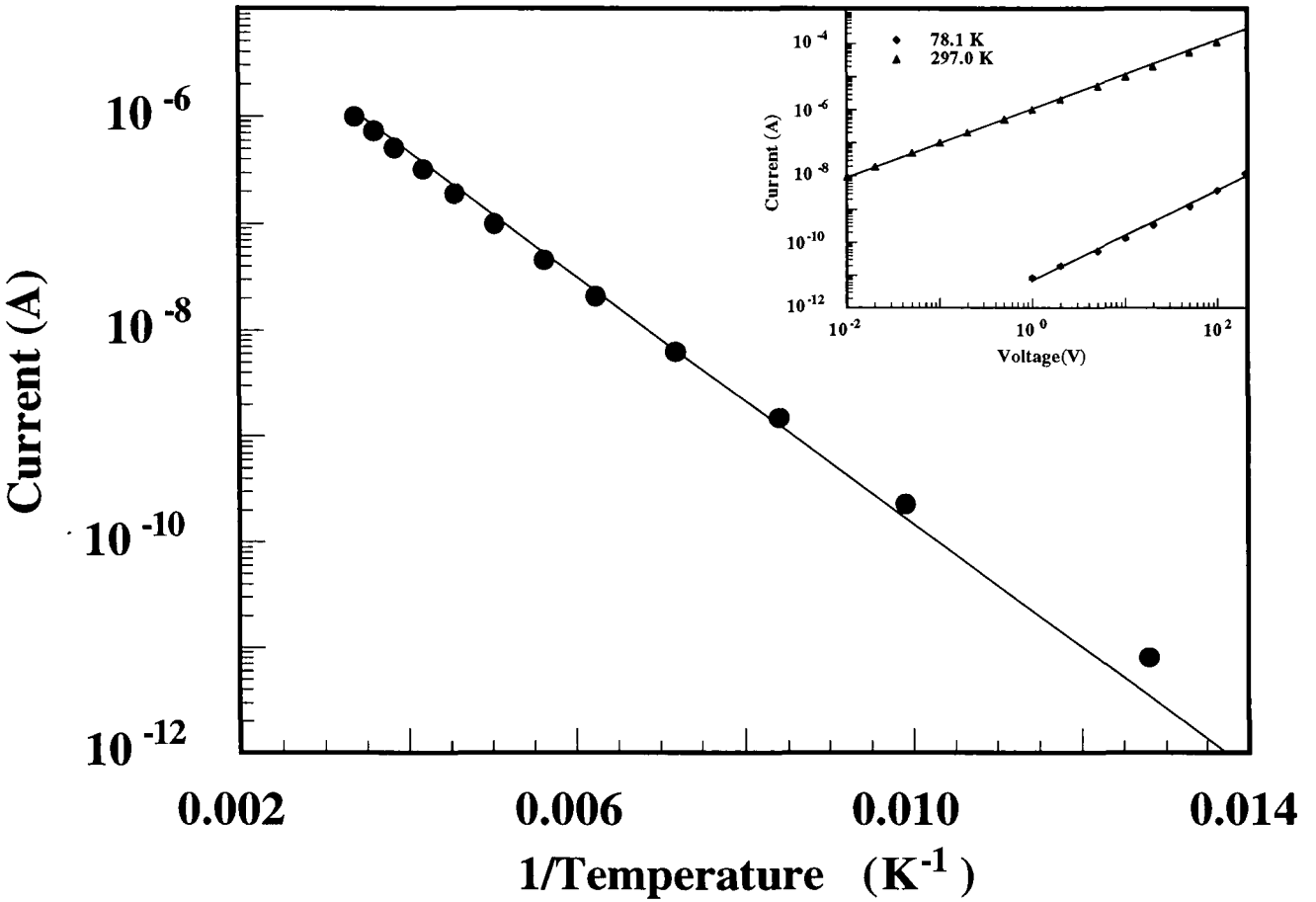

Fig. 7.32 **Semi logarithmic plot of current (with a bias voltage of 1V) versus reciprocal temperature for a 19-layer iodine doped LB sample of C_{18}Py-Pd(dmit)$_2$. The film was deposited from a floating layer formed from 1 ml of solution that was aged on the subphase for 10 minutes before compression. The current versus voltage characteristics at the extremes of the temperature range studied are shown inset.**

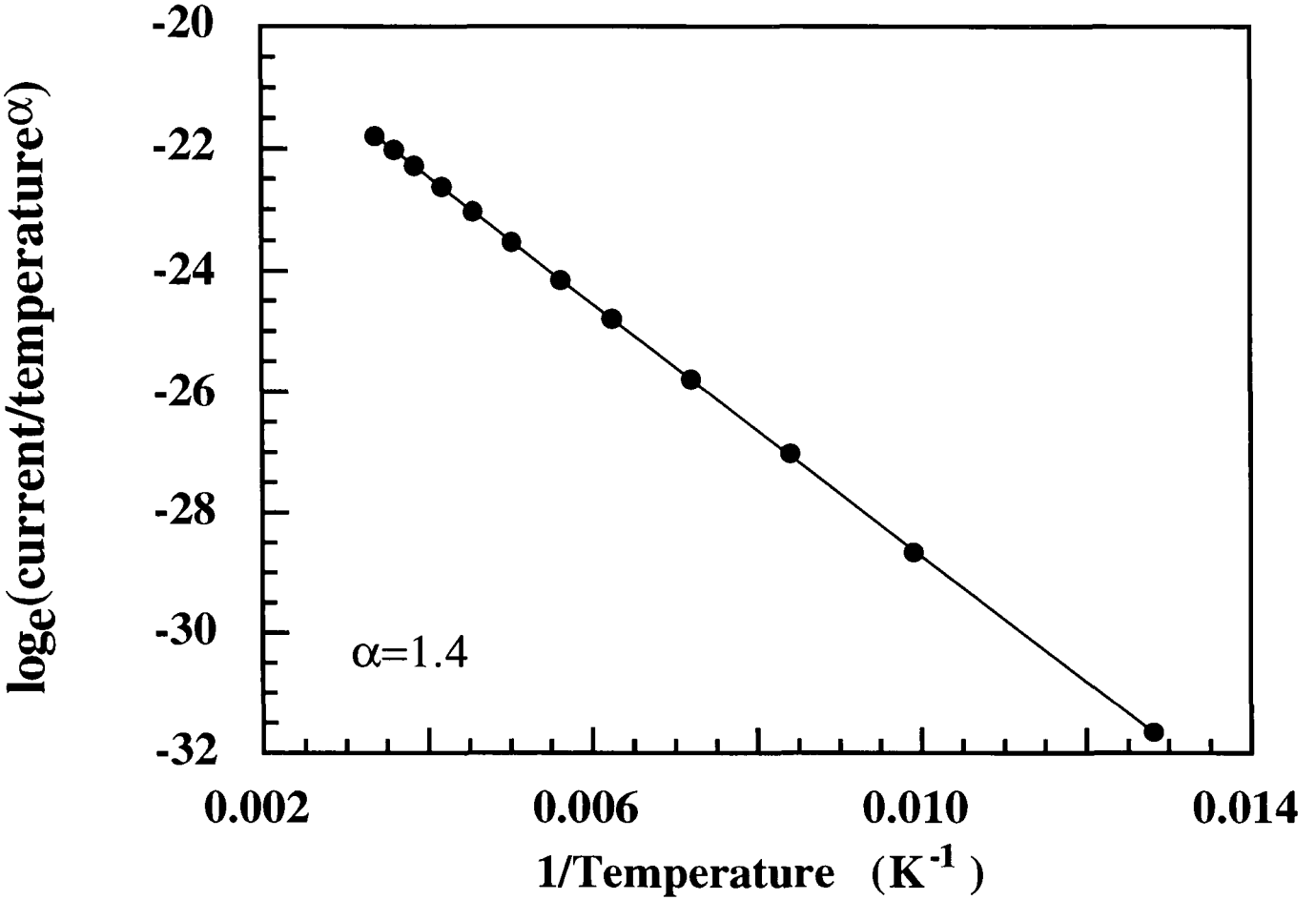

Fig. 7.33 The current versus reciprocal temperature data of Fig. 7.32 corrected for the effect of a temperature dependent carrier mobility. The 19-layer sample of C_{18}Py-Pd(dmit)$_2$ was deposited from a floating layer formed from 1 ml of solution that had been allowed to age on the surface of the subphase for 10 minutes before compression.

allowed to age on the subphase surface for 18 hours before compression were not conductive.

7.6.3 Two ml of solution spread and 10 minutes allowed before compression.

A semi-logarithmic plot of current, with a constant bias of 1V applied, versus reciprocal temperature for an as-deposited 19-layer film of C_{18}Py-Pd(dmit)$_2$ transferred from a floating layer formed from 2 ml of solution aged on the subphase for 10 minutes before compression is shown in Fig 7.34, with the current versus voltage characteristics at the extremes of the temperature range shown inset. Again, non-linearity was observed, and the same data are replotted in Fig. 7.35 after correction for a power law temperature dependence with α=1.4. A similar situation existed after exposure to iodine vapour, as shown in Fig. 7.36 where the raw data are plotted. Fig. 7.37 shows the same data after correction for a power law temperature dependence. Here a value of α=2.5 gave the best straight line fit to the data. The same activation energies i.e. 0.07±0.01 and 0.06±0.01 were calculated, before and after doping, respectively.

7.6.4 Two ml of solution spread and 21 hours allowed before compression.

The low temperature behaviour, over the range 77-300 K, of the current, I, at a fixed bias of 1V, flowing through a conductive crystallite contained in an as-deposited 39-layer film of C_{18}Py-Pd(dmit)$_2$ that was deposited from a layer formed from 2 ml of solution allowed to stand on the surface of the subphase for 21 hours before compression is shown in Fig. 7.38. The current versus voltage characteristics at the extremes of the temperature range studied are shown inset. The data deviate from a simple straight line relationship at low temperature and a graph of $\log_e(I/T^{\alpha})$ versus 1/T where α = 1.5, to provide the best straight line fit, is plotted in Fig. 7.39. From the slope of this plot, an activation energy of 0.06±0.01 eV was calculated, in agreement with the value for those films which exhibited bulk conductivity. The semi-logarithmic plot of the current with a bias of 1V versus reciprocal temperature for another such crystallite in the same LB film,

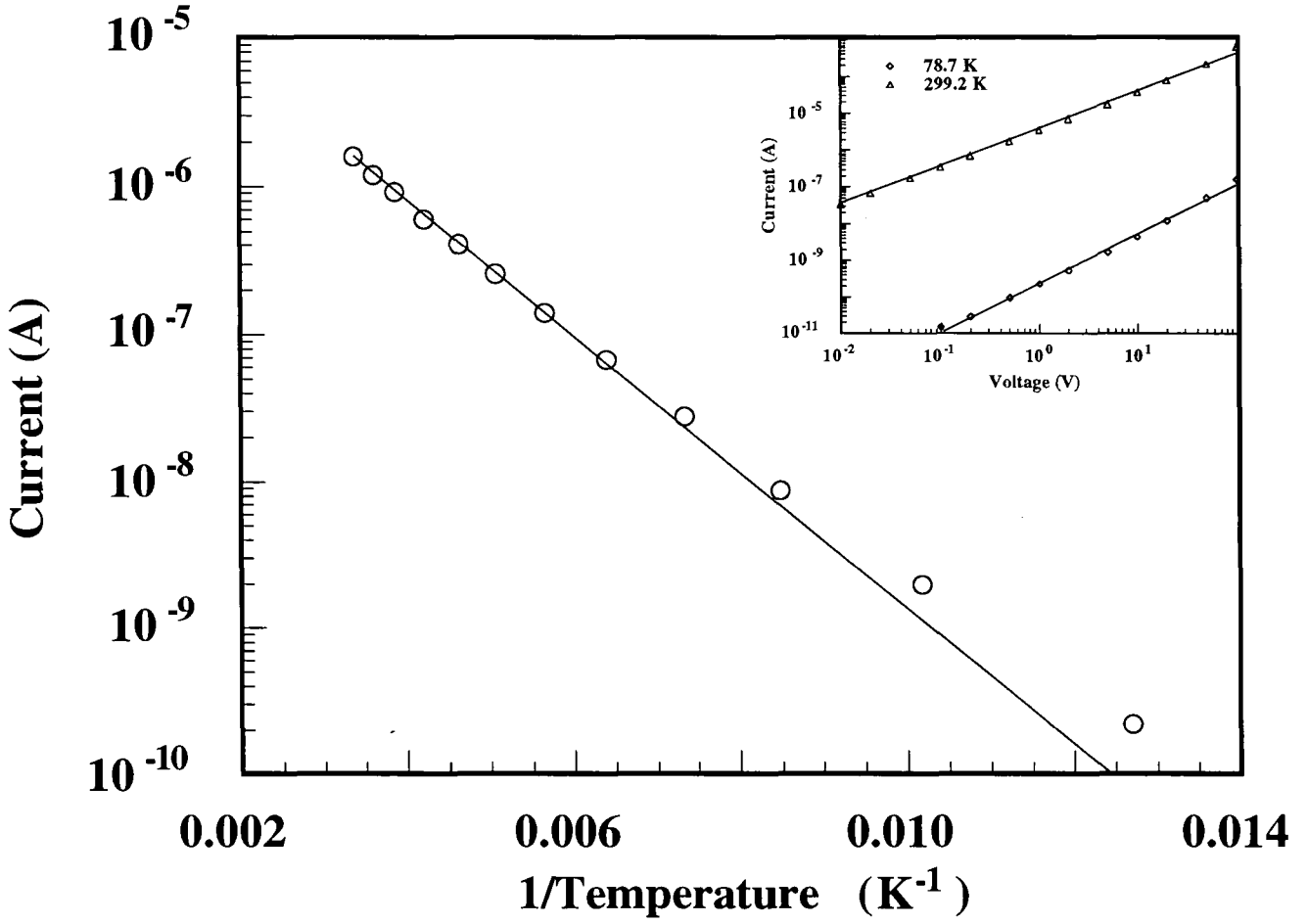

Fig. 7.34 **Semi logarithmic plot of current (with a bias voltage of 1 V) versus reciprocal temperature for a 19-layer as-deposited LB sample of C_{18}Py-Pd(dmit)$_2$. The film was deposited from a floating layer formed from 2 ml of solution that was aged on the subphase for 10 minutes before compression. The current versus voltage characteristics at the extremes of the temperature range studied are shown inset.**

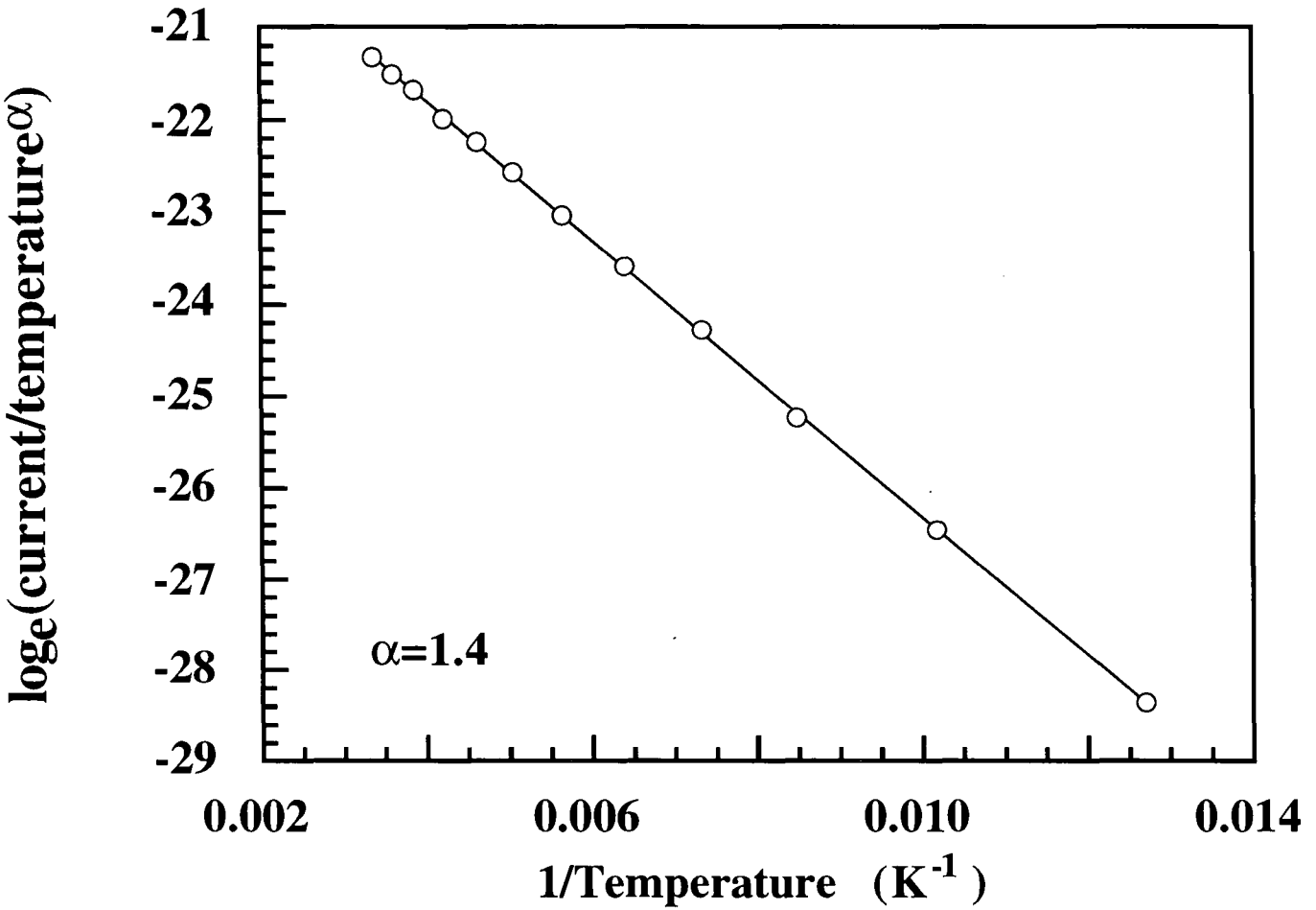

Fig. 7.35 **The current versus reciprocal temperature data of Fig. 7.34 corrected for the effect of a temperature dependent carrier mobility. The 19-layer sample of C_{18}Py-Pd(dmit)$_2$ was deposited from a floating layer formed from 2 ml of solution that had been allowed to age on the surface of the subphase for 10 minutes before compression.**

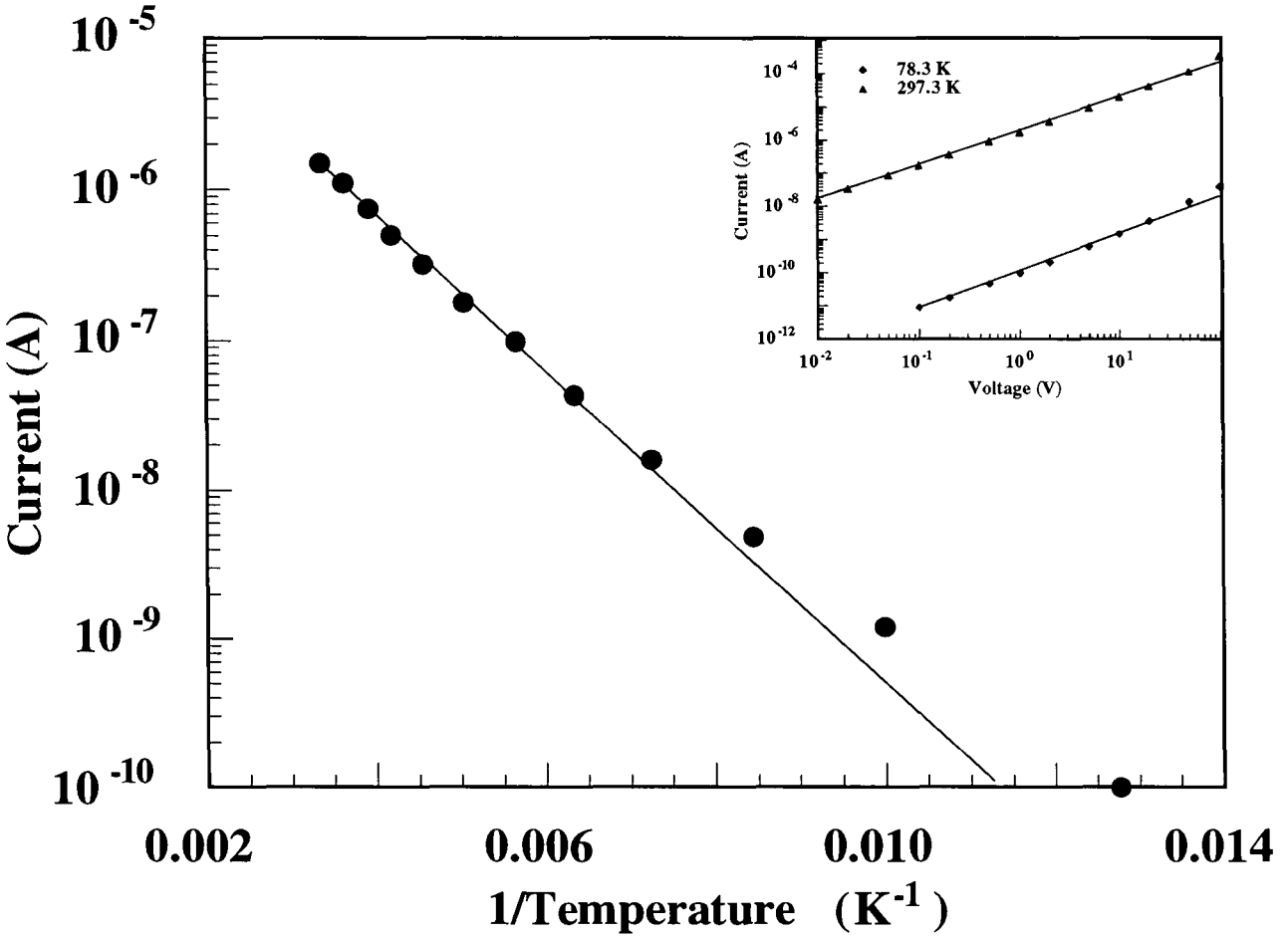

Fig. 7.36 **Semi logarithmic plot of current (at a bias voltage of 1V) versus reciprocal temperature for a 19-layer iodine doped sample of C_{18}Py-Pd(dmit)$_2$ The sample was deposited from a floating layer formed from 2 ml of solution that had been allowed to stand uncompressed on the surface of the subphase for 10 minutes. The current versus voltage characteristics at the extremes of the temperature range studied are shown inset.**

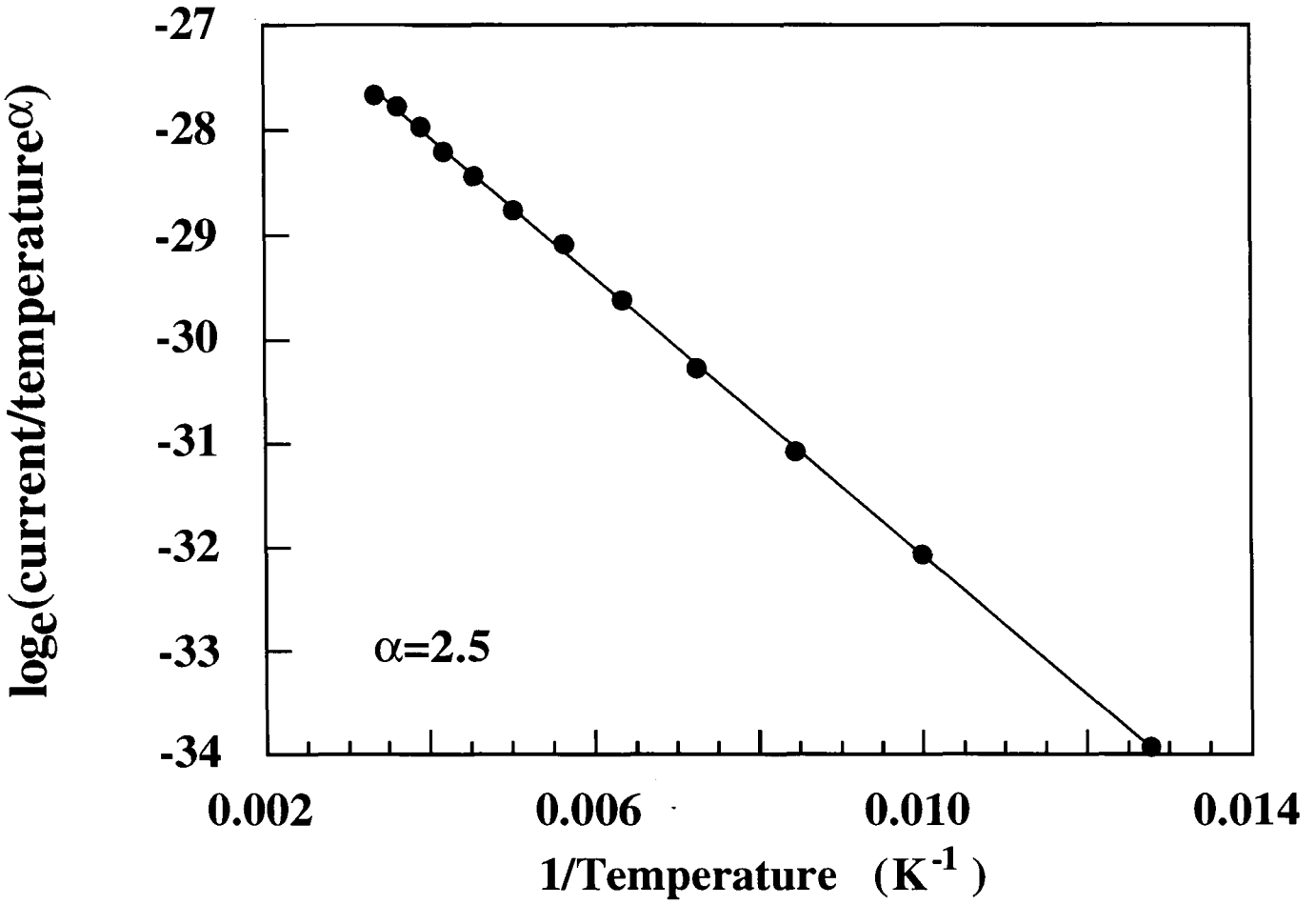

Fig. 7.37 The current versus reciprocal temperature data of Fig. 7.36 corrected for the effect of a temperature dependent carrier mobility. The 19-layer sample of C_{18}Py-Pd(dmit)$_2$ was deposited from a floating layer formed from 2 ml of solution that had been allowed to age on the surface of the subphase for 10 minutes before compression.

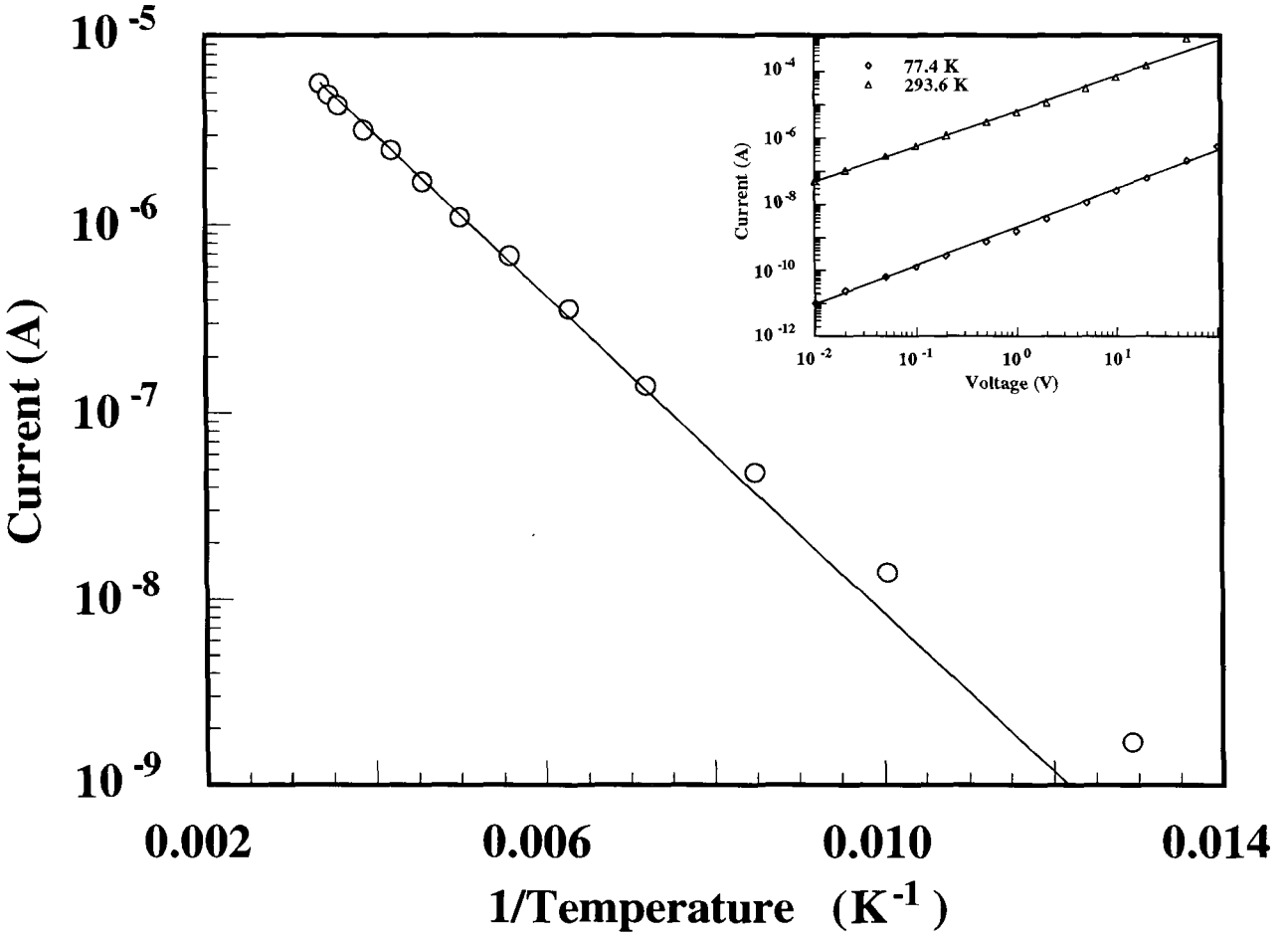

Fig. 7.38 Semi logarithmic plot of current (with a bias voltage of 1 V) versus reciprocal temperature for a 39-layer as-deposited LB sample of C_{18}Py-Pd(dmit)$_2$. The film was deposited from a floating layer formed from 2 ml of solution that was aged on the subphase for 21 hours before compression. The current versus voltage characteristics at the extremes of the temperature range studied are shown inset.

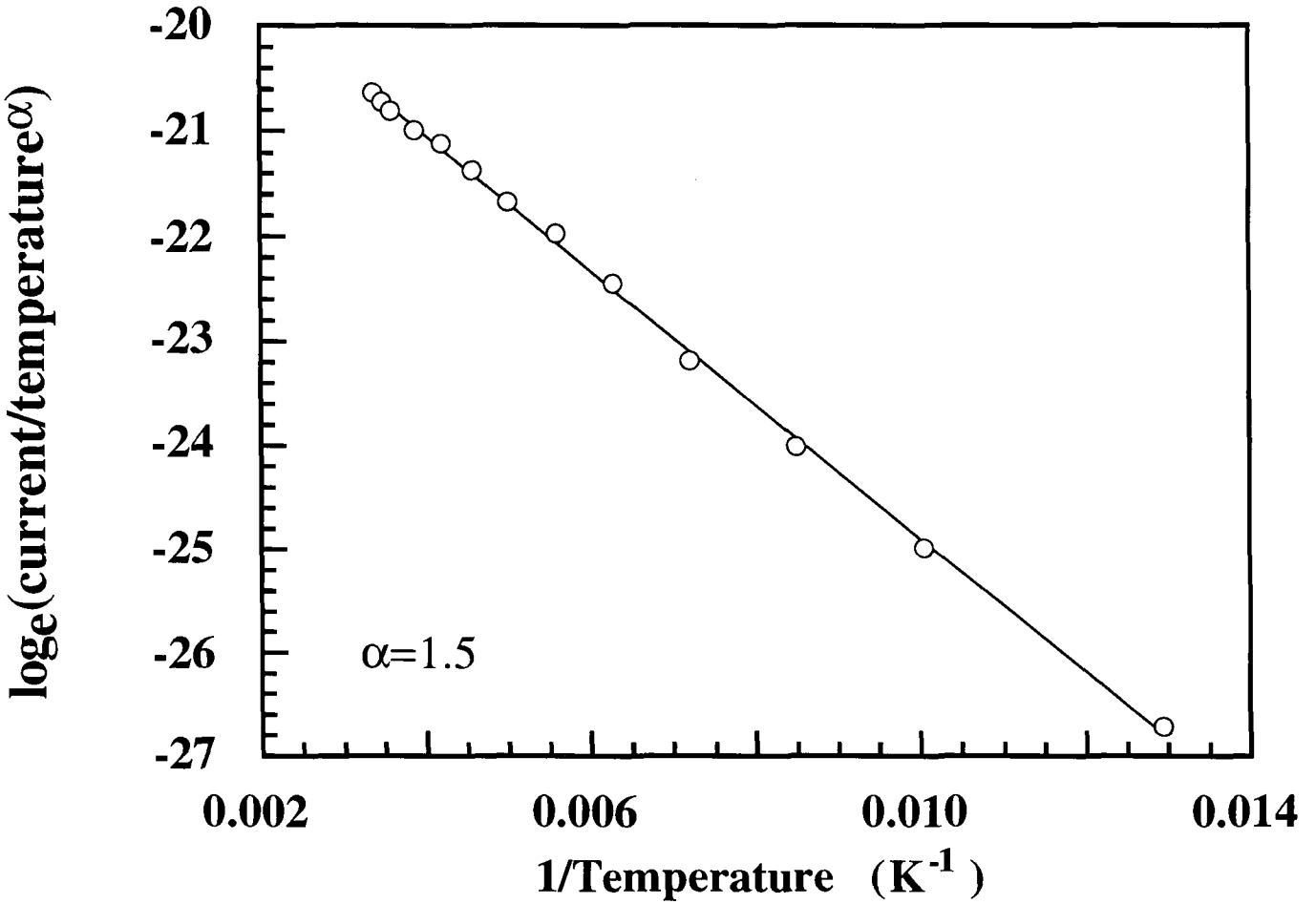

Fig. 7.39 The current versus reciprocal temperature data of Fig. 7.38 corrected for the effect of a temperature dependent carrier mobility. The 39-layer sample of C_{18}Py-Pd(dmit)$_2$ was deposited from a floating layer formed from 2 ml of solution that had been allowed to age on the surface of the subphase for 21 hours before compression.

over the temperature range 77-300 K, after iodine doping is shown in Fig. 7.40. The current versus voltage behaviour at 294.5 K and 89.8 K is shown inset. The same data, corrected for a power law temperature dependence, with $\alpha = 2.1$, are plotted in Fig. 7.41. The activation energy, calculated from the slope of this graph was found to be the same as that of the as-deposited film i.e. 0.06±0.01 eV. These results are in close agreement with those observed for multilayers deposited from a floating layer formed from 2 ml of solution compressed after 10 minutes on the subphase.

The low temperature electrical properties of the samples described in this chapter are summarised in Table 7.4.

Amount of solution spread (ml)	Time on the subphase before compression	Doping state	Applied bias (V)	ΔE (±0.01 eV)	α
1	10 mins.	As-deposited	1	0.07	4.0
			200	0.05	3.4
		Iodine doped	1	0.09	1.4
2	10 mins.	As-deposited	1	0.07	1.4
		Iodine doped	1	0.06	2.5
2	21 hours	As-deposited	1	0.06	1.5
		Iodine doped	1	0.06	2.1

Table 7.4 Thermal activation energies and values of α to give good straight line fits to experimental data for films of C_{18}Py-Pd(dmit)$_2$ prepared under different experimental conditions.

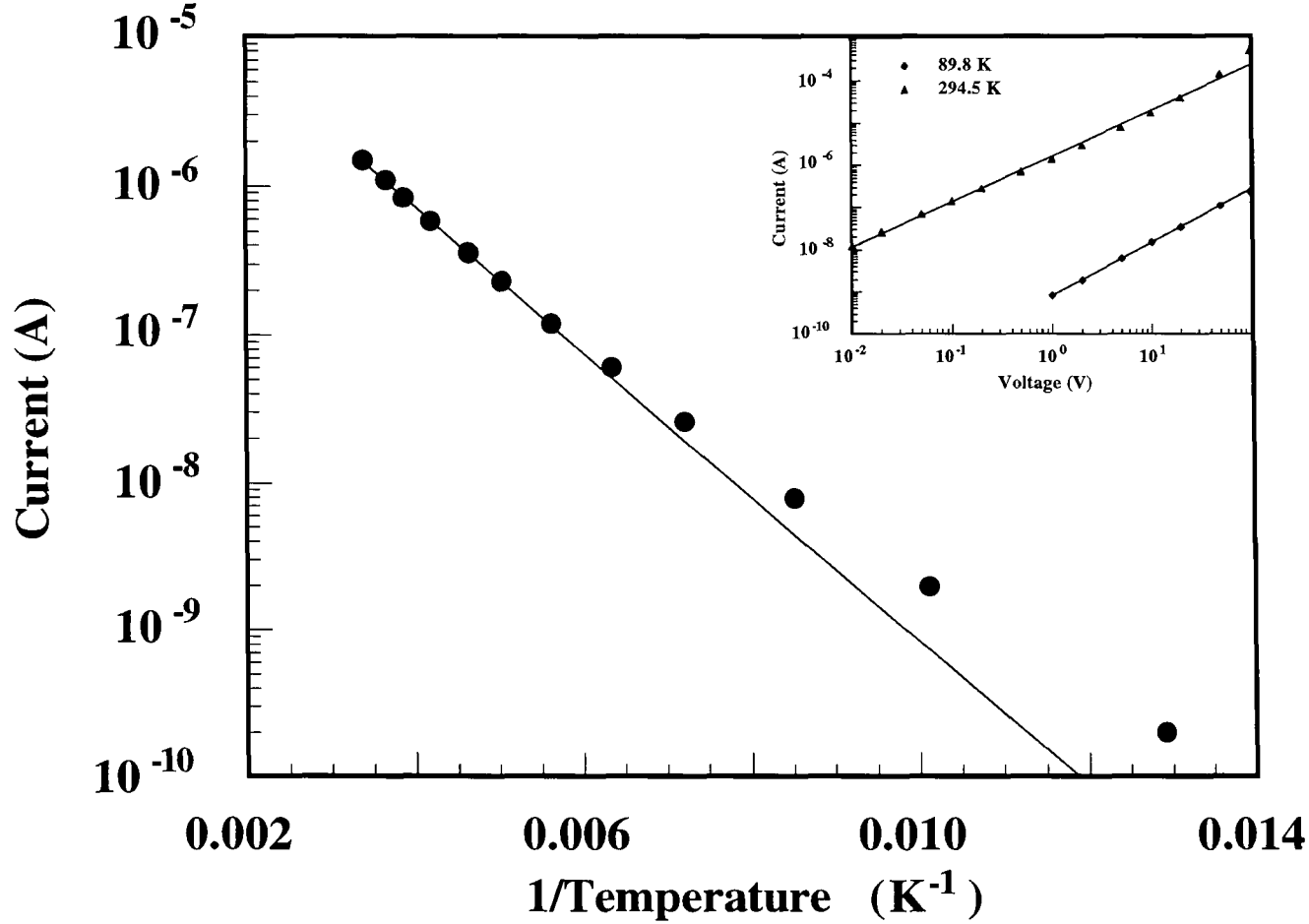

Fig. 7.40 Semi logarithmic plot of current (at a bias voltage of 1V) versus reciprocal temperature for a 39-layer iodine doped sample of C_{18}Py-Pd(dmit)$_2$ The sample was deposited from a floating layer formed from 2 ml of solution that had been allowed to stand uncompressed on the surface of the subphase for 21 hours. The current versus voltage characteristics at the extremes of the temperature range studied are shown inset.

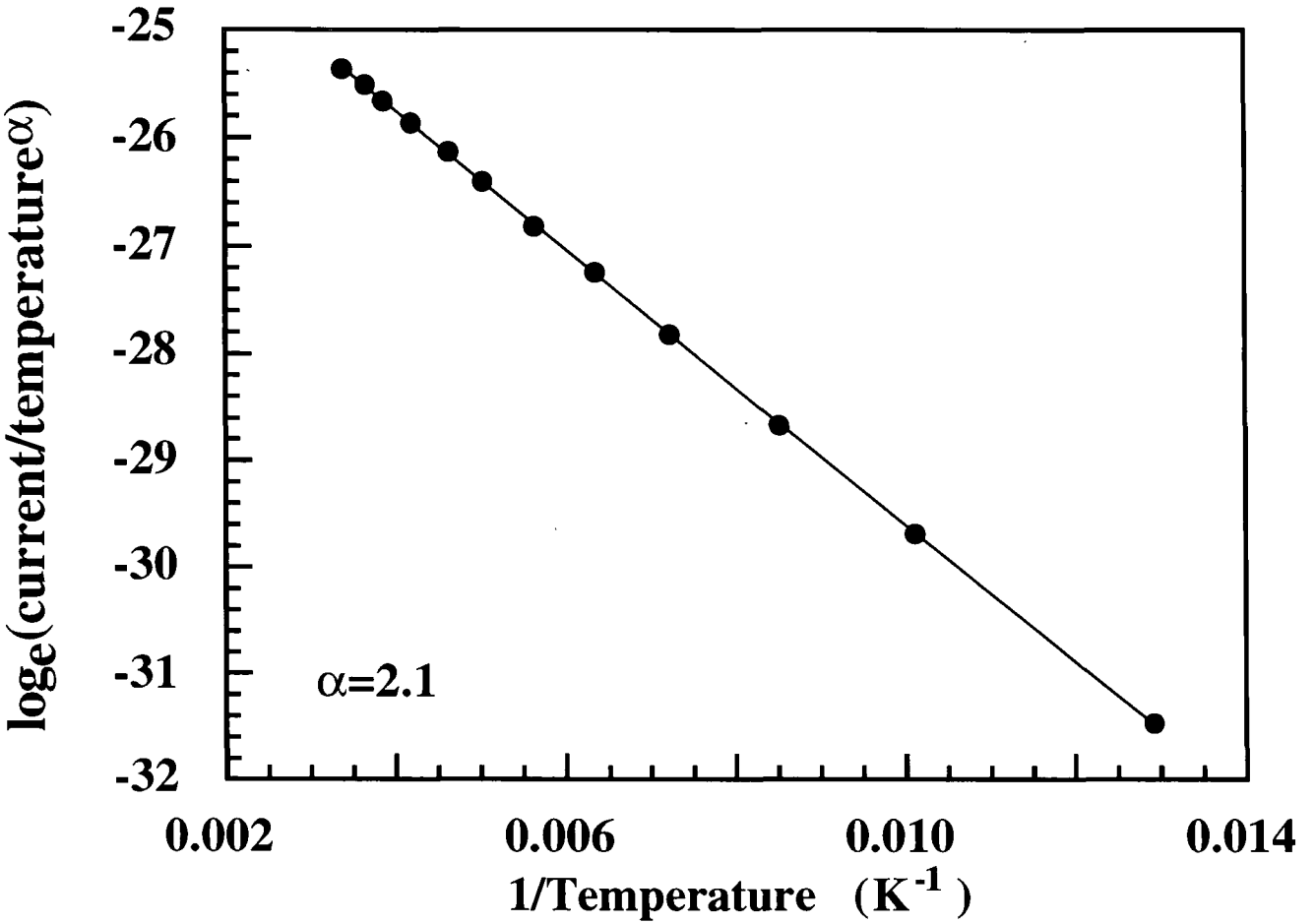

Fig. 7.41 The current versus reciprocal temperature data of Fig. 7.40 corrected for the effect of a temperature dependent carrier mobility. The 39-layer sample of C_{18}Py-Pd(dmit)$_2$ was deposited from a floating layer formed from 2 ml of solution that had been allowed to age on the surface of the subphase for 21 hours before compression.

In these films, the conductivity was thermally activated, with an activation energy of 0.07±0.02 eV recorded, a value similar to that observed for films of C_{18}Py-Ni(dmit)$_2$ after exposure to iodine vapour (chapter 8, section 8.6). There was also a power law variation of conductivity with temperature, $\sigma \propto T^{\alpha}$. α was dependent on the spreading time and doping state, and lay in the range $1.4 \leq \alpha \leq 4.0$. A value of $\alpha = 1.5$ can be attributed to the temperature dependence of the density of states in the transport band, and larger values to a combination of this effect with a contribution due to a variation of mobility with temperature.

7.7 Summary

The properties of floating layers of C_{18}Py-Pd(dmit)$_2$ were found to be dependent on the amount of material spread, and the length of time that this material was allowed to age on the surface of the subphase before compression and dipping. The material spread out well only if a small amount of material was used and a long time allowed before compression. These poor spreading characteristics were reflected in the properties of the transferred films. Large area per complex values and thin transferred layers, suggesting monolayer behaviour, were only observed if the amount of spreading solution used was small and a long spreading time allowed. High bulk conductivity that was stable with time was observed without any post deposition treatment, but only if the floating layer was compressed soon after spreading. It is thought that these films contained conductive crystallites, and that with time a reordering occurred to give a structure in which carrier transport was not favoured. In some cases, a super Ohmic dependence of current on bias voltage was observed. This behaviour has been attributed to single carrier space charge limited conductivity. By observing the low temperature electrical behaviour, an exponential dependence of conductivity on temperature was found, indicating semiconducting behaviour with a thermal activation energy of 0.07±0.02 eV. There was also a power law variation of conductivity on temperature, suggesting a contribution from fluctuations in the density of states in the transport band and/or the carrier mobility.

References

1. D.M Taylor, A.E. Underhill, S.K. Gupta and C.E. Wainwright, Makromol. Chem., Makromol. Symp., 46 (1991) 199-203.
2. S.K. Gupta, D.M. Taylor, P. Dynarowicz, E. Barlow, C.E.A. Wainwright and A.E. Underhill, Langmuir, 8 (1992) 3057-3062.
3. S.K. Gupta, D.M. Taylor, A.E. Underhill and C.E. A. Wainwright, Synth. Met., 58 (1993) 373-382.
4. M. Yumura, T. Nakamura, M. Matsumoto, S. Ohshima, Y. Kuriki, K. Honda, M. Kurahashi and Y.F. Miura, Synth. Met., 55-57 (1993) 3865-3870.
5. A.E. Underhill, R.A. Clark, I. Marsden, M. Allan, R.H. Friend, H. Tajima, T. Naito, M. Tamura, H. Kuroda, A. Kobayashi, H. Kobayashi, E. Canadell. S. Ravy and J. P. Pouget, J. Phys.: Condens. Matter, 3 (1991) 933-954.
6. Y.F. Miura, M. Takenaga, A. Kasai, T. Nakamura, M. Matsumoto and Y. Kawabata, Jpn. J. Appl. Phys., 30 (1991) 3503-3509.
7. R.J. Ward, A.S. Dhindsa, M.R. Bryce, M.C. Petty and H.S. Munro, Thin Solid Films, 198 (1991) 363-367.
8. D.M. Taylor, SD.K. Gupta, A.E. Underhill and A.S. Dhindsa, Thin Solid Films, 243 (1994) 530-535.
9. C. Pearson, A.S. Dhindsa, M.C. Petty and M.R. Bryce, Thin Solid Films, 210,211 (1992) 257-260.
10. G.G. Roberts, N. Apsley and R.W. Munn, Physics Reports, 60(1980)61-150.
11. G.G. Roberts in *'Transfer and Storage of Energy by Molecules'*, eds A.M. North and G.M. Burnet, Wiley (1974) 153-221.
12. A.S. Dhindsa, G. H. Davies, M. R. Bryce, J. Yarwood, J. P. Lloyd, M. C. Petty, and Y. M. Lvov, J. Mol. Electron., 5 (1989) 135-142.
13. D.M. Taylor, S.K. Gupta, A.E. Underhill and C.E.A. Wainwright, Thin Solid Films, 210-211 (1992) 287-289.
14. Y. Xiao, Z. Yao and D. Jin, Thin Soild Films, 223 (1993) 173-177.

15. A.J. Epstein, E.M. Conwell and J.S. Miller, Ann. N. Y. Acad. Sci., (1978) 183-209.

16. T. Nakamura, H. Tanaka, M. Matsumoto, H. Tachibana, E. Manda and Y. Kawabata, Synth. Met., 27 (1988) B601-B608.

17. Y.F. Miura, M. Takenaga, A. Kasai, T. Nakamura, Y. Nishio, M. Matsumoto and Y. Kawabata, Thin Solid Films, 210/211 (1992) 306-308.

Chapter 8

Multilayer Films of *N*-octadecylpyridinium-Ni(dmit)$_2$

8.1 Introduction

In this chapter, the film forming properties, LB deposition and characterisation of transferred multilayer films of *N*-octadecylpyridinium-Ni(dmit)$_2$ (C_{18}Py-Ni(dmit)$_2$) are described. The effect of the time between spreading and compression of the organic layer (spreading time) on the characteristics of the floating film on the subphase and the properties of transferred multilayer films on solid substrates is considered, using isotherm measurements, ellipsometry and surface profiling, optical and electron microscopy and EDS. The effect of iodine doping on film morphology, optical absorption spectra, room temperature and low temperature electrical conductivity is examined. By using the material as the dielectric in a parallel plate capacitor, the relative permittivity, before and after doping with iodine, is also measured.

8.2 Monolayer forming properties

Fig. 8.1 shows the chemical structure and space filling models of C_{18}Py-Ni(dmit)$_2$. The solid was only slightly soluble in chloroform, and although it could be dissolved in dichloromethane, subsequent spreading on the subphase was very poor since the solvent quickly evaporated. Like C_{18}Py-Pd(dmit)$_2$, it was possible to deposit this material in pure form using a mixed solvent consisting of dichloromethane and benzene in the volume ratio 3:2. 3 ml of dichloromethane was added to ~1.2 mg of solid material in a volumetric flask. After ultrasonic agitation for 10 minutes to ensure complete dissolution of the solid, 2 ml of benzene was added to give a solution with concentration of ~ 0.24 g l^{-1}. A suitable amount of this solution (1-5 ml) was applied dropwise over the whole surface of a pure water subphase using a micro syringe. This floating layer was then allowed to stand uncompressed on the surface of the subphase for a time between 1

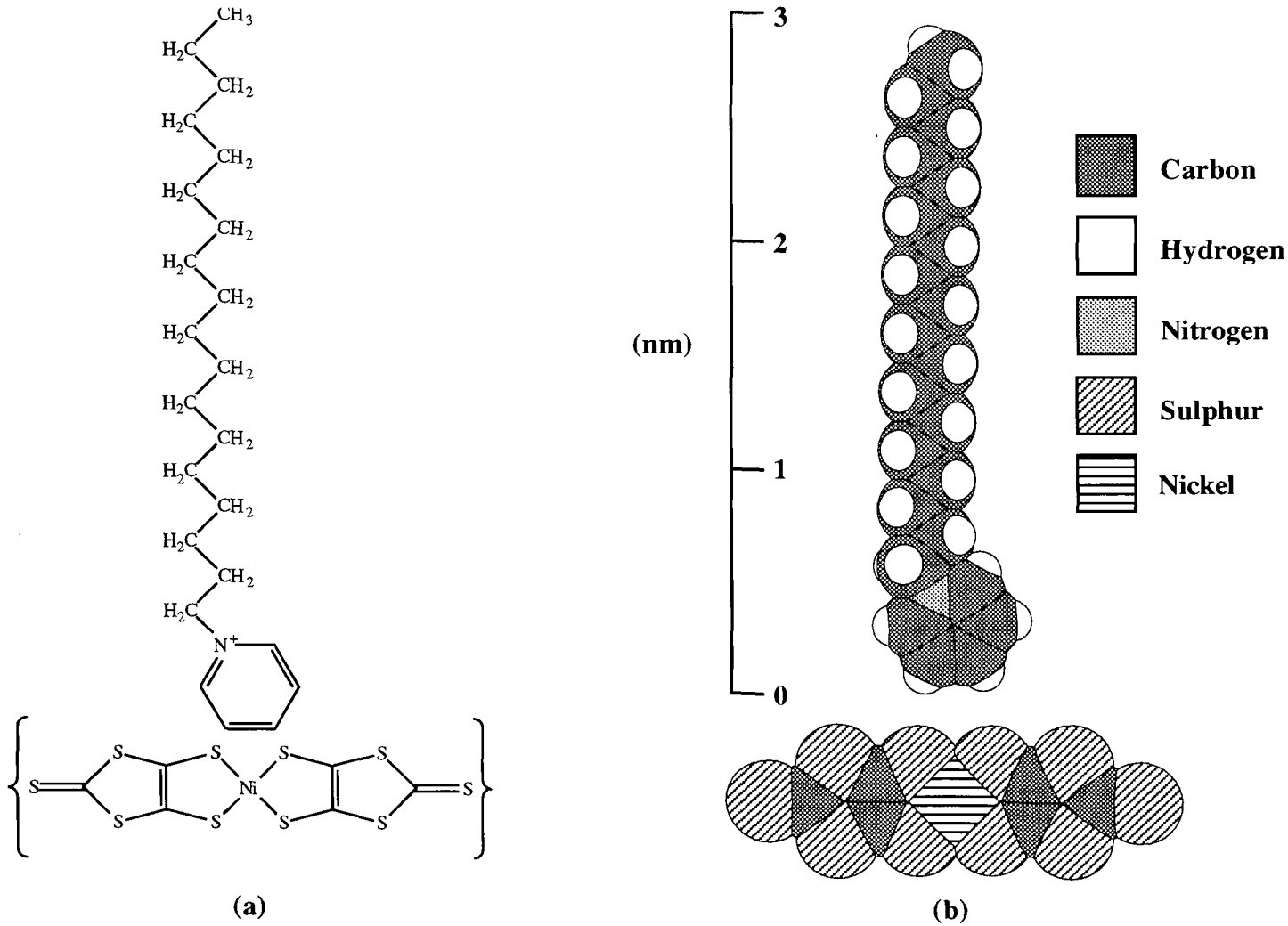

Fig. 8.1 (a) Chemical structure and (b) space filling molecular model of $C_{18}Py\text{-}Ni(dmit)_2$.

minute and 68 hours before pressure versus area isotherms were plotted at a speed of $9\pm3x10^{-4}$ nm^2 $complex^{-1}$ s^{-1}. Condensed isotherms were recorded, of similar shape to those previously reported for the 2:1 stoichiometry complex (*N*-octadecylpyridinium)$_2$-Ni(dmit)$_2$[1]. Like floating layers of C_{18}Py-Pd(dmit)$_2$ (chapter 7, section 2), the curves were strongly dependent on the time that the material was aged on the subphase before the initial compression and on the amount of solution spread, although no plateau regions were evident here. Fig 8.2 compares isotherms for three different times after spreading 1 ml of solution. After 5 minutes, the area per molecule at a surface pressure of 30 mN m^{-1} was *ca.* 0.05 nm^2. Considerably larger values were observed after longer spreading times. After 3 hours, the area per molecule at 30 mN m^{-1} was *ca.* 0.25 nm^2, and this value increased to *ca.* 0.30 nm^2 after 68 hours. Fig 8.4 shows how the area per complex at 30 mN m^{-1} changed as a function of the time that the uncompressed monolayer was aged on the subphase surface. The area per complex reached a maximum value of 0.30 nm^2 after approximately 5 hours.

Fig. 8.3 shows isotherms recorded 15 minutes after spreading of 1, 3 and 5 ml of C_{18}Py-Ni(dmit)$_2$ solution. The area per complex at 30 mN m^{-1} depended on the amount of material applied to the subphase, with the isotherm moving to smaller areas as the volume was increased. The area per complex at 30 mN m^{-1} changed from 0.085 nm^2 to 0.035 nm^2 as the volume of solution increased from 1 ml to 5 ml. This behaviour has been reported by Gupta *et al*[2] for floating layers of the 2:1 salts bis(didodecylmethylammonium)-M(dmit)$_2$ (M=Pt, Pd, Ni). From a standard molecular model, the *N*-octadecylpyridinium cation has a cross sectional area of approximately 0.25 nm^2 and the Ni(dmit)2 anion has dimensions of 1.61 nm x 0.623 nm x 0.366 nm.[2] Therefore, in common with floating films of C_{18}Py-Pd(dmit)$_2$, it is impossible to relate the maximum area per molecule measured in these experiments with a monomolecular film in which both of the components are in contact with the surface of the subphase. It is possible that a multilayer film is formed, or that the value may be associated with the

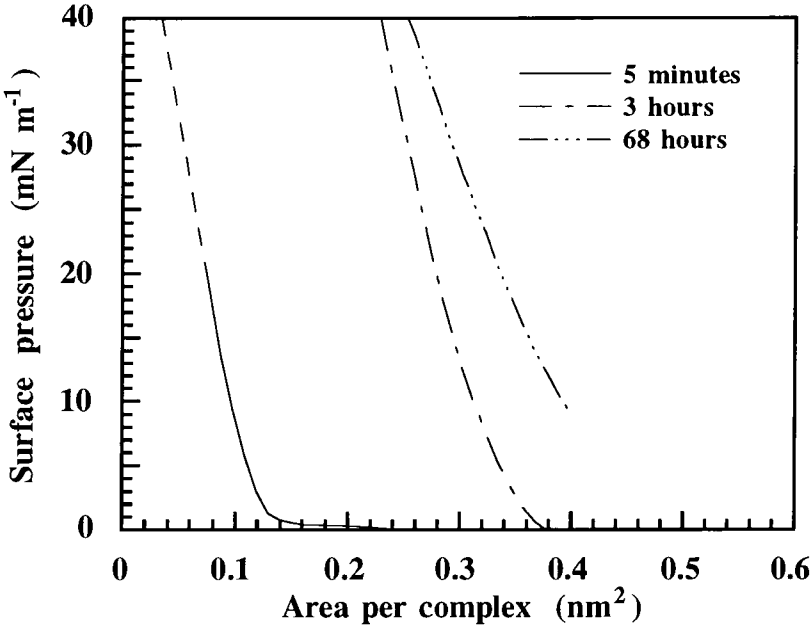

Fig. 8.2 Surface pressure versus area isotherm plots for C_{18}Py-Ni(dmit)$_2$ films, 5 minutes, 3 hours and 68 hours after the spreading of 1 ml of solution on a pure water subphase. The data for the film compressed after 5 minutes were extrapolated (dashed line) so that a value for the area per complex at 30 mN m^{-1} could be obtained.

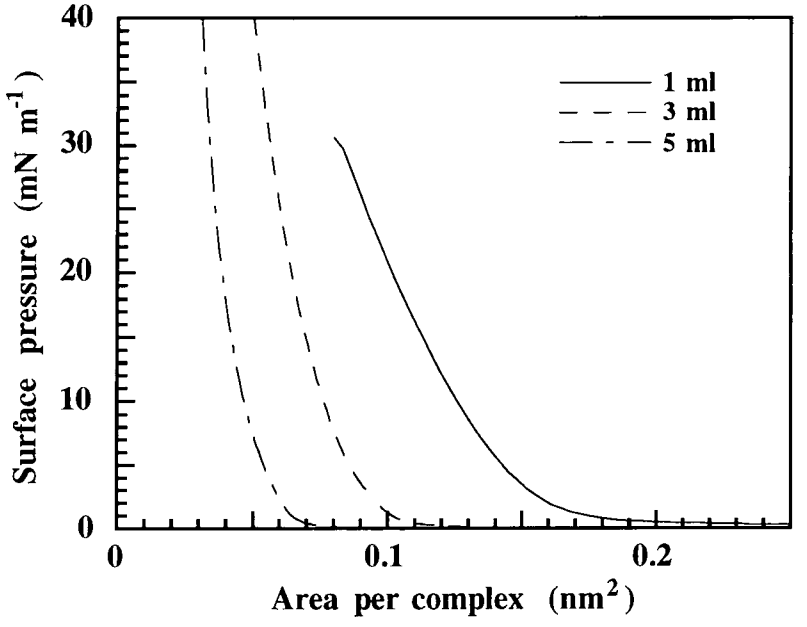

Fig. 8.3 Surface pressure versus area isotherm plots for C_{18}Py-Ni(dmit)$_2$ films, 10 minutes after the spreading of 1 ml, 3 ml and 5 ml of solution on a pure water subphase.

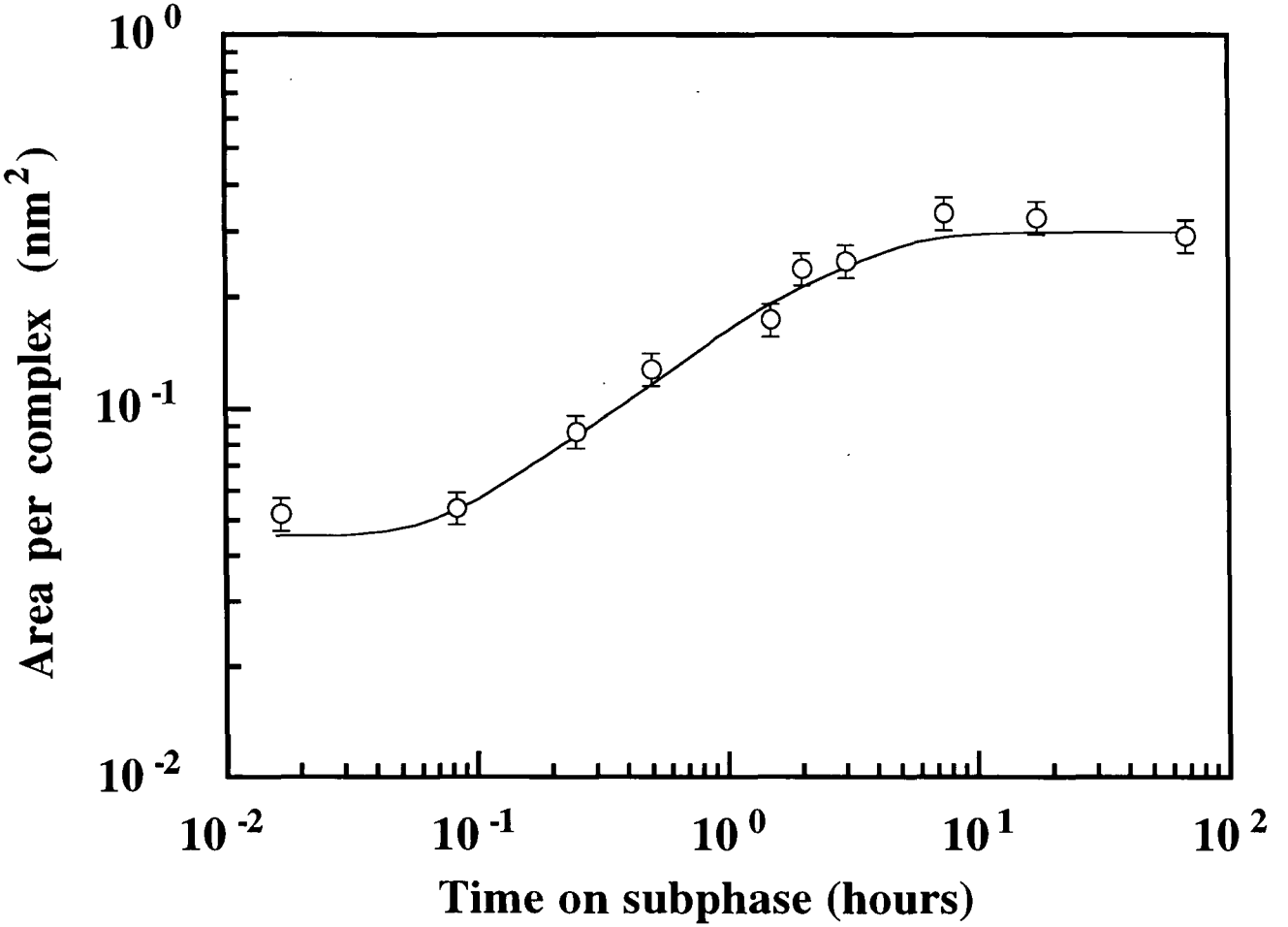

Fig. 8.4 Area per complex measured at a surface pressure of 30 mN m^{-1} versus the time that floating layers formed from 1 ml of C_{18}Py-Ni(dmit)$_2$ spreading solution were aged on the surface of the subphase before isotherms were recorded.

cross sectional area of the pyridinium cation, in which case the $Ni(dmit)_2$ molecules may be arranged above, below or interleaved between the long chain pyridinium molecules. A structure similar to that suggested for aged floating films of $C_{18}Py\text{-}Pd(dmit)_2$ is possible (Fig. 7.22).

8.3 LB film deposition

LB deposition was performed at a surface pressure of 38 mN m^{-1}. Dipping, onto hydrophilic glass slides or single crystal silicon, was started with the substrates in air above the surface of the subphase. A speed of 6 mm min^{-1} was used, and the transferred layers were allowed to dry for 15 minutes between cycles. The deposition type depended on the spreading time before compression. For layers compressed soon after application to the subphase, dipping was Y-type with a transfer ratio, $\tau = 1.0\pm0.1$. If the film had been aged for several hours before compression and deposition, dipping was Z-type, with a transfer ratio of 1.0 ± 0.1 on the upstroke. This contrasts with the behaviour of aged floating layers of $C_{18}Py\text{-}Pd(dmit)_2$, where Y-type transfer was recorded with $\tau = 1.1\pm0.1$ in both directions. In the following experiments, the number of layers transferred onto each sample was obtained from the dipping record of trough area versus time.

8.4 Film properties

8.4.1 Thickness measurements

The thickness of films which had been deposited onto single crystal silicon substrates from floating layers that had been allowed to stand uncompressed on the surface of the subphase for 10 minutes and 20 hours were measured using surface profiling and ellipsometry. As with multilayer films of $C_{18}Py\text{-}Pd(dmit)_2$ (chapter 7, section 7.4.1), the thickness per layer depended on the spreading time. For films deposited from aged floating layers, the Alpha-step data were extremely noisy, and accurate measurements were difficult. An average value of 2.5 ± 1.0 nm per layer was obtained from measurements on two different films having 11 and 22 layers. Using ellipsometry, a

value of 2.1±0.1 nm per layer was recorded for the same two films. This was an average value calculated from six separate measurements on each film. Alpha-step measurements on films transferred from a floating layer that had been aged on the subphase surface for only 10 minutes were much more reliable. Fig 8.5 shows a typical trace taken from a 59-layer as-deposited film on a silicon substrate. The film was continuous with a thickness of ca. 1.9 μm, but the surface was undulating, and micron sized features were evident. Alpha-step measurements on multilayer films of C_{18}Py-Pd(dmit)$_2$ produced similar results (cf. Fig. 7.5). Data obtained from surface profiling and ellipsometry measurements on films with different numbers of layers are plotted in Fig. 8.6. By fitting a straight line to both sets of results, an average layer thickness of 31±4 nm was obtained. This is a larger value than that obtained from multilayer films of C_{18}Py-Pd(dmit)$_2$ prepared under similar conditions, where a thickness per layer of 4.7±0.2 nm was recorded. However, this is in agreement with the observations of Gupta *et al*[2] who reported that the isotherm of their Pd salt exhibited a weaker dependence on spreading time than that of the Ni compound, with the curve moving to larger areas with increasing time. No change in thickness of C_{18}Py-Ni(dmit)$_2$ layers was recorded after exposure to iodine vapour.

8.4.2 Electron microscopy and energy dispersive spectroscopy.

Fig 8.7 shows an electron micrograph taken from a 59-layer iodine doped multilayer of C_{18}Py-Ni(dmit)$_2$ which had been deposited from a floating layer compressed after 20 minutes on the surface of the subphase. Micron sized particles were evident in the film, and one of these can be seen in the micrograph. In Fig. 8.8, the results of two EDS measurements are plotted, one for each of the electron probe positions marked on the micrograph. The two positions correspond to the particle (position A) and the background (position B). Large signals due to sulphur, nickel and iodine were recorded when the particle was probed, and traces of these elements were also seen in the background spectrum, indicating the presence of Ni(dmit)$_2$ and iodine. Using this

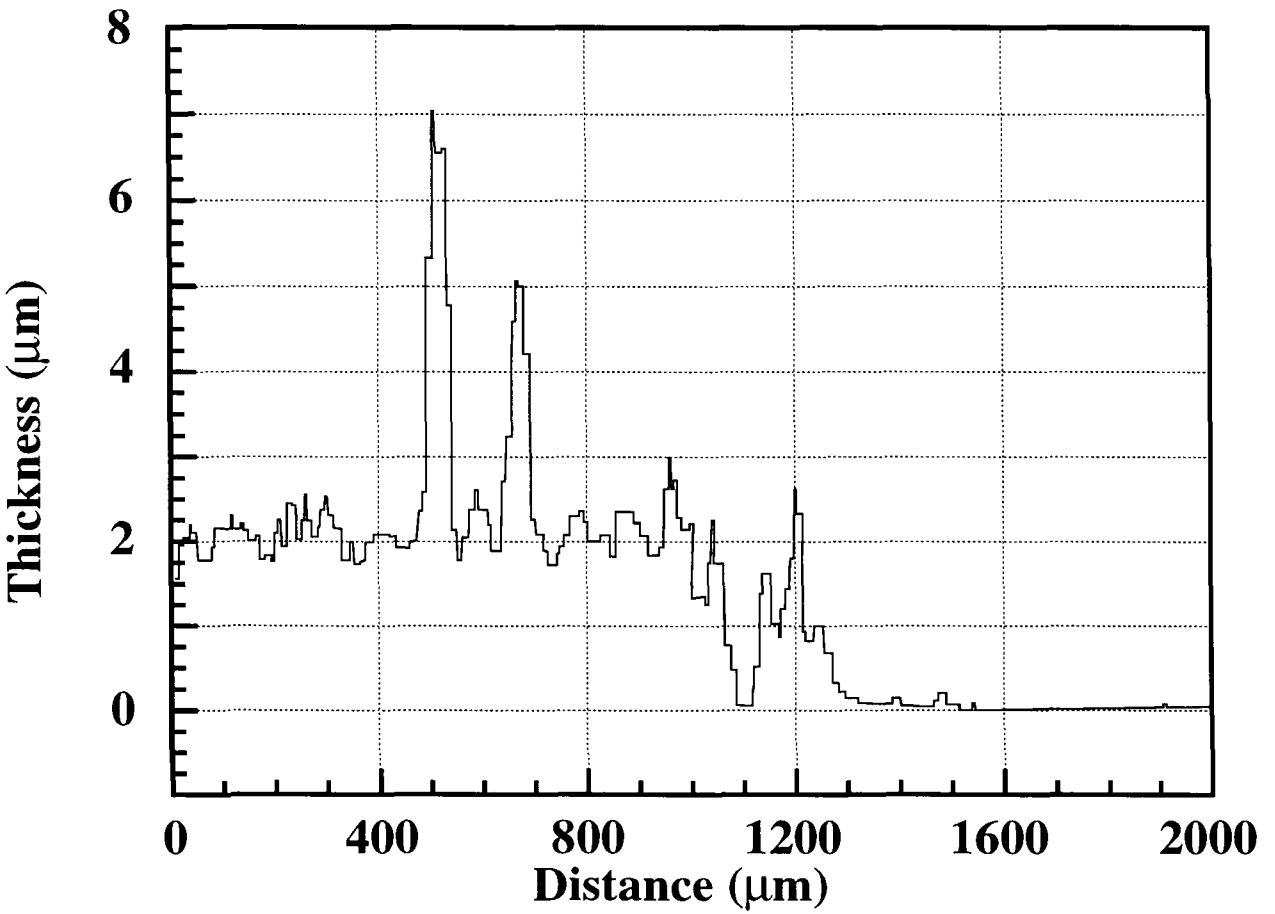

Fig. 8.5 A typical surface profiling Alpha-step trace, recorded from a 59-layer C_{18}Py-Ni(dmit)$_2$ film. The sample was deposited from a floating layer formed from 5 ml of solution that had been aged on the subphase for 10 minutes before compression.

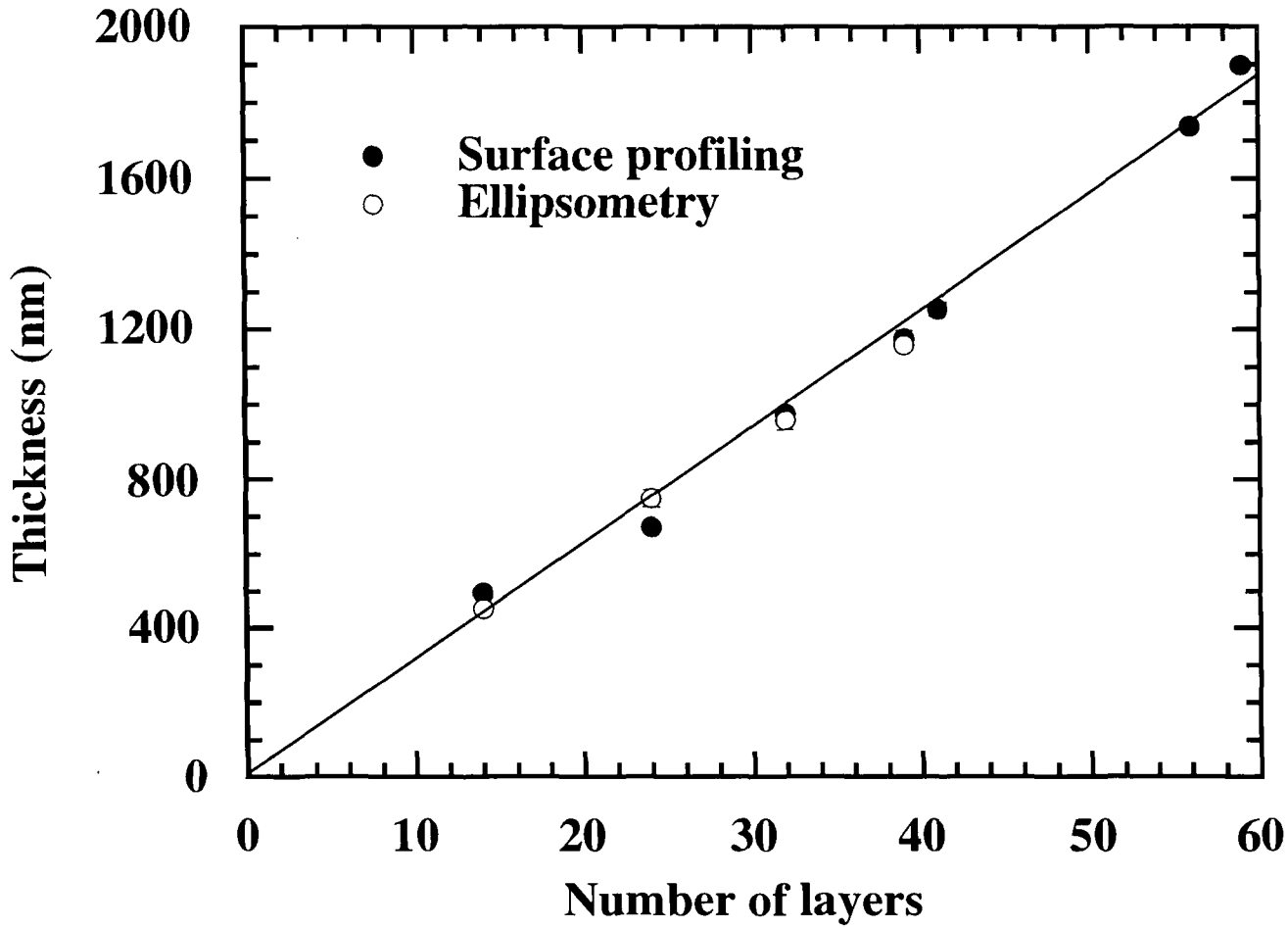

Fig. 8.6 Film thickness (measured using surface profiling and ellipsometry) versus number of layers of C_{18}Py-Ni(dmit)$_2$ deposited onto single crystal silicon. The floating film, formed from 1 ml of solution, was aged for 10 minutes on the surface of the subphase before compression.

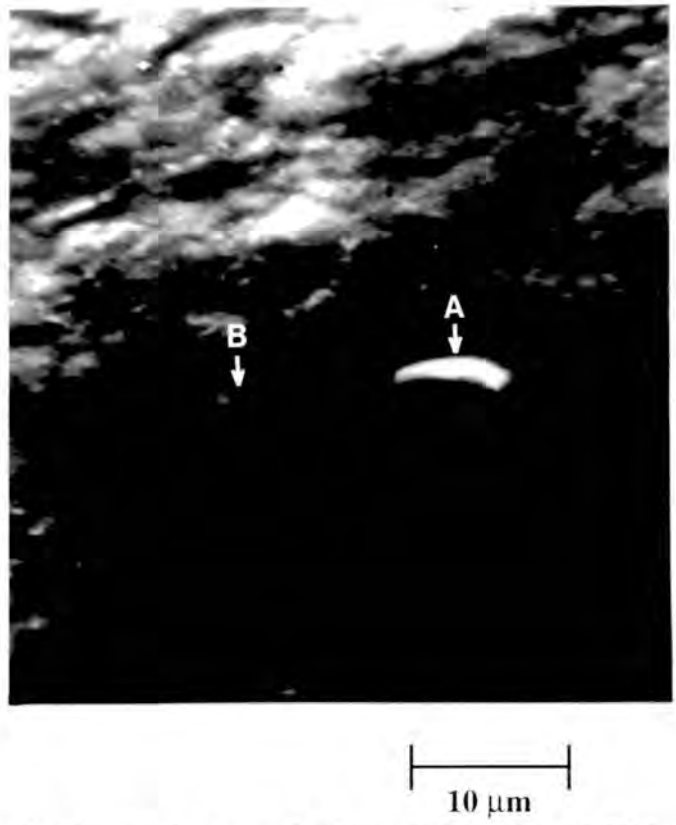

Fig. 8.7 **Scanning electron micrograph of an iodine doped 59-layer film of C_{18}Py-Ni(dmit)$_2$. The sample was transferred from a layer that had been allowed to age on the surface of the subphase for 10 minutes before compression.**

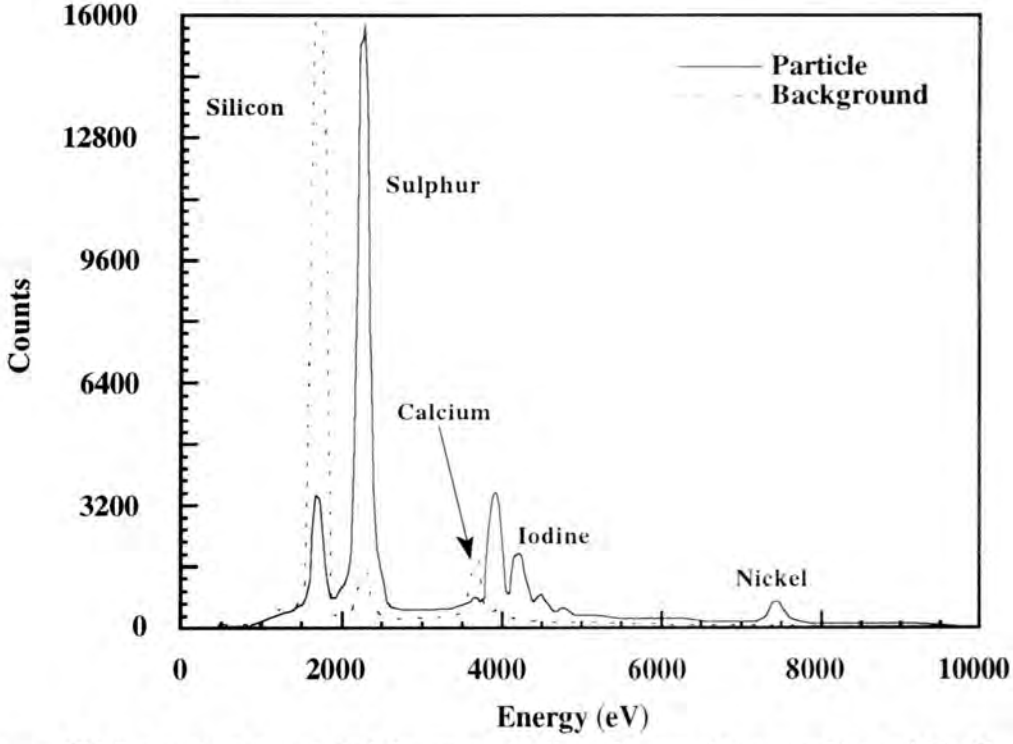

Fig. 8.8 **EDS spectra recorded from an iodine doped 59-layer film of C_{18}Py-Ni(dmit)$_2$. The sample was transferred from a layer that had been allowed to stand on the surface of the subphase for 10 minutes before compression. The electron probe was directed at point A on the micrograph shown in Fig. 8.7 when the solid line was recorded and at point B for the data represented by the dotted line.**

technique it was not possible to detect the long chain pyridinium cation. By performing a measurement on an uncoated piece of glass, it was confirmed that the peaks due to silicon and calcium seen in the spectra were generated by the glass substrate. Similar results were observed when a multilayer film of the related Pd complex, prepared under similar conditions, was investigated (chapter 7, section 7.4.2).

8.4.3 Optical microscopy

Multilayers deposited from floating films which had been aged on the subphase surface for several hours had a structure that was polycrystalline, as shown in the micrograph of Fig 8.9, which was taken from a 10-layer as-deposited sample transferred from a floating film that had been aged for 19.5 hours before compression. No significant change was observed after chemical doping with iodine vapour. Fig 8.10 shows optical micrographs for a 59-layer film deposited from a floating layer that had been aged on the subphase for only 20 minutes before compression. The as-deposited film, shown in Fig. 8.10(a), had a two phase structure, with small aggregates 5-20 μm in size distributed in a light background matrix. No substantial change was observed after a short exposure to iodine vapour, as illustrated in Fig 8.10(b), which shows the film after doping for 30 seconds. After an exposure time of 2000 seconds, however, several much larger particles appeared, as shown in Fig. 8.10(c), and the texture of the background changed to a very fine polycrystalline structure. These large aggregates were observed under the electron microscope (Fig 8.6) and, using EDS, found to contain $Ni(dmit)_2$ and iodine. To discover the origin of the particles, different numbers of layers were built up from a floating film which was compressed after 20 minutes on the subphase. These layers were then doped with iodine for 2000 seconds before observation under the microscope. Micrographs taken from 1,19 and 39-layers are shown in Fig. 8.11(a), (b) and (c), respectively. The number of particles increased as the number of layers increased, suggesting that these aggregates are present in floating layer. No precipitate could be seen in the spreading solution, and it seems likely that the aggregates form on the surface of

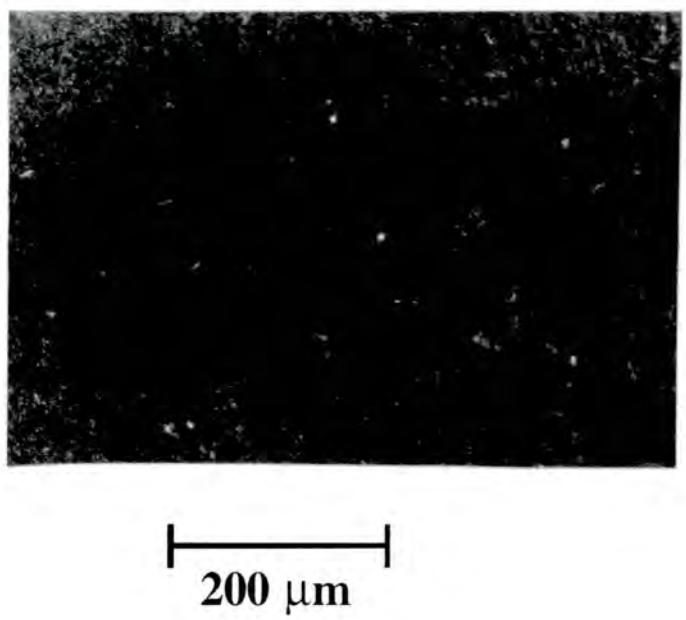

Fig. 8.9 **Optical micrograph taken from a 10-layer as-deposited sample of C_{18}Py-Ni(dmit)$_2$ transferred from a floating film that had been aged for 19.5 hours before compression.**

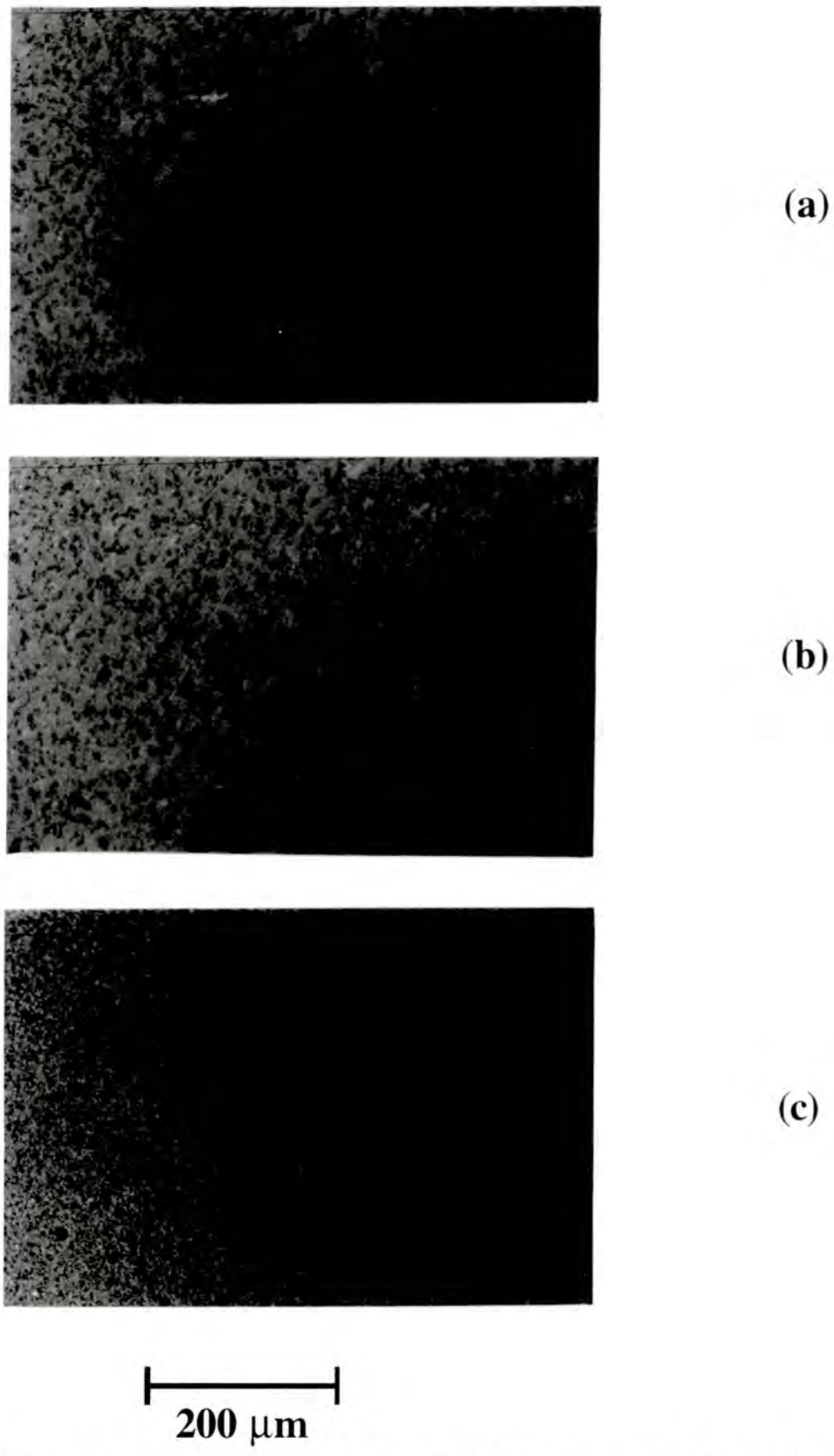

Fig. 8.10 **Optical micrographs for a 59-layer film of C_{18}Py-Ni(dmit)$_2$ transferred from a floating film that had been aged for 20 minutes before compression**

(a) **as-deposited.**
(b) **after iodine doping for 30 seconds.**
(c) **after iodine doping for 2000 seconds.**

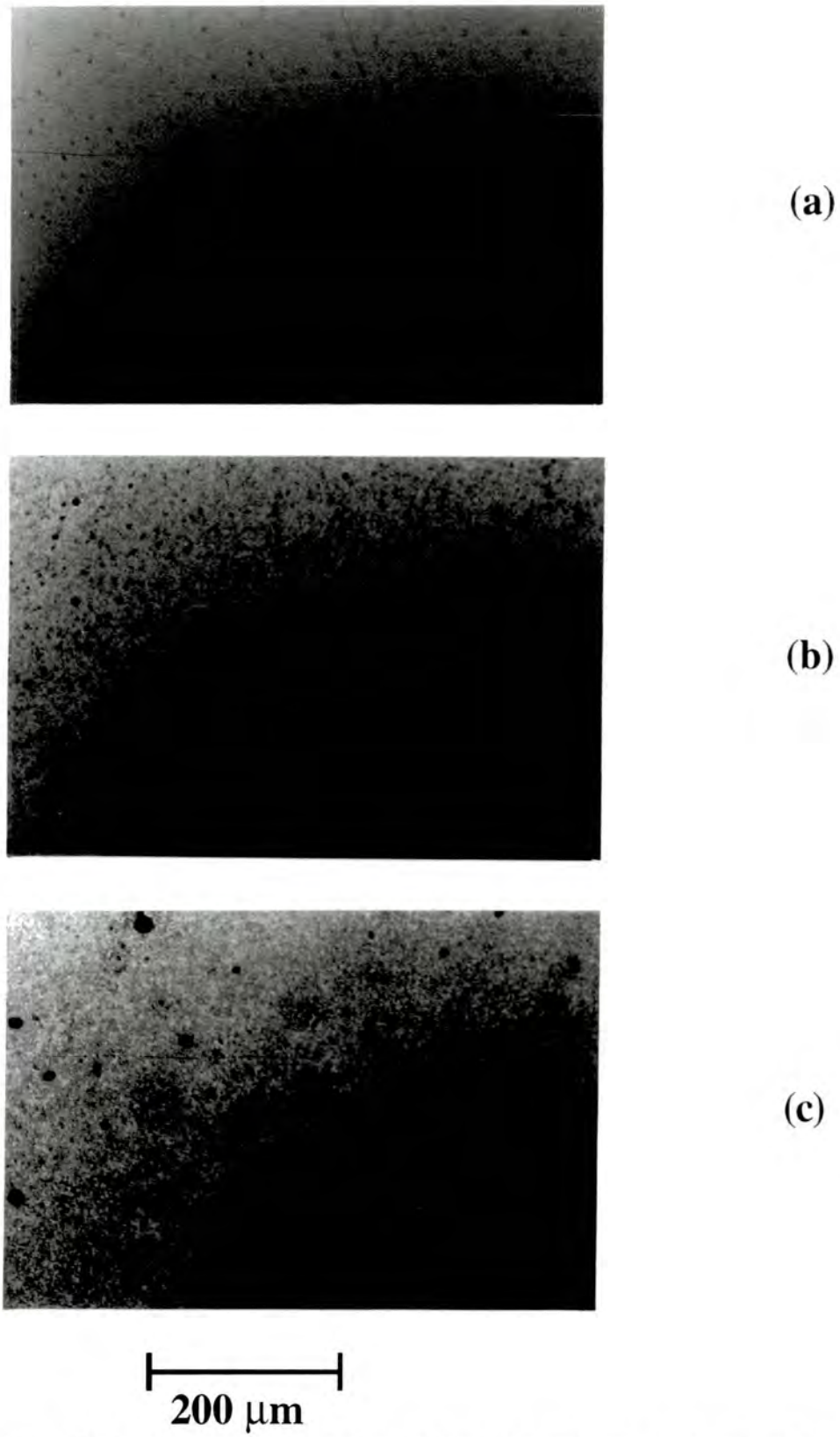

Fig. 8.11 **Optical micrographs for different numbers of layers of C_{18}Py-Ni(dmit)$_2$ transferred from a floating film that had been aged for 20 minutes before compression. The films were doped with iodine vapour for 2000 seconds.**

(a) 1-layer.
(b) 19-layers.
(c) 39-layers.

the subphase.

8.4.4 Optical absorption

Fig 8.12 shows optical absorption spectra for 9-layer as-deposited films transferred from floating layers that were aged on the subphase for 1 minute, 15 minutes, 1.5 hours and 3 hours before compression and LB deposition. Absorption bands were observed at 320, 360, 430, 640, 1100 and 1310 nm, with a shoulder evident at *ca.* 480 nm. The bands in the UV and visible range are likely to be associated with electronic transitions within the $Ni(dmit)_2$ molecules, whereas bands in the infra red have been associated with intermolecular charge transfer transitions in single crystals of $Cs[Pd(dmit)_2]$[3] and LB layers of tridecylmethylammonium-$Au(dmit)_2$.[4] The decrease in the intensity of the absorption bands with spreading time is a consequence of the diminished thickness of floating layers that had been left for a longer time on the subphase. The effect of exposure to iodine vapour for 2000 seconds on the spectrum of a 19-layer sample transferred from a floating layer compressed after 10 minutes on the subphase is shown in Fig. 8.13. 5 minutes after the completion of doping, the peaks at 640 nm, 1100 nm and 1310 nm could no longer be seen, and a new broad band appeared at *ca.* 900 nm. After 3.5 hours, it became evident that this peak was actually a combination of two absorption bands. It is possible that one or both of these absorptions is due to the charge transfer band associated with the formation of a mixed valence complex. A peak was observed, at *ca.* 800 nm, in conductive films of $C_{18}Py$-$Pd(dmit)_2$.

8.5 Room temperature conductivity

8.5.1 Contact resistance and conductivity of the organic layers

Room temperature in-plane dc conductivity was measured using evaporated gold, air drying silver paint and carbon cement as electroding materials. The conductivity of as-deposited films, regardless of spreading time, was very low. In contrast, multilayers of $C_{18}Py$-$Pd(dmit)_2$ that were transferred from floating layers compressed soon after

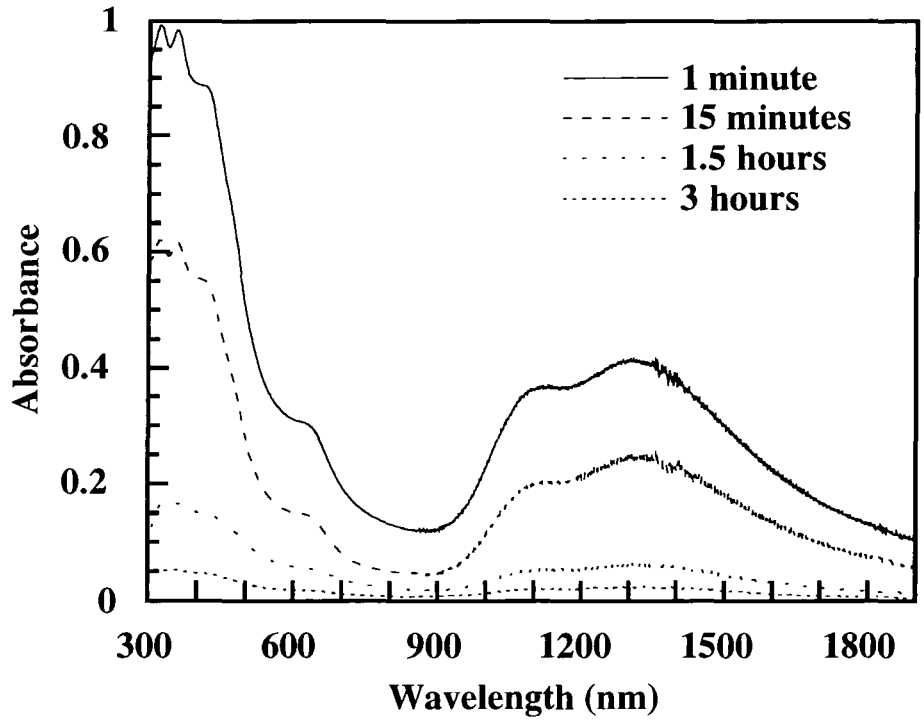

Fig. 8.12 Optical absorption spectra for 9-layer as-deposited LB films of C_{18}Py-Ni(dmit)$_2$ prepared from floating films that had been allowed to age on the subphase for different lengths of time.

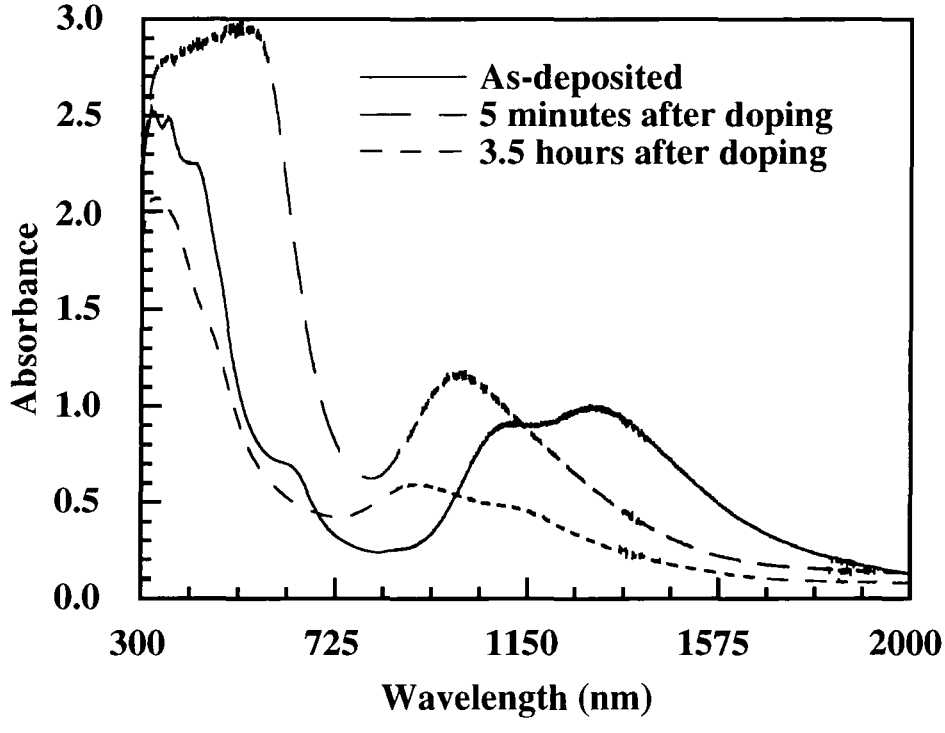

Fig. 8.13 Optical absorption spectra for 19-layer LB films of C_{18}Py-Ni(dmit)$_2$ at various times after doping with iodine vapour for 33 minutes.

spreading had a conductivity of $3.5\pm2.5\times10^{-3}$ S cm^{-1} (chapter 7, section 7.5.1). The current versus voltage characteristic for a 19-layer as-deposited film transferred from a floating layer that had been aged for 10 minutes before compression is shown in Fig. 8.14. The electrodes were 1 mm apart, and formed from gold that was evaporated on top of the LB film. Control data, measured for identical electrodes deposited directly onto the glass substrate, are plotted on the same graph. A room temperature in-plane dc conductivity of $5\pm1\times10^{-9}$ S cm^{-1} was calculated from the data for the LB sample. LB films built up from floating layers that had been aged on the subphase for many hours exhibited conductivities up to 10^{-4} S cm^{-1} immediately after exposure to iodine, but the value rapidly fell back to the as-deposited level upon evacuation of the sample chamber. The conductivity of multilayers deposited from floating films that were compressed after a short time on the surface of the subphase was seen to increase by several orders of magnitude following iodine doping.

Fig. 8.15 shows the current versus voltage characteristics for an iodine doped 19-layer film deposited from a floating layer that was compressed after 10 minutes on the surface of the subphase. The behaviour of the three different electroding materials is compared on the same graph. Evaporated gold and carbon cement exhibited similar electrical characteristics, with current proportional to voltage over the entire bias range studied. A conductivity of 0.13 ± 0.08 S cm^{-1} was calculated using the measured film thickness. No anisotropy of this conductivity was observed in the plane of the film. Fig. 8.16 is a plot of sample resistance, measured using a bias voltage of 10 V, versus the distance between carbon cement contacts applied to a 39-layer iodine doped film of C_{18}Py-Ni(dmit)$_2$. The sample was transferred from a floating layer formed from 4.5 ml of solution that was aged for 15 minutes before compression. The data points lay on a straight line through the origin, indicating that the contact resistance was negligible. When silver paint contacts were used, a departure from Ohmic behaviour was seen at low bias voltages, with a superlinear current versus voltage dependence observed. In multilayer LB films of

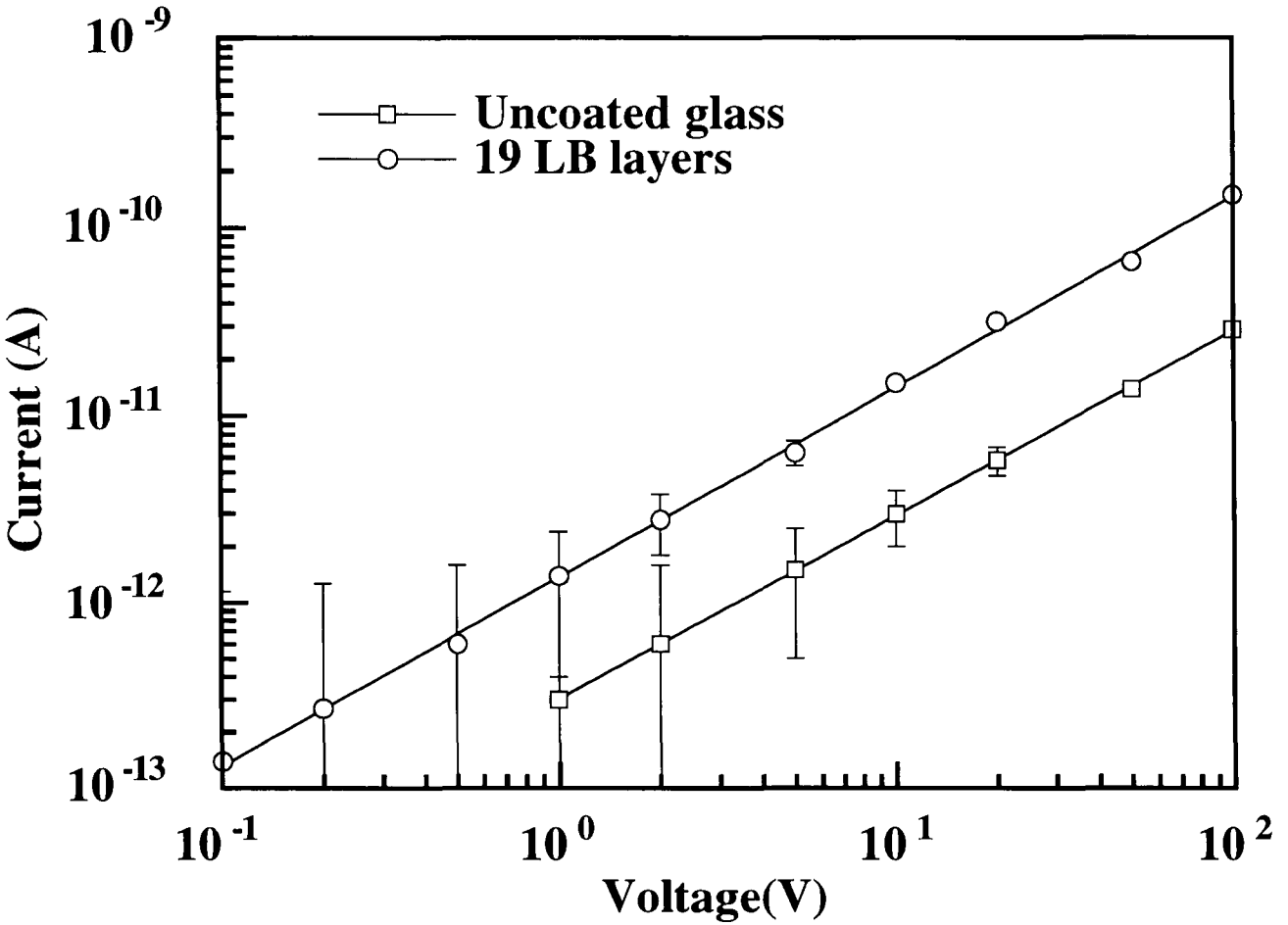

Fig. 8.14 Current versus voltage characteristics for a 19-layer as-deposited LB film of C_{18}Py-Ni(dmit)$_2$ with evaporated gold top contacts 1 mm apart. The sample was transferred from a floating layer formed from 4 ml of solution that had been aged for 10 minutes before compression. The results of a control experiment with identical electrodes deposited on the uncoated glass substrate are also plotted for comparison.

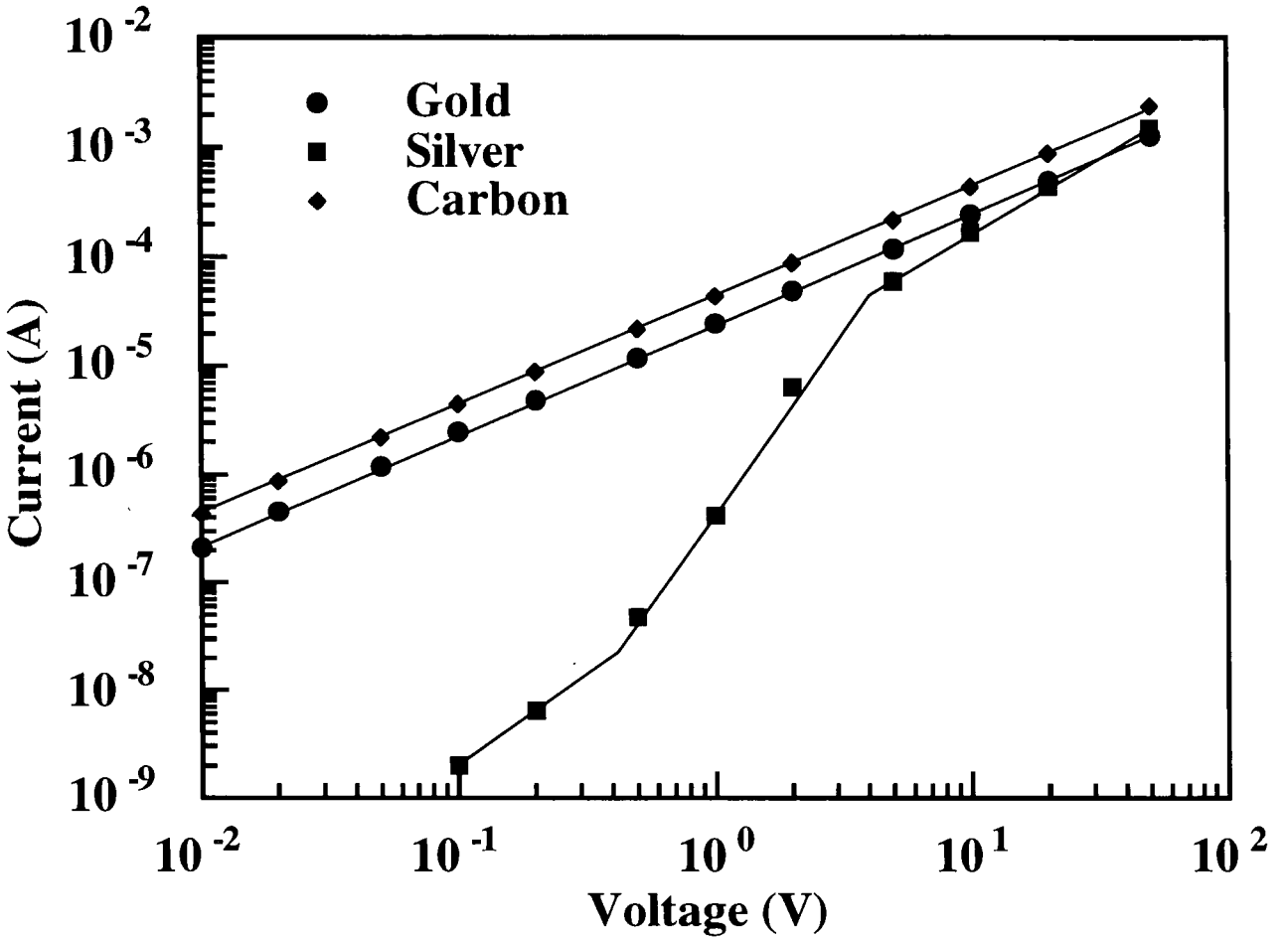

Fig. 8.15 Current versus voltage characteristics for a 19-layer iodine doped LB film of C_{18}Py-Ni(dmit)$_2$ with silver paint, carbon cement and evaporated gold contacts. The sample was transferred from a floating layer formed from 4 ml of solution that had been aged for 10 minutes before compression.

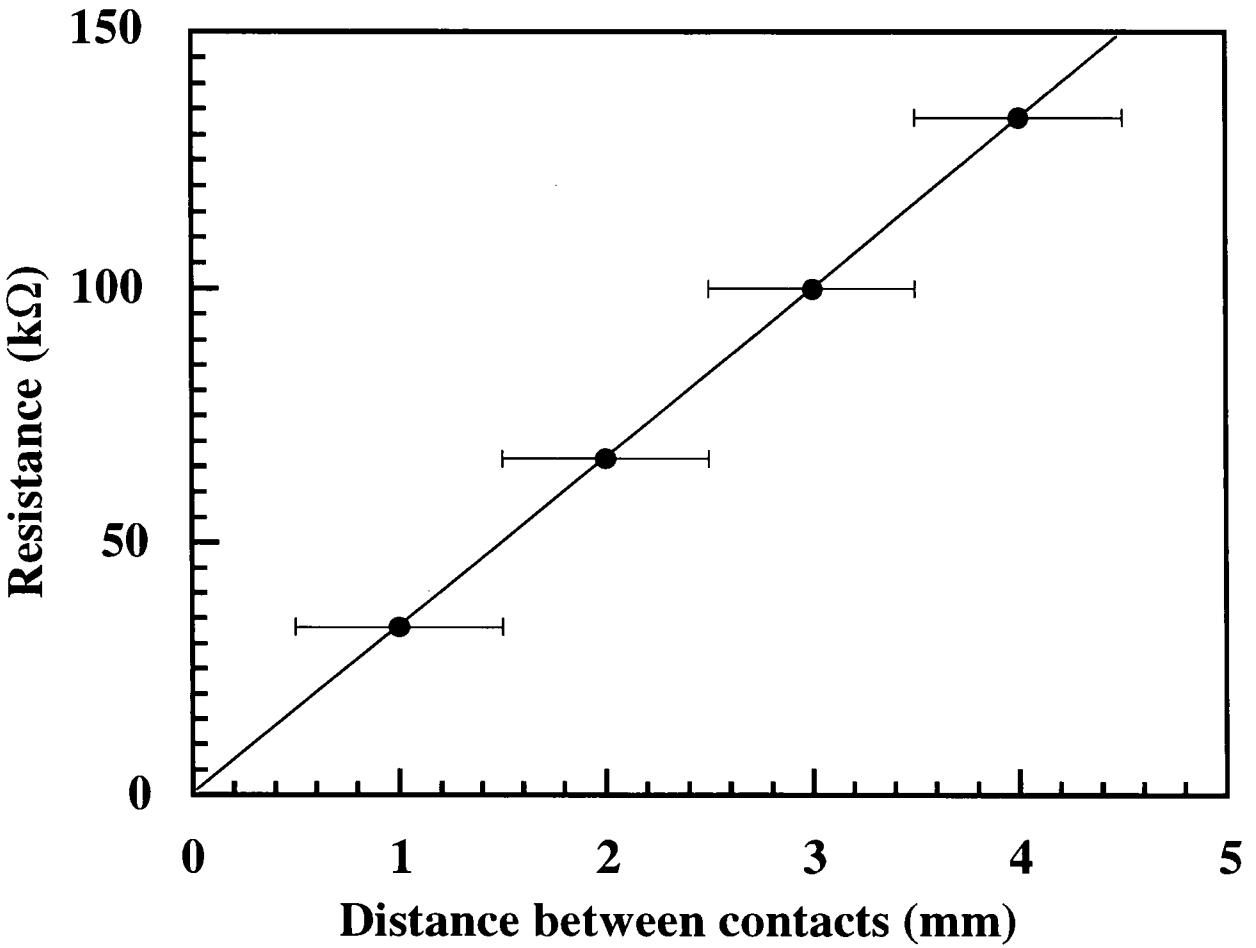

Fig. 8.16 Sample resistance, measured using a bias voltage of 10 V, versus the distance between carbon cement contacts on a 39-layer iodine doped film of C_{18}Py-Ni(dmit)$_2$. The floating layer was formed from 4.5 ml of solution that had been allowed to age on the surface of the subphase for 15 minutes before compression.

C_{18}Py-Pd(dmit)$_2$ (chapter 7, section7.5.1) and (*N*-octadecylpyridinium)$_2$-Ni(dmit)$_2$,[5] super Ohmic behaviour was attributed to space charge limited conductivity, but the situation seems to be different in this case. The superlinear characteristic observed when silver paint was used to provide contacts lay below the I∝V characteristics recorded using the other two electroding materials. Sample resistance versus the distance between silver paint contacts on a 25-layer film of C_{18}Py-Pd(dmit)$_2$ after doping with iodine, with bias voltages of 1 V and 50 V applied, are plotted in Fig. 8.17(a) and (b), respectively. At low bias, the resistance was independent of electrode spacing, indicating that the electrical behaviour was dominated by the contacts. With a high bias voltage applied, however, the data lay on a straight line through the origin, and the resistance of the LB film was dominant. It seems likely that resistive barriers were formed at the interface between the silver paint and the LB film. At low bias, a large proportion of the applied voltage was dropped across these contact resistances, and the current versus voltage characteristics were limited by the properties of the barriers. As the bias was increased, however, these barriers broke down and the current became limited by the organic film.

8.5.2 Contact stability

Fig. 8.18 is a plot of conductivity, measured with a bias of 1 V applied to carbon cement contacts that were 5.0±0.5 mm long and 5.0±0.5 mm long, versus number of layers of C_{18}Py-Ni(dmit)$_2$. These films were deposited from a floating layer formed from 4.5 ml of solution that had been aged for 15 minutes before compression. The conductivity value, which was calculated using an experimentally measured thickness, remained constant for films of between 9 and 79 layers. The carbon cement was applied using an organic solvent, and it seems likely that this dissolved through the LB layers, allowing contact to be made to the entire thickness of the film.

The electrical stability of contacts formed from different materials, after exposure to iodine vapour has been studied. The results of these experiments are shown in Fig. 8.19.

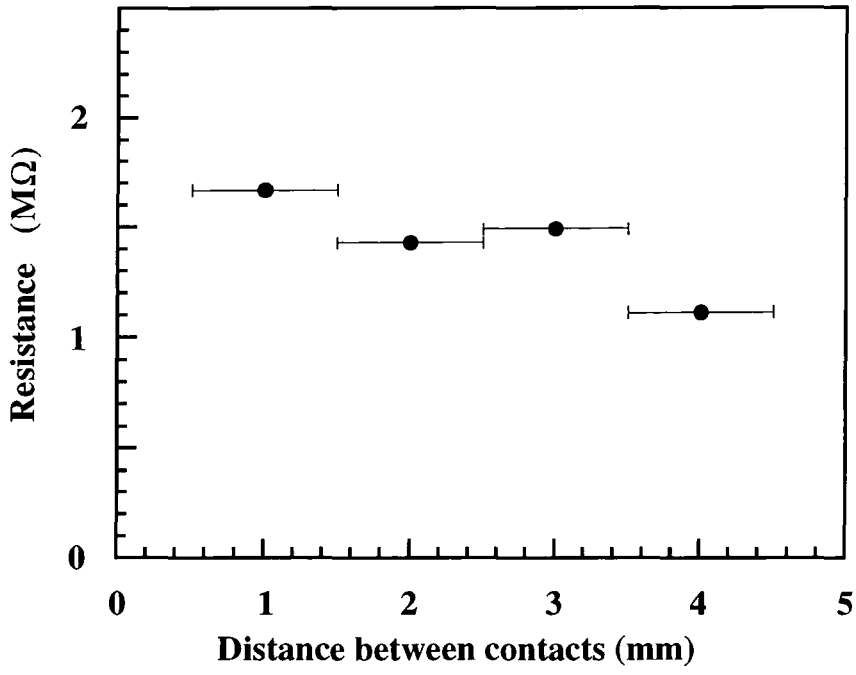

(a)

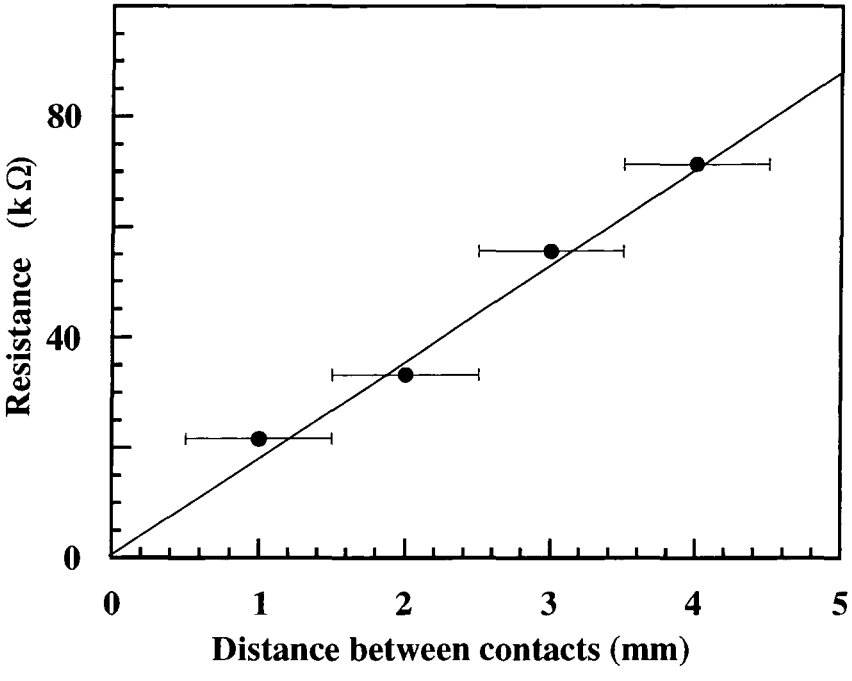

(b)

Fig. 8.17 **Resistance versus the distance between silver paint contacts applied to a 25-layer LB film of C_{18}Py-Pd(dmit)$_2$ after iodine doping.**

(a) 1V bias.
(b) 50 V bias.

The films were transferred from a floating layer formed from 5 ml of solution aged for 15 minutes before compression.

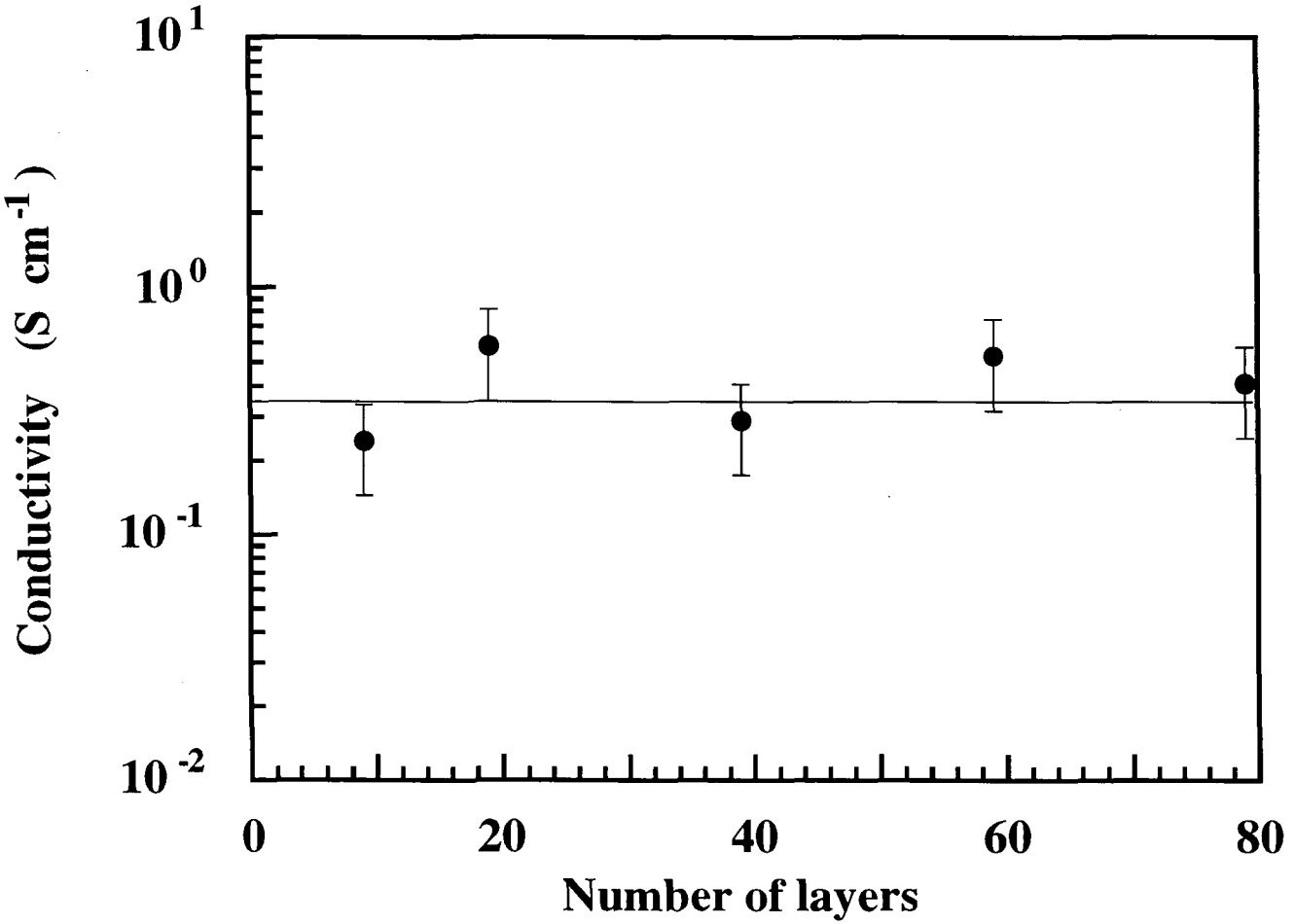

Fig. 8.18 Conductivity, measured using a bias of 1 V appied to carbon cement contacts 5 mm long and 5 mm apart, versus number of iodine doped layers of C_{18}Py-Ni(dmit)$_2$. The films were deposited from a floating layer formed from 4.5 ml of solution that had been aged on the surface of the subphase for 10 minutes before compression.

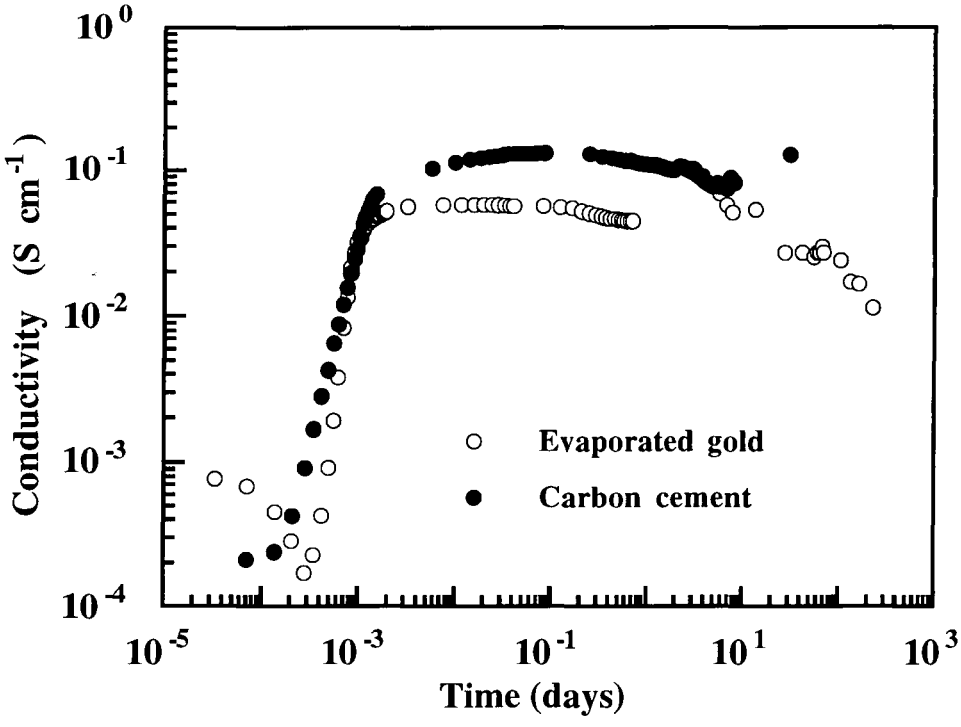

(a)

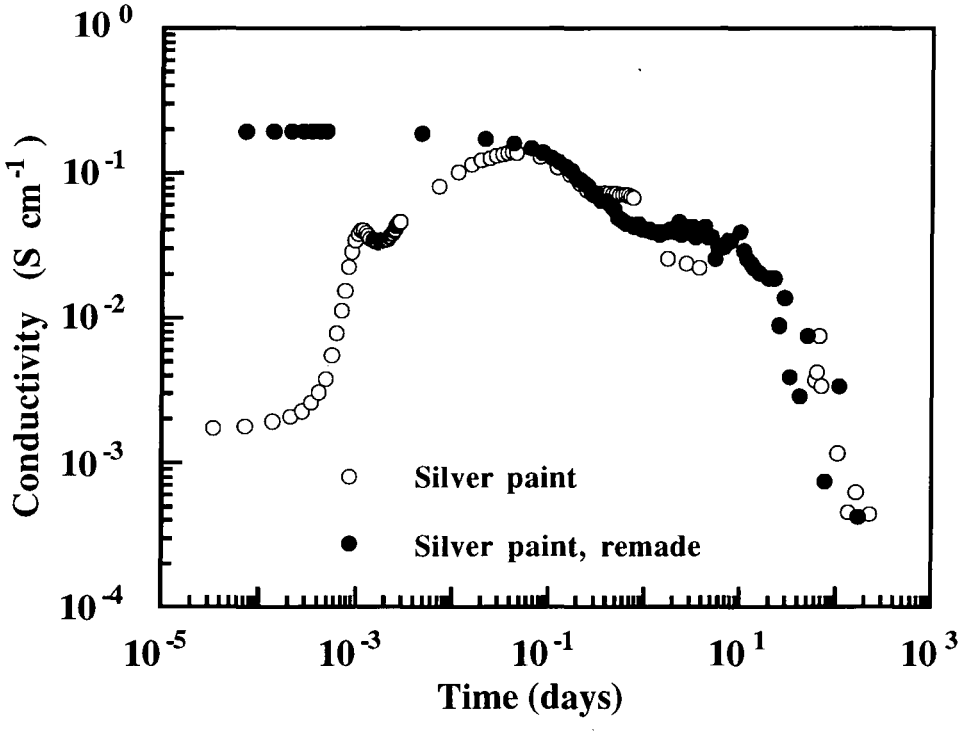

(b)

Fig. 8.19 **Conductivity versus time after doping, illustrating the stability of different electroding materials.**

(a) **Evaporated gold and carbon cement.**
(b) **Silver paint.**

The 19-layer samples used here were deposited from a floating layer formed from 5 ml of solution that was compressed after 10 minutes on the subphase. Measurements were made with a bias voltage of 10V.

For the initial measurements, up to 10 days after doping, the samples were stored and measurements made (using a bias voltage of 10 V) under vacuum. Subsequently, the films were stored and measurements performed in air. Immediately after doping, the in-plane conductivity measured for samples with carbon and gold contacts was seen to increase to 10^{-3} - 10^{-4} S cm^{-1} (Fig 8.19(a)). The conductivity then continued to increase over a time period of a few minutes to maxima of the order of 10^{-1} S cm^{-1}. This behaviour is thought to be caused by the removal of excess dopant from the film with the subsequent formation of a mixed-valence complex. The final conductivity was quite stable for several months for films stored in air at room temperature. It can be sen that similar conductivity values were measured whether the electrodes were formed from evaporated gold or carbon cement. This result contrasts with the observations made for films of C_{18}Py-Pd(dmit)$_2$, where the conductivity measured using thermally evaporated gold was significantly lower than that recorded when carbon cement was used (Chapter 7, section 7.5.3). In that case, the films had a layer thickness of 11.4±0.2 nm and were transferred from a floating layer with an area per complex at the deposition pressure of 0.15 nm^2. It was thought that the layers were partially isolated from each other by the insulating alkyl chains so that the evaporated gold would only make contact to the organic layers at the surface of the film leaving much of the sample isolated. The C_{18}Py-Ni(dmit)$_2$ films investigated here were deposited from a floating layer having an area per complex of *ca.* 0.05 nm^2, and had a layer thickness of 31±4 nm. These values suggested that the films were more disordered, allowing the evaporated gold to make contact to all of the sample.

The conductivity of films with silver paint contacts exhibited similar behaviour soon after iodine doping, as seen in Fig. 8.19(b). A few hours after the maximum conductivity was reached, however, a drop in conductivity was observed, and after three months, the value had fallen to 10^{-3} - 10^{-4} S cm^{-1}. If fresh silver contacts were now made to the same film, the current was restored to its original maximum value for a few hours before beginning

to fall again. These results suggest that the reduced current value was due to the formation of a barrier at the contact rather than deterioration in the conductivity of the film.

8.5.3 The effect of spreading time on conductivity

The in-plane dc conductivity as a function of time that the floating film was left on the subphase before compression has been studied, and the results are shown in Fig. 8.20. The area per complex information from Fig. 8.4 is also reproduced here for comparison. All of the films used in these measurements had been built up over five deposition cycles. In each case, the exact thickness was obtained from surface profiling studies. Electrical measurements were made in vacuum, and current values recorded when the conductivity was seen to be stable with time. High conductivity values were recorded for iodine doped samples deposited from floating films that were compressed after a short time on the subphase. A rapid decrease in conductivity was seen when films were left on the subphase for times greater than about 30 minutes, however. Optical and electron microscopy and EDS studies have revealed that fresh floating films contained $Ni(dmit)_2$ aggregates in a polycrystalline background matrix. These clusters were well distributed through the film, and did not form a continuous path for carrier transport. Hence, current flow must be possible through the background matrix. After doping, this background is likely to consist of a mixed-valence charge transfer salt. Films transferred from floating layers that were allowed to age for many hours before compression exhibited very low conductivity. A similar effect was observed in films of $C_{18}Py\text{-}Pd(dmit)_2$ prepared in the same way, and this behaviour was attributed to a film structure in which the $(dmit)_2$ molecules were unable to pack closely together, precluding high in-plane conductivity (chapter 7, section 7.5.2).

8.6 Low temperature conductivity

The temperature dependence of the electrical conductivity of a 19-layer as-deposited film of $C_{18}Py\text{-}Ni(dmit)_2$ transferred from a floating layer formed from 4.5 ml of solution that

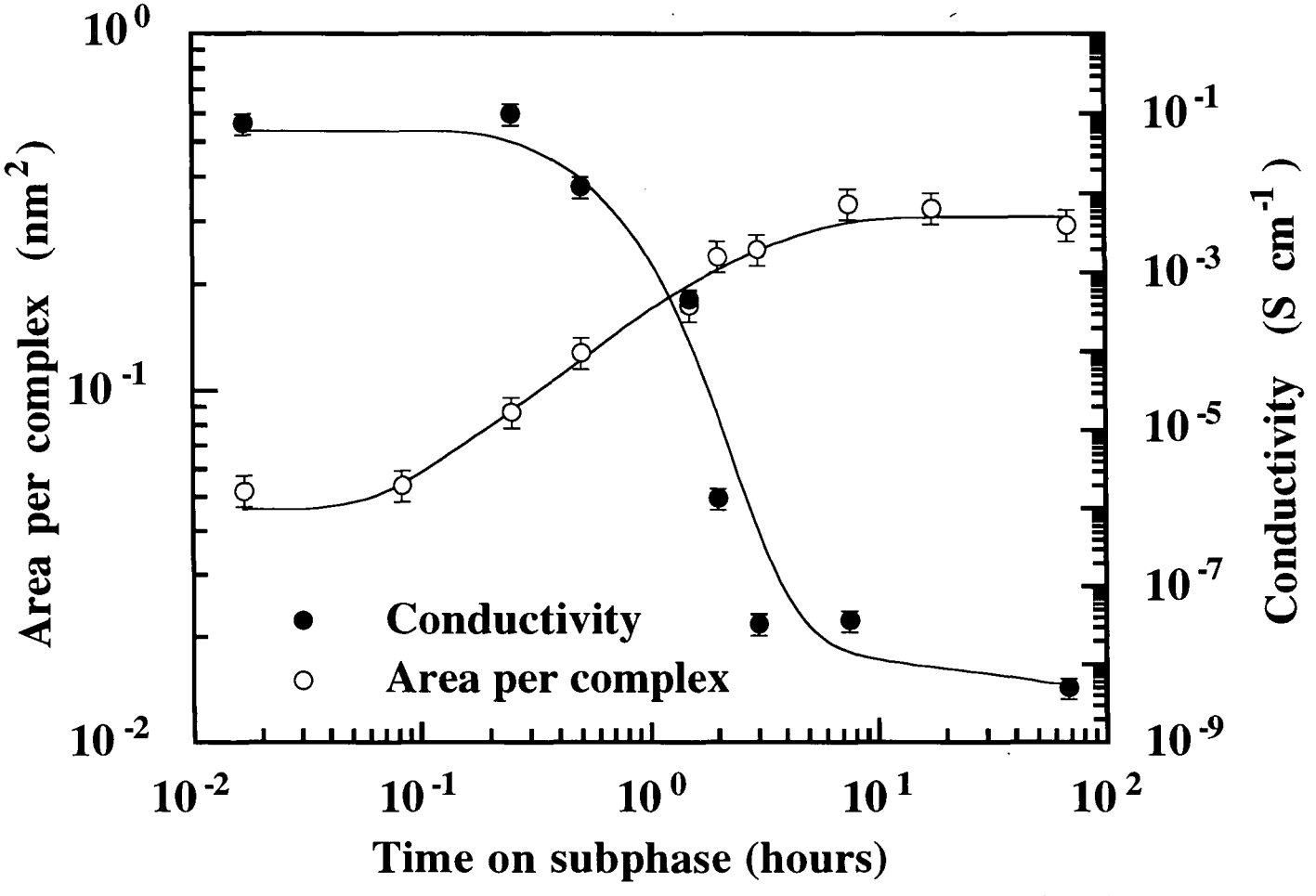

Fig. 8.20 In-plane dc conductivity versus the time that floating layers, formed from 1 ml of C_{18}Py-Ni(dmit)$_2$ solution, was allowed to age on the surface of the subphase before compression. LB films were transferred onto glass substrates, and doped with iodine for 2000 seconds before silver paint electrodes were applied. Conductivity was measured using a bias voltage of 100 V. The area per complex at 30 mN m^{-1} (data from Fig. 8.4) is also shown here.

had been aged on the surface of the subphase for 10 minutes before compression is shown in Fig. 8.21. The contacts here were silver paint 5.0±0.5 mm apart and 5.0±0.5 mm long. The current versus voltage characteristics at the extremes of the temperature range studied are shown inset to the figure. The electrical conductivity followed an exponential dependence on temperature, indicating semiconducting behaviour, with an activation energy of 0.6±0.1 eV. After doping with iodine, the activation energy for silver contacted devices was dependent on bias voltage and time. This behaviour is illustrated in Fig. 8.22. Soon after exposure to iodine, the same activation energies were recorded, within the limits of the experimental error, i.e 0.08±0.01 and 0.09±0.01 eV at bias voltages of 20 V and 1 V, respectively. After 24 hours, however, although the activation energy at a bias voltage of 20 V remained unchanged, that at 1 V increased to 0.12±0.05 eV. This change reflects the formation of barriers at the contacts, and is accompanied by an increase in the slope of the current versus voltage characteristics, shown inset to Fig. 8.21. In agreement with conductivity versus time experiments, samples with carbon cement contacts were more stable. The low temperature behaviour of a 19-layer film with carbon cement contacts, 5.0±0.5 mm apart and 5.0±0.5 mm long, after iodine doping is illustrated in Fig. 8.23, with the current versus voltage characteristics at the extremes of the temperature range studied shown inset. The data fit well to straight lines, in contrast to the behaviour observed in conductive multilayers of C_{18}Py-Pd(dmit)$_2$, where deviations from linearity due to a power law dependence of conductivity on temperature was observed (chapter 7, section 7.6). Activation energies of 0.05±0.01 eV were recorded in all cases, for fresh and aged films, with bias voltages of 1 V and 20 V applied. It is likely that the 0.09±0.05 eV and 0.12±0.05 eV activation energies measured for silver contacted devices are dominated by the contact barrier regions, and that the value of 0.05±0.01 eV obtained with carbon cement contacts represents the activation energy for electrical conductivity in the LB film of C_{18}Py-Ni(dmit)$_2$. This value is smaller than that of the 2:1 stoichiometry complex (*N*-octadecylpyridinium)$_2$-Ni(dmit)$_2$,[5] but similar to the figure of 0.056 eV reported by Miura *et al* [6] for films of didecyldimethylammonium-Pd(dmit)$_2$,

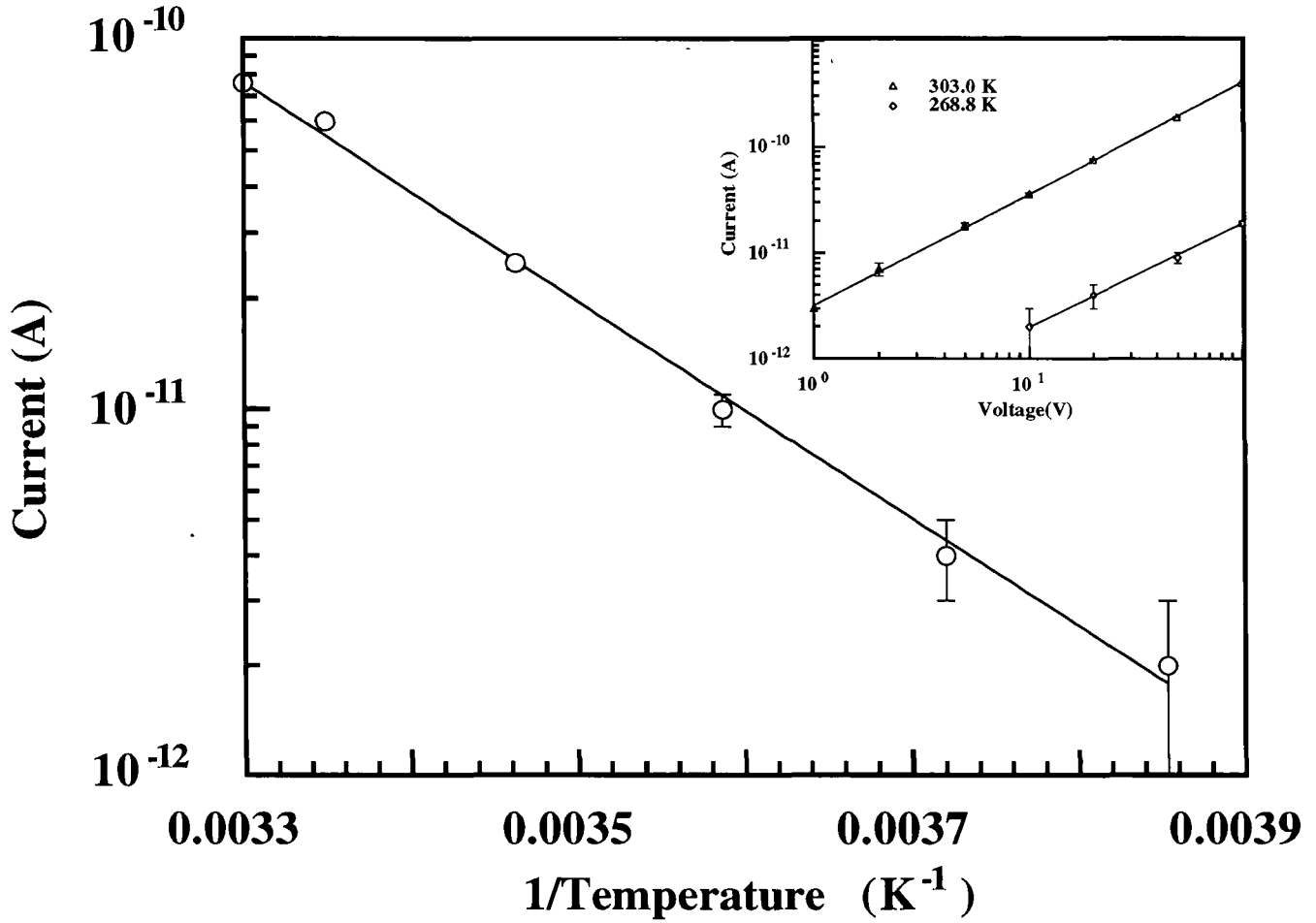

Fig. 8.21 Semi logarithmic plot of current (with a voltage of 20 V applied) versus reciprocal temperature for a 19-layer as-deposited LB sample of C_{18}Py-Ni(dmit)$_2$ with silver paint contacts 5 mm long and 5 mm apart. The film was deposited from a floating layer formed from 4.5 ml of solution that was aged on the subphase for 10 minutes before compression. The current versus voltage characteristics at the extremes of the temperature range studied are shown inset.

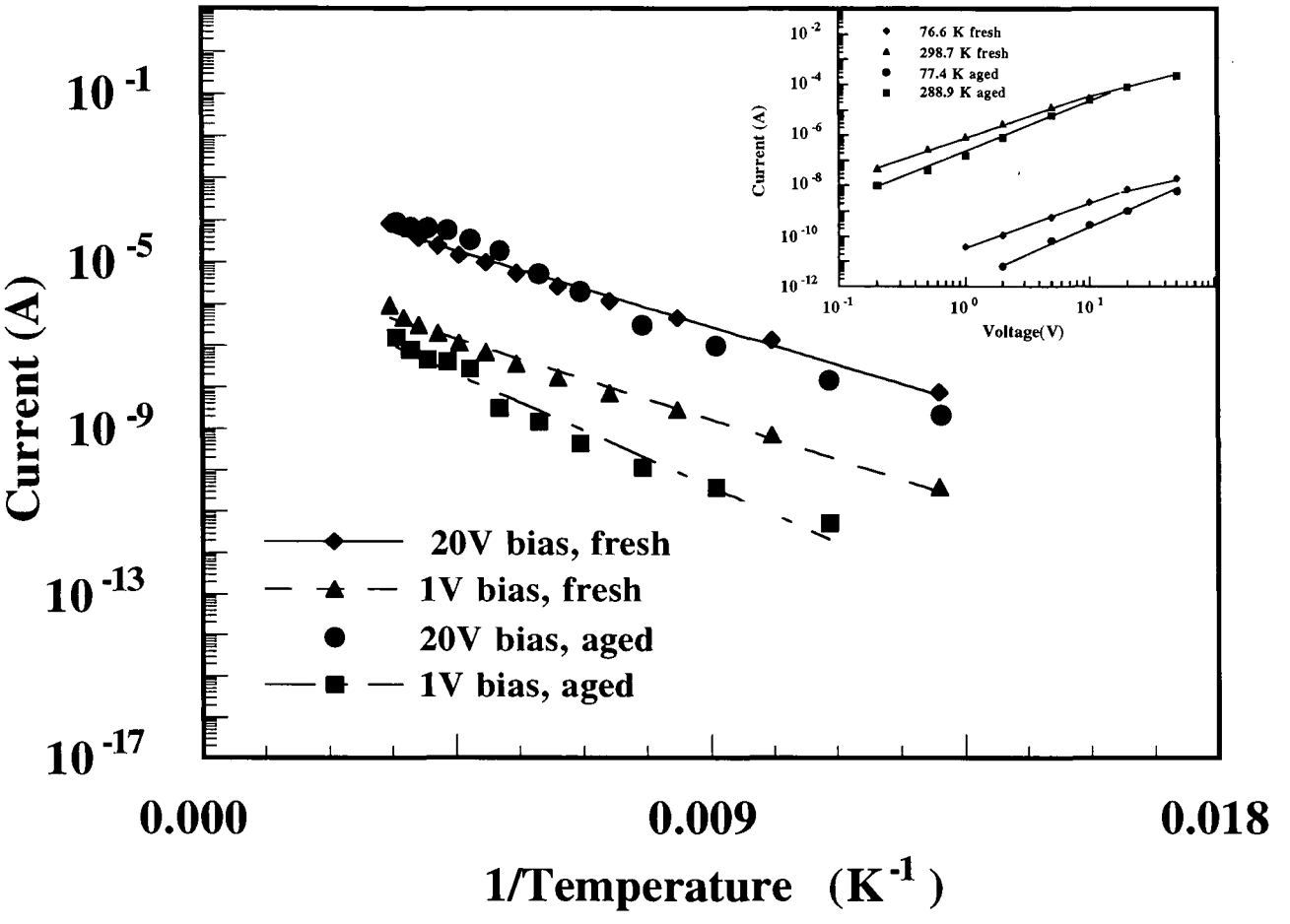

Fig. 8.22 Semi logarithmic plots of current (with bias voltages of 1 V and 20 V applied) versus reciprocal temperature for a 19-layer iodine doped LB sample of C_{18}Py-Ni(dmit)$_2$ with silver paint contacts 5 mm long and 5 mm apart. The film was deposited from a floating layer formed from 4.5 ml of solution that was aged on the subphase for 10 minutes before compression. Measurement were made when the contacts were fresh and then again 24 hours later The current versus voltage characteristics at the extremes of the temperature range studied are shown inset.

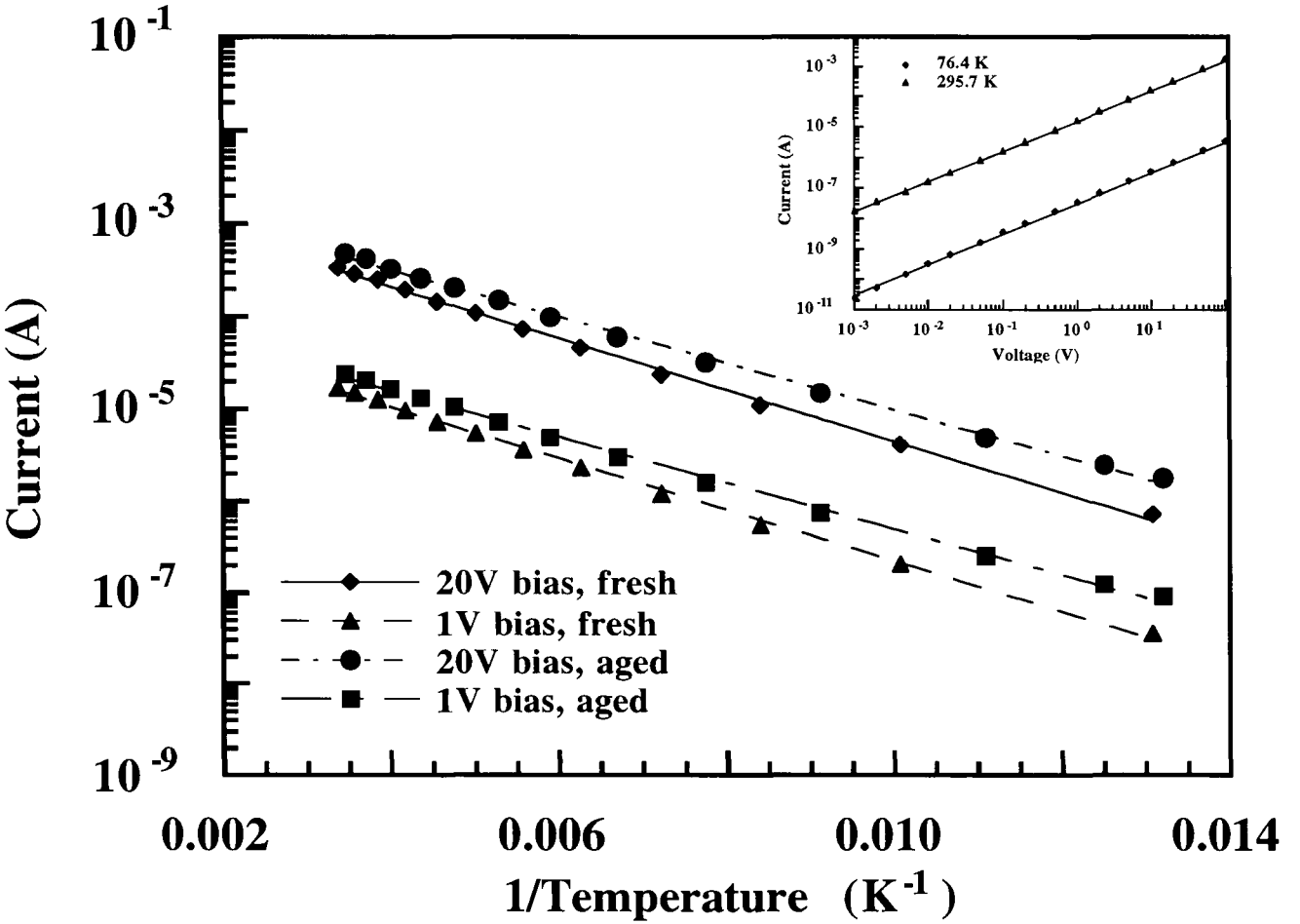

Fig. 8.23 Semi logarithmic plots of current (with bias voltages of 1 V and 20 V applied) versus reciprocal temperature for a 19-layer iodine doped LB sample of C_{18}Py-Ni(dmit)$_2$ with carbon cement contacts 5 mm long and 5 mm apart. The film was deposited from a floating layer formed from 4.5 ml of solution that was aged on the subphase for 10 minutes before compression. Measurement were made when the contacts were fresh and then again 24 hours later. The current versus voltage characteristics at the extremes of the temperature range studied are shown inset.

and similar to those measured for multilayers of C_{18}Py-Pd(dmit)$_2$ (chapter 7, section 7.6).

8.7 Capacitance

To measure the capacitance of LB multilayers of C_{18}Py-Ni(dmit)$_2$, substrates consisting of glass slides covered with gold undercoated with chromium (to improve the adhesion of the gold to the glass) were used. These were initially covered with a base layer consisting of 40 LB layers of 22-tricosenoic acid (22-TA). Stepped thickness structures of C_{18}Py-Ni(dmit)$_2$ were then deposited from a floating layer formed from 1 ml of solution that had been aged on the subphase surface for 30 minutes before compression. Top electrodes were provided by silver dots, carefully evaporated onto the organic film to give the parallel plate capacitor geometry shown in Fig. 8.24(a). This structure can be modelled by a series combination of two separate capacitors, as shown in Fig. 8.24(b). The capacitance of the 22-tricosanoic acid layer was measured at a frequency of 1 MHz, and the value obtained ($C_{22\text{-}TA}$ = 240 pF) was used in the equation

$$\frac{1}{C_{dmit}} = \frac{1}{C_{measured}} - \frac{1}{C_{22\text{-}TA}} \qquad 8.1$$

to extract the capacitance of the C_{18}Py-Ni(dmit)$_2$ layers from the experimental values of $C_{measured}$ i.e. the value of the series combination of $C_{22\text{-}TA}$ and C_{dmit}. The capacitance of a parallel plate capacitor is given by

$$C = \frac{\varepsilon_0 \varepsilon_r A}{d} \qquad 8.2$$

where ε_0 is the permittivity of free space, ε_r the relative permittivity of the dielectric, A the area of the plates and d the distance between them. A plot of 1/C versus d is a straight line with slope $1/\varepsilon_0\varepsilon_r A$. Fig. 8.25 is a plot of reciprocal capacitance versus number of layers for the C_{18}Py-Ni(dmit)$_2$ films, as-deposited and after iodine doping. Both sets of

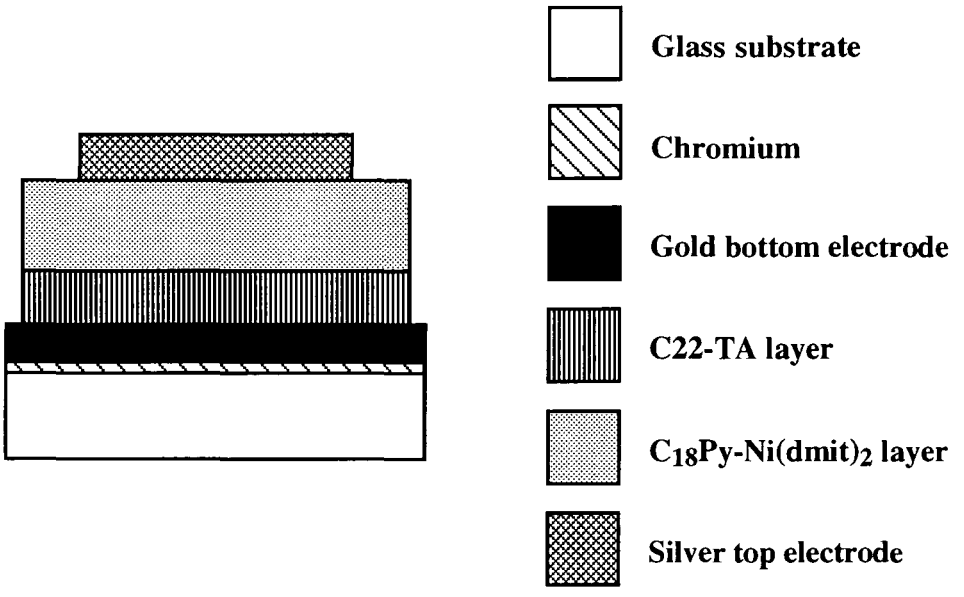

(a)

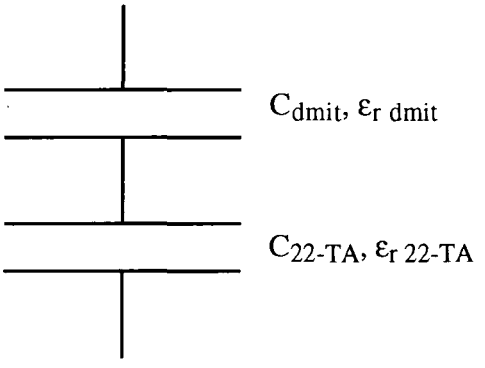

(b)

Fig. 8.24 (a) **The parallel plate geometry used to measure the dielectric properties of LB films, showing the separate layers of C22-TA and C_{18}Py-Ni(dmit)$_2$.**

(b) **The structure can be modelled by two separate capacitors in series.**

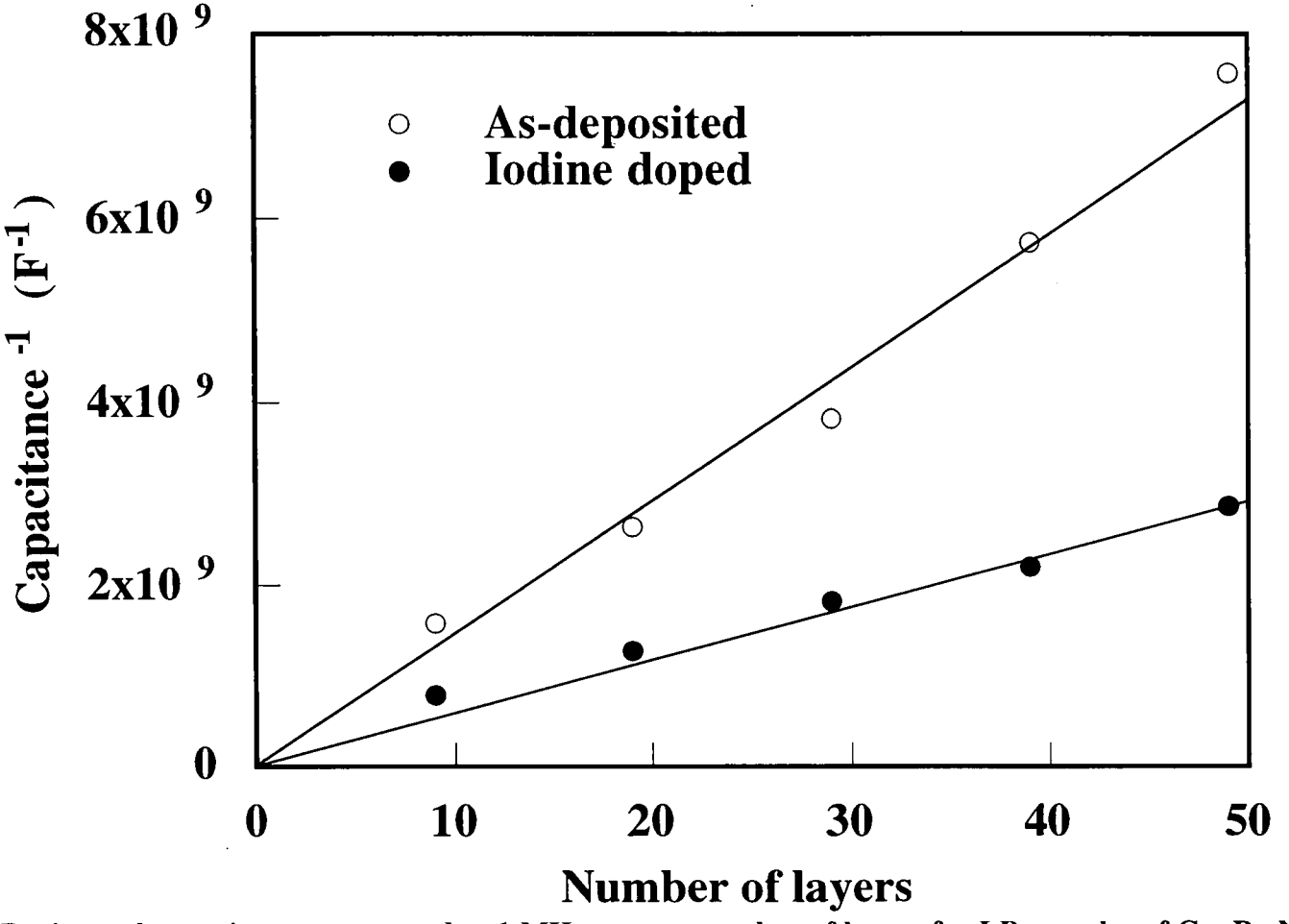

Fig. 8.25 Reciprocal capacitance, measured at 1 MHz, versus number of layers for LB samples of C_{18}Py-Ni(dmit)$_2$. The films were deposited onto a glass slide coated with a chromium/gold electrode and 40 LB layers of C_{22}-TA. The floating layer of C_{18}Py-Ni(dmit)$_2$ was formed from 1 ml of solution that had been aged for 30 minutes on the subphase surface before compression.

data lie on straight lines, confirming the reliability of film transfer. The thickness of the 49-layer C_{18}Py-Ni(dmit)$_2$ film, obtained from Alpha-step measurements, was 170±20 nm and, using this value to calculate the slopes of the straight lines in Fig. 8.25, the relative permittivity of the C_{18}Py-Ni(dmit)$_2$ layers was calculated to be 3.4±0.6 in the as-deposited state and 6.7 ±1.3 after doping with iodine.

8.8 Summary

The preparation and characterisation of LB multilayer films of N-octadecylpyridinium-Ni(dmit)2 have been described. Like the related compound, C_{18}Py-Pd(dmit)$_2$ (chapter 7), spreading of the material on the surface of the subphase was poor, and the properties of the floating layer and transferred films on solid substrates was dependent on the time between spreading and compression of the layer. The area per complex value obtained from isotherm measurements was seen to increase with spreading time, with true monolayer films only obtained after several hours. LB films built up from aged floating layers were electrically insulating, in the as-deposited state and after iodine doping. It is thought that the structural arrangement of the molecules in these films did not favour carrier transport. Films deposited from floating layers that were compressed soon after spreading were also insulating in the as-deposited state, unlike those of C_{18}Py-Pd(dmit)$_2$ that were prepared under similar conditions, which were conductive without post deposition doping. After exposure to iodine vapour, however, a significant increase in conductivity to a maximum value of 0.13±0.08 S cm^{-1} was observed. Optical and scanning electron microscope studies with EDS revealed that these films were two-phase structures, with μm sized particles of Ni(dmit)$_2$ in a polycrystalline background matrix. The stability of different electroding materials has been investigated. Evaporated gold and carbon cement contacts were stable for at least several months, but when silver paint was used, the sample resistance was seen to increase with time. This has been attributed to the formation of resistive barriers at the contacts. Observation of the variation of conductivity with temperature revealed semiconducting behaviour with a thermal activation energy for

conductivity in the organic layers of 0.05±0.01 eV. By incorporating C_{18}Py-Ni(dmit)$_2$ layers in a parallel plate capacitor structure and measuring the capacitance at a frequency of 1 MHz, it was possible to calculate the relative permittivity of the organic material at this frequency. Values of 3.4±0.6 and 6.7±1.3 were obtained, for films as-deposited and after iodine doping, respectively.

References

1. A.S. Dhindsa, J.P. Badyal, C. Pearson, M.R. Bryce and M.C. Petty, J. Chem. Soc., Chem. Commun., (1991) 322-323.
2. S.K. Gupta, D.M. Taylor, P. Dynarowicz, E. Barlow, C.E.A. Wainwright and C.E.A. Underhill, Langmuir, 8 (1992) 3057-3062.
3. A.E. Underhill, R.A. Clark, I. Marsden, M. Allan, R.H. Friend, H. Tajima, T. Naito, M. Tamura, H. Kuroda, A. Kobayashi, H. Kobayashi, E. Canadell. S. Ravy and J. P. Pouget, J. Phys.: Condens. Matter, 3 (1991) 933-954.
4. Y.F. Miura, M. Takenaga, A. Kasai, T. Nakamura, M. Matsumoto and Y. Kawabata, Jpn. J. Appl. Phys., 30 (1991) 3503-3509.
5. C. Pearson, A.S. Dhindsa, M.C. Petty and M.R. Bryce, Thin Solid Films, 210/211 (1992) 257-260.
6. Y.F. Miura, M. Takenaga, A. Kasai, T. Nakamura, Y. Nishio, M. Matsumoto and Y. Kawabata, Thin Solid Films, 210/211 (1992) 306-308.

Chapter 9

The *N*-octadecylpyridinium-Ni(dmit)$_2$ Field Effect Transistor

9.1 Introduction

In this chapter, the electrical characterisation of an organic thin film transistor incorporating an LB film of *N*-octadecylpyridinium-Ni(dmit)$_2$ as the active layer is described. The procedure used to produce gate contacts and the measurement of the capacitance of the insulating gate oxide layer are both explained. The drain characteristics of a device, measured before and after chemical doping with iodine, are presented and the data are used to calculate the mobility of the charge carriers in the channel.

9.2 Gate contacts

Four different methods were investigated to establish the best evaporated metal/substrate treatment combination for the production of gate contacts on silicon substrates. These were: (a) aluminium with no substrate treatment; (b) gold undercoated with chromium with no substrate treatment; (c) plain gold with no substrate treatment; and (d) plain gold deposited after etching of the substrate with HF. An array of contacts were evaporated in each case so that the contact resistance, R_C, could be measured from the intercept on the vertical axis of a plot of sample resistance versus contact spacing. The results of these experiments are shown in Fig. 9.1. When aluminium was used, the overall resistance was very high (*ca* 40 kΩ), and independent of the distance between contacts, indicating that R_C dominated. This is because aluminium evaporated onto silicon without any subsequent annealing (to alloy the metal with the surface of the semiconductor and produce a heavily doped p-type layer) will form a rectifying contact. When chromium was evaporated before a gold overlayer, the overall resistance was reduced, and R_C was found to be *ca.* 300 Ω. Using plain gold reduced R_C to 45 Ω, and etching the silicon with HF before evaporation of plain gold contacts provided the lowest contact resistance of

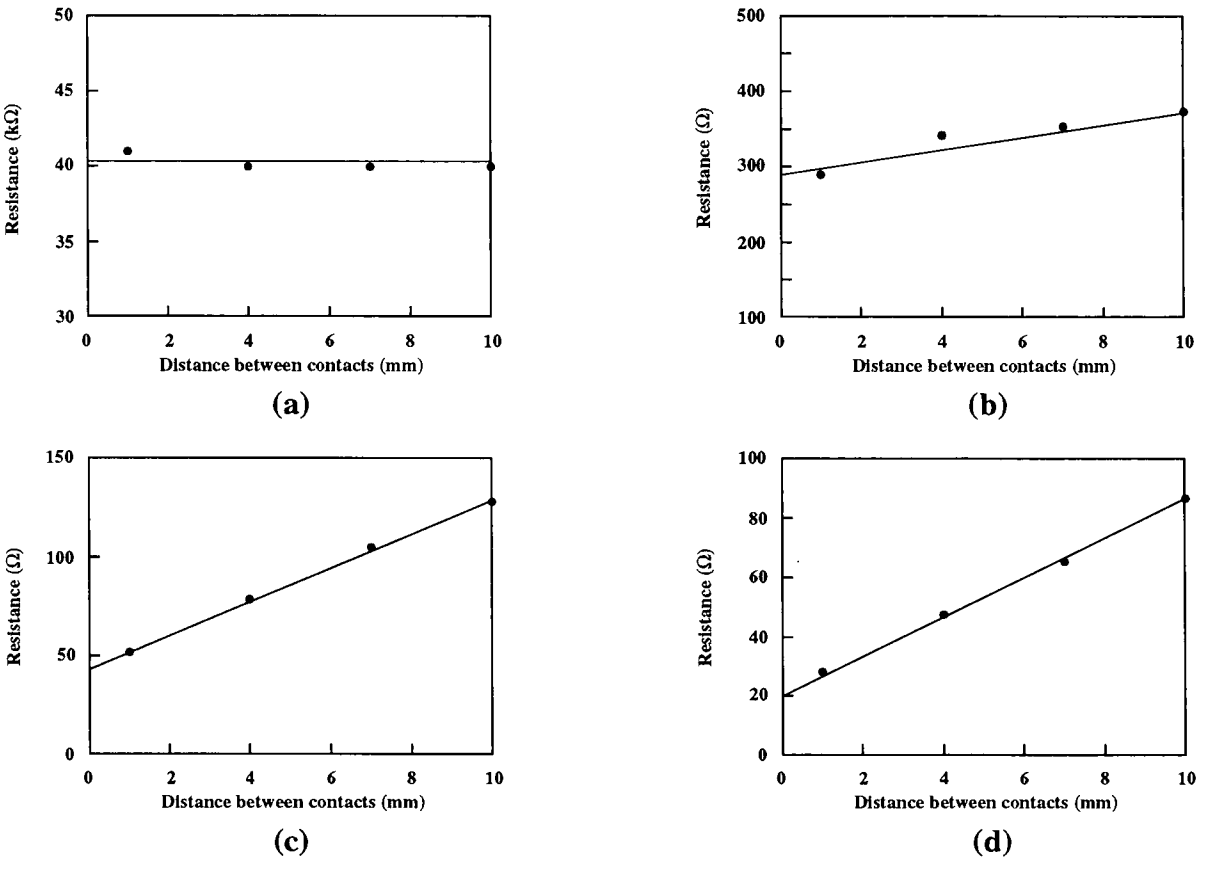

Fig. 9.1 **Plots of sample resistance versus distance between contacts for four different gate electroding techniques.**

(a) **Aluminium with no substrate treatment.**
(b) **Gold undercoated with chromium with no substrate treatment.**
(c) **Gold with no substrate treatment.**
(d) **Gold deposited after the substrate was etched with 10 % HF solution.**

all, i.e. 20 Ω. The etching would remove any insulating oxide layer from the surface of the substrate. In practice, to ensure that the resistance of the gate contact was as low as possible, a portion of the thermally grown gate oxide was removed using a 10 % HF solution, and the substrates were immediately placed under vacuum for metallisation. In Fig. 9.2, the current versus voltage plot for a pair of gold contacts 1 mm apart is shown. The characteristic was linear, indicating Ohmic behaviour.

9.3 Oxide capacitance

The growth of an oxide layer on a silicon substrate to act as the gate insulator in a TFT structure has been described in chapter 5, section 5.7.2, and the measurement of the capacitance versus voltage characteristics of a MIS capacitor incorporating this oxide as the dielectric was discussed in chapter 5, section 5.8.1. The capacitance versus voltage plot for a 280 ± 10 nm thick (measured using ellipsometry) thermally-grown oxide layer on a p-type silicon substrate is shown in Fig. 9.3. Contact to the silicon was achieved using gold that was evaporated after the substrate had been etched with a 10 % HF solution, and the top electrodes were thermally evaporated gold dots, 1 mm in diameter. Stepped dc bias voltages were applied and the capacitance, measured at a frequency of 1 MHz, allowed to stabilise before the data were recorded. The capacitance of the structure in accumulation, due to the device geometry as defined by the top electrode area and the oxide thickness, was 80 ± 1 pF. From this value, an oxide capacitance per unit area, C_i = $1.0 \pm 0.1 \times 10^{-8}$ F cm^{-2} was calculated. The curve is not monotonic as expected for a high frequency CV plot, and an increase in the measured capacitance can be seen in the inversion region. In a p-type MIS structure, positive charge in the insulator can induce an inversion layer in all areas under the oxide, including those away from the gate metallisation. This effectively increases the area of the lower plate of the capacitor, leading to an elevated capacitance value in the inversion region.[1] However, the presence of charge in the oxide should also causes a shift of the CV plot to the left. No significant shift was observed here and it seems likely that the increased capacitance observed in the inversion

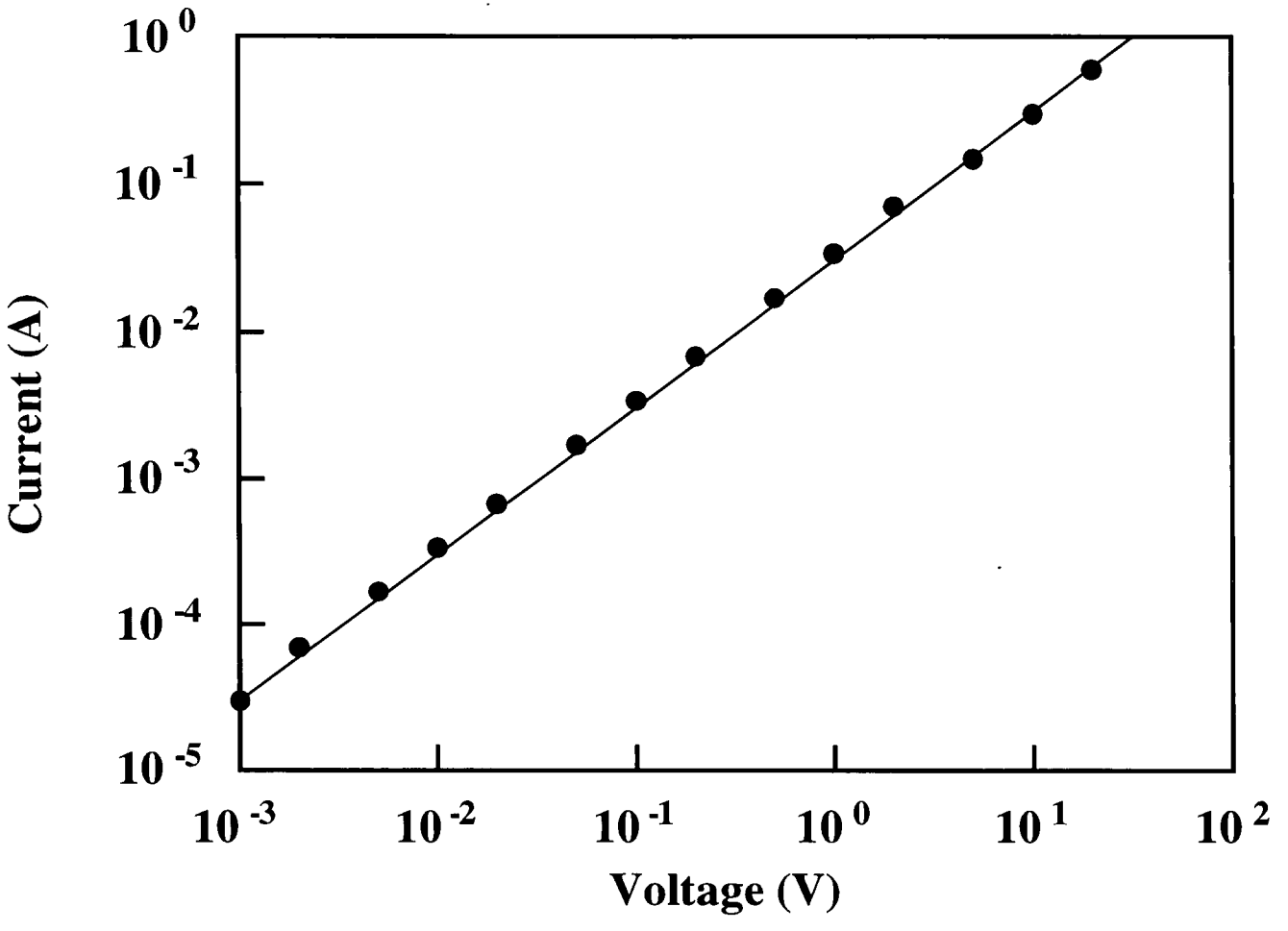

Fig. 9.2 Current versus voltage plot for evaporated gold contacts, 1 mm apart, on a p-type silicon substrate. The substrate was etched with a 10 % HF solution to remove any oxide layer before metallisation. The plot is linear, indicating Ohmic behaviour.

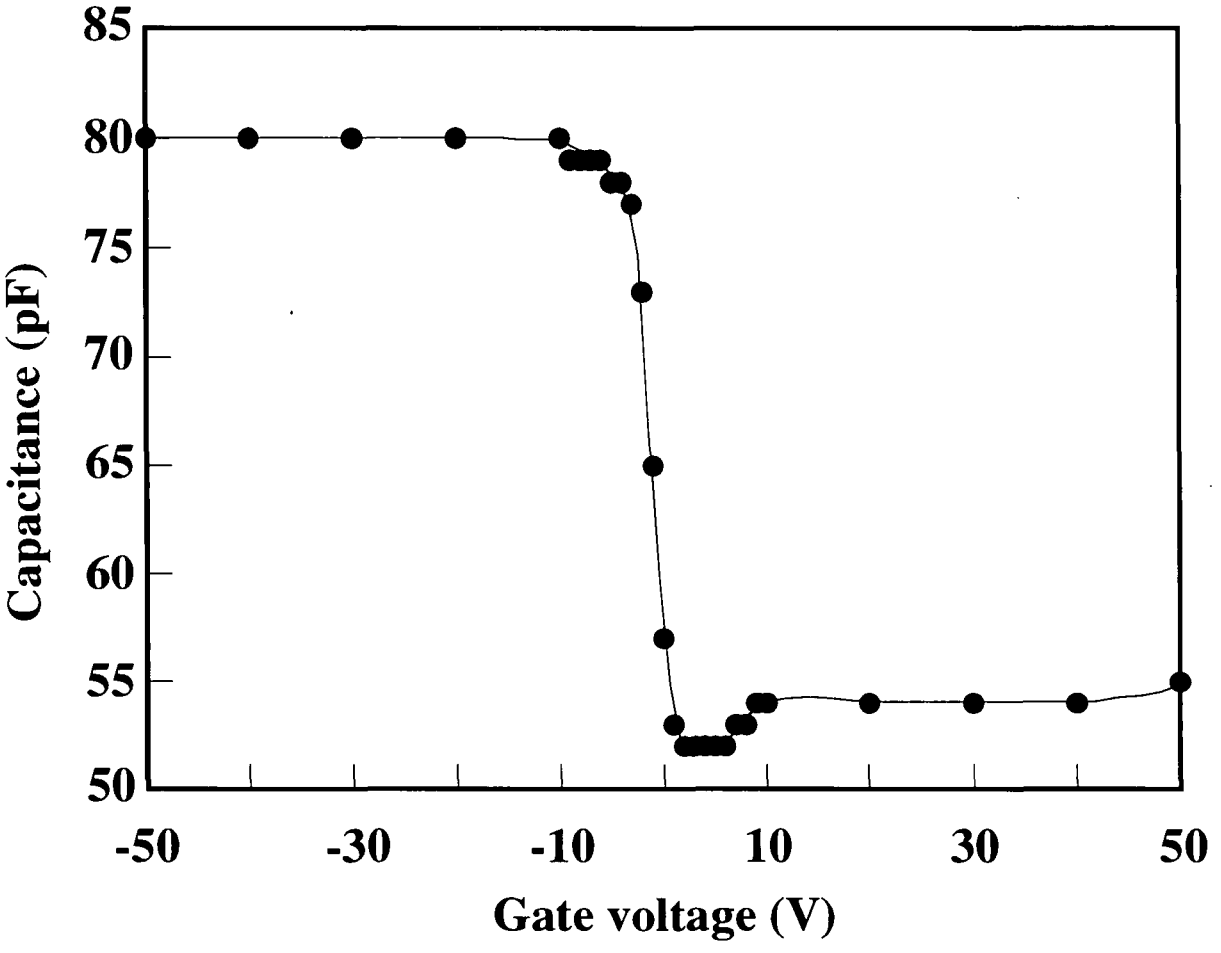

Fig. 9.3 **The capacitance at 1 MHz versus voltage behaviour of a MIS capacitor consisting of a 280 ± 10 nm thick thermally grown oxide layer on a p-type silicon substrate. Contacts to the substrate and top electrodes, 1 mm in diameter, were formed from thermally evaporated gold. Dc bias voltages were applied and the capacitance reading allowed to stabilise before data were recorded.**

region was due to the presence of fast states in the semiconductor that were able to respond to the field at the measurement frequency of 1 MHz.

9.4 Source and drain contacts

The fabrication of interdigitated source and drain contacts is described in chapter 5, sections 5.7.3 - 5.7.5. An optical micrograph illustrating the structure of one pair of electrodes, before the deposition of LB layers, is shown in Fig. 9.4.

9.5 LB film deposition

The LB film forming properties of *N*-octadecylpyridinium-Ni(dmit)$_2$ (C_{18}Py-Ni(dmit)$_2$) have been described in chapter 8, section 8.2. For incorporation in TFT devices, multilayer stepped structures were transferred from floating layers formed from 1 ml of solution that had been aged on the surface of the subphase for 30 minutes before compression.

9.6 Electrical characteristics

Before deposition of LB layers, the drain current (I_D) due to the conductivity of the gate oxide (with a drain bias voltage (V_{DS}) of 100 V applied) was very small, with typical values of the order of 2±1 pA. The yield of operational devices was low, and only a few working structures were produced. In some cases, there were short circuits between the source and drain electrodes, probably caused by the presence of particulate contamination during the photolithographic processing. Sometimes, although the electrodes were not defective, no drain current modulation was observed. The operation of an organic thin film transistor depends strongly on the nature of the interface between the gate insulator and the organic layer. It is possible that the presence of contamination on the surface of the gate oxide prevented the operation of some devices.

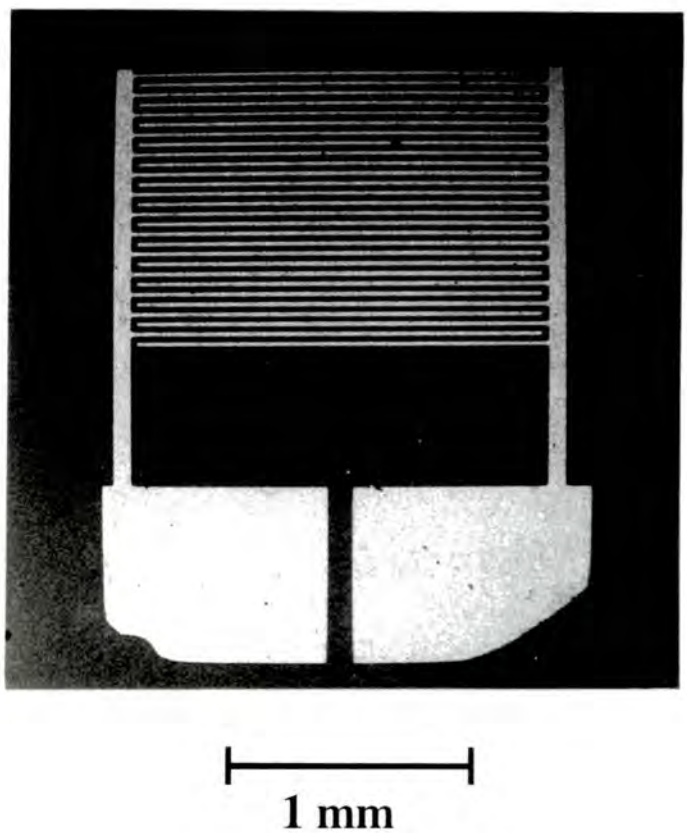

Fig. 9.4 **Optical micrograph of the interdigitated source and drain electrodes used in the fabrication of organic thin film transistors.**

9.6.1 As-deposited

The I_D vs V_{DS} characteristics, at various gate voltages, for a working TFT having an organic film consisting of 59 as-deposited layers of C_{18}Py-Ni(dmit)$_2$ on top of the interdigitated source and drain electrodes are shown in Fig 9.5. The drain current flowing with gate bias voltages below threshold was a result of Ohmic conduction between the drain and source contacts through the bulk of the organic layer. From this characteristic, the Ohmic conductivity of the C_{18}Py-Ni(dmit)$_2$ layer was calculated to be $1.3 \pm 0.2 \times 10^{-7}$ S cm^{-1}, using a thickness per layer of 3.5 ± 0.4 nm obtained from surface profiling measurements. This value is significantly higher than that measured using gold, silver paint and carbon cement contacts in previous experiments (chapter 8 section 8.5.1). It is possible that the 20 μm gap between the interdigitated electrodes could be bridged by the crystallites that were present in the organic layers (observed using optical microscopy, chapter 8, section 8.4.3), and that the measured value here reflected the conductivity of these aggregates. Drain current modulation was achieved by the application of a positive voltage to the gate, indicating that the carriers involved in conduction were electrons. To date, all of the organic materials used in TFTs have been p-type semiconductors. This is the first time that n-type conduction has been observed in an organic charge transfer complex.

From the standard treatment of TFTs (chapter 4, section 4.2) the saturation drain current $I_{D,sat}$ is given by equation 4.15. and a plot of $(I_{Dsat})^{1/2}$ versus V_G has a slope of

$$S = \frac{(I_{D,sat})^{1/2}}{V_G} = \left(\frac{WC_i\mu}{2L}\right)^{1/2} \qquad 9.1$$

the carrier mobility, μ, is given by

$$\mu = \frac{2LS^2}{WC_i} \qquad 9.2$$

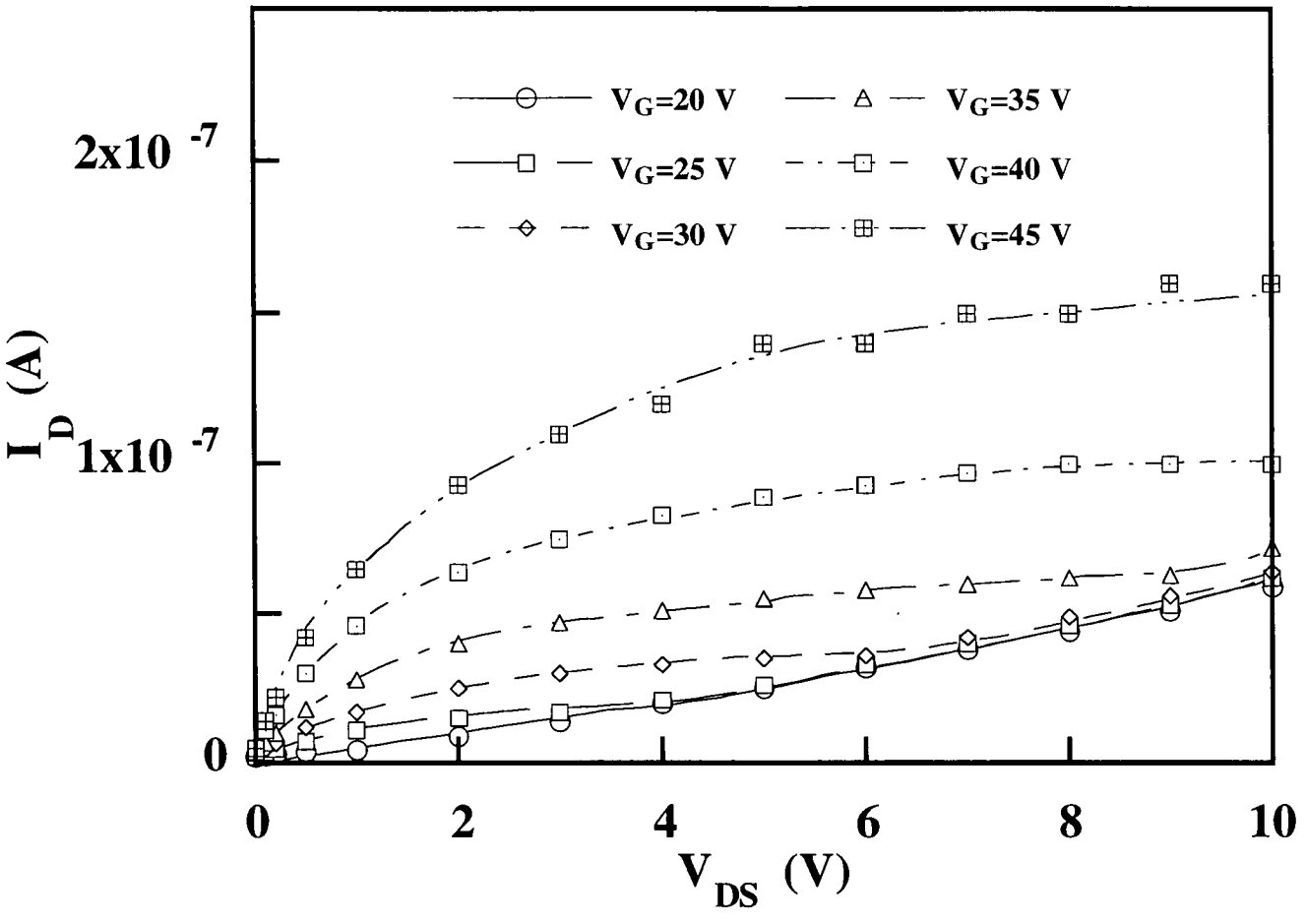

Fig. 9.5 The drain current versus drain voltage characteristics, at various values of gate bias, for a TFT having an organic film consisting of 59 as-deposited layers of C_{18}Py-Ni(dmit)$_2$ on top of the interdigitated source and drain electrodes.

and the threshold voltage, V_t, by the intercept on the V_G axis. Fig. 9.6 is a plot of $(I_{D,sat})^{1/2}$ versus V_G for the same as-deposited 59-layer device. $I_{D,sat}$ readings were corrected by subtracting the bulk Ohmic current from the measured value so that only the channel current was included. A straight line fit to the points with $V_G \geq 25$ V gave a threshold voltage of 22 ± 1 V. High threshold voltages are often observed in organic TFTs, and can be attributed to traps in the organic layer.[2] V_t correspond to the gate voltage at which the free carrier density equals the trap density. From the slope of the linear fit, a carrier mobility of $1.9 \pm 0.5 \times 10^{-5}$ cm^2 V^{-1} s^{-1} was calculated. This is a similar value to that reported by Paloheimo *et al* for the mobility of carriers in a TFT using an LB film of quinquethiophene mixed with arachidic acid as the active layer.[3]

The transfer characteristic for the same as-deposited C_{18}Py-Ni(dmit)$_2$ device, I_D (with V_{DS} fixed at 5V) versus V_G, is plotted in Fig. 9.7. The bulk Ohmic current at low gate bias voltages is apparent on this graph.

9.6.2 Iodine doped

After doping, I_D was seen to increase by 5 orders of magnitude, reflecting the large increase in the conductivity of the organic film. The I_D vs V_{DS} characteristics, at various gate voltages, for a TFT having an active region consisting of 59 iodine doped layers of C_{18}Py-Ni(dmit)$_2$, are shown in Fig 9.8. From the Ohmic characteristic with $V_G \leq V_t$, a conductivity value of $3.7 \pm 0.4 \times 10^{-3}$ S cm^{-1} was calculated. This figure is comparable to that measured for iodine doped films of C_{18}Py-Ni(dmit)$_2$ that were prepared under similar conditions in previous experiments (chapter 8, Fig. 8.19). Again, modulation of the drain current was observed with positive bias voltages applied to the gate, indicating that the charge carriers were electrons. Values of $(I_{D,sat})^{1/2}$ versus V_G (as before, $I_{D,sat}$ readings were corrected by subtracting the bulk Ohmic current from the measured value) for the same device are plotted in Fig. 9.9. From the slope of the straight line fit to points with $V_G \geq 25$ V, a carrier mobility of 0.3 ± 0.1 cm^2 V^{-1} s^{-1} was calculated, and the intercept of this line with the V_G axis revealed a threshold voltage $V_t = 22 \pm 1$ V. The

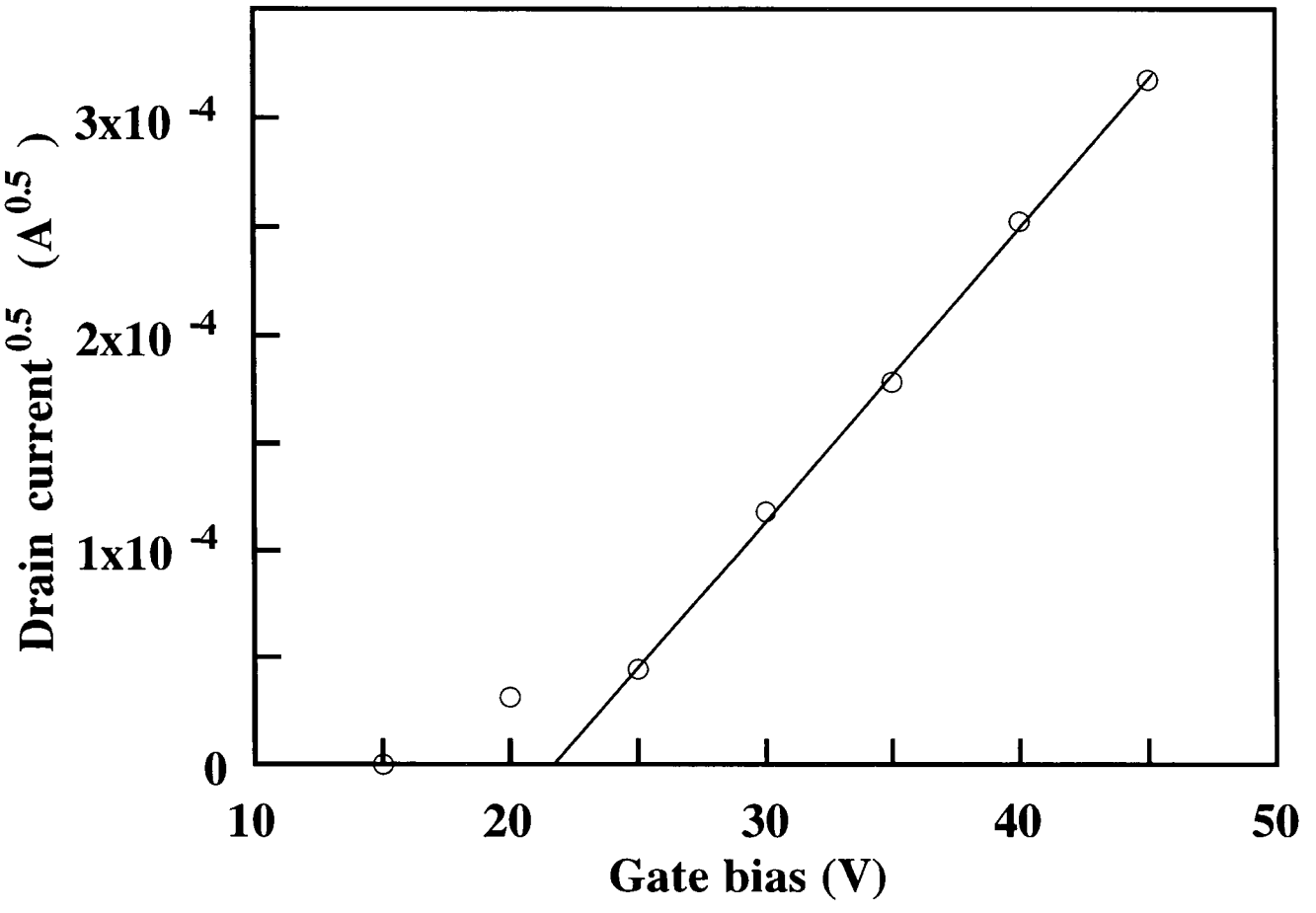

Fig. 9.6 $I_{D,sat}^{1/2}$ versus gate bias voltage for a TFT having an organic film consisting of 59 as-deposited layers of C_{18}Py-Ni(dmit)$_2$ on top of the interdigitated source and drain electrodes. The drain current values were corrected, by subtracting the Ohmic current below threshold, so that only the channel current was included.

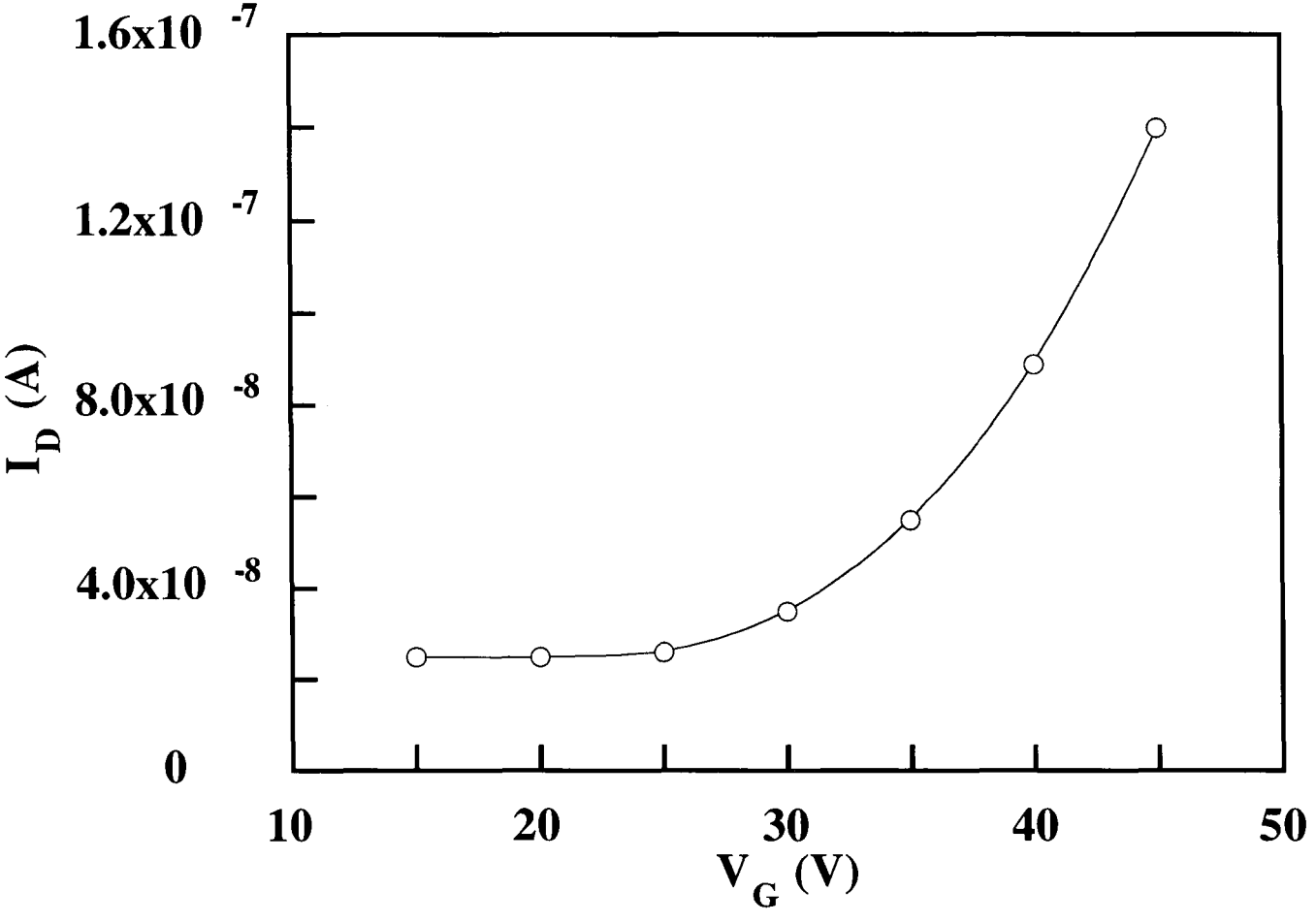

Fig. 9.7 Transfer characteristic for a thin film transistor using 59 as-deposited layers of C_{18}Py-Ni(dmit)$_2$ as the active region. V_{DS} was fixed at 5V. The current flowing through the bulk of the organic layer below threshold is apparent here.

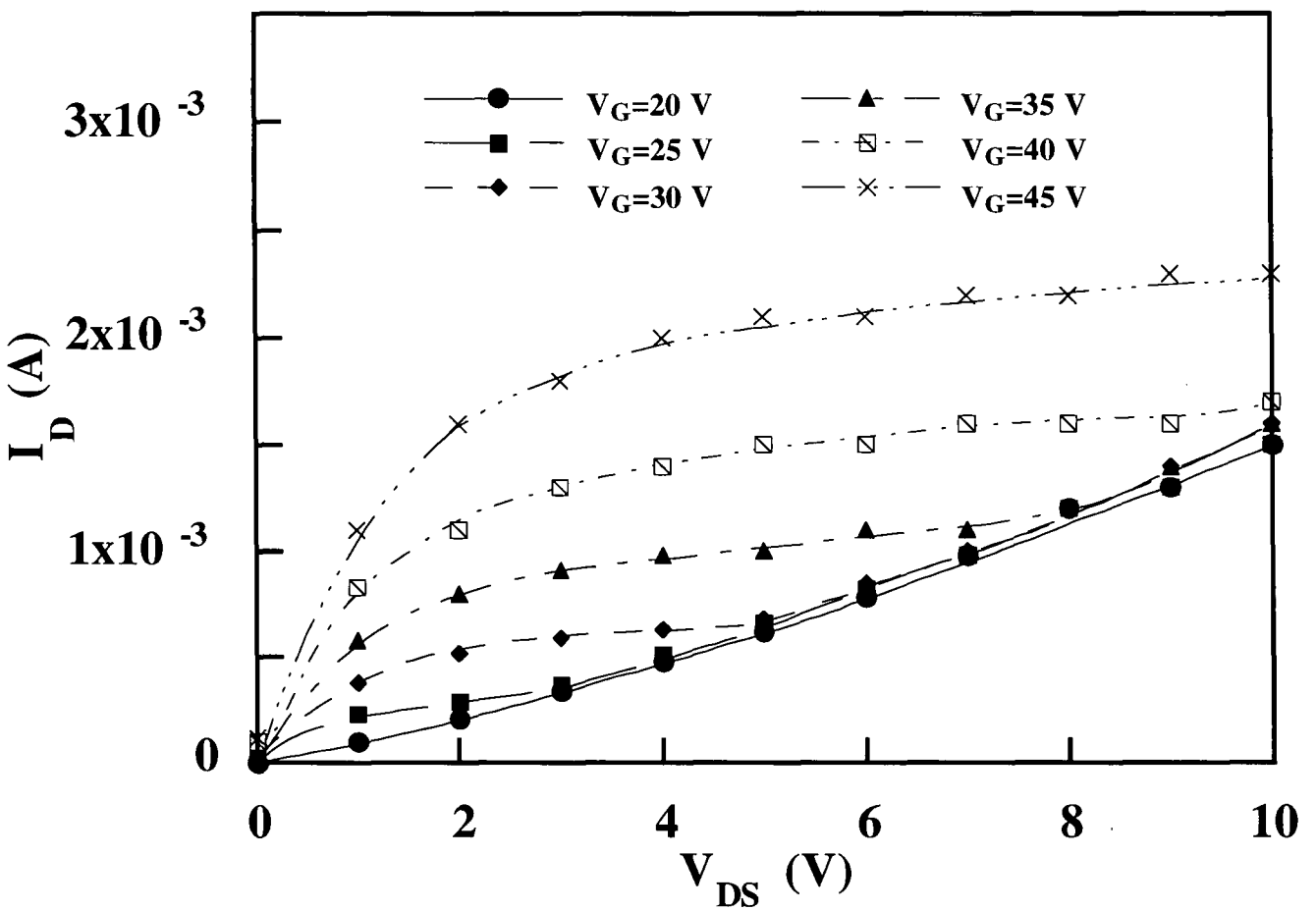

Fig. 9.8 **The drain current versus drain voltage characteristics, at various values of gate bias, for a TFT having an organic film consisting of 59 iodine doped layers of C_{18}Py-Ni(dmit)$_2$ on top of the interdigitated source and drain electrodes.**

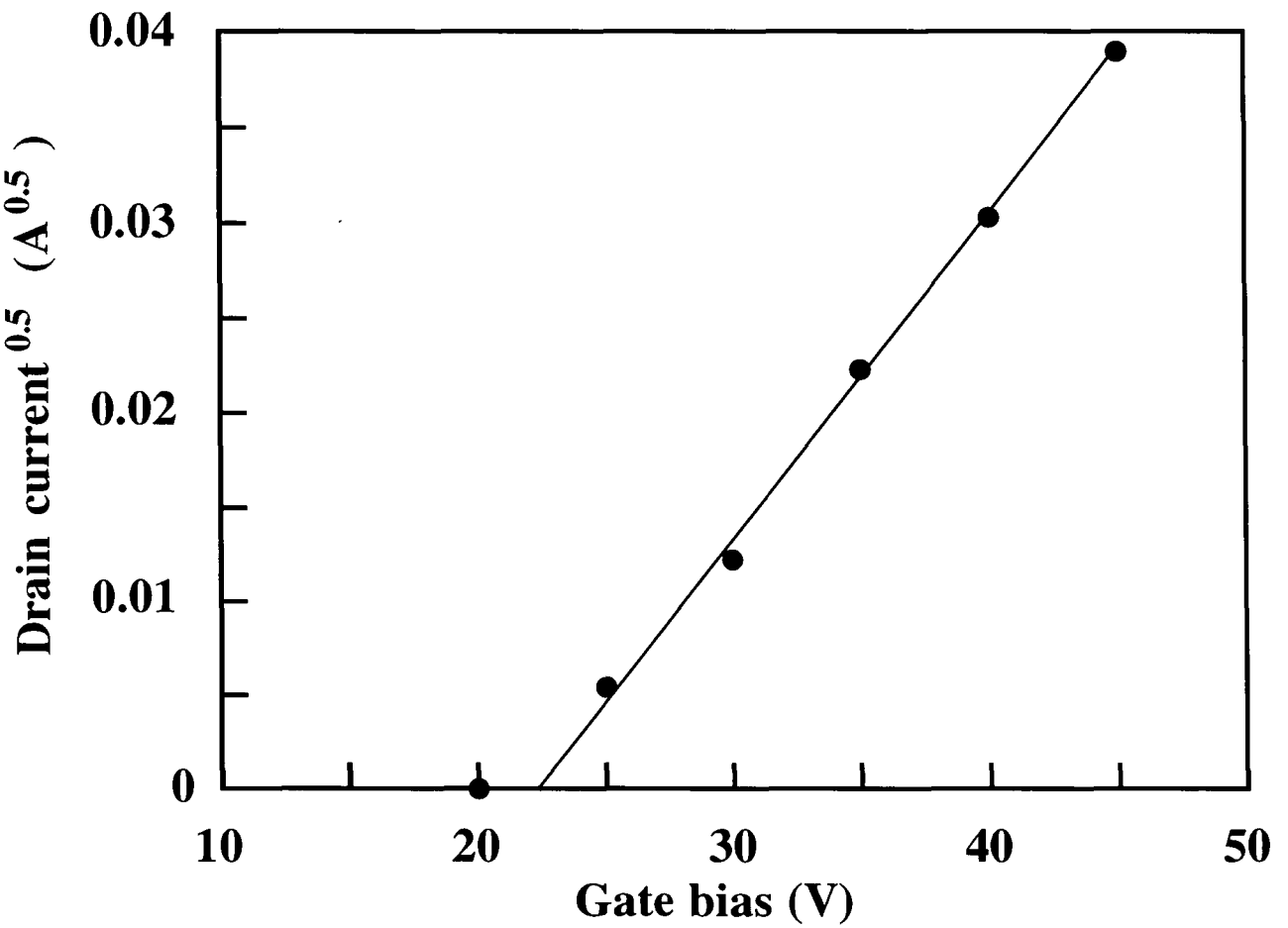

Fig. 9.9 $I_{D,sat}^{1/2}$ versus gate bias voltage for a TFT having an organic film consisting of 59 iodine doped layers of C_{18}Py-Ni(dmit)$_2$ on top of the interdigitated source and drain electrodes. The drain current values were corrected, by subtracting the Ohmic current below threshold, so that only the channel current was included.

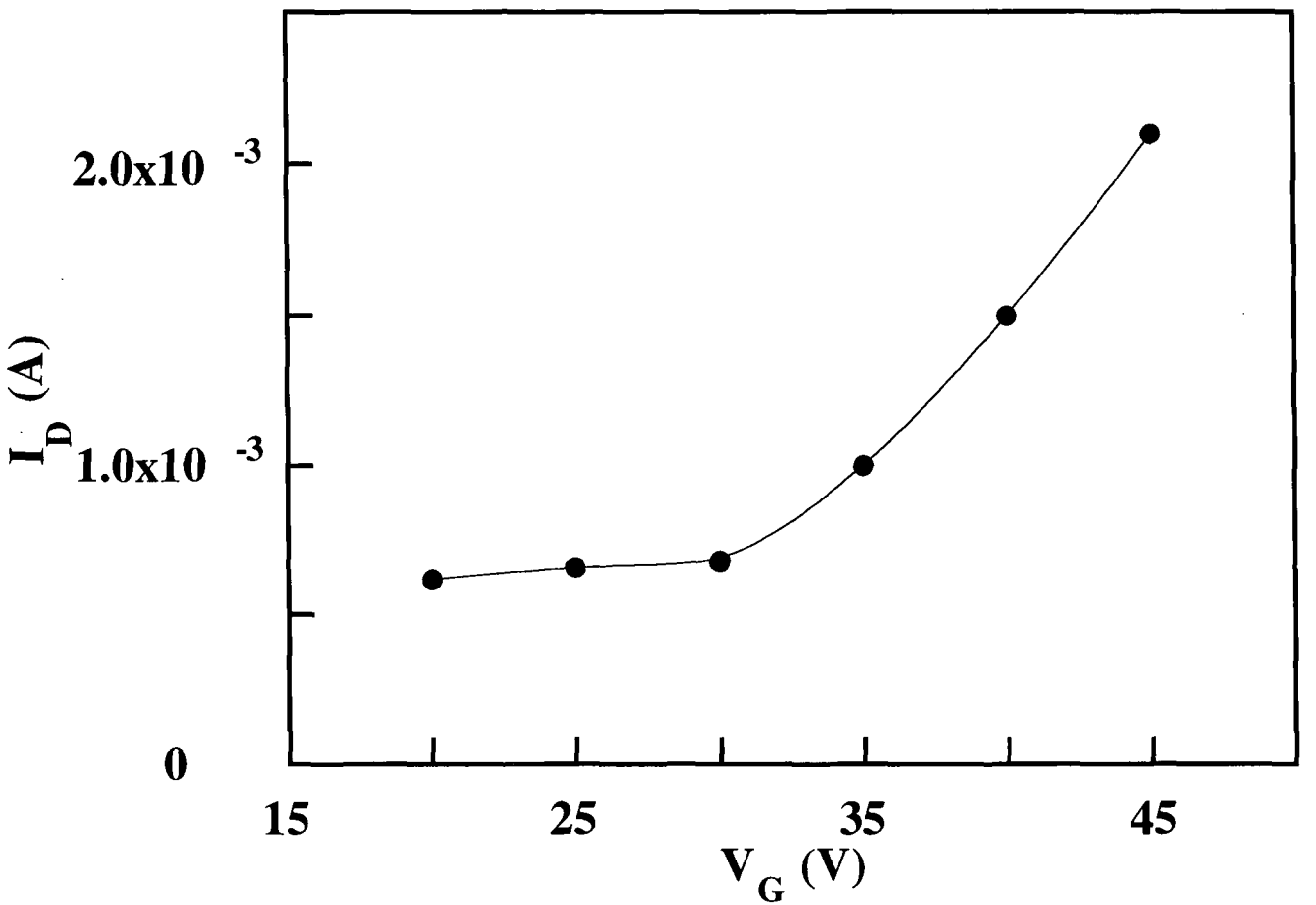

Fig. 9.10 Transfer characteristic for a thin film transistor using 59 iodine doped layers of C_{18}Py-Ni(dmit)$_2$ as the active region. V_{DS} was fixed at 5V.

mobility measured here is similar to the value reported by Garnier *et al* in a device using vacuum evaporated α-sexithienyl as the active layer and poly(-parabanic acid) resin and cyanoethylpullulan as the substrate and gate insulator, respectively.[4]

The transfer characteristic for the same iodine doped C_{18}Py-Ni(dmit)$_2$ device is shown in Fig. 9.10

9.7 Summary

An organic thin film transistor (TFT) has been fabricated using LB layers of C_{18}Py-Ni(dmit)$_2$ as the semiconducting layer. The conductivity of the LB layer in the as-deposited state was higher than that measured previously. It is thought that the small gap between the interdigitated electrodes used here could have been bridged by the μm sized aggregates that were observed in these films. The conductivity after iodine doping was similar to that obtained in previous experiments. Field effect transistor (FET) characteristics were recorded before and after doping, and the data used to calculate the mobilities of the charge carriers in the organic layer. Values of $1.9 \pm 0.5 \times 10^{-5}$ cm^2 V^{-1} s^{-1} and 0.3 ± 0.1 cm^2 V^{-1} s^{-1} were calculated, before and after doping with iodine, respectively. A threshold voltage of 22 ± 1 V was observed in both cases.

References

1. E.H. Nicollian and A. Goetzberger, IEEE Trans. on Electron. Devices, ED-12 (1965) 108-117.
2. G. Horowitz and P. Delannoy, J. Appl. Phys. 70 (1991) 469-475.
3. J. Paloheimo, P. Kuivalainen, H. Stubb, E. Vuorimaa and P. Yi-Lahti, Appl. Phys. Lett., 56 (1990) 1157-1159.
4. F. Garnier, G. Horowitz, X. Peng and D. Fichou, Adv. Mater. 2, (1990) 592-594.

Chapter 10

Conclusions and Suggestions for Further Work

10.1 Conclusions

The preparation of Langmuir-Blodgett (LB) films containing the long chain tetrathiafulvalene (TTF) derivative octadecanoyl-TTF and the organometallic charge-transfer complexes *N*-octadecylpyridinium-bis-(4,5-dimercapto-1,3-dithiole-2-thione) palladium (C_{18}Py-Pd(dmit)$_2$) and *N*-octadecylpyridinium-bis-(4,5-dimercapto-1,3-dithiole-2-thione) nickel (C_{18}Py-Ni(dmit)$_2$) has been investigated.

It was necessary to mix ODTTF with either octadecanoic acid (OA) or pentacosa-10,12-diynoic acid to aid transfer to solid substrates. The area per molecule values obtained from isotherms revealed that spreading of the molecules was complete, i.e. monomolecular films were formed. After compression, the mixed floating films could be deposited onto microscope glass slides or single crystal silicon wafers, with a transfer ratio of 1.0±0.1, to give good quality Y-type multilayers.

C_{18}Py-Pd(dmit)$_2$ and C_{18}Py-Ni(dmit)$_2$ could be deposited without the addition of fatty acid. The spreading of these materials on the surface of a pure water subphase was influenced by the amount of material spread and the spreading time (the time between the application of the molecules to the subphase and the initial compression of the floating layer). In both cases, the layer dispersed most effectively when a relatively small amount of material was spread and the spreading time was long. Otherwise, the small area per complex values obtained from isotherms revealed that spreading was incomplete, suggesting that multilayers and/or aggregates were formed on the subphase. Although both materials behaved in a similar way, comparison of the area per complex data revealed that C_{18}Py-Pd(dmit)$_2$ spread more easily than C_{18}Py-Ni(dmit)$_2$. This shows

that variation of the central metal ion in an organometallic charge-transfer complex can influence the properties of the material. Dipping of these floating layers onto glass microscope slides also depended on the spreading conditions. For C_{18}Py-Pd(dmit)$_2$, the best transfer ratios were recorded when a large amount of material was spread, regardless of the time allowed before compression. In the case of C_{18}Py-Ni(dmit)$_2$, good Y-type dipping was observed when the spreading time was short, with Z-type transfer recorded when the layer was aged for a long time before compression.

The thickness per layer of films containing ODTTF was lower than that expected from the lengths of the molecules that were obtained from standard models. This is thought to be due to tilting of the molecules and/or interdigitation of the hydrocarbon chains/head groups. Further work is required to confirm this assumption. X-ray scattering measurements could be used to provide more information.

LB samples containing ODTTF were conductive as-deposited, with room temperature in-plane dc values of $2.0\pm0.2\times10^{-3}$ S cm^{-1} and $2.3\pm0.6\times10^{-5}$ S cm^{-1} recorded for films diluted with OA and PA, respectively. The origin of this conductivity is not known, since undoped TTF should be insulating. It is thought that inadvertent oxidation of the TTF by an unidentified ion during the preparation of the films may have been responsible. Electrical conductivity was increased by chemical doping with iodine vapour. Maximum values of $2.4\pm0.1\times10^{-2}$ S cm^{-1} and $8.4\pm0.4\times10^{-4}$ S cm^{-1} observed in films containing OA and PA, respectively. This increase was attributed to the formation of a mixed valence complex, evidence for which was provided by optical absorption measurements that revealed the appearance of a charge-transfer band in the infra-red after doping. These films were semiconducting, with thermal activation energy (ΔE) values, obtained from low temperature electrical measurements, of 0.45±0.02 eV and 0.25±0.02 eV measured before and after doping, respectively. The peak conductivity values given here were observed when the amount of fatty acid contained in the samples was below 50%.

Increasing the proportion of acid beyond this point resulted in a decrease in conductivity. This behaviour has been explained using a two-site classical percolation model. Optical and scanning electron microscope (SEM) studies and energy dispersive spectroscopy measurements have revealed a two-phase structure, with separate regions of ODTTF and fatty acid. When the amount of acid in the film was high, the ODTTF regions became isolated so that no continuous path was available for carrier transport. The conductivity of these films was not stable with time, with the value beginning to fall after only a few hours.

The room temperature in-plane dc conductivity of multilayer films of C_{18}Py-Pd(dmit)$_2$ was influenced by the technique used to prepare the floating film. When the layer was aged for a long time before compression, the bulk conductivity was very low, regardless of the amount of material applied to the subphase. From the area per complex values measured when a small amount of solution was spread, a model has been suggested in which the (dmit)$_2$ molecules are interleaved between the long chain cations. X-ray scattering measurements could be used to obtain further structural information. When a large amount of material was spread, visible aggregates were evident in the layer on the surface of the subphase and in the film subsequently transferred to the substrate. By carefully making contact to these aggregates, they were found to be conductive in the as-deposited state, with a conductivity value of $1.2\pm1.0\times10^{-1}$ S cm^{-1} measured. Doping with iodine reduced this figure by a factor of 2-3. Energy dispersive spectroscopy measurements revealed that these particles contained palladium and sulphur, indicating the presence of the organometallic molecule. LB samples deposited from floating layers that were compressed soon after spreading were conductive without any post deposition treatment. When a small amount of solution was spread, a room temperature dc conductivity of $3.5\pm2.5\times10^{-3}$ S cm^{-1} was measured. Iodine doping increased this value by an order of magnitude to $2.6\pm1.7\times10^{-2}$ S cm^{-1}. At high dc bias, super Ohmic current versus voltage characteristics were observed suggesting space charge limited behaviour.

This was confirmed by measuring the thickness dependence of the current in the super Ohmic region. Films transferred from a floating layer formed from a large amount of solution exhibited a higher conductivity of $1.5\pm1.0\times10^{-1}$ S cm^{-1} as-deposited, a value that was stable with time. Iodine doping reduced this figure to $6.0\pm4.0\times10^{-2}$ S cm^{-1}. Observations of film morphology using optical and electron microscopy have revealed the presence of crystallites in the films. The behaviour of these particles depended on the amount of solution spread and the spreading time. After short spreading times, the particles remained and the film was conducting. If a small amount of solution was spread and the spreading time long, the particles dispersed and an insulating film was the result. This observation agrees with the model, developed from the area per complex measurements, where the $Pd(dmit)_2$ molecules are separated from each other by the long chain cations, precluding high conductivity. If a large amount of solution was spread and the spreading time long, the particles aggregated together to form much larger conductive crystallites in an insulating background matrix. The conductivity of these films was thermally activated, with $\Delta E=0.07\pm0.02$ eV. A power law variation of conductivity with temperature was also observed, however, suggesting a contribution from the temperature dependence of the density of states in the transport band and/or the carrier mobility.

The conductivity of multilayer samples of $C_{18}Py\text{-}Ni(dmit)_2$ was dependent on the spreading conditions. Films built up from aged monolayers were insulating, in the as-deposited state and after iodine doping. Films transferred from floating layers with a short spreading time were insulating in the as-deposited state, but a significant increase in conductivity was observed, to a stable value of $1.3\pm0.8\times10^{-1}$ S cm^{-1}, after exposure to iodine vapour. The current versus voltage characteristics that were measured were found to depend on the material used to form contacts to the film. When silver paint was used, a super Ohmic region was observed at low bias voltages. Gold and carbon cement contacts gave linear behaviour over the whole voltage range studied. The super Ohmic data measured with silver paint electrodes lay below the linear characteristic that was obtained

with the other two materials, and has been attributed to the formation of resistive barriers between the organic film and the contacts. These films were semiconducting, with $\Delta E=0.05\pm0.01$ eV. By using this material as the dielectric in a parallel plate capacitor and measuring the capacitance at 1 MHz, the relative permittivity at this frequency could be calculated. Values of 3.4 ± 0.6 and 6.7 ± 1.3 were obtained for layers before and after doping, respectively.

A thin-film field-effect transistor has been fabricated using a LB multilayer of C_{18}Py-Ni(dmit)$_2$ as the active region. From the characteristics of the device, the mobilities of the charge carriers in the channel have been calculated. Values of $1.9\pm0.5\times10^{-5}$ cm^2 V^{-1} s^{-1} and 0.3 ± 0.1 cm^2 V^{-1} s^{-1} were obtained before and after iodine doping, respectively.

10.2 Suggestions for further work

The electrical conductivities reported here are in-plane values. It may be useful to measure the electrical characteristics perpendicular to the plane of these films to determine whether the materials exhibit any rectifying properties.

The thin film transistor prepared here had a high threshold voltage, i.e. 22 ± 1 V, and a low yield of operational devices was observed. The successful operation of an organic thin film transistor is dependent on the nature of the interface between the gate insulator and the organic layer. Garnier *et al*[1] have demonstrated that the carrier mobility in a transistor using evaporated α-sexithienyl as the active layer can be increased from 10^{-5}-10^{-4} cm^2 V^{-1} s^{-1} to 4.6×10^{-1} cm^2 V^{-1} s^{-1} by replacing the SiO_2 gate insulator and substrate with organic materials, i.e. cyanoethylpullulan and poly(-parabanic acid) resin. Fig 10.1 shows a proposed structure for a thin-film transistor using LB layers of an organic fatty acid or a polymeric material as the gate insulator. This would allow close control over the thickness of the insulator, and may reduce operating voltages and enhance saturation behaviour. The low mobilities measured here mean that these organic devices could not

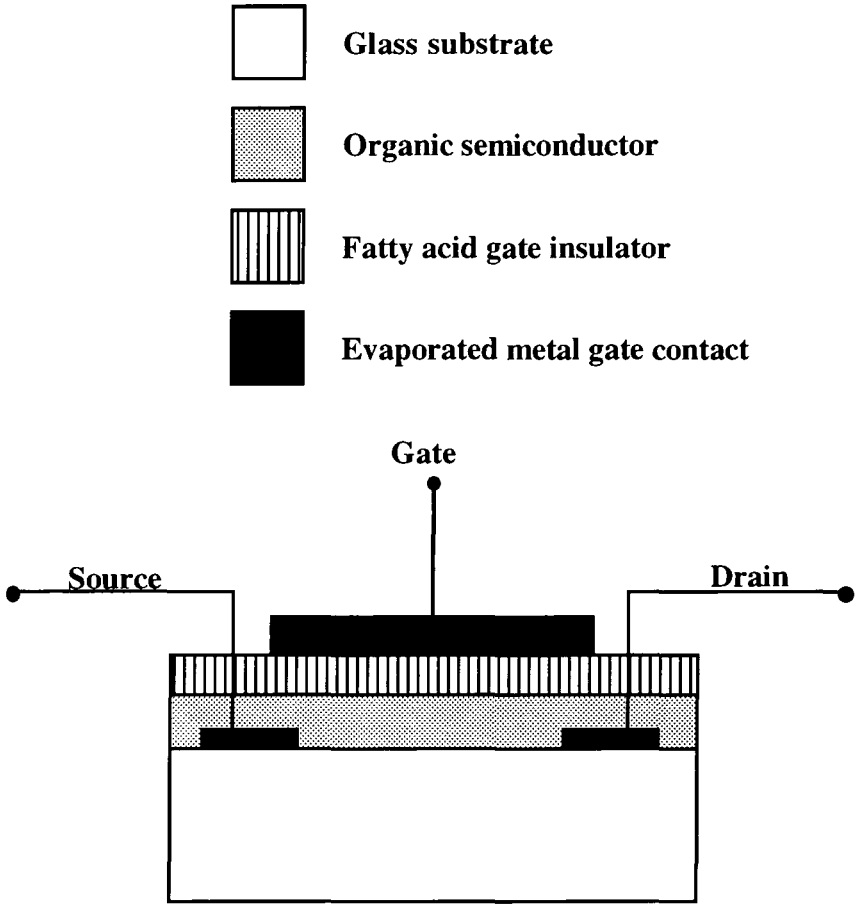

Fig. 10.1 **Proposed structure for an organic thin-film field-effect transistor using LB layers of a fatty acid as the gate insulator.**

compete with those fabricated from inorganic materials such as silicon. If the yield and electrical characteristics could be improved, however, they may be useful as the driver transistors in liquid crystal display panels.

The charge injection properties observed may make these compounds suitable for use in optoelectronic devices. Williams *et al*[2] have demonstrated that an LB film of C_{18}Py-Ni(dmit)$_2$ could be used as an electron injecting layer to reduce the bias voltage required for the onset of light output from an anthracene electroluminescent cell, and it may also be possible to fabricate solar cells using these materials.

References

1. F. Garnier, G. Horowitz, X. Peng and D. Fichou, Adv. Mater. 2, (1990) 592-594.
2. G. Williams, A.J. Moore, M.R. Bryce and M.C. Petty, Thin Solid Films, 244 (1994) 936-938.